FireFlight Final Report

AE3200: Design Synthesis Exercise

Group 29 – Tuesday 24th June, 2025

Kelsey Bozic	5757142	Carolina Silvestre	5480833
Tomás Dias	5715660	Rufus Sundaram	5699797
Damian Games	5240077	Louis Taillandier	5295793
Mario Piñeiro	5761549	Kevin Wibowo	5712122
Primož Perko	5726492	Christopher Wille	5692709

Delft University of Technology

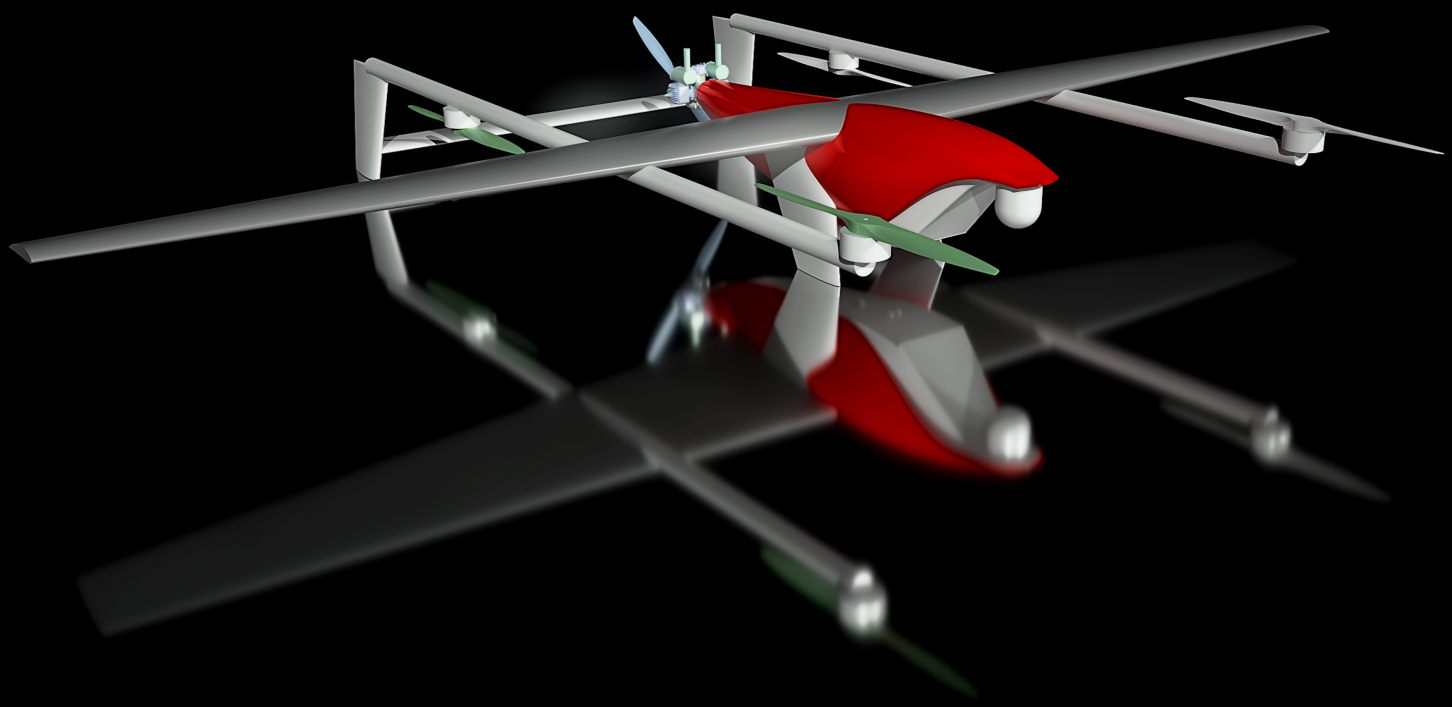

Instructors:	Dr. Ir. L. Laguarda & Dr. Ir. A. H. van Zuijlen
Coaches:	Ir. E. Sticchi & Ir. S. de Boer
Project Duration:	April - June 2025
Faculty:	Faculty of Aerospace Engineering, Delft
Report Style:	TU Delft, by Daan Zwaneveld

Acknowledgements

We would like to express our sincerest gratitude to our tutors, Dr.ir. Luis Laguarda and Dr.ir. Alexander van Zuilen, for their outstanding guidance and encouragement offered throughout the DSE project. Moreover, a special thanks goes to our coaches, ir. Emanuele Sticchi and ir. Stefan de Boer, for contributing immensely to our work and providing your input and expertise down to the minute details. Without all of your support, FireFlight would not have manifested into a concrete project, and we wish you all the best on your work in the future. We would also like to give recognition to the firefighting professionals, Jelmer Dam, Richard Vergouwen, Peter Phillips, and Tealand Stender, for their valuable input into aiding our understanding of firefighting. We also give a word of thanks to the OSCC, to Joris Melkert, Erwin Mooij, and the numerous people behind the scenes ensuring our time spent in the DSE was an enriching experience that will guide us on our careers ahead.

Lastly, our appreciation lies with our parents, siblings, family, and friends, who have always cheered us on in our endeavours. Your support all through our lives has shaped us into the engineers we have become today, and we love you all so much!

Kelsey, Tomás, Damian, Mario, Primož, Carolina, Rufus, Louis, Kevin & Christopher

Delft, 24th June 2025

Executive Overview

With global warming increasing wildfire risk year-by-year, the need for a system that reduces damages made by wildfires becomes more and more apparent. The FireFlight project aims to develop an aerial support system to assist firefighting brigades in their fight against wildfires through their surveillance, monitoring, and extinguishing. To provide a complementary service to existing operations, market analyses and interviews conducted indicate a demand for surveillance of fire-prone areas to enable early detection, improving the resolution of fire risk area monitoring, early suppression of wildfires, monitoring wildfire development, and providing information to fire brigades during firefighting.

Functions

After the overall project is defined, the detailed functions of the system must be described. To this end, the functions that must be performed by the system of systems (SoS) and corresponding systems are broken down chronologically in a functional flow diagram detailing the entire project cycle from design to end of life, ensuring all functions required for the effective execution of the mission are included. The functions are then arranged in a functional breakdown diagram, displaying the functional hierarchy.

Market Analysis

To find more about whether there is a need in the market for a system like this, and what exactly is desired from that system, a market analysis is performed.

Market Gap and Strategy

A market gap is identified in the wildfire fighting market as damages for uncontrollable wildfires can exceed €1M in the Netherlands, and are orders of magnitude larger in other countries, both within and outside Europe. There is a need for early detection, which is currently serviced by expensive satellite systems that lack resolution, or by remote-operated unmanned aerial vehicle (UAV) systems that lack the autonomy, flight time, detection ability, and range of a dedicated unmanned aerial system (UAS).

A further market gap is identified in existing UAV systems, as heavy-lift surveillance UAV swarms with a high autonomy level are currently non-existent. There are systems for defence capabilities, but they are currently in the Research & Development (R&D) phase, so FireFlight has the potential to break through several industries.

The project is currently set to target the Dutch government fire agencies, keeping design criteria in mind to eventually expand into Europe and worldwide. This is expected to have a cost-reducing effect on the client, as the development costs are shared between financial stakeholders that see use in the operation of the system. Additional revenue streams may be generated through licensing software developed for UAV swarming and fire detection, or by leasing the system to be able to operate year-round in the northern and southern hemispheres.

Key Stakeholders

When it comes to the entities that are directly affected by the FireFlight project, several key stakeholders are identified:

- Air Traffic Control (ATC)
- European Environmental Agency (EEA)
- Firefighter Union
- National Government/Customer
- System Insurance Company
- Investors
- Local Government
- Manufacturers
- Firefighters/Operators
- Regulators

The stakeholders directly set the mission requirements that drive the technical requirements of the project. This means that they are directly related to the outcome of the project.

Verification & Validation Plan

A detailed plan is provided for all verification and validation (V&V) procedures, which includes:

- **Requirements Validation:** Checking if requirements are well written.
- **Model Verification and Validation:** Checking if all models are well implemented and perform as needed.
- **Sensitivity Analysis:** Analysis on how design outputs change when different design parameters are varied.
- **Product Verification:** Verifying that final product meets all requirements.

- **Product Validation:** Checking if the final product works as intended.

Each subsystem chapter includes a section on verification and validation, and here a preliminary compliance matrix is also added to show whether requirements are met.

Trade-off Summary

The trade-offs performed during the preliminary design phase, prior to the start of this report, and the design choices made, were the following:

- **UAV Configuration:** Hybrid vertical take-off and landing (VTOL) fixed-wing UAV;
- **Base Station:** Container;
- **Vertical-to-Horizontal Transition Method**: Dual propulsion;
- **Propulsion:** Parallel-hybrid configuration;
- **Aircraft Configuration:** Conventional wing-plus-tail;
- **Wing Positioning:** High-wing configuration;
- **Wing Airfoil:** NACA 4415 at wing root and NACA 4412 at wing tip

In all trade-offs where the highest-scoring options had very similar scores, further technical analysis was done to obtain a more reliable trade-off decision. With the preliminary design finalised, Phoenix was born, and it is showcased in Figure 1

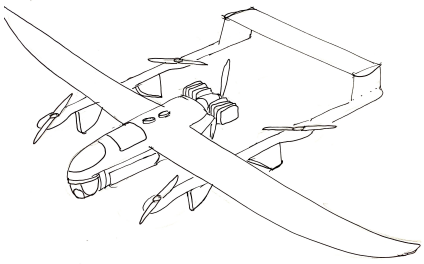

(a) Full preliminary design of the UAV.

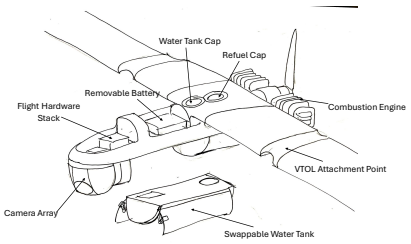

(b) Labelled breakdown of the preliminary design of the UAV, excluding the booms and empennage.

Figure 1: Drawings of the preliminary design of the UAV.

Detailed and Subsystem Design

With the preliminary design finalised, the Class II estimations followed, subsequently leading to subsystem design.

Class II

The Class II weight estimation attempts to find a more realistic estimate of the subsystem weights, when compared to the Class I weight estimation, leading to results that require less contingencies. First, an estimate was made on the fuselage and VTOL propulsion sizing. This was then used to perform the total weight estimation, which was based on both empirical and physical formulae. The final maximum take-off weight obtained was $71.8\,\mathrm{kg}$.

The Class II drag estimation sums up the drag contributions from all the individual components of the UAV, to arrive at a final zero lift drag estimate.

Finally, a sensitivity analysis is performed to assess the robustness of the design; it is concluded that the final maximum take-off weight (MTOW) never increased drastically due to a small increase in any parameter.

Propulsion

System sizing is followed by subsystem design. The propulsion subsystem includes the design of both propulsion systems: horizontal and VTOL. Once again, functional and requirement analyses are performed, followed by the design of the horizontal propulsion system, where the engine and propeller blades are sized. The engine chosen is the DLE60, with 7HP and weighing $2\,\mathrm{kg}$. The propeller blades are sized according to the engine chosen, and are thus $30\,\mathrm{cm}$ in size (radius). The rotational frequencyfor maximum engine efficiency during cruise is then calculated to be 5100 RPM (revolutions per minute). This finalises the design of the horizontal propulsion, which leads to the VTOL system design. The total power required by the four VTOL propellers is found to be $22.6\,\mathrm{kW}$, after including a safety factor of 1.5. To fulfill this VTOL requirement, the VL1035 motor is chosen, which weighs $1.2\,\mathrm{kg}$. To operate this motor, the cables, battery, propeller blades, and relay switches are then sized. Finally, a mass and cost budget is performed, including all components of the propulsion system.

Structures

The structures subsystem consists of the design of all structures present in the UAV. A functional and requirement analysis is performed here as well to guide the design. Since the UAV will operate with relative proximity to fires, an estimate of the operating temperature is made. This showed that the maximum increase in the UAV's structural temperature is of $62\,^{\circ}\mathrm{C}$ when operating near the fire, resulting in $102\,^{\circ}\mathrm{C}$ operating temperature. Then, the structural loading cases are identified, which includes: maximum gust load (highest load factor of n = 6), vertical take-off, and stacked landed on-ground. With the loading defined, a tubular sizing tool is created to size tail booms, fuselage, and the landing gear. This tool outputs the loading diagram, shear force, and bending moment on an analysed boom. To size the wingbox, in the start it is assumed that it could be tubular, similarly to the booms, but after analysis with the tool, it is shown that this would not withstand the required loads. This then leads to the design of a full wingbox and the creation of a dedicated tool for this, also with the same outputs. A three-cell wingbox design is created, and this is followed by buckling analysis, where it is concluded that buckling is the limiting factor for the structure, particularly at the wing root. In terms of material selection, it is found that carbon fibre is necessary, as using aluminium would increase the mass of the wingbox by 70%, which makes it higher than the allocated budget. The final wingbox weighs $6.18\,\mathrm{kg}$.

Aerodynamics

A higher-fidelity aerodynamic analysis of the wing is performed using ANSYS Fluent, resulting in a lift coefficient of $C_L = 0.8479$ and a drag coefficient of $C_D = 0.0451$ at a cruise angle of attack (AoA) of 7.45°. This is a lower C_L than was initially estimated from XFLR5 and Class II estimations, therefore other ways of increasing the lift should be investigated such as increasing the cruise angle of attack or including winglets. More accurate data—such as pressure distributions—is also obtained, and these more accurate loads can be implemented in the structures simulations.

Stability and Control

Stability and control entails the design of the empennage and control surfaces to ensure the aircraft is stable and controllable in all axes, as well as the positioning of components. A functional and requirement analysis is first given to provide a guideline for the design. Afterwards, a trade-off is performed on the empennage configuration, which includes four design options (U-tail, inverted U-tail, V-tail, inverted V-tail), and the final design choice is the U-tail. With this, the vertical tails can be used as landing gear, reducing weight. A trade-off is then performed on the airfoil for the empennage. Separate trade-offs are done for the vertical and horizontal empennage, but both conclude that the optimal option is the NACA 0012. This is followed by the centre of gravity (CG) analysis, where the locations of all components are chosen; the final CG location at operational empty weight (OEW) lies at the quarter chord point of the main wing. As the fuel and water are placed on the location of the OEW, the location of the maximum take-off weight (MTOW) remains at the quarter chord. This leads onto the preliminary horizontal tail sizing, which is used to create the scissor plot. The plot is used to find the required tail size for the UAV to be both stable and controllable. However, the size that is found would result in a tail chord length lower than $5\,\mathrm{cm}$, which is too low to obtain enough structural integrity, so, a more appropriate size of $20\,\mathrm{cm}$ is chosen. The vertical tails are sized with empirical data. With the tails sized, control surface sizing (elevators, rudders, ailerons) is also done to enable the UAV to achieve its required pitch, roll, and yaw rates. Afterwards, a dynamic stability analysis is performed to check for any unstable modes. The phugoid, short period, aperiodic roll, and Dutch roll modes were found to be stable, while the spiral mode is slightly unstable. A static stability analysis conducted to analyse this instability also concluded that the spiral mode is unstable. However, the instability is small enough to be ignored, as several aircraft have it as well. The stability and control design is then finalised by performing sensitivity analysis.

Flight Performance

Flight performance includes the analysis of climb and descent, turning, cruise, emissions, and noise. Starting with climb and descent performance, a climb requirement of $2\,\mathrm{m{\cdot}s^{-1}}$ was met. Meanwhile, a maximum descent rate of $2.78\,\mathrm{m{\cdot}s^{-1}}$ is possible, while $0.565\,\mathrm{m{\cdot}s^{-1}}$ is achieved for controlled descent. Moving onto turning performance, the UAV is able to achieve a turn rate of $42.88\,^{\circ}{\cdot}\mathrm{s^{-1}}$, which is essential for suppressing a smaller fire. The analysis of cruise showed that the cruise range achieved by the UAV is $479\,\mathrm{km}$. This value is enough to cover the entire operational area, so the UAV is able to make a full surveillance pass before having to return to the ground station for refuelling. Since the UAV runs on fuel, its emissions must be analysed, and these are calculated to be $4\,\mathrm{kt}$ for the entire swarm over 20 years. Finally, the noise produced by the swarm is analysed, and it was concluded that it meets the European Union Aviation Safety Agency (EASA) guidelines on noise produced by light-weight aircraft.

Embedded Systems

The UAV embedded systems design defines the onboard electronics architecture for autonomous wildfire surveillance and suppression. Required functionality is identified, requirements formulated, and the layout of onboard hardware defined. Component selection is justified through power, data, and control interfacing. Key domains include sensing, computing, power distribution, communications, and actuation. A full communications architecture is established, including UAV–GCS–remote user data links and a mesh network for swarm operation. SoS-level data flow is also defined. All design claims are tied to verifiable interfaces and supported by a requirement compliance matrix.

Operations and Simulations

Operations and Logistics Concepts

Operations and logistics concepts entails all details regarding how the system will operate. It starts with the operational environment, where some detail is given on what kind of airspace the system will operate in, and what risk category it belongs to. This is followed by an overview of the general operational concept, which provides details on how the ground station will be deployed, the logistics of the surveillance, the suppression, the monitoring of an ongoing large fire, irregular and emergency operations, and how maintenance of the system will be done. Afterwards, an explanation is given on how the design of the UAV is affected by operations, which includes factors such as the need for disassembling the UAV, and having a modular payload attachment. Following this, the ground station (GS) design is done, which includes UAV landing zone, replacing batteries, refuelling, replenishing suppressant, a rover to transport UAVs, methods to protect the ground station from external harm, water and fuel storage, power and mass budgets, and the ground station's spatial footprint.

(a) User interface concept during surveillance mission.

(b) Visualisation of battery swap at the ground station with a robotic arm.

Figure 2: Operational concepts of the mission.

Wildfire Suppression

A proper analysis of components needed for wildfire suppression must be done, along with the suppression strategy. Here, a design for the water tank that will be inside the UAV is developed. To open and close the tank, a sealing mechanism is also designed, and the size of this is as large as possible to deploy water at a faster rate. With the design of the tank and sealing mechanism finished, the speed of water deployment is calculated to be $2\,\mathrm{s}$. Lastly, a detailed suppression strategy is provided, which is crucial to ensure that UAVs deploy their water payload effectively and are thus able to suppress fires.

Simulations

Simulations are crucial to assess the feasibility of the aerial operations. It starts with the simulation of the fire spread, where a neural network (NN) was used on training data to obtain a model of how fire propagates in an area. Validation is done by comparing the results of the model with a wildfire that occurred in Portugal, and an accuracy of 78% is obtained over a propagation period of $33\,\mathrm{h}$, which shows very promising results. A model for optimising the path followed during surveillance is also created, and it makes use of genetic algorithms. For fire detection, the UAV will first use its infrared camera to detect a fire, and then switch to using a convolutional neural network (CNN) on its RGB (Red Green Blue) camera to confirm whether the fire truly exists. A detailed plan is provided on how this model will be developed. Afterwards, a model for the swarm coordination is done, which is based on speed and heading changes, and works differently depending on the mission phase. This model ensures UAVs do not collide. Lastly, a suppression simulation is created as well to model how well the swarm can suppress wildfires. To combine everything, a holistic simulation is done, where the full behaviour of the UAV, from take-off to fire circulation, is modelled. With this simulation, it is possible to find the maximum wind speed at which complete fire extinguishing is possible. The following simulation parameters are used.

- Fire model used: Dutch forests [1]
- Number of UAVs: 24
- Fire area extinguished per UAV: $8\,\mathrm{m}^2$
- Initial fire size: $0.09\,\mathrm{m}^2$

With these conditions, the maximum wind speed possible is $7\,\mathrm{km{\cdot}h^{-1}}$. The time at which the fire is detected is $3.7\,\mathrm{min}$, and the time at which the first UAV deploys its water payload is $4.7\,\mathrm{min}$.

[1] See: https://www.hogeveluwe.nl/nl/ontdek-het-park/natuur-en-landschap/bomen, Accessed 01/05/2025.

Technical Budgets and Risk

Technical Resources and Budgets

To ensure mass and power requirements of a single UAV are met, a technical resource budget is needed. For this, an initial estimate was given at the start of the project. With the current detailed design, these budgets have been updated with the current mass and power values, as well as estimates for how these values may still change. Furthermore, a more detailed mass budget is provided, where the mass of different subsystems is shown over several iterations. At the current state of the project, the mass budget is complied with as the maximum take-off weight is still below the requirement. The power budget was increased, but this was necessary for the VTOL system. The mass budget can be seen in Table 1.

Table 1: Comparison of initial and current mass budget for the UAV.

Subsystem	**Actual Mass [kg]**		**Target Mass [kg]**		**Margin [%]**		**Current Mass [kg]**		**Specification Mass [kg]**	
	Init.	Curr.	Init.	Curr.	Init.	Curr.	Init.	Curr.	Init.	Curr.
Structure	n/a	17.0	12.0	18.9	40	10	n/a	18.9	20.0	21.0
Power Sources	n/a	18.1	9.6	19.8	40	10	n/a	20.1	16.0	22.0
Payload	n/a	15.9	15.0	18.0	40	10	n/a	17.7	25.0	20.0
Avionics	n/a	1.4	2.4	1.8	40	10	n/a	1.6	4.0	2.0
Propulsion	n/a	12.3	9.0	13.5	40	10	n/a	13.7	15.0	15.0
Total	n/a	**64.7**	**48.0**	**72.0**	n/a	n/a	n/a	**72.0**	**80.0**	**80.0**

Technical Risk Management

The technical risk management strategy is outlined by first identifying technical risks that affect the project, determining their impact, defining mitigation strategies and planning contingencies. Risk maps are made before and after risk mitigation, clearly showcasing the risk reductions imposed by the mitigation. Risk is determined as a product of likelihood and severity. Severity is split into four classes – negligible, marginal, critical, and catastrophic – and likelihood is split into five classes – very low, low, moderate, high, and very high. Each identified risk is assigned a unique identifier and its likelihood and severity is determined. A mitigation action is assigned to each risk, as well as a contingency plan in the event of the realisation of the risk. A responsible authority is also established for each risk. The risks are then re-evaluated based on the assigned mitigation measures, and the risk maps present the final state of technical risks. Risk management has been done periodically since the start of the project.

Sustainability Implementation

Sustainability is considered in all subsystem designs. Each implementation is briefly explained to illustrate how sustainability is embedded in both the system design and the mission and is related to the sustainability indicators. Additionally, a life cycle assessment has been performed, providing an overview of the total equivalent CO2 emissions during the UAV lifespan. The total amount of emitted CO2 is estimated to be 3,398,183 kg.

Design Overview

Table 2 shows the main design and operational parameters of the system. With renders for the uav in Table and ground station in Figure 4 with a three-view drawing in Appendix A.

Table 2: Summary of final design and operational parameters.

Item	**Value**	**Unit**	**Item**	**Value**	**Unit**	**Item**	**Value**	**Unit**
$MTOW$	65	kg	$P_{h_{\max}}$	2600	W	System Cost	2.7M	EUR
OEW	31	kg	N_{prop}	4+1	-	$P_{\text{VTOL}_{\max}}$	22.4	kW
W_{PLD}	18	kg	R	350	km	A_{covered}	400	km2
S	1.87	m^2	L/D_{cruise}	11.7	-	h_{VTOL}	30	m
b	4.32	m	t_{refill}	180	s	N_{UAV}	35	-
L_t	1.7	m	t_{VTOL}	240	s	h_{cr}	450	m
S_h	0.32	m^2	t_{loiter}	300	s	Cost ops	292K	EUR/yr
S_v	0.18	m^2	Cost GS	800K	EUR	$V_{\text{H}_{\max}}$	33	m/s
V_{cr}	25.9	m/s	Cost UAV	54K	EUR	t_{detect}	220	s

Figure 3: Phoenix UAV render.

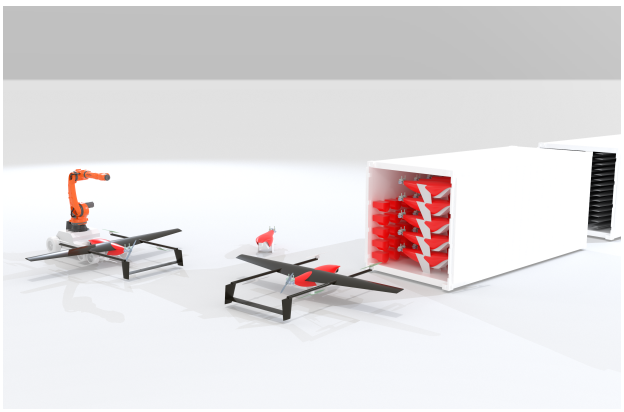

Figure 4: Ground station operations of FireFlight swarm.

User Requirements Compliance

Table 3: User requirements.

ID	Requirement	Status
Performance		
USR-PERF-001	The system shall cover an area of at least 20 km by 20 km.	Completed
USR-PERF-002	The system shall provide capacity for up to 50 simultaneously operating drones.	Completed
USR-PERF-003	The system shall maintain operational ability without visible spectrum detection.	Completed
USR-PERF-004	Each UAV within the swarm shall measure temperature level with a precision of at least 1 °C.	Completed
USR-PERF-005	Each UAV within the swarm shall measure relative humidity with a precision of at least 5%.	Completed
USR-PERF-006	Each UAV within the swarm shall measure smoke level with a precision of at least 10 $\mu g \cdot m^{-3}$.	Completed
USR-PERF-007	The system shall be capable of operating in winds up to 160 $km \cdot h^{-1}$.	Partially Met
USR-PERF-008	Each UAV within the swarm shall withstand temperatures up to 200 °C for a minimum time of 30 seconds.	Completed
Safety and Reliability		
USR-SAFE-001	The swarm shall adapt in real time to fire conditions.	Completed
USR-SAFE-002	The swarm shall use AI algorithms for coordination.	Completed
USR-SAFE-003	Each UAV within the swarm shall have collision avoidance capability.	Completed
USR-SAFE-004	Each UAV within the swarm shall have redundant flight control system.	Completed
USR-SAFE-005	Each UAV within the swarm shall allow handover to human operator within 1 second.	Completed
USR-SAFE-006	The system shall have a relocatable servicing platform supporting deployment and charging.	Completed
USR-SAFE-007	Each UAV in the system shall return to the servicing station in the event of a system malfunction.	Completed
USR-SAFE-008	The swarm shall be reliably operational for at least 99% over a 20 year lifespan.	Completed
Sustainability		
USR-SUST-001	Fire retardant chemicals used shall meet EPA and EEA environmental standards.	Completed
USR-SUST-002	Each UAV within the swarm shall have a modular design.	Completed
USR-SUST-003	At least 80% of drone materials by mass shall be recyclable.	Partially Met
USR-SUST-004	Batteries used shall be recyclable under EU regulations.	Completed
Engineering Budgets		
USR-ENG-001	Each UAV within the swarm shall provide a standardised payload interface with a minimum capacity of 15 kg.	Completed
USR-ENG-002	Each UAV shall have a maximum takeoff mass of 80 kg.	Completed
USR-ENG-003	Fire-retardant refilling time shall not exceed 3 minutes.	Completed
USR-ENG-004	Water refilling time shall not exceed 3 minutes.	Completed
Cost		
USR-COST-001	System costs shall be split into development, production, delivery and operational costs.	Completed
USR-COST-002	The total cost of the system (purchase + operations + end-of-life) over a period of 20 years shall be under €10 000 000.	Completed
Operations		
USR-OP-001	System shall comply with EU regulations for drone operations in class E airspace.	Completed
USR-OP-003	Navigation system shall provide a positional precision of 99 centim.	Completed
USR-OP-004	The System shall be able to perform detection activities 24/7 during high-risk periods.	Completed
USR-OP-005	The System shall be able to perform suppression activities for at least 6 hours on a given day.	Completed
USR-OP-006	The System shall be able to continuously assess the state of the zone.	Completed

Table 3 shows the compliance matrix for the requirements that were set by the user. Two requirements are marked as partially met. The first is the wind requirement, as the final design that was developed can fly in only $100\,\mathrm{km{\cdot}h^{-1}}$ winds. This was decided upon because wind speeds higher than SI100 are rarely achieved during wildfires. Furthermore, attempting to fully achieve the requirement would result in a costly and heavy design. The second requirement that is partially met is on recyclability, and the value achieved is 50%, as carbon fibre is required to have a design that performs well enough structurally.

Project Outlook

This entails all process that ought to be handled following the first 10 weeks of the project. In addition related costs for the system are outlined.

Cost and Return on Investment

A full system cost breakdown was performed, including operational expenses. The system production cost is €2.7 million, with suggested purchase price of €4.2 million. These results were used to estimate the system's return on investment (ROI), which was calculated at 15% over the 5 year design period. The user will spend approximately €290K per year as such €10 million for all system expenses including acquisition over 20 years.

Next Phases

After the Design Synthesis Exercise (DSE), the design must be developed into a market-ready product. A post-DSE plan is defined, including a Gantt chart and development logic covering prototyping, hardware verification, manufacturing, and launch preparation. Client and stakeholder needs are considered throughout.

Contents

List of Symbols

Abbreviations

ac	Aerodynamic Centre	-
AI	Artificial Intelligence	-
AoA	Angle of Attack	-
ATC	Air Traffic Control	-
AWG	American Wire Gauge	-
BLDC	Brush-Less Direct Current	-
CFRP	Carbon Fibre Reinforced Polymer	-
CG	Centre of Gravity	-
CNN	Convolutional Neural Network	-
DSE	Design Synthesis Exercise	-
EASA	European Union Aviation Safety Agency	-
EEA	European Environmental Agency	-
EOL	End Of Life	-
EPNL	Effective Perceived Noise Level	dB
ESC	Electronic Speed Controller	-
FLAME	Fire Luminosity Airborne-based Machine learning Evaluation	-
FR	Fineness Ratio	-
GCS	Ground Control Station	-
GS	Ground Station	-
HLD	High Lift Device	-
HTOL	Horizontal Take-off and Landing	-
ICE	Internal Combustion Engine	-
IR	Infrared	-
MTOW	Maximum Take-Off Weight	-
N/A	Not Applicable	-
NN	Neural Network	-
OEW	Operating Empty Weight	-
OTA	Over-The-Air	-
PWL	Sound Power Level	dB
R&D	Research and Development	-
RGB	Red Green Blue	-
ROI	Return on Investment	-
RPM	Revolutions Per Minute	-
SoS	System of Systems	-
SPL	Sound Pressure Level	dB
TBD	To Be Determined	-
TRL4	Technology Readiness Level 4	-
UAS	Unmanned Aerial System	-
UAV	Unmanned Aerial Vehicle	-
USD	United States Dollar	-
UTS	User Terminal System	-
V&V	Verification & Validation	-
VALID	Verifiable, Achievable, Logical, Integral and Definitive	-
VLOS	Visual Line of Sight	-
VTOL	Vertical Take-off and Landing	-

Greek Letters

α	Angle of Attack	$^\circ$
β	Prandtl-Glauert Correction Factor	-
β	Sideslip	$^\circ$
Δ	Change In Value	-
δ	Deflection Angle	$^\circ$
ϵ	Downwash Angle	$^\circ$
η	Efficiency	-
η_h	Tail Dynamic Pressure Ratio	-
η_v	Dynamic Pressure Ratio	-
Γ	Dihedral	rad
κ	Curvature	-
λ	Eigenvalue	-
λ	Taper Ratio	-
Λ_x	Sweep at x	$^\circ$
μ	Mean	-
ω_0	Undamped Natural Frequency	Hz
ρ	Density	$\mathrm{kg{\cdot}m^{-3}}$
σ	Sidewash Angle	rad
σ	Standard Deviation	-
σ	Stress	Pa
τ	Control Surface Effectiveness Factor	-
θ	Angle	$^\circ$
ζ	Damping Ratio	-

Roman Letters

$\bar{c}$	Mean Chord	m
$\bar{x_{ac}}$	Aerodynamic Centre	-
$\Delta_{fus}C_{m_{ac}}$	Change In Moment Coefficient	-

A_h	Horizontal Tail Aspect Ratio	-
b_h	Horizontal Tail Span	m
C_{bat}	Battery Capacity	Ah
C_{D0}	Zero Lift Drag Coefficient	-
C_{fc}	Flat Plate Skin Friction Coefficient	-
c_h	Horizontal Tail Chord	m
C_{Lp}	Half Amplitude Time	-
$C_{n\beta}$	Half Amplitude Time	-
C_r	Root Chord	m
C_t	Tip Chord	m
$C_{Y\beta}$	Half Amplitude Time	-
$C_{D_{\text{cr}}}$	Cruise Drag Coefficient	-
$C_{D_{\text{misc}}}$	Miscellaneous Drag Coefficient	-
C_{D_y}	Side Drag Coefficient	-
C_{L_α}	Lift Curve Slope	-
$C_{L_{\text{cr}}}$	Cruise Lift Coefficient	-
$C_{L_{\alpha_h}}$	Tail Lift Curve Gradient	-
$C_{l_{\delta_\alpha}}$	Roll Control Derivative	-
$C_{L_{A-H}}$	Tail-less Lift Curve Slope	-
C_{L_h}	Horizontal Tail Lift Coefficient	-
C_{l_P}	Roll Stability Derivative	-
$C_{m_{ac}}$	Aerodynamic Moment Coefficient	-
D	Drag	N
E	Young's Modulus	Pa
FF_c	Form Factor	-
FR_{fus}	Fineness Ratio of Fuselage	-
g	Gravitational Aceleration	$\text{m}\cdot\text{s}^{-2}$
I	Cross-Section Moment of Inertia	m^4
i_h	Tailplane Incidence Angle	$^\circ$
I_{yy}	Moment of Inertia Y	m^4
I_{zz}	Moment of Inertia Z	m^4
IF_c	Interference Factor	-
J	Advance Ratio Coefficient	-
K_{rho}	Fuselage Density Coefficient	-
L	Beam Length	m
L_{cable}	Length of Cable	m
L_{fus}	Length of Fuselage	m
l_V	Vertical Tail Moment Arm	m
m	Mass of Item	kg
M_F	Fuselage Mass	kg
M_W	Wing Mass	kg
N_r	Number of Rotors	-
P	Electric Power	W
P	Period	1/s
p	Roll Rate	$^\circ/\text{s}$
P_{bat}	Battery Power	W
$P_{\text{line loss}}$	Line Loss Power	W
P_{mot}	Motor Power	W
P_{prop}	Propeller Power	W
q_{xy}	Shear Flow of Section xy	$\text{N}\cdot\text{m}^{-1}$
S	Wing Surface Area	m^2
S_{ref}	Reference (Wing) Area	m^2
S_{wet_c}	Wetted Area	m^2
S_h	Horizontal Tail Surface	m^2
t/c	Thickness to Chord Ratio	-
$T_{\frac{1}{2}}$	Half Amplitude Time	s
V_{cr}	Cruise Speed	$\text{m}\cdot\text{s}^{-1}$
V_{hor}	Horizontal Velocity	$\text{m}\cdot\text{s}^{-1}$
$V_{H_{\text{max}}}$	Max Horizontal Speed	$\text{m}\cdot\text{s}^{-1}$
V_h	Horizontal Tail Volume	m^3
W_{ai}	Air Induction Weight	lbs
W_{Emp}	Empenage Weight	lbs
W_{Engine}	Engine Weight	lbs
W_{fuel}	Fuel Weight	lbs
W_{LG}	Landing Gear Weight	lbs
W_{nac}	Nacelle Weight	lbs
W_{OE}	Operating Empty Weight	kg
W_{Paint}	Paint Weight	lbs
W_{Prop}	Propeller Weight	lbs
W_{pwr}	Powertrain Weight	lbs
W_{TO}	Take-off Weight	lbs
W_{VTOL}	VTOL system Weight	kg
W_{PLD}	Payload Weight	-
X_{F}	Fuselage Group Location	m
X_{LEMAC}	Leading Edge of Mean Chord Position	m
$X_{\text{CG}_{\text{OEW}}}$	OEW centre of Gravity	m
X_h	Horizontal Tail Length	m
A	Wing Aspect Ratio	-
b	Wingspan	m
I	Electric Current	A
R	Electric Resistance	Ω
V	Electric Voltage	V

1 Introduction

Wildfires are highly destructive phenomena, claiming hundreds of lives and billions in damages yearly. The Netherlands sees the majority of its wildfires occur during the spring and summer seasons, when factors such as dry vegetation, strong winds, and higher temperatures compound to increase wildfire risk [1]. These conditions are only expected to culminate due to climate change, with current projections indicating increasing dangers of wildfires, not only in the Netherlands, but around the world [2, 3]. Thus, early wildfire detection and suppression become evermore imperative. As existing systems often exhibit delayed response times or limited area coverage, the need for a novel solution is apparent. With fire suppressant resources increasing exponentially with the time a fire propagates for [4], response speed becomes a focal performance indicator — to do this cheaply while minimising damage, a solution should ideally be rapidly deployed and operated autonomously.

A **project objective** arises — designing a fire response UAV system capable of supporting continuous monitoring, early detection, targeted suppression, and support to firefighting units. This report describes the initial design phase of the Phoenix UAV - a VTOL system to be used in a swarm of 35 combination with an autonomous ground station to execute its mission: surveil, suppress and assess wildfires.

The structure of this report aims to guide the reader through all phases of system development. Chapter 2 defines the system's functions and requirements; Chapter 3 examines the market context, identifying potential users and gaps in existing systems; Chapter 4 outlines the sustainability strategy; Chapter 5 presents the verification and validation framework. Chapter 6 summarises trade-offs that shaped system-level design; Chapter 7 details the sizing approach and configuration convergence. Chapters 8 to 13 cover the design of different subsystems depth. Namely, they cover stability and control, structures, propulsion, aerodynamics, flight performance, and embedded systems. Chapter 14 addresses operational logistics and deployment; Chapter 16 summarises simulation outcomes; Chapter 15 introduces the suppressant system architecture. Chapter 17 presents resource budgets; Chapter 18 discusses sustainability implementations. Chapter 19 identifies system risks and mitigation strategies; Chapter 20 provides a requirement compliance matrix. Lastly, Chapter 21 presents an outlook on the project's future, complete with financial planning and timeline forecasting.

2 Functional Analysis

The system functional flow is presented in Figures 2.2 to 2.1, in the form of functional breakdown and flow diagrams, where functions are grouped into packages that collectively outline the operation of the complete SoS. Subsystem-specific functional analyses are provided in the respective chapters. Functions within domains extending past the scope of direct system design (such as marketing and manufacturing) are addressed in Subsection 21.3.1.

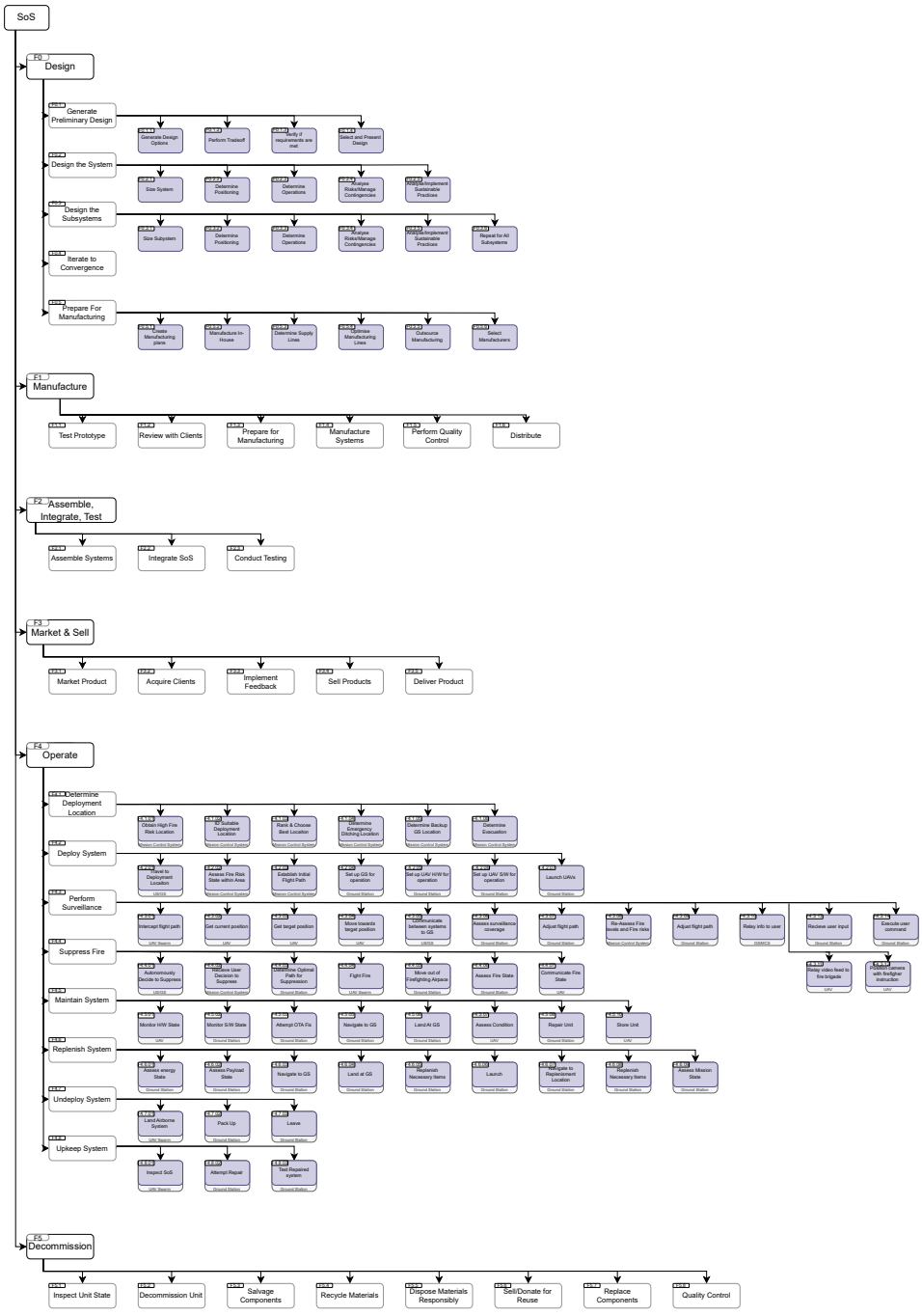

Figure 2.1: Functional breakdown structure.

Figure 2.2: Functional flow diagram (1/2).

Figure 2.3: Functional flow diagram (2/2).

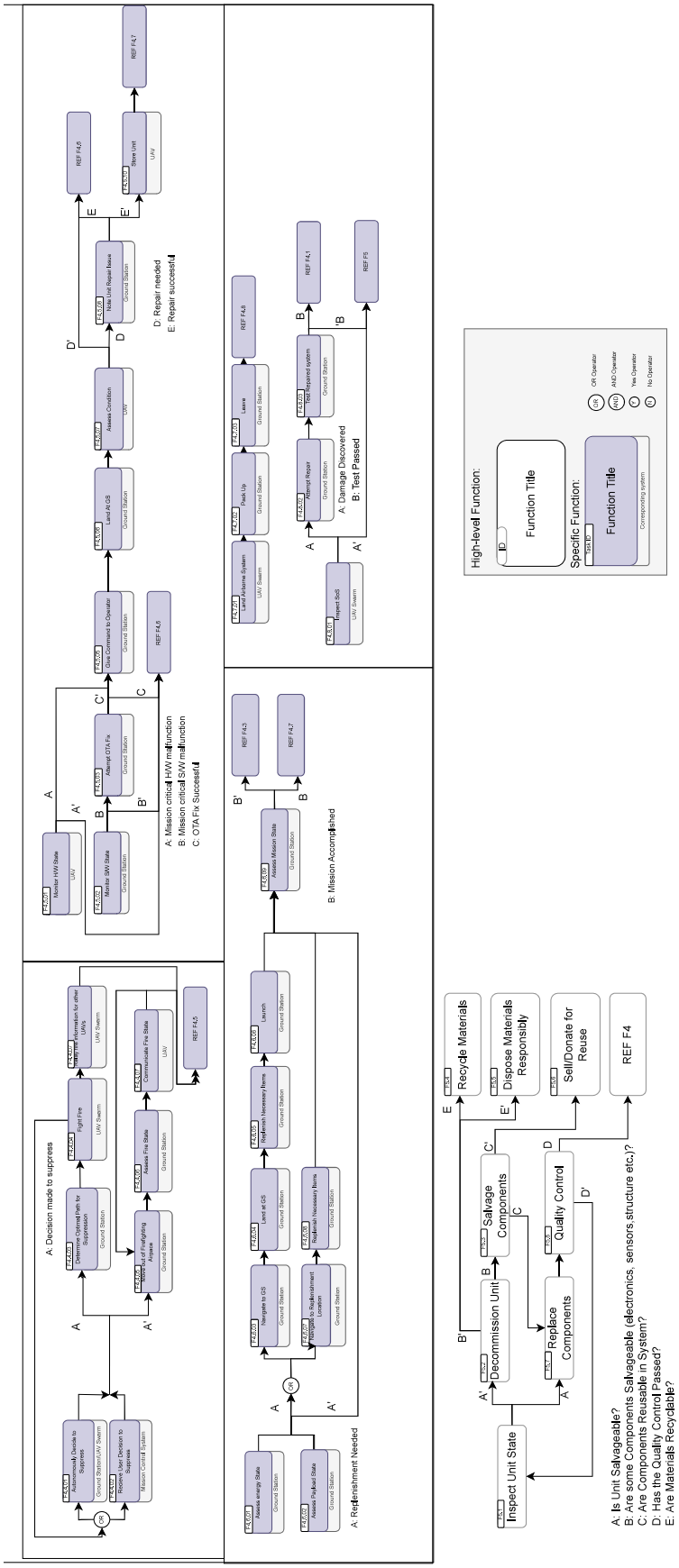

3 Market Analysis

This section describes the market gap for the proposed system. Note that due to the reserve currency status of the United States Dollar (USD), it is used for global market metrics, while the Euro currency is used for estimates due to the initial target market being in the Netherlands.

Wildfires created approximately $6.8B in damages in 2023[1]. European Joint Research Centre estimates wildfire damages in Europe at €2B in 2024[2]. However, quantifying the total damage of these fires is unreliable due to the high variability in estimation methods. If the effect of the release of carbon dioxide and reduced carbon sink area is included, these damages are likely significantly higher.

3.1.Project Objective

Project Objective: "Design a wildfire fighting UAV swarm to monitor and assess high fire-risk areas, and detect and suppress early-stage fires, by 10 students within 10 weeks."

The project aims to improve the current firefighting methods by leveraging artificial intelligence and improvements in UAV swarming capability. The goal is to design a system that will reduce the occurrence of devastating wildfires by extinguishing them before they exceed available suppression capabilities and become uncontrollable, leaving containment as the only remaining option.

3.2.Wildfire Fighting Market

According to the Institute for Defence and Government Advancement, global wildfire management market totals $3B in 2024 with compound annual growth rate of 2.5% per annum [5]. $1.9B per annum is attributed to aerial firefighting capability and $61.4M for UAS technology. Of the total budget, aerial capacity represents 73%. While UAVs make up only 1% of the total budget, they are assumed to be UAVs only used in a piloted, information-collection role.

Estimates from the BrandWeer Nederland place the cost of fighting small fires at €1.8M in 2018, with the cost for fighting a single out of control fire at approximately €426 000 [6], excluding air support, for which costs of €20 000 per hour are reported. In addition, subsequent land management and recovery can cost up to €300 000. As such, an estimate of €1M in damages saved in the case of a single out of control fire being avoided.

The Netherlands represents 364 hectares of total burnt area, making up to 0.08% of the total area burnt in Europe from the 2013-2022 average [7]. As such, the Dutch customer may represent only a small sub-group in the global UAS firefighting market. However, as a wealthy country with dense population and climate awareness, the demand for wildfire fighting improvements is high[3]. In addition, the UAV swarm system is ideal for patrolling small, high value/risk areas, and the Netherlands provides a relatively simple operational terrain making it a prime target for initial development.

The largest burnt areas in Europe include Spain, Portugal and Greece [7]. Table 3.1 shows the relative sizes of fire management markets for aerial, advanced sensing technology, and UAS systems [5]. The United States provides the largest market by a high margin, but presents a significantly higher land area. As the UAV swarm will have a specific cost per square kilometre due to limited range, two metrics have been calculated from the aggregated market for aerial, sensing and UAS market — $ per km^2 and K$ (thousand dollars) per km^2. This metric considers total land area to normalize for size, however does not account for different risk areas.

Table 3.1: Annual market sizes by country and category.

Country	Aerial (M$)	Sensing (M$)	UAS (M$)	Land ($ per km^2)	Burned (K$ per km^2)
Portugal	50	N/A	1.0	554	55
Greece	80	N/A	1.0	613	162
Spain	40	2.0	2.0	87	141
Australia	77	9.0	5.0	12	32
United States	1600	58	44	172	309
Canada	56	16	6.1	8.0	5.0
Brazil	1.7	2.1	1.6	1.0	2.0

Data for the Netherlands is not included as the market is not considered large enough on a global scale. However, it is

[1] See: https://www.statista.com/statistics/1423714/economic-impact-due-to-wildfires-worldwide/ Accessed: 01/05/2025.
[2] See: https://joint-research-centre.ec.europa.eu/projects-and-activities/natural-and-man-made-hazards/fires_en. Accessed: 01/05/2025.
[3] See: https://nltimes.nl/2025/04/12/firefighter-warning-netherlands-unprepared-major-wildfires. Accessed: 23/04/2025.

determined that due to the high land value, low land area and direct interest in the system it is, per land area, still an interesting market to begin designing for. Beyond this it can be identified that Mediterranean and United States regions provide the highest markets per land area. It can be noted that despite Australia's large total market and wildfire occurrence, the value for a system per land area is relatively lower.

3.2.1.Identified Gap in Firefighting Capacity

In fighting wildfires, detection and response time is critical [6] as fires grow exponentially, meaning early detection and suppression can save large fire response being required. Particular interest in the market have been confirmed, based on interviews with industry experts[4] [5].

In terms of current firefighting methods, there are several challenges to tackle. A major one is the difficult terrain with limited road access [8], which prevents firefighters from reaching the fires. A second challenge is the mobilisation of air support for fire suppression, as there are significant delays due to runway and crew availability [6]; having direct and automated response can save significant damages and costs. Challenges for manned air support for firefighting also include the lack of night-time operability, and capacity in low visibility conditions.

UAVs include an improved sensor suite and reduced requirements on structural safety[6], so they will provide improved coverage in harsh weather conditions as pilot safety and visibility is not needed for consideration. In terms of sensors, infrared (IR) imaging is a proven tool in firefighting operations for detecting fire hotspots and guiding firefighting efforts[7]. With this, and recognising that current aerial options provide low flexibility [8], it is clear that there is a large gap in the market for automated monitoring of large areas with continuous operations, using UAVs. As such, there is interest in the usage of UAVs in surveillance and monitoring operations, as well as detection and suppression of early-stage fires[8] .

3.3.UAV Market

There is currently a boom in UAV capacity, generating high levels of funding and competition. Available UAV systems provide conditional operational autonomy for example auto-follow or waypoint navigation, which creates an opportunity for becoming the first to market a UAV system with the ability to autonomously complete missions. As of now, operations are limited to visual line of sight (VLOS) flights made by individual operators per UAV with manual coordination with ground assets.

Numerous companies selling UAVs provide solutions for single human pilot and some conditional autonomy features. Costs for UAV swarms are not readily available due to their secretive development for military applications. For civilian applications, UAV swarms are mainly present in university projects, and thus have technology readiness level 4 (TRL4), with tests in controlled environments.

In terms of interest in general UAV applications, multiple industries have a need for autonomous UAV technology and UAV swarm technologies. Performing autonomous surveillance of an area, or autonomous delivery of packages, extends to numerous markets. This includes defence, border security, high-security facility surveillance, building-interior mapping, search and rescue, environmental observation, and agricultural crop spraying[9].

3.4.Similar Projects and Competitors

UAV swarms in general have a low TRL level and are only well designed university research and military projects. However, there are a high number of single UAV systems in the consumer and military markets. The specified mission for firefighting falls between consumer UAV and military UAV systems. The gap in costs is extremely high due to differing capability, production volumes, and target markets.

In addition, the effect of established research and development (R&D) programs is difficult to estimate. For example, large UAV companies such as DJI or Parrot have many years of experience, established supply chains, and economies of scale in their favour. These organisations operate closer to consumer electronics companies rather than companies in the aerospace industry, such as Lockheed Martin, General Atomics, and Airbus. Due to the specific market, high carrying capacity, and advanced sensors required for firefighting, costs are estimated to be higher than for consumer UAVs, and closer to the low end for defence industry projects.

The following lists detail some reference costs used to estimate the production and total costs of the system. The list includes various cost due to variability in availability; it can, however, be broken down into total project costs for military UAV systems that may indicate upper bounds and consumer heavy lift drones that may indicate values closer to production cost.

[4]Personal communication with Jelmer Dam, the Landelijk Coördinator Natuurbrandbeheersing (19/05/2025).
[5]Personal communication with Peter Phillips, a volunteer firefighter for County Fire Authority Victoria, Australia (01/05/2025)
[6]See: https://www.easa.europa.eu/en/domains/drones-air-mobility/operating-drone/specific-category-civil-drones. Accessed: 08/05/2025.
[7]See: https://bushfirefront.org.au/historical-facts/how-do-we-do-it/. Accessed: 08/05/2025.
[8]Personal communication with Tealand Stender, UAV Pilot for the United States Forest Service (29/04/2025).
[9]See: https://www.sysgo.com/blog/article/autonomous-drones-revolutionizing-industries-with-precision-and-efficiency. Accessed: 08/05/2025.

UAV Development Contracts and Program Costs

- Newspace Research & Technologies Pvt Ltd signed a $15M contract for 100 UAVs[10];
- RQ7 shadow signed a $152M contract for 36 UAVs with ground stations and support systems[11];
- NASA Altair total project cost for development of single autonomous UAV of &18M[12].

Consumer Heavy Lift UAVs

- DJI Flycart at €19 500 base price[13];
- DJI Agras at €13 000 base price[14];
- FreeFly Systems Alta X at $28 000 base price (Used by United States Forest Service)[15].

Other Missions of Interest:

- Zipline logistics service in Rwanda at $20 per delivery[16];
- FireWatch AI Cameras in Germany €1.13M [17];
- Helicopter cost at €20 000 per hour [6].

3.5.Market Trends

UAV systems are a key technology in firefighting and national roadmaps for technology development. As of 2024, the Bushfire Research Centre of Excellence envisions UAV mission profiles reaching individual task autonomy in 3–8 years, followed by full mission autonomy in 8–15 years [8]. They focus on integration of multiple sensing modalities and all weather operations.

The UAV market has also seen high levels of growth due to hardware solutions being well developed for piloted VLOS missions. However, large market opportunities still exist in increasing autonomy levels to allow expansion of operations beyond direct control.

3.6.Market Barriers

Firefighting for wildfires is focused on extinguishing capacity. The hereby proposed UAV swarm provides a support role to reduce the frequency of fires. However, it will not be able to replace true firefighting capacity in case of fires become uncontrollable. As such, there may be organisational resistance to allocating budget to unproven technology.

Regulatory environment presents challenges due to the lack of definition for UAV integration in airspace. However, this issue can possibly have a low effect, since the operating environment of the system will not be in densely populated areas and airports, particularly in the Netherlands.

Lastly, the general UAV market has high competition, presenting risk that swarm technologies will eventually become available in consumer markets, and thus making this project's system less unique. As such, awareness and adaptability is paramount to ensuring the project maintains market viability.

3.7.Target Customer

The target customer for the system is the government of countries that experience significant damages due to wildfires. As previously stated, secondary customers for the UAV swarm and surveillance capability include government defence, facility surveillance, search and rescue, among others.

The project will begin with targeting the Dutch market. However, it will also take into account requirements for tougher terrains and vegetation in the design process so that development costs may be split amongst a larger customer base. Due to this consideration, and the existence of a single certification procedure for European Union countries, the system may then be marketed to other European countries. Eventually, after further certification, it can be marketed internationally.

[10] See: https://www.janes.com/osint-insights/defence-news/defence/indian-army-receives-swarming-uavs. Accessed: 02/05/2025.
[11] See: https://www.defenseindustrydaily.com/aai-receives-up-to-1026m-in-new-contracts-for-its-rq7-shadow-uavs-02725/. Accessed: 02/05/2025.
[12] See: https://www.nasa.gov/reference/altair-uav/. Accessed: 02/05/2025.
[13] See: https://UAVland.nl/dji-flycart-30. Accessed: 02/05/2025.
[14] See: https://UAVshop.nl/dji-agras-t50. Accessed: 02/05/2025.
[15] See: https://store.freeflysystems.com/collections/alta-x. Accessed: 02/05/2025.
[16] See: https://www.bbc.com/news/technology-40935773. Accessed: 02/05/2025.
[17] See: https://www.land.nrw/pressemitteilung/ministerin-gorissen-eroeffnet-erste-waldbrandueberwachungszentrale-fire-watch-am. Accessed: 02/05/2025.

3.7.1.Market Contingencies

There is a high value in having continual monitoring of fire front for firefighters. In the case that fire suppression does not make a cost effective strategy, there is still value in a UAV system that is able to provide a continuous picture of the situation on the ground. In addition, pivoting and providing swarm capability to other UAV systems in other industries is possible.

3.8.Market Situational Analysis

A strengths, weaknesses, opportunities and weaknesses aalysis distinguishing the position of the product in the market is performed in Table 3.2.

Table 3.2: Analysis for firefighting UAV swarm market position.

	Helpful	**Harmful**
Internal	– Direct improvement to current firefighting methods; – Development of valuable intellectual property and experience in UAV swarming; – Use in emergency services may reduce regulatory requirements.	– Scaling UAV swarm to large areas for market results in high cost; – Cannot replace firefighting capacity in case of out of control fire; – Multiple technologies developed simultaneously.
External	– There is no direct competition for firefighting UAV swarm in the market; – There is limited development of UAV swarms in secondary markets; – Research funding for UAV technology, emergency services is available;	– High level of competition in UAV market; – UAV Operation regulation is not well defined and restrictive; – Onboarding fire organisations is not guaranteed.

3.9.Stakeholder Analysis

The final section of the market analysis relates to the stakeholders considered for the present mission. It is essential to obtain a complete list of all stakeholders to be able to identify all the needs and requirements for the system. Firefighters and operators are considered the same stakeholder following the decision that the firefighters will operate the system; firefighters are the most qualified people to provide commands to the system when it comes to fire monitoring and fighting operations provided receive prior specific training.

The stakeholders are placed in the stakeholder map in Figure 3.1 to determine whether they should be monitored, kept informed, kept satisfied, or managed closely, depending on their influence on and interest in the project outcome.

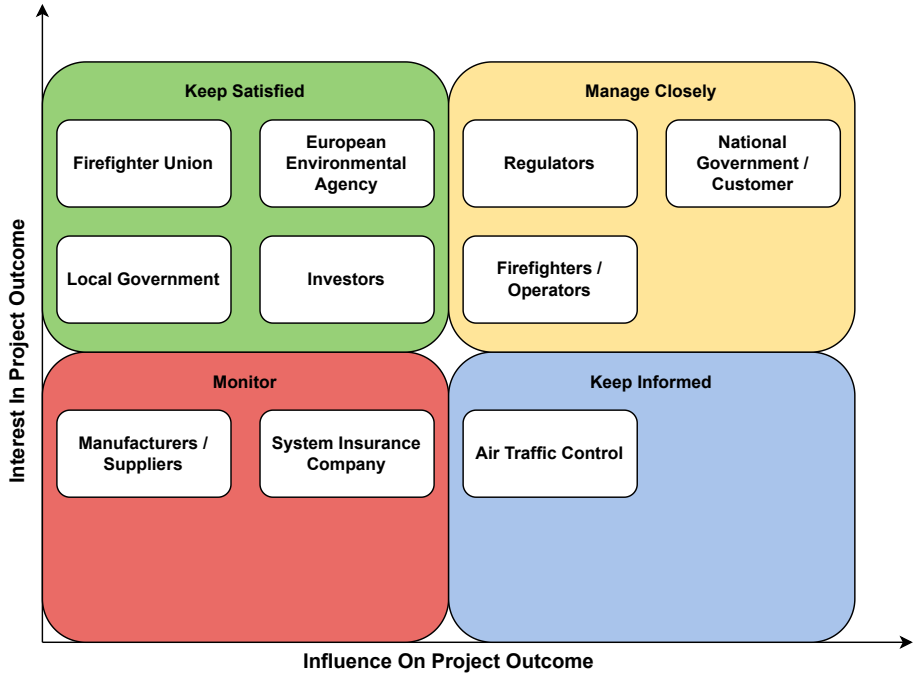

Figure 3.1: Stakeholder map describing how each stakeholder must be taken into account during the design process.

4 Sustainable Development Strategy

This chapter provides the strategy and guidelines that will be followed during the design of the UAV system. The key to increasing sustainable development of the project is to identify essential indicators and develop a strategy to tackle them. Section 4.1 concerns the indicators used to assess sustainability. The sustainability strategy in the development phase is discussed in Section 4.2. Section 4.3 mentions the sustainability strategy in the production phase. Finally, for the operational phase the sustainability strategy is laid out in Section 4.4.

4.1.Sustainability Indicators

The impact of products can be quantified by dividing their global effect into several categories. A typical division is provided by M. H. Abbasi et al. [9], who argue that sustainability can be categorised into environmental, economic, and social contributions; each category can be defined in terms of a series of sustainability indicators that further quantify complex sustainability information. Considering the organisational sustainability during the FireFlight project, the sustainability indicators defined in Table 4.1 are deemed relevant.

Table 4.1: Sustainability categories and respective indicators.

Environmental	Economic	Social
Pollutant emission	Research and development costs	Safety
Energy consumption	Production costs	Reliability
Energy efficiency	Operation costs	Security
Share of renewable energy	Maintenance costs	Availability
Share of recyclable materials	Budget	Functionality
Required space	Produced value	Social acceptance
Water consumption	Transport cost	Job creation
Ecosystem disruption		Noise production
Noise production		Aesthetic aspects

Pollutant emission describes the emission of all pollutants (CO_2, NO_x, particulate matter, etc.), but particularly focuses on carbon dioxide as the most critical driver of climate change. Ecosystem disruption is a combination of factors that have a direct impact on the environment and wildlife, such as the destruction of animal habitats. The produced value measures the financial benefits produced by the product, such as the reduction of wildfire suppression and damage costs.

These parameters require constant attention during the product's development phase; quantifying their impact and identifying whether the indicator has a positive or negative impact on the sustainability cycle is required. Furthermore, sustainability will be used as a driving performance criterion for each design consideration and trade-off table.

4.2.Development Phase

Sustainability in development is addressed by selecting sustainable materials, prioritising repairability, and minimising prototyping waste through simulation. Measures are summarised in Table 4.2.

Table 4.2: Developmental sustainability strategy.

Measure	Indicator
The product should be designed to cover the area most efficiently	Energy consumption, Pollutant emission
The product should be produced and operated using renewable energy	Share of renewable energy
The product should be a modular design, having easily replaceable components, creating less waste in case parts need to be discarded	Energy efficiency
Digital twins should be used, reducing the number of prototypes created by using high-fidelity simulations and virtual testing [10]	Pollutant emission, Energy efficiency, Required space
Project expenses should be monitored and controlled to prevent exceeding the expected budget	Budget, Production costs, Operation costs, Maintenance costs, Research and development costs, Produced value
The product should only be designed to fulfil the defined mission objective	Safety, Security, Functionality, Energy efficiency

4.3.Production Phase

In the production phase, sustainability efforts focus on minimising environmental impact through local sourcing, circular supply chains, and energy-efficient manufacturing. Measures are summarised in Table 4.3.

Table 4.3: Production sustainability strategy.

Measure	Indicator
Use local suppliers, minimising transport and promoting local businesses	Energy efficiency, Transport cost, Social acceptance, Job creation
Circular supply chain: Work with suppliers that use recycled or recyclable materials. Implement take-back agreements for used parts	Share of recyclable materials
Energy monitoring of production process	Energy consumption, Energy efficiency
Sustainable Manufacturing Processes: Use additive manufacturing to reduce waste. Recycle scraps from manufacturing processes	Share of recyclable materials
Implement quality controls to improve product lifetime (fewer replacements)	Production cost, Reliability
Co-production with other European UAV projects to share tooling costs	Share of renewable energy, Production costs, Required space

4.4.Operational Phase

Sustainability during operation emphasises smart resource usage and minimal ecological disruption, through AI-based mission planning, predictive maintenance, and renewable energy solutions. Measures are summarised in Table 4.4.

Table 4.4: Operational sustainability strategy.

Measure	Indicator
Smart Mission Planning: Use AI to optimise flight paths and minimise flying time. Enables UAVs to accomplish more with less energy	Required space, Energy efficiency, Operation costs, Water consumption
Preventive Maintenance: Use predictive analytics to identify component wear early, preventing unnecessary failures and replacements	Share of recyclable materials, Energy efficiency
Battery Management: Use battery health monitoring to extend the lifecycle. Implement battery swapping and recharging hubs that use solar panels or wind energy	Energy consumption, Energy efficiency, Safety
The product should minimise the disturbance of any natural habitats and avoid activities causing ecosystem disruption	Required space, Ecosystem disruption, Noise production
The product should not disturb or pose a threat to humans	Safety, Reliability, Security, Noise production, Aesthetic aspects
The product should be operational whenever the risk for a wildfire is high	Reliability, Availability, Functionality, Job creation

4.5.End-of-Life Phase

End-of-life strategies focus on recycling, reuse, and responsible disposal to reduce landfill waste and recover materials. These are summarised in Table 4.5.

Table 4.5: End of Life sustainability strategy.

Measure	Indicator
Material Recycling: Partner with certified e-waste recyclers for electronic components. Design using mono-materials or separable mixed materials for easier sorting	Share of recyclable materials, Safety
Battery Recycling: Use standardised battery packs that can be returned to manufacturers for safe disposal or recycling	Share of recyclable materials, Safety
Carbon Offsetting: For emissions that cannot be eliminated, invest in reforestation or verified carbon credits as an offset strategy	Pollutant emission, Budget, Social acceptance
Reuse components of partly broken systems	Share of recyclable materials, Reliability

5 Verification & Validation Plan

Verification and validation are essential to ensure that the design meets all requirements across all facets of the mission. Given the complexity of the system, and the coupling between design and mission, this phase is highly resource intensive, and an approach plan is required. Section 5.1 describes how requirements were validated, Section 5.2 discusses the verification and validation for different models, Section 5.3 explains the approach to sensitivity analyses and their value, Section 5.4 describes how it will be confirmed that the product complies with all requirements, and lastly, Section 5.5 describes the constant process of ensuring that the different aspects of the design indeed work as expected.

5.1.Requirements Validation

System requirements were based on stakeholder and market analyses, and reviewed with expert contacts for early validation. Each requirement was checked against the VALID criteria: Verifiable, Achievable, Logical, Integral, and Definitive.

5.2.Model Verification & Validation

To validate the performance of models multiple comparisons to external data need to be drawn. Table 5.1 shows a summary of the models that are predicted to be used and the methods to confirm their capability. The definition of how verification and validation are handled across the system follows. This entails requirement compliance checks, testing, and result validation where applicable. Each method is selected to match the nature of the data or implementation being verified.

Table 5.1: Verification and validation plan for planned simulation models.

Simulation Model	Verification Approach	Validation Approach
Fire Simulation Model (custom)	Unit testing for nominal and edge cases	Compare simulations to historical data, comparison to existing fire models
Finite Element Structural (3rd-party)	Analyse by hand calculation for simple cases	Reference validation from software supplier
Aerodynamic Simulation Models (3rd-party)	Compare to approximate hand calculated estimate	Reference validation from software Supplier
Operations Simulation Models (custom)	Unit testing for nominal and edge cases	Field trials with scaled prototype swarms, Comparison with Manual Operations Data, Monte Carlo Simulations
Weight Estimation Models (custom)	Hand calculation	known model, comparison to existing Missions
Fire Detection Model (custom)	Unit testing for simplified and edge cases	Physical testing (Phone Camera)
Cost models (custom)	Unit testing for simplified and edge cases	Compare predicted costs to existing missions or components

Compliance Matrix: Each subsystem has defined requirements, which must be verified. To track this, a compliance matrix is included per subsystem, assigning each requirement a status: “yes” (verified), “preliminary yes” (likely met, but untested), or “TBD” (undetermined).

Unit Testing: Unit testing is a fundamental part of software testing where individual units or components of a program are tested in isolation. This entails testing individual methods and different simple scenarios in code. The main unit tests that are done in the report include initialisation unit tests, setter and getter unit tests, computational unit tests (ensuring values are equal to expected), and edge-case tests (where unusual values that may break the program are tested).

These have been implemented for all code files used for the generation of data. All code was developed using version control from a central repository. On this repository, an automated testing pipeline was applied, and each version of the program shall be confirmed to be passing all tests before adding to main codebase.

System Testing: Unit tests check individual functions in isolation, but fail to identify issues in the interaction between different methods. For larger implementations, system tests are required. These verify interactions between methods and may include visual tests (checking if outputs look correct), performance tests (checking that methods run within a reasonable time), integration tests (checking whether components communicate correctly), and edge-case tests (checking how the system handles unusual inputs).

All methods have been completely verified using unit and system tests. A target of 90% coverage — described as ”exemplary” by Google testing[1] — has been achieved in all code.

Validation: Validation checks if the model matches reality. This can be done by comparing results to existing data, running field tests, or testing after deployment (which will happen post-DSE, since the system is not being built yet). Validation

[1] See: https://testing.googleblog.com/2020/08/code-coverage-best-practices.html. Accessed: 18/06/2025.

is only applied where it makes sense — some software is non-physical or uses standard methods that do not need it (like Class II estimations).

5.3.Sensitivity Analysis

Sensitivity analysis checks how much results change when inputs are varied. This helps confirm that results are not overly sensitive to assumptions or uncertainties, and ensures that results are robust. It is usually done by tweaking inputs and observing the effect. Like validation, it is only used where relevant.

5.4.Product Verification

Verification of the product is defined as the process of confirming that the product complies with all requirements defined in the Baseline Report. The methods planned to be used for the verification of each requirement are described.

In order to perform all verification activities, significant resources will be required. As such, in the cost budget outlined in the Baseline Report, a significant element of the total development costs were allocated to laboratory and field testing. Key resources and stakeholders beyond standard engineering items identified are as follows:

- Wind tunnel facility capable of testing UAVs at wind speeds up to $45\,\mathrm{m{\cdot}s^{-1}}$ while carrying maximum payload;
- Controlled airspace permission for testing up to 50 simultaneous UAVs;
- Fire testing facility with permissions for controlled burns and fire suppressant deployment;
- Environmental testing facility for simulating wildfire conditions including smoke, heat, and variable visibility;
- Regulatory coordination with EASA and the Dutch Transport Institute (Inspectie Leefomgeving en Transport) for certification testing;
- Firefighting agency partnership for operational validation of fire suppression techniques;
- Local conservation authority coordination for testing in natural reserves/protected areas;
- Communication interference testing equipment for validating system performance in emergency conditions;
- ISO 27001 security audit resources and certified personnel.

5.5.Product Validation

Product validation is occurring at all stages of the product design. In the initial project planning phase, a market analysis was performed along with detail stakeholder and risk analysis. These form the initial basis of the validation to understand the real world need of the system. During the design, as options are developed further, the suitability compared to the market analysis is continually evaluated. Depending on the estimated performance of the system as it is evaluated in the design process, the extent of the operation for the aircraft is compared to desired mission. In the event that there is divergence, this will be brought to the attention of the customer and a further strategy will be developed.

5.5.1.Test Campaign

The test campaign will consist of numerous field testing exercises, for which a budget of €7M has been specified due to the high number of organisations and facilities involved. The following list covers the tests to be performed, with a description of the successful outcome for each item:

- **Camera Subsystem Field Testing:** Check that the camera system detects fires when ground-mounted.;
- **Single UAV Ground Integration Test:** Verify data and communications across all subsystems on one UAV.;
- **Ground Integration Test:** Verify data and communications across all systems within the SoS;
- **Initial Single UAV Test Flight:** Demonstrate flight capability of one UAV under nominal flight profile;
- **Swarm Subset Test Flight:** Demonstrate swarming capability using three UAVs to confirm capability (without excessive risk);
- **Nominal Surveillance Testing:** Demonstrate continued operations and ability to survey desired area;
- **Simulated Stress Testing:** Demonstrate capability to mobilise all units in response to a simulated fire warning;
- **Full Fire Testing:** Demonstrate ability of system to detect and suppress controlled fire with appropriate safety contingencies.

5.5.2.Certification

In addition to validation, certification may be required depending on the operational use case. Relevant documentation for V&V must be collected throughout and early engagement with regulatory authorities is essential to ensure compliance and demonstrate it adequately.

6 Trade-off Summary

This chapter summarises the design decisions made in earlier reports. It first outlines the trade-off methodology used throughout the project (Section 6.1). Then, trade-offs already performed and previously documented are recapitulated (Section 6.2). Finally, it consolidates all trade-offs into a single, selected design concept, in Section 6.3.

6.1.General Trade-Off Methodology

Since multiple trade-offs are required for UAV swarm design, a standard method was defined and applied across all trade-offs performed by the team.

6.1.1.Determining Trade-Off Criteria, Weights, and Scoring

The first step in the trade-off is determining the relevant criteria. Only after can the design options be considered, as the criteria are used to discard some of the options in the design option tree. The criteria are determined by analysing the system requirements (see Chapter 20), and the subsystem requirements, that are found in their respective chapters, recognising the most important performance metrics for a system or subsystem. The metrics that best help differentiating between design concepts are chosen as the trade-off criteria. Once the criteria are defined, a diagram is generated to show the requirements represented by each criterion.

The weight of each trade-off criterion must then be determined. First, it is defined that the sum of all weights must be equal to one, the minimum weight attributed to a criterion must be 0.1, and all weights shall be multiples of 0.05. Thus, the maximum weight of a criterion is limited by the number of criteria.

To determine the weights, a tabular method was developed by the group. Here, all criteria are placed as both the column titles and row titles of a table. Then, for each column and row, an assessment is made on whether the criterion represented by that column is more, equally, or less important than the criterion represented by that row. This assessment is made by analysing the system requirements that each criterion represents and estimating to which extent they are crucial for the mission. Depending on the assessment, a value of two (more important), one (equally important), or zero (less important), is given to that table entry. The values on each column are then summed, providing a final importance score for each criterion. These are then used to arrive at the final weights. However, the final weights are not directly proportional to the importance scores, as this would result in weights that are not multiples of 0.05, or are lower than 0.1.

When it comes to the scoring of design options with regard to trade-off criteria, a scoring method is defined as well. A qualitative score is to be assigned to each design option for each criterion. The scores and colours they correspond to are as follows (some colours span two consecutive scores):

1. Critical Concern (Red)
2. Major Deficiency (Orange)
3. Needs Improving (Orange)
4. Acceptable (Green)
5. Good Performance (Green)
6. Excellent (Blue)

Each trade-off uses a scoring rubric to evaluate design options. Scores from 1 to 6 are assigned to each criterion, with an explanation provided for each entry. This method supports consistency and transparency in design option evaluation. The rubric reflects insights from the earlier risk analyses and the sustainability plan.

6.1.2.Design Options Considered

After criteria and their weights are found, the design options to be considered in the trade-off must be decided upon. Initially, all feasible options in the design option tree are gathered. Then, the ones that perform significantly worse than all other options, according to the trade-off criteria, are removed. The non-discarded options are then taken to the trade-off.

6.1.3.Trade-Off Summary Table

The trade-off is performed using a weighted sum approach: rubric-based scores are multiplied by criterion weights and summed to rank designs. A table is generated with criteria (weights in parentheses) as columns and design options as rows. Each cell includes a short justification and a colour and score tag (e.g. [Blue, 6]). Column widths are kept uniform for readability. As this is a preliminary assessment, only qualitative reasoning is provided per score.

6.1.4.Sensitivity Analysis

Due to uncertainty in both scores and weights at this design stage, a sensitivity analysis is performed to assess the impact of small variations. For score sensitivity, a delta is computed per score–design pair, representing the score increase needed for that option to reach first place. Deltas under two points indicate sensitivity and require justification. For weight sensitivity, a delta is computed per criterion, showing the weight change (with normalisation) needed to alter the top-ranked design. If

no change affects the outcome, the entry is marked N/A. Deltas below 0.2 indicate sensitivity and also require justification. Results are summarised in a single table, with sensitive entries highlighted in yellow.

6.2.Previously Performed Trade-Offs

This section summarises the important trade-offs performed in the earlier design stages.

6.2.1.UAV Configuration Trade-Off

The first trade-off performed was on the UAV configuration, where the following configurations were considered:

- **Rotorcraft:** Aircraft including helicopters and multi-copters using a rotating wing to generate lift;
- **HTOL (Horizontal Take-off and Landing) Fixed-Wing:** Aircraft using static lifting surface in combination with forward propulsion only;
- **VTOL Fixed-Wing:** Aircraft using static lifting surfaces in combination with both forward propulsion and VTOL capability through vertical propulsion system;
- **Airship:** Lighter-than-air aircraft.

Since some concepts favour suppression and others surveillance, two separate trade-offs were conducted with mission-specific criteria. This also served to assess whether distinct designs were needed. In both cases, the VTOL fixed-wing emerged as the top-ranked option — as seen in Table 6.1 — due to its versatility: long range, high speed, runway-independent operation, and hover capability. A single design is therefore sufficient for both mission types.

Table 6.1: Resulting scores for vertical-to-horizontal.

Option	Rotorcraft	HTOL Fixed-Wing	VTOL Fixed-Wing	Airship
Surveillance Score (weighted)	3.5	4.0	4.75	3.05
Suppression Score (weighted)	3.4	4.0	5.1	3.1

6.2.2.Base Station Trade-Off

The next trade-off is for the type of base station to transport, operate, and store UAVs. This trade-off evaluates the following options:

- **Truck:** Acts as the base station itself, containing and redeploying UAVs. It must remain at the operational site throughout the mission;
- **Container:** Functionally similar to the truck but separable from its transport vehicle, enabling one truck to service multiple containers. Assumed to offer the same UAV functionality at lower cost;
- **Water-Based:** A container deployed near a large water body, enabling UAVs to land as hydroplanes and offering direct access to water for fire suppression;
- **Aircraft:** Uses a conventional aircraft to deploy UAVs from the air. The aircraft loiters over the zone during operations until UAVs are recovered;
- **Lighter-than-Air:** A tethered balloon or blimp that hovers over the deployment zone, resupplied via the tether and relocated using propellers.

Table 6.2 shows that the container is the most suitable design option, due to its high availability, reliability, and sustainability, and low cost.

Table 6.2: Resulting scores for base station trade-off.

Option	Truck	Container	Water-Based	Airplane	Lighter-than-Air
Score (weighted)	4.5	4.9	3.95	1.95	3.65

6.2.3.Vertical-to-Horizontal Method Trade-Off

Since the UAV is a VTOL fixed-wing aircraft, a trade-off is required to assess the available transition methods between VTOL and cruise. The following options are evaluated:

- **Tilt Wing:** Concept relies on a rotational wing (around the root) to align the thrust vector vertically and transition to horizontal flight via wing rotation;
- **Tilt Rotor:** Concept is similar, instead operating by rotating the propulsive rotors only;

- **Dual Propulsion:** Concept utilises two independent systems, (typically) four vertical thrusters for VTOL, and one for horizontal flight. The systems are then toggled to transition without moving parts;
- **Tilt Body:** Lands on the tail, takes of as a helicopter and rotates in flight by using a rotor tilting mechanism or multiple thrust difference vectoring rotors.

Table 6.3 shows the final results of the trade-off, highlighting dual propulsion as the optimal design. Dual propulsion is an existing and tested technology, minimising risk, and it is cheap due to its low complexity.

Table 6.3: Resulting scores for vertical-to-horizontal transition method trade-off.

Option	Tilt Wing	Tilt Rotor	Dual Propulsion	Tilt Body
Score (weighted)	3.15	4.05	5.20	4.20

6.2.4.Propulsion Trade-Off

As dual propulsion is to be used by the UAV, a system that is able to integrate both propulsion systems must be chosen. Four systems are identified:

- **All Electric:** A fully electric aircraft allows for a single source of power (i.e., a single battery) linked to both the vertical take-off and horizontal propulsion systems;
- **Parallel Hybrid:** This combination uses an electric system for VTOL capabilities using batteries and brushless direct current (BLDC) motors, and an internal combustion engine (ICE) purely for horizontal propulsion. The two systems are completely separate;
- **Series Hybrid:** A series hybrid system runs the combustion engine through a generator to convert its mechanical energy into electricity. This is then combined with a battery to provide electrical power to both sets of rotors. This enables in-flight battery recharging using the ICE;
- **Series-Parallel Partial Hybrid:** This can be considered a consolidation of the previous two configurations. In this scenario, the ICE is directly linked to the horizontal propulsion rotors, with the addition of a power splitter connecting it to a separate generator. This is then linked to the vertical propulsion system alongside a battery. This retains the ability to recharge the battery, although this benefit is only seen for vertical capability.

Table 6.4 shows the final scores for the propulsion trade-off. Parallel hybrid scores the highest, and is thus selected. This design option is ideal due to its low complexity, cost, and mass, and its high reliability.

Table 6.4: Resulting scores for propulsion trade-off.

Option	All Electric	Parallel Hybrid	Series Hybrid	Series-Parallel Partial Hybrid
Score (weighted)	3.65	4.85	4.60	4.35

6.2.5.Aircraft Configuration Trade-Off

As the UAV is a fixed-wing aircraft, the configuration with respect to the type of wing must be chosen. The following design options are considered:

- **Conventional Wing-Plus-Tail**: The wing and fuselage are separated and the tail is placed at the rear of the fuselage, behind the wing;
- **Flying Wing**: The wing and fuselage are the same body and no tail is present;
- **Canard**: The wing and fuselage are separated and the tail is placed at the front of the fuselage, in front of the wing.

Table 6.5 shows that the conventional configuration is the preferred option. It offers inherent stability, good manoeuvrability, high payload capacity, and low design complexity. A drag analysis confirmed that its drag is only slightly higher than that of a flying wing.

Table 6.5: Resulting scores for aircraft configuration trade-off.

Option	Flying Wing	Conventional	Canard
Score (weighted)	4.55	5.20	4.60

6.2.6.Wing Positioning Trade-Off

As a conventional configuration was chosen, the vertical positioning of the wing must be decided upon, and the options included are high-wing, mid-wing, and low-wing.

The final results of the trade-off are shown in Table 6.6, and with this, a high-wing design was chosen. The main reason for this is that the wingbox is placed at the top of the fuselage, so, it does not interfere with the water and fuel tanks, and it does not block water during deployment. Moreover, it has excellent roll stability and creates a large clearance between the VTOL propellers and the ground.

Table 6.6: Resulting scores for Wing Positioning Trade-off.

Option	Low	Mid	High
Score (weighted)	3.7	3.9	4.8

6.2.7.Wing Airfoil Trade-off

Different airfoils are considered for the wing, trading off different aerodynamic, structural and operational aspects. using the elected trade-off, the wing was sized using the DATCOM method to customise it to the mission. The NACA 4412, 4415, 23015, 23012 and 2215, Seilig S1223 and Eppler E854 airfoil were considered. Since the NACA 4415 and 4412 performed similarly, they were both used for the wing, with the thicker 4415 used at the root for increased structural performance, and the thinner 4412 at the tip for aerodynamic performance.

6.3.Chosen Design

The resulting concept — the Phoenix — is born. The design chosen is a fixed-wing VTOL aircraft with a parallel hybrid propulsion system, having a conventional wing-plus-tail and high-wing configuration; the concept is shown in Figure 6.1 and will be further developed in the following chapters.

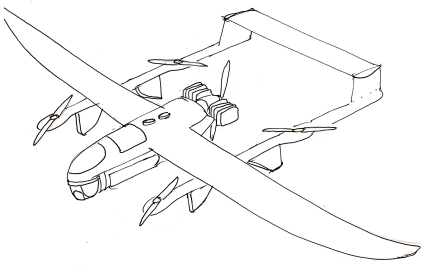

(a) Full preliminary design of the UAV.

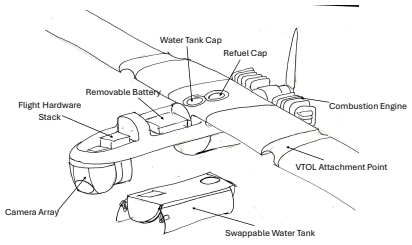

(b) Labelled breakdown of the preliminary design of the UAV, excluding the booms and empennage.

Figure 6.1: Drawings of the preliminary design of the UAV.

7 System Sizing

System sizing entails generating preliminary masses and main aircraft dimensions. It comprises estimation methods of Class I and II and statistical and data driven methods such as DATCOM. Class I and II estimations are iterated until convergence and a mass distributions as well as basic dimensions are obtained.

7.1.Approach to Sizing

To effectively size the system and determine subsystem configuration and sizing, Class II sizing, weight and drag estimations are performed. Since multiple concepts for subsystem design are used, the estimations are designed to take into account the inherent properties and efficiencies of different subsystem configurations. This allows the mass to be calculated for each configuration, aiding in early subsystem design.

The overall method for Class I and Class II estimations, along with convergence loops, is shown in Figure 7.1. Class I estimations are first iterated with aerodynamic properties until convergence. Subsystems are then sized, and their weight and drag are estimated, feeding back into the Class I loop. This process iterates until both levels are converged. The resulting subsystem configurations are then evaluated to determine the final design.

A velocity–load factor (V–N) diagram, or flight envelope, is shown in Figure 7.2. Manoeuvring loads are bounded by the stall limit in both positive and negative directions, with positive loads capped at 2.5 per Roskam [11]. Gust loads, based on Roskam's 1 cos gust model for small aircraft, are applied across a range of velocities and converted to load factor deviations. These define the gust envelope, with a resulting limit load factor of approximately 4.

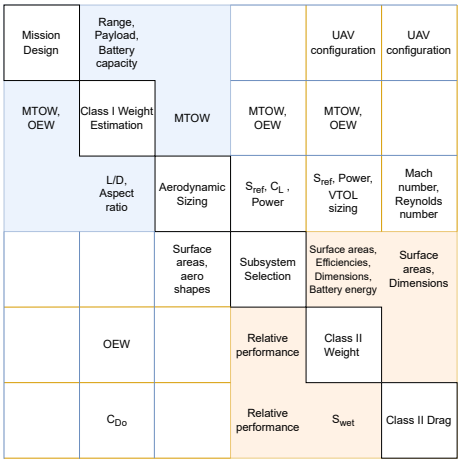

Figure 7.1: N2 chart describing feedforward and feedback in preliminary design.

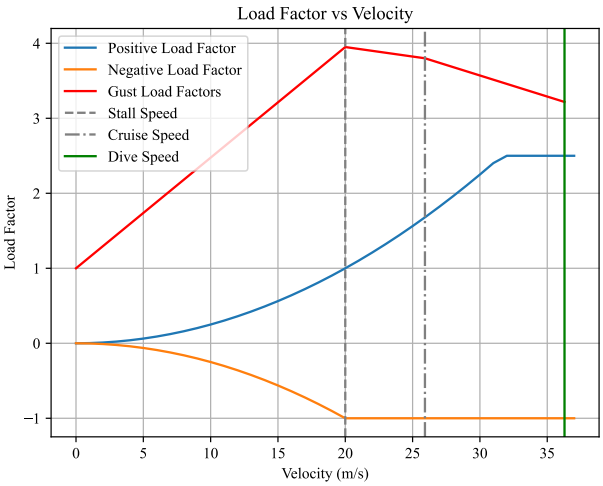

Figure 7.2: V-N loading and gust diagram.

7.1.1.Class II Fuselage Sizing

The fuselage must be carefully designed, as it adds a significant amount of mass, carries and connects most components, and greatly contributes to the overall aircraft's drag. At this stage of the design, it is common to use statistical models and preliminary estimates to obtain the relevant design parameters.

For the Class II method, the fuselage length and diameter are required. These can be obtained by following a methodology established by F. Götten et al. [12], which relates the fuselage length and the fineness ratio to the maximum take-off weight. The relation for the fuselage length is presented in Equation 7.1 and can be directly implemented into the Class II estimation.

$$L_{\text{fus}} = 0.2825 \cdot MTOW^{0.4206} \tag{7.1}$$

Moreover, following F. Götten et al.'s [12] approach, the fineness ratio can be obtained by using Equation 7.2. The fineness ratio relates the fuselage length to the maximum diameter and, in combination with the fuselage length, provides a statistical estimate for the Class II input fuselage diameter.

$$FR_{\text{fus}} = 0.7342 \cdot \ln(MTOW) + 1.6589 \tag{7.2}$$

7.1.2.VTOL Propulsion System

The VTOL propulsion system is intended to be able to overcome the gravitational force of the vehicle by generating sufficient lift. This may be done in a variety of ways; however, for small UAVs, there is essentially one way to do it: through the use of rotors[1]. This may be done through either a monocopter or a multicopter, with the UAV industry overwhelmingly opting for quadcopters. This is for two main reasons: there may be an even number of rotors, meaning that the motors may be spun in opposite directions, consequently passively cancelling torque, and that the UAV can be controlled without the use of a swashplate (using thrust differentials instead), making the UAV simple, redundant, and inexpensive (both in purchase and in use)[2]. In particular, quadcopters are the dominant configuration as they also have simple controllability (as their manoeuvring directions are directly tied to thrust differential directions), all while being the minimal number of rotors which these conditions (which is desirable for lesser inefficiencies and less elements that may be subject to failure[1].

With four rotors and motors, the main consideration for the sizing is that the combined thrust they produce exceeds the take-off weight (MTOW in particular) by a certain amount. In general, a maximal thrust-to-weight of 1.5 is recommended [13] for use in high wind conditions. With a maximal thrust value, the weight of the components can be determined. Comparing the weight of existing propulsion components (namely propellers, motors, and speed controllers) to the thrust that they produce (using independently conducted tests[3]), a statistical relation between the MTOW of the vehicle and the VTOL propulsion mass can be derived. The linear interpolation for high-thrust (order of 10^2N) yielded a relation of MTOW to VTOL mass given by Equation 7.3.

$$W_{\text{VTOL}} = 0.0839 \cdot (1.5 \cdot MTOW) + 2.733 \tag{7.3}$$

This result was obtained with a Pearson correlation coefficient of 0.86, indicating a strong linear relationship.

7.2.Class II Weight Estimation

To estimate the mass of the aircraft, the components mentioned in the sections above are added up to estimate the empty operating weight (OEW) of the UAV. The methodology used is one suggested by Jay Gundlach [14], based on several existing methodologies and emperical relationships. The wing group can be estimated using Equation 7.4:

$$W_{\text{wing}} = 0.0038 \cdot (N_Z \cdot W_{\text{TO}})^{1.06} \cdot A^{0.38} \cdot S^{0.25} \cdot (1+\lambda)^{0.21} \cdot \left(\frac{t}{c}\right)^{0.14}_{\text{root}} \tag{7.4}$$

The fuselage formula, originally from Raymer [15], is dependant on length from Equation 7.1 and diameter which is obtained with the fineness ratio FR from Equation 7.2 as well as some coefficients. The formulas to calculated are presented below.

$$W_{\text{fuselage}} = L_{\text{struct}} \frac{L_{\text{struct}}}{FF}^2 \cdot \rho_{\text{mat}} \cdot K_{\text{rho}} \cdot N_z^{0.25} \cdot K_{\text{inlet}} \tag{7.5}$$

Gundlach [14] suggests to estimate the empennage weight W_{Emp} by using a linear regression:

$$W_{\text{Emp}} = WA_{\text{Emp}} \cdot S_{\text{Emp}}, \tag{7.6}$$

$$W_{\text{nac}} = F_{\text{nac}} \cdot P_{\text{max}}^{E1}, \tag{7.7}$$

$$W_{\text{LG}} = F_{\text{LG}} \cdot W_{\text{TO}}. \tag{7.8}$$

The weight of the powertrain component W_{pwr} is the sum of the engine weight W_{Engine}, air intake weight W_{ai}, propeller weight W_{Props}, fuel system weight W_{FuelSys} and balance of propulsion system weight W_{PropSys}, as can be seen in Equation 7.9:

$$W_{\text{pwr}} = W_{\text{Engine}} + W_{\text{ai}} + W_{\text{Props}} + W_{\text{FuelSys}} + W_{\text{PropSys}} \tag{7.9}$$

$$W_{\text{Engine, rubber}} = P_{\text{max}} \cdot \frac{W}{P} \tag{7.10}$$

$$W_{\text{Engine, installed}} = F_{\text{Install}} \cdot W_{\text{Engine, rubber}} \tag{7.11}$$

$$W_{\text{ai}} = F_{\text{ai}} \cdot P_{\text{max}} \tag{7.12}$$

$$W_{\text{Prop}} = K_{\text{Prop}} \cdot N_{\text{Props}} \cdot N_{\text{Blades}}^{0.391} \cdot \left(\frac{D \cdot P_{\text{max}}}{1000 \cdot N_{\text{Props}}}\right)^{0.782} \tag{7.13}$$

$$W_{\text{FuelSys}} = F_{\text{fs}} \cdot W_{\text{Fuel}}^{E1} \tag{7.14}$$

$$W_{\text{PropSys}} = F_{\text{PropSys}} \cdot W_{\text{Engine}} \tag{7.15}$$

$$W_{\text{Paint}} = MF_{\text{Paint}} \cdot W_{TO} \tag{7.16}$$

The parameters in the equations above were chosen to fit the mission and type of aircraft. Note that Equation 7.13 and

[1] See: https://www.forbes.com/sites/quora/2013/12/23/what-makes-the-quadcopter-design-so-great-for-small-drones/. Accessed 02/06/2025.
[2] See: https://www.nasa.gov/wp-content/uploads/2020/05/aam-science-behind-quadcopters-reader-student-guide$_0$.*pdf*. Accessed 18/06/2025.
[3] See: https://database.tytorobotics.com/. Accessed 02/06/2025.

Equation 7.14 are to be used with imperial units. The range, choices and reasons for choice are given in Table 7.1. Other parameters are initialised with rough values from earlier estimations and then iterated until convergence.

Table 7.1: Parameters used in class II weight estimation.

ID	Parameter	Value range	Value used	Reason
ρ_{mat}	Fuselage material density	Per material	2810	Dense material - conservative
K_{rho}	Fuselage density coefficient	0.002-0.004	0.003	Middle value
K_{inlet}	Inlet coefficient	1-1.1	1	No inlet on fuselage
$E1$	Nacelle exponent	1	1	Recommended value
F_{nac}	Nacelle factor	0.24-0.37	0.24	Nacelle not a priority
F_{lg}	Landing gear factor	0.02-0.04	0.02	No wheels required
F_{install}	Engine installation factor	1-1.5	1.5	Mounting systems and exhausts
K_{prop}	Propeller factor	15-30	15	Composite propellers
F_{propsys}	Propulsion system factor	0.08-0.35	0.2	Average system
F_{ai}	Air induction factor	0.08-0.24	0.24	Unknown system - conservative
F_{fs}	Fuel system factor	0.05-0.1	0.05	Simple system, no reverses, jets, etc.
$E1$	Fuel sys exponent	0.6-1	1	Small tactical UAV
F_{paint}	Paint factor	0.02	0.02	Recommended value

7.3.Class II Drag Estimation

In order to improve the estimate of the zero lift drag coefficient, consideration is made to different drag inducing structures of the aircraft. The following equation is used

$$C_{D_0} = \frac{1}{S_{\text{ref}}} \sum_c C_{f_c} \cdot FF_c \cdot IF_c \cdot S_{\text{wet}_c} + \sum C_{D_{\text{misc}}} \tag{7.17}$$

In this equation, C_{D_0} is the total zero lift drag coefficient. The term S_{ref} represents the wing reference area of the aircraft. C_{f_c} is the flat plate skin friction coefficient for component c, which estimates the friction drag of that component. FF_c is the form factor, accounting for pressure drag due to viscous separation, and IF_c is the interference factor that estimates the impact of one component on the drag of others. The wetted area of each component is denoted by S_{wet_c}. Finally, $C_{D_{\text{misc}}}$ represents miscellaneous drag contributions from sources such as antennae, engine cooling drag and other surface features.

The aircraft is modelled following Raymer [15] where coefficients are given per unit wetted area and interference factor. It is modelled as 3 fuselages with sizes estimated from the other class II mass estimation representing the fuselage and 2 booms. The booms are given interference factor of engine nacelle mounted directly under the wing as this is the closest approximation available from literature. A sub-fuselage store is modelled with radius of 50mm to represent the camera module. Wings and empennage surfaces are modelled as wings in Raymer method based on surface area multiplied by 2 for total area, assuming thin surface. Finally landing gear is modelled as two surfaces mounted under the fuselage.

The assumption of turbulent flow transition at 10% of surface for the skin drag for all components as per general aviation manufacturing. Excrescence drag is taken as 10 % from Raymer as upper limit for light aircraft, as the UAV is estimated to have multiple drag inducing components such as VTOL propellers and hatches for water disposal. This includes cooling drag. The whole class II drag estimation is iterated with other parameters in the main loop.

7.4.Iteration and Results

The Class II weight and drag estimations are iterated according to Figure 7.1 until convergence is achieved. Convergence to within 1% was achieved within 10 iterations, and the results in Table 7.2 were produced and used as a base to conduct detailed subsystem design.

Note the VTOL system is taking up more than a quarter of the OEW, which is to be expected due to possibly heavy motors and electronics. The booms are also very heavy which is not too easy to explain, so it is expected that the weight will possibly drop in the detailed design phase. A summary of values obtained from the converged analysis is presented below. The values are set to evolve as more analysis is done on the aerodynamic, structural, operational, and performance characteristics of the UAV.

Table 7.2: Summary of values from Class II iteration.

ID	Value	Unit	ID	Value	Unit
MTOW	71.8	kg	W_{Fuel}	5.1	kg
W_{OE}	44.6	kg	S	1.87	m^2
b	4.32	m	Range	350	km
W_{PLD}	18	kg	V_{cr}	25.9	m/s
$V_{H\text{max}}$	30	m/s	$C_{L_{\text{cr}}}$	0.977	-
$C_{D_{\text{cr}}}$	0.04	-	L/D_{cruise}	11.7	-

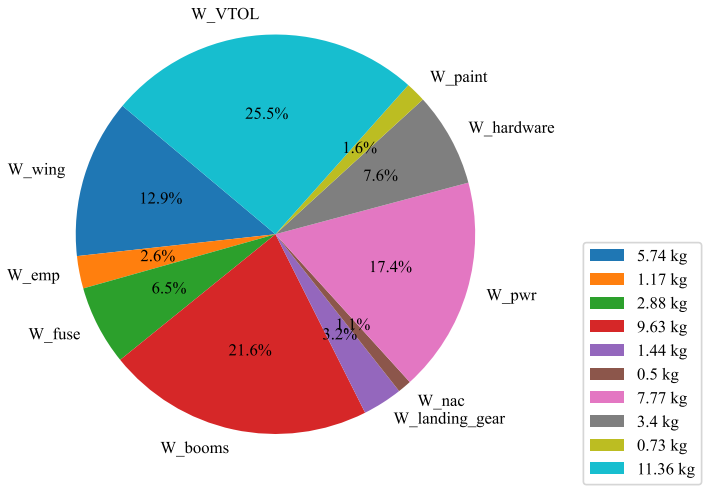

Figure 7.3: Distribution of components to Operating Empty Weight.

7.5.Sizing Sensitivity Analysis

The sensitivity of the maximum take-off weight to different parameters in the convergence loop are given below with the percentage change of MTOW shown on the y-axis. The analysis was performed on key input numerical parameters or parameters that are determined by the design group and influence the convergence loop such as the loading factor N_Z, water payload PL_{water}, specific fuel consumption c_{prop}, aspect ratio A, range or loiter time in horizontal flight mode. Note that the VTOL mode use is restricted to take-off and landing and an unsuccessful landing attempt means returning to horizontal flight to loiter. The analysis shows highest sensitivity to the load factor and the water payload, followed closely by the specific fuel consumption. This is expected and track with engineering judgement as the parameters either influence the structural, payload or fuel weight. Following these, range mission range influences the mass as well with a longer range resulting in more mass. The aspect ratio seems to be very close to optimum as it is related to the loading factor in the structural weight, but the change in MTOW is minimal in any case. All in all, the largest contribution is $\approx \pm 4\%$ for a load factor change of $\approx 12.5\%$ or a payload change of $\approx 10\%$.

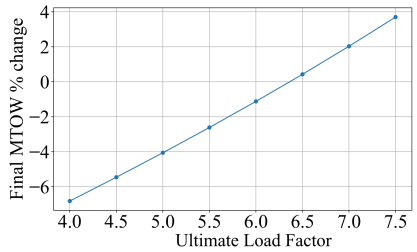

(a) Sensitivity of MTOW to ultimate load factor.

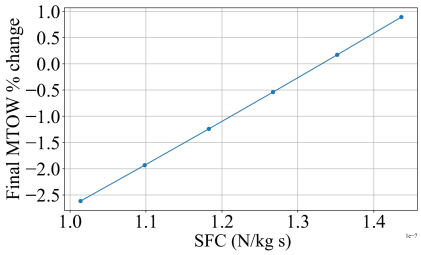

(b) Sensitivity of MTOW to SFC in kg/(Ns).

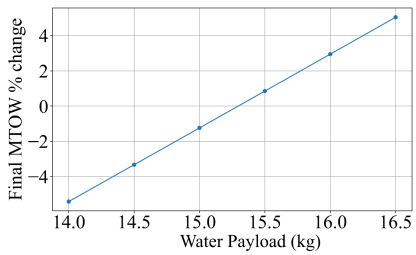

(c) Sensitivity of MTOW to water mass in kg.

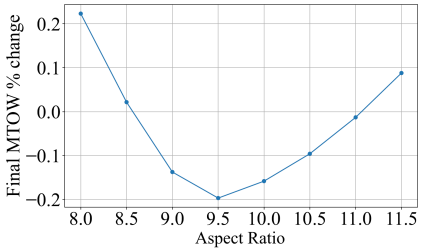

(d) Sensitivity of MTOW to ultimate aspect ratio.

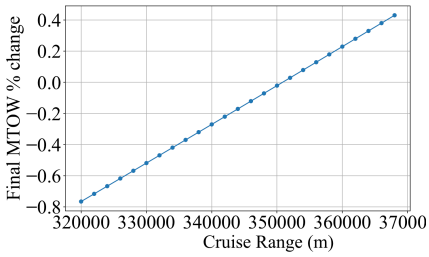

(e) Sensitivity of MTOW to cruise range in m.

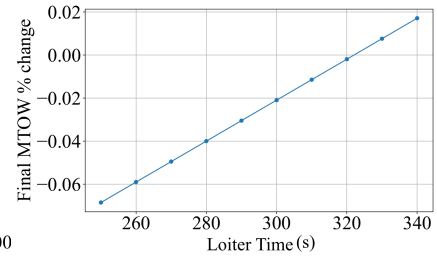

(f) Sensitivity of MTOW to horizontal flight loiter time in s.

Figure 7.4: Sensitivity analysis plots for iteration loop.

A Monte Carlo analysis with a normal distribution with $\mu = \text{value}$, $\sigma = 0.1 \cdot \text{value}$ was performed to determine the spread of MTOW values when changing the parameters used in the sensitivity analysis. the standard deviation was allocated at 10% of the mean to account for the vastly different orders of magnitude of parameters. As can be seen on Figure 7.5, the spread is generally quite narrow with the vast majority of values falling within $\pm 10\%$ of the mean MTOW.

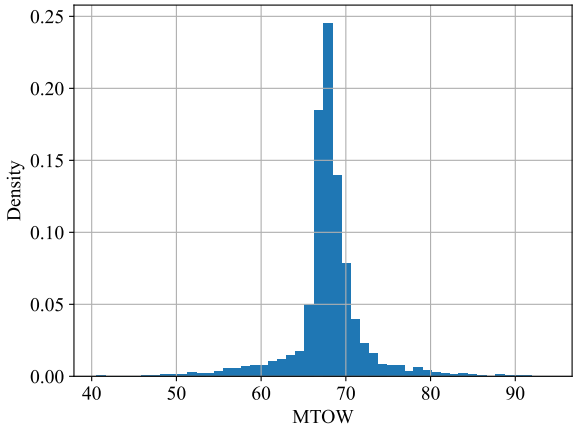

Figure 7.5: Monte Carlo Sensitivity Analysis

7.6.Sizing Verification & Validation

Seventeen individual unit tests are performed to confirm the validity of each step in the calculation, where a drag object is added and the drag computed manually and compared to the output of the estimation tool. The maximum take-off weight of comparable UAVs and missions can be plotted against the payload weight, getting a linear relationship. In Figure 7.6 it can be seen that Phoenix has very comparable capabilities, validating the obtained weights.

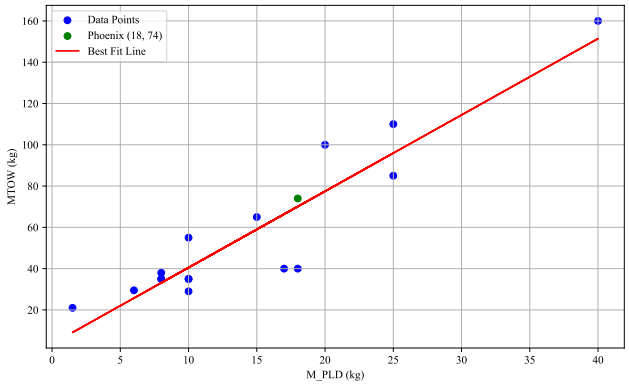

Figure 7.6: Design point compared to reference aircraft.

Class II weight estimation uses methods applicable to each specific subsystem, to ensure the accuracy and latest estimation formulas are applied. This also makes sure that newer subsystems, such as electric VTOL propulsion, are not missed in the estimation due to older research that did not take such technology into account. Furthermore, each subsystem is directly compared to other products containing similar subsystems; the advantages of this are that the final UAV will be comparatively sized to aircraft currently on the market, and aids in its fast implementation in the current landscape. Though the method is not perfect, such as the booms being too heavy, it gives an accurate estimate for the Class II preliminary design phase. Inconsistencies will be iterated in the future detailed design phase; mass changes are noted to be later analysed and combined in a technical mass budget and it is decided if iteration is needed. The sizing methods provide a good start to actually select components that are assembled into the Phoenix UAV.

8 Propulsion Design

Propulsion is an essential part of any mission that utilises long endurance to maximise its flight time and is even more important in a VTOL - fixed wing aircraft that requires two propulsion systems to operate its mission. Both systems are designed in this chapter. First, the functions and requirements of the propulsion subsystem are defined. The horizontal system is sized and components such as the engine and propeller are selected, then the VTOL system parameters are generated, as it is a more complex system, where the mass of electric parts must be minimised. Verification of the requirements is performed through a compliance matrix. Finally the impact of the systems on mass and cost is established.

8.1.Propulsion Functional Analysis and Requirements

Functions the propulsion system must execute are presented below in Figure 8.1 and requirements are derived from them in Table 8.1. The functions fit within F4, the operational section of the functional flow diagram for the project. The requirements address both the operational performance as well as RAMS and sustainability aspects.

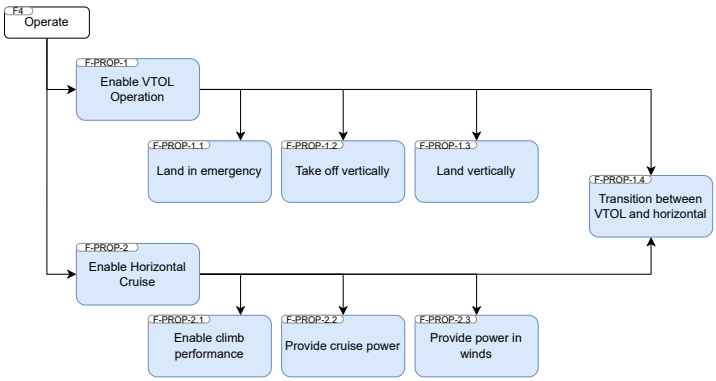

Figure 8.1: Functions for the propulsion subsystem.

Table 8.1: Requirements for the propulsion system supplementing system requirements.

ID	Requirement
REQ-UAV-PROP-01	The horizontal propulsion system shall provide at least 5 kW of power
REQ-UAV-PROP-02	The horizontal propulsion system shall weigh no more than 7 kg not including fuel
REQ-UAV-PROP-03	The VTOL propulsion system shall weigh no more than 20 kg including the battery
REQ-UAV-PROP-04	The propulsion system shall use readily available fuel
REQ-UAV-PROP-05	The propulsion system shall provide a VTOL T/W ratio of at least 1.5
REQ-UAV-PROP-06	The propulsion system shall use unleaded fuel
REQ-UAV-PROP-07	The propulsion system shall be readily maintainable
REQ-UAV-PROP-08	The propulsion system shall be able to start remotely
REQ-UAV-PROP-09	The propulsion system shall be safe for all operators
REQ-UAV-PROP-10	The propulsion system shall be used for lateral control during VTOL on the FireFlight UAV
REQ-UAV-PROP-11	The propulsion system shall produce at most 84 dB effective perceived noise when operating the FireFlight mission in cruise
REQ-UAV-PROP-12	The propulsion system shall produce at most 86 dB effective perceived noise when operating the FireFlight mission in take-off
REQ-UAV-PROP-13	The propulsion system shall produce at most 89 dB effective perceived noise when operating the FireFlight mission on approach
REQ-UAV-PROP-14	The VTOL battery shall require replacement at most once a year while operating the FireFlight mission
REQ-UAV-PROP-15	The propulsion system shall not interfere with the deployment of the payload
REQ-UAV-PROP-16	The propulsion system shall clear the ground when on the ground
REQ-UAV-PROP-17	The VTOL system can safely descend and perform an emergency landing with one propeller inoperable

8.2.Horizontal Propulsion Engine

An internal combustion engine is selected for horizontal propulsion. It is determined that the maximal power requirement is needed for climb. An engine is then sized for double the power, assuming poor propeller efficiency at max power since it is optimised for cruise.

After investigating available engines on the market it was determined that an engine with 7HP or about 5.2 kW of power

needs to be acquired. It is determined that the DLE60 engine by DLE engines [1] is a good choice as it offers reliable operation at low mass, weighing 2 kg including the electrical systems and exhaust; and fuel consumption, consuming about $1.5\,\mathrm{L{\cdot}h^{-1}}$ in flight. The engine is also selected as there is some data available, however this needs to be supplemented by testing at a later project state. Thus the choice may be re-evaluated based on test data. Since REQ-UAV-PROP-08 stipulates the system must be started remotely, an E-starter[2] is used to start the engine without human intervention and also at altitude is the engine stalls, adding to system reliability.

Additionally, a pusher configuration is chosen, mounting the engine and propeller behind the fuselage, sine an unobstructed view for the camera is required and booms are already planned for the VTOL system and can be used to support the empenage as well.

8.3.Horizontal Flight Propeller

Once an engine is selected, the propeller election follows by combining engine power with flight speed and clearance requirements to determine propeller size and pitch, as well as the the required propeller speed. If the optimal propeller speed differs significantly from the motor speed, a gearbox is introduced.

8.3.1.Initial selection

Several propellers are recommended to be paired with the engine by the engine manufacturer, and are a natural starting point. These are the 22in × 10in, 23in × 8in, 23in × 10in and 24in × 8in, where the first number is the propeller diameter and the 2nd number is the pitch, or the distance the propeller travels in one revolution, in inches.

The main constraint on propeller size is the tip speed, as it should be held under Mach 0.92 for efficiency purposes and below 0.75 for noise emission purposes. Since sustainability is a major aspect of this project, the 0.75 Mach restriction is followed. Following the methodology presented by A. Johanning [16], a larger propeller is beneficial for efficiency, however, the shaft power limitations of the engine must be considered along with the power requirements from the power-loading diagram. The propeller is therefore sized for maximum efficiency in cruise, maximum motor power utilisation and maximal climb performance.

8.3.2.Sizing for Engine Power

The different propellers are first considered when running at the maximal engine power of 7 HP or 5200 W. Efficiency is shown to be related to the disc loading by Johanning [16] in Figure 8.2.

Therefore the engine with a low disc loading is beneficial, especially at low flight speeds near the cruise speed of $25\,\mathrm{m{\cdot}s^{-1}}$, where a marginal decrease in disc loading has significant benefits. The disc loading is determined by Equation 8.1 where P is power in kilo Watts, A is the propeller area and ρ is the air density, taken as $1.225\,\mathrm{kg{\cdot}m^{-3}}$.

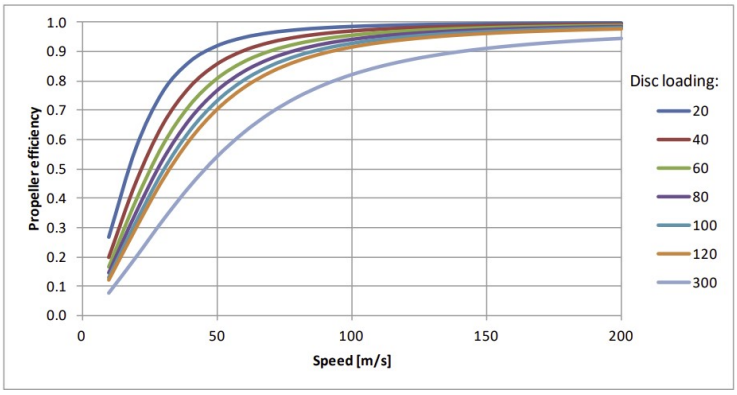

Figure 8.2: Efficiency of propellers at different speeds and disc loadings from Johanning [16].

$$\text{Loading} = \frac{P}{A\rho} \tag{8.1}$$

This yields the following results in Table 8.2 for disc loadings, essentially proving that a larger propeller will have a higher efficiency.

The largest propeller is thus selected, noting that the radius of the propeller is $\approx 30\,\mathrm{cm}$ which is still sufficient for ground clearance with proper landing gear sizing.

Table 8.2: Propeller disc loading with diameter.

Propeller	Disc Loading
24in	$14.544\,\mathrm{kW{\cdot}m{\cdot}kg^{-1}}$
23in	$15.83\,\mathrm{kW{\cdot}m{\cdot}kg^{-1}}$
22in	$17.30\,\mathrm{kW{\cdot}m{\cdot}kg^{-1}}$

8.3.3.Sizing For RPM efficiency

The propeller must also be sized to operate at an optimal RPM at cruise. Using Johanning [16] and Freeman [17] an approximation mapping for propeller efficiency is obtained. The data used is for older Clark-Y airfoil propellers which offer conservative performance compared to newer optimized composite propellers. Note that the propeller advance coefficient is displayed on the x-axis. It is essentially a measure of how the propeller speed compares to the horizontal travel speed and is defined by Equation 8.2, where the rotational velocity is

[1] See: https://www.dlengine.com/en/rcengine/dle60/. Accessed: 08/06/2025.
[2] See: https://www.bigplanes.nl/contents/en-uk/p26554_Electric-starter-for-DLE60.html. Accessed: 08/06/2025.

given in $1\,1/\mathrm{s}$. Note that this is not the actual ratio of velocities but remains the industry standard. A higher advance ratio corresponds to lower RPM, and a sharp drop of efficiency is seen in Figure 8.3 as the propeller spins too slowly. The RPM required to maintain cruise speed is therefore positioned on the left side of the maximum efficiency point ensuring that the UAV does not lose propulsion in the presence of a disturbance that slows the propeller leading to a less sensitive, more robust system.

$$J = \frac{V_{\text{hor}}}{D \cdot \text{rps}} \tag{8.2}$$

The advance speed can then be related to propeller RPM, where a larger propeller can spin slower, thus allowing the engine to run at a lower RPM, consuming less fuel. Moreover, it is determined that using a 1.5:1 reduction gearbox would match optimal efficiency of the propeller with the engine, ensuring the $24\text{in} \times 8\text{in}$ propeller can run at 5100 engine RPM at $2.2\,\mathrm{k}$ for cruise speed and allow a maximum horizontal speed of $33\,\mathrm{m{\cdot}s^{-1}}$ at 8500 RPM and $5.2\,\mathrm{kW}$.

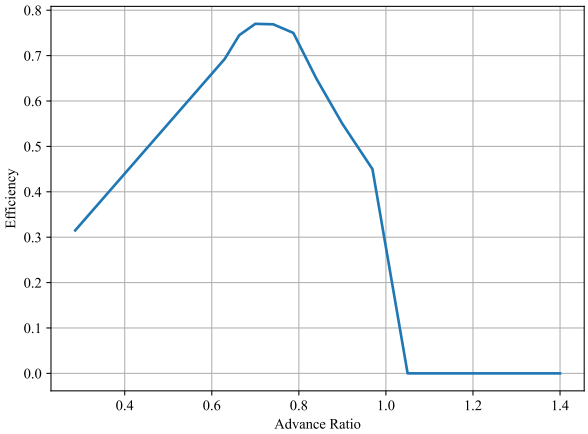

Figure 8.3: Efficiency trend with advance coefficient.

8.4.VTOL Flight System

The VTOL propulsion system consists of four motors and propellers, which provide the thrust during the VTOL and transition phase of the UAV. To size the propulsion system, the propeller type first needs to be selected. A simple relation of thrust equalling to weight is not sufficient here due to propellers providing less thrust when moving compared to the stationary thrust performance and manoeuvrability in winds. This deficit is characterised by Octonius [13] combining blade element theory and momentum theory and is determined to be $1.5mg$ for sufficient manoeuvrability where m is the UAV mass and g is the gravitational acceleration this also allows for wind resistance on level 5 or 6 on the Beaufort scale as the large drone mass helps with inertial resistance. This, however required wind tunnel tests and full scale demonstrations to verify. Furthermore, the power required for the thrust of an unducted fan can be obtained from momentum theory displayed in Equation 8.3 where r is the propeller radius, N_r is the number of rotors and ρ is the air density.

$$P = \sqrt{\frac{\left(\frac{1.5mg}{N_r}\right)^3}{\pi r^2 \rho}} \tag{8.3}$$

Using the MTOW obtained from Class II weight estimation of $69\,\mathrm{kg}$ and a propeller diameter of $0.9\,\mathrm{m}$, a max power per propeller of $4200\,\mathrm{W}$ is found, which is significantly more than the initial estimate of $850\,\mathrm{W}$, as that was a significant underestimation due to not implementing momentum theory. Nonetheless it is possible to design for this new power. Note that it is assumed that VTOL operations in their entirety may need to take place at max load due to winds, which is a very conservative assumption.

8.5.VTOL Power and Energy Budget

To determine the components that need to be used, the power and energy budgets for executing the mission must first be established. This is done by estimating losses in the system and defining the mission parameters to arrive at a full set of VTOL system sizing parameters.

8.5.1.Losses

After the propeller power was established, this must be transformed into correct power figures for sizing the motors and the batteries. This means that efficiencies must be determined where η_{mot} is the motor efficiency and η_{line} is the line loss due to high-current cables.

$$P_{\text{mot}} = P_{\text{prop}}\eta_{\text{mot}} \tag{8.4}$$

$$P_{\text{bat}} = P_{\text{prop}}\eta_{\text{line}}\eta_{\text{mot}} \tag{8.5}$$

Motor Losses Motor losses roughly break down into ohmic losses, mechanical losses and iron core losses according to de Swardt[18], all of which depend heavily on operating conditions such as load, temperature and rotational speed. Due to this, a data driven approach is taken, comparing current high-performance drone motor efficiencies, given in grams of thrust per Watt consumed $\mathrm{g{\cdot}W^{-1}}$.

Ohmic losses are the consequence of high currents running through the coils in the motor electromagnet. They are most commonly caused by heat excess and drive coil design. Drone VTOL motors are optimised to run high currents for several minutes at a time but should not be operated at the highest currents for too long as higher operational power causes more energy dissipation.

Mechanical losses are mainly due to friction and ventilation. Motors are usually assembled with low friction bearings but some friction still persists. Since the motor operates in air that may also be sued for cooling, some energy is also lost to air resistance. Like before, higher power draw usually means more speed causing higher losses.

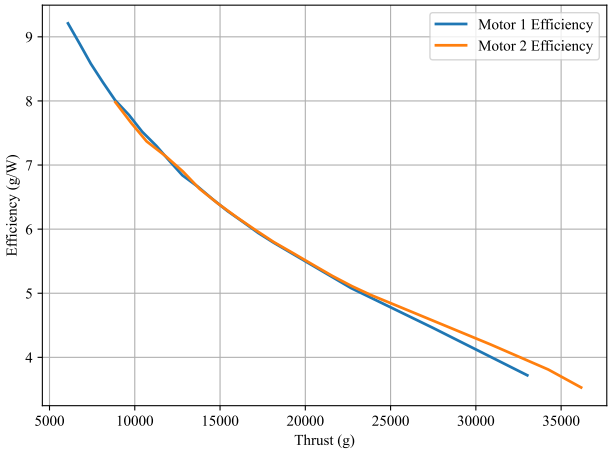

Figure 8.4: Sample efficiencies of high power UAV electro-motors for UAVs.

Iron losses are a consequence of magnetisation physics due to hysteresis of the iron core, losses in eddy currents and additional losses due to magnetic interactions with other parts of the motor. These depends on the magnetic flux which is dependant on velocity, thus being connected to power draw as well.

In all cases, it is apparent that higher loading conditions cause the motor to operate at lower efficiencies. A series of motors from T Motor[1] is investigated and plotted in Figure 8.4 at the required thrust level per motor to determine an average loading of $\approx 4.7\,\mathrm{g \cdot W^{-1}}$, leading to a final conservative motor power of $\approx 5550\,\mathrm{W}$.

Line Losses Assuming a high power copper cable with silicon insulation and a diameter equivalent to AWG10, it is determined that the resistance of the wire is $\approx 1\Omega$ per 1000 ft [2]. Converting to SI units and using the maximum current of $120\,\mathrm{A}$ and a wire length of $2\,\mathrm{m}$ from the battery through the wing and VTOL boom to the ESC and to the motor, a line power loss of $95\,\mathrm{W}$ is found with Equation 8.6. This finally determines the power draw from the battery per rotor of $\approx 5650\,\mathrm{W}$ equalling a total battery power draw of $\approx 22.6\,\mathrm{kW}$

$$P_{\text{line loss}} = R_{\text{line loss}} I^2 L_{\text{cable}} \tag{8.6}$$

8.5.2.System Sizing

After considering all the losses and efficiencies, the system can be sized to provide enough power for operation. During VTOL operation, the UAV must clear any surrounding tree tops and transition to horizontal flight. It is determined that an altitude of $30\,\mathrm{m}$ must be achieved to clear most trees in Europe according to Gelabert [19]. Assuming that a conservative ascent time would be 30 seconds, with 30 seconds assumed for landing as well as the same speed is adopted. Using a safety factor of four for any transition operations, wind conditions, battery degradation and emergency hover operations, a capacity for a total VTOL time per mission of $240\,\mathrm{s}$ at maximum power is designed for. This is used to determine the required battery capacity, which is presented in Figure 8.3 along with other important parameters for the design of the VTOL system.

8.6.Element Selection

From the requirements given in Subsection 8.5.2, elements can be selected from the elements available on the market. This is the preferred method since development of components in-house is not considered beneficial given the wide array of UAV and drone components available on the market.

Table 8.3: Required VTOL system performance.

Quantity	Value	Unit
Propeller Power	4500	W
Motor Peak Power	5500	W
Battery Power	22.6	kW
Max Wire current	108	A
Battery voltage	51.8	V
Battery Capacity	29	Ah

8.6.1.VTOL Motor

Following the parameters determination, an electric motor had to be selected to best fit the mission and required drone operations. It was determined that the VL1035 [3] motor from T Motor was selected. The selection was made as it satisfies the requirements at a relatively low weight, weighing $\approx 1.5\,\mathrm{kg}$ and providing a peak power of $\approx 8000\,\mathrm{W}$ and is in the only motor line of such capacity identified to have available test data with efficiencies and power values, which makes further analysis possible and enables system optimisation. Additionally, it is capable of performing the mission as it can produce thrust values with power values outlined in Figure 8.3, it has an air cooling system to prevent overheating and has IPX5 water resistance, meaning it can sustain water exposure such as rain or mist.

An electronic speed controller compatible with the motor is also selected, following manufacturer recommendations to ensure it can operate at its rated current during the operation. The T Motor V200A [4] controller is selected as it can

[1] See: https://store.tmotor.com/categorys/vl-series-propulsion-system. Accessed: 08/06/2025.
[2] See: https://www.engineeringtoolbox.com/copper-wire-d_1429.html. Accessed: 08/06/2025.
[3] See: https://store.tmotor.com/product/vl1035-large-drone-motors-for-heavy-lift-uavs.html. Accessed: 08/06/2025.
[4] See: https://uav-en.tmotor.com/2024/V-Series _ 1101/1245.html. Accessed: 08/06/2025.

provide 200 A peak current and 120 A continuous current. It also features options for propeller locking, which ensures the propellers stop in their lowest drag orientation during cruise. It weighs 500 grams and has cooling channels to ensure seamless VTOL operation.

8.6.2.Cables

To be able to carry the high currents required by the motors, sufficient cabling must be adopted. High current copper silicone insulation cables of American Wire Gauge 10 (AWG10) are selected as they can withstand currents of up to $120\,\mathrm{A}$. To allocate sufficient length budget for connecting each propeller in the VTOL arm to the battery in the fuselage, a length of $2.5\,\mathrm{m}$ per cable is used with 8 cables in total (two cables per motor). Using the weight of $100\,\mathrm{g{\cdot}m^{-1}}$, a cable weight of $2\,\mathrm{kg}$ is determined for the high power systems.

8.6.3.Battery

To supply the appropriate voltage a 14S LiPo battery must be used as assumed before. Furthermore, rounding to the nearest commonly accessible battery capacity a 30 Ah capacity is used, along with at least a 20C discharge rate to satisfy the 22.6 kW requirement. The nearest available battery is the Herewin 14S 60.9V 30000mAh 25C Agriculture Drone Battery with a C-rating of 25C, which exceeds the requirement. It weighs approximately $10.8\,\mathrm{kg}$ and is commonly used for heavy agriculture drones. It also allows smart charging and discharging by balancing cells to ensure longevity. Smart charging also allows it to fully charge in $\approx 1\,\mathrm{h}$, meaning that each UAV can operate with 2 batteries, one always charging on the ground during operation.

8.6.4.Propeller

A propeller fitting with the motor is selected based on manufacturer recommendations and thrust and efficiency figures given in the motor test data. The propeller used measures 32in diameter and 11in pitch (32x11)[1], which provides good thrust at high efficiency RPM values for the motor, allowing optimised operation. The propeller is made of carbon fibre, meaning it only weighs $\approx 150\,\mathrm{g}$ while remaining structurally strong enough to carry the designated weight of $\frac{1.5}{4}MTOW$. It can also provide momentary power bursts resulting of thrusts of up to 1.6 MTOW.

8.6.5.Relay Switches

Since the motors have an idle current of 4.2 and voltage of $15\,\mathrm{V}$, they consume power when not in use. This is a critical problem for the mission since the cruise phase is orders of magnitude longer than the VTOL phase. Essentially, the battery size would need to double if the motor were to draw idle power for the entirety of the cruise phase. It is therefore necessary to physically isolate the ESC and motor to prevent unwanted power consumption while in cruise. This is done by a relay switch that can reliably and quickly cur the power to the motors via an electric signal from the onboard computer.

Existing relays for cars can be used since they are expected to cut power only when the engine is in its idle state and therefore doesn't draw excessive power. They must nonetheless sustain maximum current on operation but this is much less containing than the 'switching current' at which the switch must actively operate. Due to this alleviating circumstance the relays can be sized smaller and only weight $\approx 100\,\mathrm{g}$ each, with four necessary, one for each rotor. A manual master cut-off switch in combination to a grounding port and anti-spar leads for battery removal must also be included to cut power during maintenance.

8.6.6.Note on Operations, Mass and Cost

Certain assumptions were made when first sizing the propeller. It was assumed that the propeller would be $0.9\,\mathrm{m}$ in diameter, however, the final selected propeller diameter measures only $0.81\,\mathrm{m}$. While this will increase the power draw assumed, data obtained from the manufacturer on the combined operation of the motor and the propeller show that operational thrust is achievable within the motor's power budget, verifying that sizing is appropriate.

Table 8.4: Selected components and their properties.

Component	Selected	Mass	Cost
ICE Engine	DLE60	$\approx 2\,\mathrm{kg}$	€ 200
Horizontal Propeller	Any 24×8 in	$100\,\mathrm{g}$ each	≈ € 70 each
VTOL Battery	Herewin 14S 60.9V 30Ah 25C or eq.	$10\,\mathrm{kg}$	≈ € 440 each
VTOL Propeller	T-Motor 32×11 in	$100\,\mathrm{g}$ each	€ 70 each
VTOL Motor	T-Motor VL1035	$1.2\,\mathrm{kg}$ each	€ 175 each
VTOL ESC	T-Motor 200A	$\approx 0.5\,\mathrm{kg}each$	€ 436 each
VTOL Cable	Any AWG10	$\approx 2\,\mathrm{kg}$ total	≈ € 18 total
VTOL Relay	Any car relay	$\approx 80\,\mathrm{g}$ each	≈ € 18 each

An overview of selected components along with their masses and cost is visible in Table 8.4.

The system as a whole is considered maintainable and safe since the components are relatively simple and commonly used. Nonetheless since the propellers are large they necessitate an exclusion zone when operating. This is not a detriment to the mission since the system is expected to operate autonomously. Electrical safety around the high power system

[1] See: https://store.tmotor.com/product/g32x11prop-2pcs-1pair-glossy-carbon-fiber.html. Accessed: 08/06/2025.

is critical so a grounding port and a manual battery isolation switch must be used for maintenance and proper protocol must be followed. Non-authorised personnel should not operate the system. Furthermore the system is able to perform controlled descent if one of the motors/propellers fails and is inoperable by dropping the water payload immediately, thus reducing the mass. The remaining operational propellers can provide a thrust-to-weight ratio of ≈ 1.4 in that scenario ensuring some controllability and limiting system damage. note that there will be a torque mismatch since an odd number of propellers is operating, so a margin of the thrust excess must be used to manage rotation and perform an emergency landing, sacrificing smoothness for damage limitation.

Finally, the reliability and degradation of the VTOL battery must be considered. Using a depth discharge of 75 to 80%, which is expected on average assuming most UAV missions will not need additional drain due to emergency operations or high wind, a cycle count of ≈ 500 cycles is found until the battery has a capacity 80% of its original, which is deemed the cut-off for power supply and safety margin used in sizing. The lifetime of the battery is detailed along with other components in the RAMS analysis.

8.7.Propulsion Verification & Validation

The requirements outlined in Table 8.1 are subject to verification. Since some requirements are sized for but ultimately require testing to fully confirm system capability, they are marked with 'Preliminary yes' meaning that the requirement has been considered in the design and should be met pending test. Some requirements also require other subsystems to be fully verified and are therefore marked 'TBD' .The full list of requirements and their status is found in Table 8.5

The requirements that can be verified by analysis require verification tests while most aspects of this chapter require validation with the actual components and hardware in the loop tests. Note that the mass requirements is on the edge of being met with any uncertainty tipping it over the line. This must be clearly monitored to reduce weight increases in the future. The lower mass of the horizontal propulsion system allows for some leniency, however. No code was required in this section beyond simple graphing of data that can be verified by inspection of the graph and data. Beyond that, most V&V activities are performed in the prototyping and integration phase after the completion of the design synthesis exercise.

Table 8.5: Compliance matrix for propulsion subsystem.

ID	Verification Method	Status	Value
REQ-UAV-PROP-01	Test	Preliminary yes	5200 W
REQ-UAV-PROP-02	Inspection	Preliminary yes	3.7 kg
REQ-UAV-PROP-03	Inspection	Preliminary yes	20.0 kg
REQ-UAV-PROP-04	Analysis	Yes	30:1 2-stroke
REQ-UAV-PROP-05	Demonstration	Preliminary yes	1.6
REQ-UAV-PROP-06	Analysis	Yes	2-stroke
REQ-UAV-PROP-07	Demonstration	Preliminary yes	N.A.
REQ-UAV-PROP-08	Test	Preliminary yes	N.A.
REQ-UAV-PROP-09	Analysis	Preliminary yes	N.A.
REQ-UAV-PROP-10	Demonstration	TBD	N.A.
REQ-UAV-PROP-11	Demonstration	TBD	N.A.
REQ-UAV-PROP-12	Demonstration	TBD	N.A.
REQ-UAV-PROP-13	Demonstration	TBD	N.A.
REQ-UAV-PROP-14	Demonstration	TBD	500 cycles
REQ-UAV-PROP-15	Demonstration	TBD	N.A.
REQ-UAV-PROP-16	Demonstration	Yes	N.A.
REQ-UAV-PROP-17	Demonstration	Preliminary yes	1 eng. INOP

8.8.Propulsion Recommendations

When sizing the horizontal propeller, there was a lack of data and most calculations were based on conservative assumptions for engine power and propeller efficiency since no data is provided for the actual propellers and engines in this size range as most are targeted for hobby aircraft. The available power from the engine at different RPM must be obtained from a test in the prototype phase to determine the engine can actually provide the power at the RPM speed required for cruise. Any mismatch between propeller and engine speed should be accounted for by differing the gear ratio based on the data obtained. The engine selection may also be reconsidered at the prototype stage subject to market availability at that time and the data obtained.

Moreover, the VTOL system must be tested, ensuring safety when handling high voltage and fast rotating propellers. Additionally, a test similar to the horizontal propulsion test should be performed, so the thrust-power loadings for the motor-propeller combination can be obtained. Finally, battery drainage tests should be done to determine the actual capacity since battery listings can be unreliable. Nonetheless the sizing and selection is sufficient for the performance for the mission and any modifications can be outlined during prototype development.

9 Structural Design

To perform the structural design of the airframe, first the functions and requirements are described in Section 9.1. The operating temperature is estimated in Section 9.2. Section 9.3 discusses the loading cases of the aircraft. The tubular sizing tool for designing beams is described in Section 9.4. Moreover, the wing sizing is performed in Section 9.5. For the production of the airframe, a manufacturing, assembly and integration plan is given in Section 9.6. The sustainability is described in Section 9.7. For validation and verification, the methodology is described in Section 9.8. Finally, the recommendations are given in Section 9.9.

9.1.Functional Analysis and Requirements

The functional analysis can be found in Figure 9.1. The following requirements are described in Table 9.1.

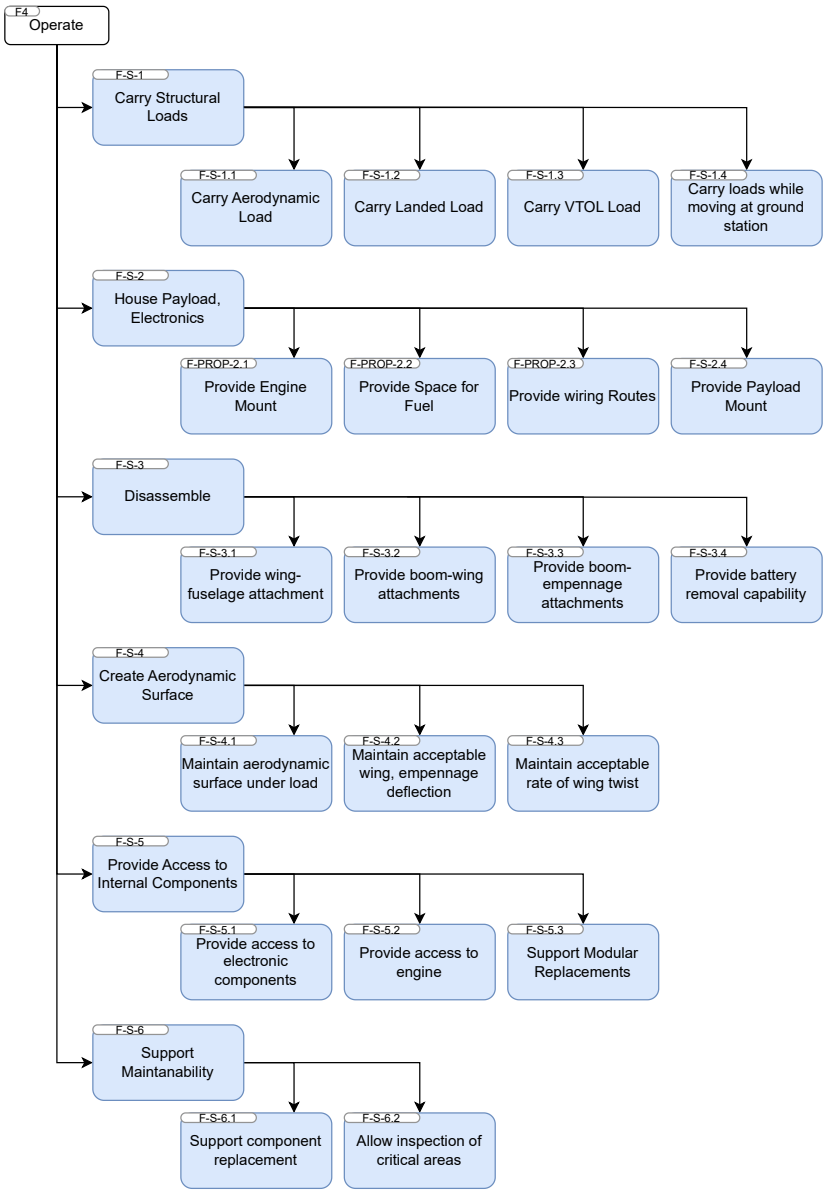

Figure 9.1: Functional breakdown structure for airframe.

Table 9.1: Requirements for the airframe system supplementing system requirements.

ID	Requirement
REQ-UAV-STRUCT-01	The airframe shall carry all determined loading cases without structural failure
REQ-UAV-STRUCT-02	The airframe shall provide sufficient volume for storage and mounting of all subsystems
REQ-UAV-STRUCT-03	The airframe shall support a detachable water payload
REQ-UAV-STRUCT-04	The airframe shall provide internal routing for subsystem wiring
REQ-UAV-STRUCT-05	The airframe shall be detachable into wings, booms, empennage, and fuselage
REQ-UAV-STRUCT-06	The airframe shall withstand operating temperatures up to $102\,^{\circ}\mathrm{C}$
REQ-UAV-STRUCT-07	The airframe shall be constructed from at least TBD% recyclable materials by mass
REQ-UAV-STRUCT-08	The airframe shall maintain the aerodynamic shape of all lifting surfaces under load
REQ-UAV-STRUCT-09	The wingtip deflection angle shall not exceed 10° during cruise flight
REQ-UAV-STRUCT-10	The total mass of the airframe shall not exceed $22.24\,\mathrm{kg}$
REQ-UAV-STRUCT-11	The total cost of the airframe shall not exceed €15 000
REQ-UAV-STRUCT-12	The airframe shall withstand a gust load factor of 6 without structural failure
REQ-UAV-STRUCT-13	The wing shall have a maximum wingtip twist of TBD
REQ-UAV-STRUCT-14	The airframe shall allow access to internal electronics
REQ-UAV-STRUCT-15	The airframe shall allow removable battery

9.2.Operating Temperature Estimation

The net radiative heat flux from the fire to the UAV surface is given by the Stefan-Boltzmann law:

$$\dot{q}_{\text{rad}} = \epsilon \sigma A (T_f^4 - T_s^4) \tag{9.1}$$

where:

- ϵ: emissivity of UAV surface material [-]
- σ: Stefan-Boltzmann constant = 5.67×10^{-8} [W/m^{2}K^4]
- A: exposed surface area [m^2]
- T_f: fire temperature [K]
- T_s: surface temperature [K]

For transient heating over short duration Δt, the temperature rise is:

$$\Delta T = \frac{\dot{q}}{m c_p} \tag{9.2}$$

- m: mass of heated component [kg]
- c_p: specific heat capacity [J/kg·K]

For a flyby scenario with constant exposure time, assuming $T_s \ll T_f$, the equation simplifies to:

$$\Delta T = \frac{\epsilon \sigma A T_f^4 \Delta t}{m c_p} \cdot \frac{1}{d^2} \tag{9.3}$$

- Surface area: $A = 11.43$ m²
- Absorptivity: $\epsilon = 0.85$
- Specific heat: $c_p = 800$ J/kg·K
- Flyby duration: $\Delta t = 5$ s
- Fire temperature: $T_f = 1473$ K [1]
- Flyby distance: d = 1.5 m

Worst case situation is considered, with structure composed of CFRP with glass temperature 120°C, absorptivity of 0.85 and specific heat of 800 J/kgK, with solid rectangular area of wingspan (4.2 m) by boom length (2.7 m) 11.43 m. The view factor for geometric radiation exchange decreases approximately as $1/d^2$ for point source approximation, where d is the distance from fire to UAV. This relationship allows scaling of the basic calculation for different flyby distances.

With these values for a flyby of 5 seconds at 2 m a ΔT of 62°C is estimated. Assuming a maximum ambient temperature of 40°C[2] this results in a maximum operating temperature of $102°C$ which is within acceptable limit.

[1] https://www.usgs.gov/media/images/how-hot-are-wildfires Accessed 16/06/2025

[2] https://www.knmi.nl/over-het-knmi/nieuws/temperatuur-door-historische-grens-van-40-c Accessed 16/06/2025

9.3.Aircraft Loading

The basic aircraft loads considered come from propulsion system, weight and aerodynamic loading. A simplified model is used comprising of the distributed lift load, the weights for various components. From the loads on the structure internal normal, shear and bending stresses are calculated. Each load bearing structure is considered as a beam for which internal layout is calculated. In python a numerical integration scheme is used to combine the effect of various forces on each structural beam.

Three fundamental limiting loading cases are considered on every structure of the aircraft: maximum gust load, vertical take-off and stacked landed on-ground configuration. The exact aerodynamic loads from manoeuvring is not simple to discern as it depends on manoeuvrability requirements and aircraft moment of inertia in each axis which are not clearly defined at this point of design due to time constraint. However the current approximation of a gust loading factor of 4 with a safety factor 1.5 provides a high level oof loading that is designed for.

Loading diagrams are generated from the loads applied to the aircraft and the shear and bending moment diagrams plotted. Internal normal stresses are not plotted due to their simple distribution in the landing gear and fuselage cases. The bending moment is related to the shear force through integration:

9.4.Tubular Sizing Tool

All structural elements are initially modelled and sized as hollow tubes. This is done as hollow tubes are easily manufacturable, provide good moment of inertia for their weight, and hollow structure will allow routing of electronics if necessary. After initial sizing they can be modified to improve weight estimate. Loading distributions are added for shear and moments. The shear is found by directly computing the

The bending moment is related to the shear force through integration:

$$M(x) = \int V(x)\,dx \tag{9.4}$$

The deflection is obtained through double integration of curvature:

$$\frac{d\theta}{dx} = \kappa = \frac{M(x)}{EI} \tag{9.5}$$

$$\frac{d^2y}{dx^2} = \frac{M(x)}{EI} \tag{9.6}$$

where θ is the slope and y is the deflection.

Numerical Integration Scheme

The numerical integration is performed using forward Euler method with uniform spacing $\Delta x = \frac{L}{n}$, where n is the number of discrete points along the beam length L. For the first integration (curvature to slope) and second integration (slope to deflection):

$$\theta_{i+1} = \theta_i + \kappa_i \cdot \Delta x = \theta_i + \frac{M_i}{EI} \cdot \Delta x \tag{9.7}$$

$$y_{i+1} = y_i + \theta_i \cdot \Delta x \tag{9.8}$$

The cumulative sum gives:

$$\theta_i = \sum_{j=0}^{i-1} \kappa_j \cdot \Delta x \tag{9.9}$$

$$y_i = \sum_{j=0}^{i-1} \theta_j \cdot \Delta \tag{9.10}$$

9.4.1.Tail Boom Sizing

Booms are modelled from side view with max gust loads shown in Figure 9.2a, VTOL loading shown in Figure 9.2c and pullup manoeuver shown in Figure 9.2b. The length of 2700 mm is taken from a minium clearance of VTOL propellers with margin. Max load factor of 6 is used, with VTOL acceleration of 1.5g assumed. The pullup manoeuver is considered with a load factor of 3.5 with an additional downforce at the tail of 60 N per side to simulate an aggressive pull up. In the loading diagram there is a large discontinuity in the bending and shear stresses at the wing. Geometry may be further optimized based on this distribution, however as the mass is within budget this is not yet considered.

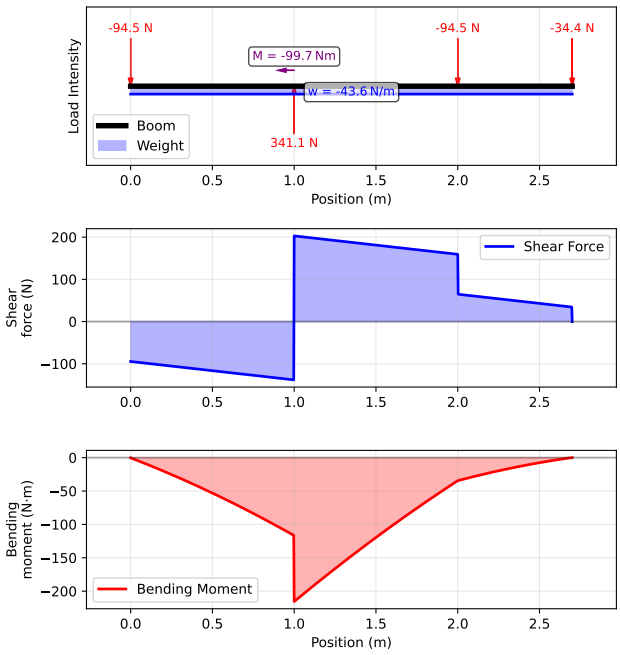

(a) Gust Condition Loading

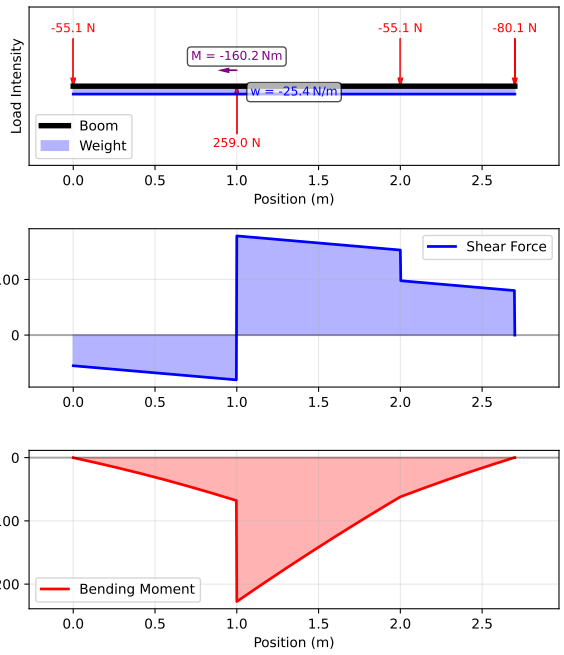

(b) Pullup Manoeuvre Loading

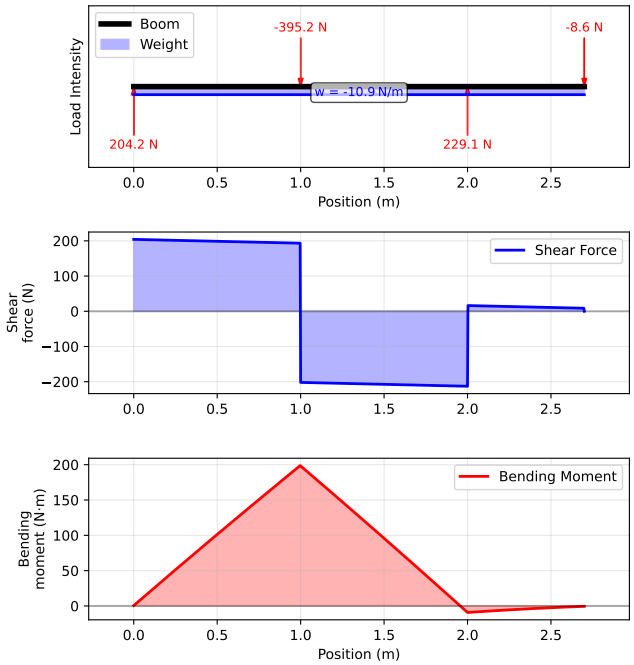

(c) VTOL manoeuvre loading

Figure 9.2: Shear and moment diagrams of side view boom under various load conditions.

9.4.2.Fuselage Sizing

Fuselage is initially sized with a concept in mind of a single beam from which components are attached underneath. This is to get a confirmation for sizing for which either a monocoque or truss structure can be further designed for, which is required for design completion. The camera and engine is modelled as point force at its location with the bending analysed. It is assumed water, battery and fuel mass will be attached as a uniform distributed load on the airframe shown in Figure 9.3a. The additional compressive force due to thrust is negligible compared to bending stress at max load factor.

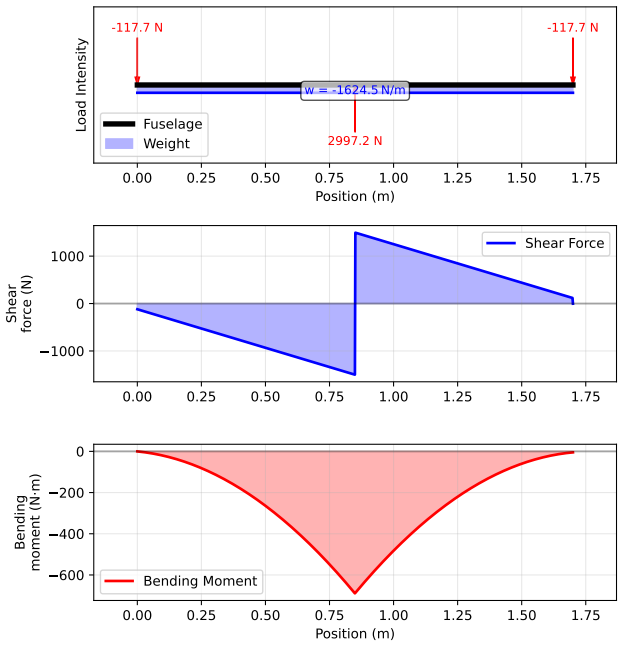

(a) Simplified side view fuselage during gust loading, shear, and moment diagram.

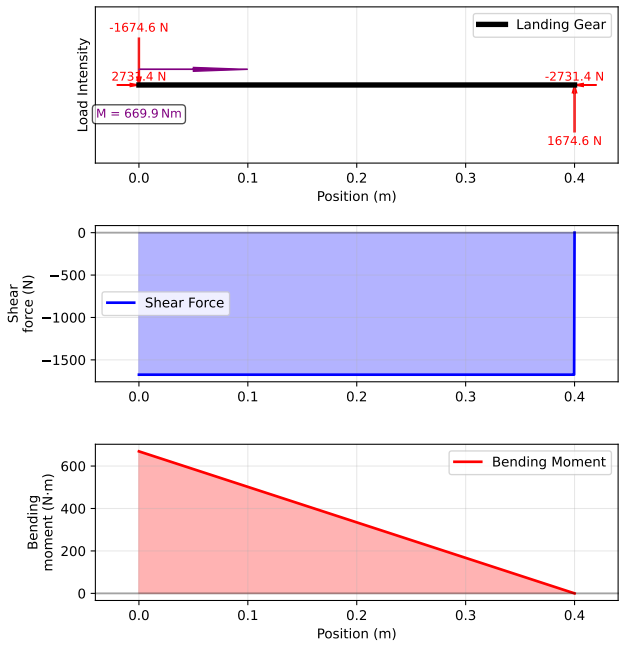

(b) Landing gear in stacked configuration loading, shear, and moment diagram.

Figure 9.3: Loading, shear, and moment diagram of fuselage and landing gear

9.4.3.Landing Gear Sizing

The load on the landing gear is modelled from a tube stacked at an angle of 32 degrees with vertical reaction force at the ground equivalent to 5 UAVs given the stacked load case. In addition it is assumed worst case loading of all weight on a single landing gear in case of angled placement allowing only a single front gear to take loads resulting in a compressive force of approximately 3000N shown in Figure 9.3b.

9.4.4.Tubular Wingbox Sizing

The loads on the wing are primarily lift shown in Figure 9.4a with secondary drag component shown in Figure 9.4b, both of which are computed from the distributions provided by XFLR5. The weight of the fuselage and the booms including VTOL motors are modelled as point masses. The weight of the wing is modelled as a distributed load based on approximation from class II weight estimation. The structure limited by volume is the wing as it must maintain aerodynamic shape. It was determined a tubular wingbox was not sufficient as the minimum viable size exceeded the maximum airfoil thickness which was 35mm.

9.4.5.Sizing Results

Table 9.2 shows the results of the sizing.

Table 9.2: Structural properties of selected UAV components (per unit).

Structural Element	Length (mm)	Diameter (mm)	Thickness (mm)	Mass (kg)	Sized by
Boom	2700	60	2	2.71	Deflection
Landing Gear	400	56	2	0.386	Deflection
Fuselage Stiffener	1700	56	1	0.824	Deflection
Tubular Wingbox	4200	55	2	3.92	Bending Stress

9.4.6.Assumptions

For calculation of shear stresses thin wall assumption is made for the sizing of the tubes whereby the shear is evenly distributed in the cross section. It is assumed that for cutouts for electronics, joints will be locally reinforced and are not designed for at this stage. In addition joins in the structure will also be assumed to be locally reinforced. In addition beams are assumed to have point forces and moments applied while in reality, all forces will be distributed over small area. Across design Euler-Bernoulli beam theory is used which requires small deflections and linear elastic theory to be true, as these are ranges that are designed for these assumptions are not limiting.

9.4.7.Vibrational Analysis

At current design point only boom are modelled for natural frequency as they are determined a critical case due to their length and interaction with the horizontal stabilizer. They are modelled as a boom with the boom mass, a characteristic length from the wing to the tip and with a point mass modelling the empennage attached to the end. It is assumed each boom will have frequency with half the mass of the empennage and no interaction between them. The wing is modelled with the tubular wing box and a characteristic length of 1 half span with 0 mass added to the tip.

For a cantilever beam with a point mass at the tip, the natural frequency is:

$$f = \frac{1}{2\pi}\sqrt{\frac{k_{\text{eff}}}{m_{\text{eff}}}} \tag{9.11}$$

Effective Stiffness

The effective stiffness of a cantilever beam is:

$$k_{\text{eff}} = \frac{3EI}{L^3} \tag{9.12}$$

Effective Mass

The effective mass includes both the point mass and a portion of the distributed beam mass:

$$m_{\text{eff}} = m_{\text{point}} + \alpha \cdot m_{\text{beam}} \tag{9.13}$$

where m_{point} is the point mass at tip, m_{beam} is the total mass of the beam, and $\alpha = \frac{33}{140} \approx 0.236$ is the mass participation factor for the first mode of a cantilever.

$$f = \frac{1}{2\pi}\sqrt{\frac{3EI}{L^3\left(m_{\text{point}} + \frac{33}{140}m_{\text{beam}}\right)}} \tag{9.14}$$

The factor $\frac{33}{140} \approx 0.236$ represents the effective mass participation of the distributed beam mass in the first bending mode of a cantilever. This factor accounts for the fact that different parts of the beam move with different amplitudes during vibration.

On analysis of the boom a natural frequency of **11.1Hz** is found. The short period has frequency of 1Hz. As such the natural frequency of 10Hz of the booms is considered acceptable. This will provide a maxiumum control input frequency of 8Hz in the pitch.

On analysis of the wing a natural frequency of 5.23Hz is found. This is very approximate and should not be considered a final value as it is for wing box that will not be used. However, the risk that this frequency will interact is significant and must be closely monitored.

9.4.8.Thermal Analysis

A basic calculation of thermal expansion under the design temperature difference of 62 degrees, with a thermal expansion coefficient of $23 \cdot 10^{-6} C^{-1}$ a temperature induced expansion of approximately 4mm is found. This is approximately 0.1% of the boom length and is as such considered negligible at this point in the design. It must be monitored during the design of joints in the structure.

9.5.Wing Sizing

In order to design the internal wing structures, first the loading cases are analyzed. Cruise flight, landing, take-off and landing using VTOL propellers and gust loading form the main loading cases. After plotting the internal shear and moment diagrams, it is evident that horizontal flight with a gust (i.e. with a load factor of 6) forms the limiting load case, as the internal forces and moments are the highest. The gust load case can be seen in Figure 9.4a and Figure 9.4b for the lift and drag respectively.

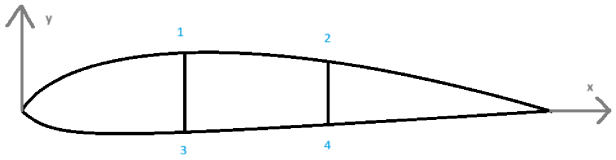

Figure 9.5: Wingbox cross-section

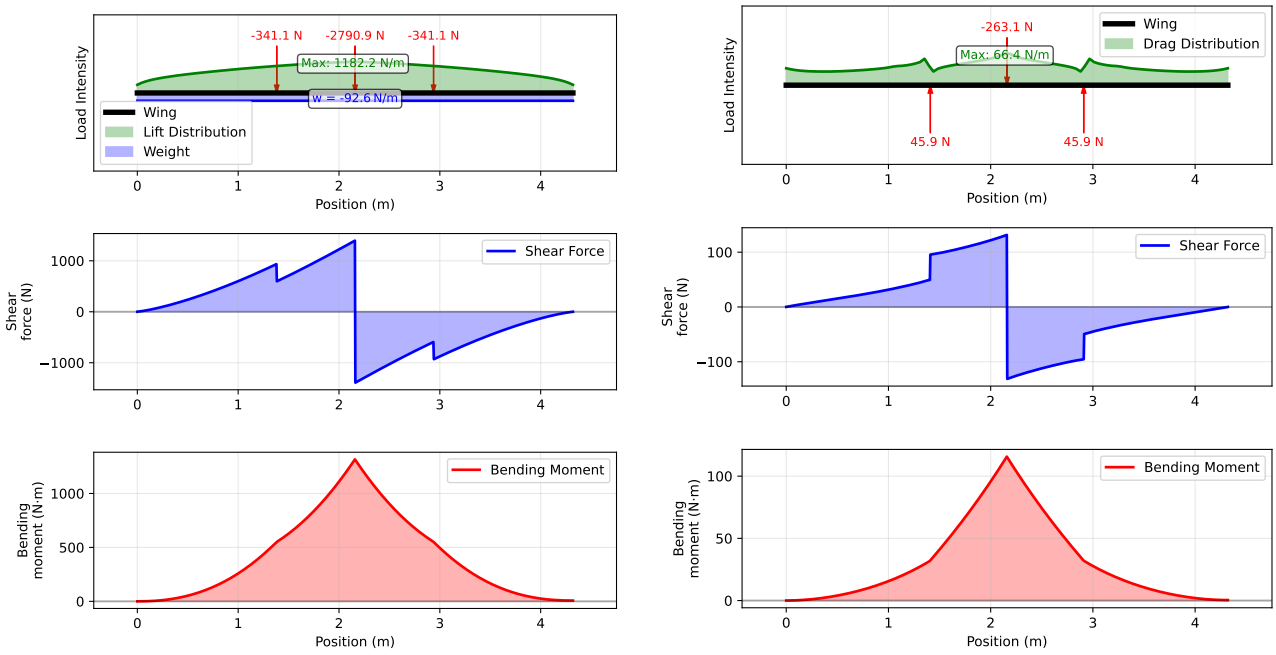

(a) Front view wing loading diagram gust condition.

(b) Top view wing loading diagram gust condition

Figure 9.4: Comparison of shear and moment diagrams for boom under gust and pull-up manoeuvre conditions.

There are several things that can be constraining the wingbox design: deflection, bending stresses, shear stresses, buckling and other failure modes that are not yet considered in this preliminary design stage. The lift and drag force act at the local centre of pressure of each section of the wing. As the centre of pressure does not correspond with the shear centre of the cross-section, an additional torque is experienced on top of the bending moment, resulting in higher shear stresses. Additionally, the empennage is connected with the booms to the wing, applying a large torque on the wing when using the elevator. To limit these effects, the concept of a multicell wingbox with two spars is chosen (see Figure 9.5). The forward spar is located at $0.25\left(\frac{x}{c}\right)$, close to the centre of pressure for the web to carry the shear force, and the aft spar is at $0.75\left(\frac{x}{c}\right)$ for attaching the ailerons. First the structure is considered with only a load-carrying skin and spars, and varying the thickness of each element. If this is insufficient to limit deflection and bending stresses, inertia can be added by using spar caps or stringers. Buckling can be countered by adding stringers and/or increasing the thickness of the corresponding panel. More details on the methodology and analysis for each failure mode is described below.

In order to have a safe design, a safety factor of 1.2 is applied to all forces and moments. According to the wing design in the midterm report, the root is a NACA 4415 and the tip a NACA 4412 airfoil; a linear interpolation is assumed between these.

9.5.1.Bending stresses

In order to estimate the bending stresses in each span wise section, Equation 9.15 is used [20].

$$\sigma_z = \frac{(M_x I_{yy} - M_y I_{xy})y + (M_y I_{xx} - M_x I_{xy})x}{I_{xx} I_{yy} - I_{xy}^2} \tag{9.15}$$

According to Megson [20], the effect of taper can be neglected when estimating bending stresses. To obtain a decent accuracy, the geometric properties (I_{xx}, I_{yy} and I_{xy}) are calculated per section considered and Equation 9.15 is used per section.

9.5.2.Deflection

Recall that the airfoils used are asymmetric. The horizontal and vertical curvature u'' and v'' can be found using Equation 9.16 [20].

$$\begin{bmatrix} u'' \\ v'' \end{bmatrix} = \frac{-1}{E(I_{xx}I_{yy} - I_{xy}^2)} \begin{bmatrix} -I_{xy} & I_{xx} \\ I_{yy} & -I_{xy} \end{bmatrix} \begin{bmatrix} M_x \\ M_y \end{bmatrix} \tag{9.16}$$

Integrating the curvature twice yields the deflection, as can be seen in Equation 9.17. Note that the integration constants are zero, as the boundary conditions at the root ($z = 0$) are $u' = u = v' = v = 0$. The total deflection δ is then $\delta = \sqrt{u^2 + v^2}$. [20]

$$u = \iint \frac{M_x I_{xy} - M_y I_{xx}}{E\left(I_{xx}I_{yy} - I_{xy}^2\right)} \qquad v = \iint \frac{M_y I_{xy} - M_x I_{yy}}{E\left(I_{xx}I_{yy} - I_{xy}^2\right)} \tag{9.17}$$

9.5.3.Shear stresses

The lift and drag force act at the local centre of pressure of each section of the wing. As the centre of pressure does not correspond with the shear centre of the cross-section, an additional torque is experienced on top of the bending moment, resulting in higher shear stresses.

In order to determine base shear flow q_b of each cell of the wingbox, cuts are made at the leading edge in the skin of section 1-3, the upper airfoil section 1-2 and at the trailing edge skin 2-4. Note that as a cut is made in these sections, there the base shear flow is equal to 0.

For calculating q_b for the other sections, recall that the shear flow The base shear flow is given by Equation 9.18 [20]:

$$q_b = -\frac{V_y I_{yy} - V_x I_{xy}}{I_{xx}I_{yy} - I_{xy}^2} \int_0^s t y ds - \frac{V_x I_{xx} - V_y I_{xy}}{I_{xx}I_{yy} - I_{xy}^2} \int_0^s t x ds \tag{9.18}$$

The base shear flow of the front spar $q_{b_{13spar}}$ is given by Equation 9.19:

$$\begin{aligned} q_{b_{13\text{ spar}}} &= -\frac{V_y I_{yy} - V_x I_{xy}}{I_{xx}I_{yy} - I_{xy}^2} \int_0^s t_{13\text{ spar}} y ds - \frac{V_x I_{xx} - V_y I_{xy}}{I_{xx}I_{yy} - I_{xy}^2} \int_0^s t_{13spar} x_{\text{front spar}} ds \\ &= -\frac{V_y I_{yy} - V_x I_{xy}}{I_{xx}I_{yy} - I_{xy}^2} t_{13\text{ spar}} \int_0^s y ds - \frac{V_x I_{xx} - V_y I_{xy}}{I_{xx}I_{yy} - I_{xy}^2} t_{13\text{ spar}} x_{\text{front spar}} L_{13\text{ spar}} \end{aligned} \tag{9.19}$$

Similarly, Equation 9.20 gives the base shear flow of the aft spar $q_{b_{24spar}}$:

$$\begin{aligned} q_{b_{24\text{ spar}}} &= -\frac{V_y I_{yy} - V_x I_{xy}}{I_{xx}I_{yy} - I_{xy}^2} \int_0^s t_{24\text{ spar}} y ds - \frac{V_x I_{xx} - V_y I_{xy}}{I_{xx}I_{yy} - I_{xy}^2} \int_0^s t_{24\text{ spar}} x_{\text{aft spar}} ds \\ &= -\frac{V_y I_{yy} - V_x I_{xy}}{I_{xx}I_{yy} - I_{xy}^2} t_{24\text{ spar}} \int_0^s y ds - \frac{V_x I_{xx} - V_y I_{xy}}{I_{xx}I_{yy} - I_{xy}^2} t_{24\text{ spar}} x_{\text{aft spar}} L_{24\text{ spar}} \end{aligned} \tag{9.20}$$

The base shear flow of segment 3-4 is given by Equation 9.21

$$\begin{aligned} q_{b_{34\text{ skin}}} &= -\frac{V_y I_{yy} - V_x I_{xy}}{I_{xx}I_{yy} - I_{xy}^2} \int_0^s t_{34\text{ skin}} y ds - \frac{V_x I_{xx} - V_y I_{xy}}{I_{xx}I_{yy} - I_{xy}^2} \int_0^s t_{34\text{ skin}} x ds \\ &= -\frac{V_y I_{yy} - V_x I_{xy}}{I_{xx}I_{yy} - I_{xy}^2} t_{34\text{ skin}} \int_0^s y ds - \frac{V_x I_{xx} - V_y I_{xy}}{I_{xx}I_{yy} - I_{xy}^2} t_{34\text{ skin}} \int_0^s x ds \end{aligned} \tag{9.21}$$

The rate of twist for each cell i is given by Equation 9.22. Assuming no distortion between cells, the rate of twist for each cell is the same.

$$\left(\frac{d\theta}{dz}\right)_i = \frac{1}{2A_i} \oint \frac{q_{b_i} + q_{s_{0_i}}}{t_i G_i} ds \tag{9.22}$$

For cell I this becomes

$$\begin{aligned}\left(\frac{d\theta}{dz}\right)_I = \left(\frac{d\theta}{dz}\right) &= \frac{1}{2A_I}\left(\int_{1_{\text{skin}}}^{3}\frac{q_{s_{0_I}}}{t_{13\text{ skin}}G_{13\text{ skin}}}ds + \int_{1_{\text{spar}}}^{3}\frac{q_{s_{0_I}} - q_{s_{0_{II}}}}{t_{13\text{ spar}}G_{13\text{ spar}}}ds + \oint\frac{q_{b_I}}{t_I G_I}ds\right) \\ &= \frac{1}{2A_I}\left(\frac{q_{s_{0_I}}L_{13\text{ skin}}}{t_{13\text{ skin}}G_{13\text{ skin}}} + \frac{\left(q_{s_{0_I}} - q_{s_{0_{II}}}\right)L_{13\text{ spar}}}{t_{13\text{ spar}}G_{13\text{ spar}}} + \oint\frac{q_{b_I}}{t_I G_I}ds\right)\end{aligned} \tag{9.23}$$

The rate of twist of cell II is given by Equation 9.24

$$\begin{aligned}\left(\frac{d\theta}{dz}\right)_{II} = \left(\frac{d\theta}{dz}\right) = \frac{1}{2A_{II}}\Bigg(&\frac{q_{s_{0_{II}}}L_{12\text{ skin}}}{t_{12\text{ skin}}G_{12\text{ skin}}} + \frac{\left(q_{s_{0_{II}}} - q_{s_{0_I}}\right)L_{13\text{ spar}}}{t_{13\text{ spar}}G_{13\text{ spar}}} + \frac{q_{s_{0_{II}}}L_{34\text{ skin}}}{t_{34\text{ skin}}G_{34\text{ skin}}} \\ &+ \frac{\left(q_{s_{0_{II}}} - q_{s_{0_{III}}}\right)L_{24\text{ spar}}}{t_{24\text{ spar}}G_{24\text{ spar}}} + \oint\frac{q_{b_{II}}}{t_{II}G_{II}}ds\Bigg)\end{aligned} \tag{9.24}$$

Finally, for cell III the rate of twist is Equation 9.25

$$\left(\frac{d\theta}{dz}\right)_{III} = \left(\frac{d\theta}{dz}\right) = \frac{1}{2A_{III}}\left(\frac{q_{s_{0_{III}}}L_{24\text{ skin}}}{t_{24\text{ skin}}G_{24\text{ skin}}} + \frac{\left(q_{s_{0_{III}}} - q_{s_{0_{II}}}\right)L_{24\text{ spar}}}{t_{24\text{ spar}}G_{24\text{ spar}}} + \oint\frac{q_{b_{III}}}{t_{III}G_{III}}ds\right) \tag{9.25}$$

The moment equilibrium of a closed section beam can be found using Equation 9.26, taking counterclockwise moments as positive [20]:

$$-V_x\eta_O + V_y\xi_O = \sum_{i=1}^{n}\oint pq_{b_i}ds + \sum_{i=1}^{n}2A_i q_{s_{0_i}} \tag{9.26}$$

For the wingbox of this UAV, the moment equilibrium in Equation 9.27 applies.

$$T - V_x\eta_O + V_y\xi_O = q_{b_{13\text{ spar}}}d_{\text{front spar}}L_{13\text{ spar}} + q_{b_{24\text{ spar}}}d_{\text{front spar}}L_{24\text{ spar}} + 2A_I q_{s_{0_I}} + 2A_{II}q_{s_{0_{II}}} + 2A_{III}q_{s_{0_{III}}} \tag{9.27}$$

The above equations together result in a system of equations $A\bar{x} = b$. The column vector $\bar{x}$ is

$$\bar{x} = \begin{bmatrix} q_{s_{0_I}} & q_{s_{0_{II}}} & q_{s_{0_{III}}} & \frac{d\theta}{dz}\end{bmatrix}^T \tag{9.28}$$

The first row of the system of equations is formed by Equation 9.23, the second by Equation 9.24 and the third by Equation 9.25. As the line integrals in these equations contain all known values, these form the right hand side vector b Finally, the moment equilibrium in Equation 9.27 forms the fourth and final row. Solving these leads to the unknown values in $\bar{x}$. The resulting shear flows in the wingbox are calculated using Equation 9.29 according to the directions and coordinate system defined above. The shear stresses per segment are then found by dividing the shear flow by the corresponding thickness.

$$\begin{aligned} q_{13\text{ skin}} &= q_{s_{0_I}} & q_{13\text{ spar}} &= q_{b_{13\text{ spar}}} + q_{s_{0_I}} - q_{s_{0_{II}}} \\ q_{12\text{ skin}} &= q_{s_{0_{II}}} & q_{34\text{ skin}} &= q_{b_{34\text{ skin}}} + q_{s_{0_{II}}} \\ q_{24\text{ spar}} &= q_{b_{24\text{ spar}}} + q_{s_{0_{II}}} - q_{s_{0_{III}}} & q_{24\text{ skin}} &= q_{s_{0_{III}}}\end{aligned} \tag{9.29}$$

9.5.4.Buckling

As the top side of the wingbox is in compression when the wing generates lift, a potential failure mode is buckling. The segment with the highest compressive force is the skin 1-2 and is therefore most likely to buckle. As the leading and trailing edge of the cross-section are also partially in compression, these could also buckle. However, due to the strong curvature this is far less likely than the buckling of a straight thin panel. Therefore the following buckling analysis is only performed on segment 1-2.

The critical stress when buckling will occur for a thin plate can be found with Equation 9.30 [20]. The buckling coefficient C depends on the boundary conditions and aspect ratio of the plate. For a conservative estimation, the upper surface of the wing between both spars is considered simply supported on both sides, resulting in $C \approx 4$. As the Young's modulus E and Poisson ratio ν are material properties, it is evident that for a given material only the thickness t and width b of the plate

can be changed to prevent buckling. The width b can be reduced by adding stringers. Note that C is also dependent on the aspect ratio, so it is also an option to add ribs to reduce the length and increase C. This is however a much less efficient option as C quickly reaches it asymptote value of 4, meaning that many ribs would be required. As adding stringers is therefore the most efficient way of preventing buckling, this is the only option considered.

$$\sigma_{cr} = C\frac{\pi^2 E}{12(1-\nu^2)}\left(\frac{t}{b}\right)^2 \tag{9.30}$$

As the wing has a significant amount of taper, and b changes throughout the span, b is taken at the root value to perform a conservative analysis. Moreover, it is assumed that this method yields representative results for quasi-isotropic composites.

9.5.5.Material Selection

For designing the wing structure, two materials are considered. First the properties of the widely used aluminium 7075-T6 alloy can be found in Table 9.3. Note that this is an isotropic material and the tensile and compressive strength can be considered equal. Yao Sun et al. determine that after exposure to $200°$ aluminium properties are only moderately affected [21]

Another option is using carbon fibre. The option considered is the plain weave F6273C-11M prepreg, using standard modulus T700S-12K fibers and 2511 resin system[3]. The high T_g of 153°C makes it an attractive option for flying over fires[4]. The ply properties can be found in Table 9.5 at 22°C and 82°C. As is is a plain weave ply, the properties in 0 and 90 direction are similar. To estimate the properties of the laminate, classical laminate theory has to be used. However, due to time constraints a more simple approximation is given in Table 9.4. Taking the minimum value for each parameter in 0 and 90 direction and operating temperature, and applying a material knockdown factor of 0.8 gives a decent first estimate of laminate properties for the preliminary design phase. Finally, note that the methodology for bending, shear and buckling all assume an isotropic material. Therefore, only quasi-isotropic layups are considered.

Table 9.3: Material properties of Aluminium 7075-T6[5]

Property	Value	Unit
σ_y	503	MPa
E	71.7	GPa
τ	331	MPa
G	26.9	GPa
ν	0.33	-
ρ	2.81	g/cm^3

Table 9.4: Material properties of laminate

Property	Value	Unit
σ_t	722.4	MPa
σ_c	361.6	MPa
E	38.8	GPa
τ	38.16	MPa
G	2.368	GPa
ν	0.024	-
ρ	1.51	g/cm^3
Cured ply thickness	0.218	mm

Table 9.5: Material properties of F6273C-11M (T700S-12K PW) carbon fibre ply[6]

Property	Value RTA (22°C)	Value ETW (82°C)	Unit
$\sigma_{t,0}$	1089	1089	MPa
$\sigma_{t,90}$	993	903	MPa
$\sigma_{c,0}$	674	514	MPa
$\sigma_{c,90}$	638	452	MPa
$E_{t,0}$	59.2	62.9	GPa
$E_{t,90}$	56.7	59.2	GPa
$E_{c,0}$	53.3	57.9	GPa
$E_{c,90}$	48.5	56.4	GPa
τ	86.2	47.7	MPa
G	4.01	2.96	GPa
ν	0.054	0.024	-
ρ	1.51	1.51	g/cm^3
Cured ply thickness	0.218	0.218	mm

Table 9.6: Comparison of CF and Alu

Parameter	CF Value	Alu Value	Unit
Max compressive stress	86.0	93.8	MPa
Max tensile stress	43.8	47.8	MPa
Max shear stress	27.6	30.1	MPa
Total mass	6.18	10.5	kg
Max total deflection	7.3	4.3	cm
Thickness	0.872	0.8	mm

Table 9.6 contains the comparison of stresses, deflection and mass for aluminium and carbon fibre for the gust load case. Note that no failure occurs due to bending and shear for both materials, and the deflection is well within acceptable limits. For aluminium a thickness of $0.8\,\mathrm{mm}$ is used, which is the minimum (off-the-shelf) thickness for sheet metal. However,

[3]https://www.toraycma.com/wp-content/uploads/2511-Prepreg-System.pdf
[4]https://www.toraycma.com/wp-content/uploads/Toray-Aerospace-Selector-Guide.pdf
[5]https://www.matweb.com/search/datasheet.aspx?MatGUID=4f19a42be94546b686bbf43f79c51b7d&ckck=1, Accessed: 17-06-2025
[6]https://www.toraycma.com/wp-content/uploads/2511-Prepreg-System.pdf, Accessed: 17-06-2025

the total mass of $10.5\,\mathrm{kg}$ goes well over the mass budget by a factor of almost 2. Therefore the option of using aluminium 7075-T6 is discarded, and the further analysis is only performed on T700S plain weave prepreg.

After iterating through different thicknesses in the front spar, aft spar and skin, it is clear that the structure is not strength limited nor deflection limited. Therefore, a lay-up of four plies is chosen to obtain a thickness of 0.872 mm. For the lay-up to be quasi-isotropic, the plies will have the orientations of 0, 90, +45 and -45 in any order. Note that this is not a symmetric lay-up, meaning bending behaviour and stretching from shearing deformations are coupled, potentially leading to laminate failure unaccounted for in this methodology [22]. Although generally symmetric lay-ups are preferred for this reason, the aim of this chapter is to obtain a preliminary sizing of the wingbox, and the effects are therefore neglected. The precise lay-up design is left as a recommendation for future development.

9.5.6.Results

The maximum tensile and compressive bending stresses for a gust load along the halfspan can be seen in Figure 9.6. It is clear that the highest stresses are experienced at the root, gradually reducing along the span. A small kink can be seen where the boom attaches at $0.75\,\mathrm{m}$. The internal stresses at the root are plotted in Figure 9.8. The location of the neutral axis is where the stresses are zero. As the top surface of the airfoil is further located from the neutral axis than the bottom side, the magnitude of stresses is higher at the top. The maximum compressive stress is $86.0\,\mathrm{MPa}$, and the maximum tensile stress is $43.8\,\mathrm{MPa}$. Note that both of these are well below yielding failure.

Recall that due to the asymmetric cross-section and moments in x and y direction, the wing will experience a vertical and horizontal deflection. Figure 9.7 shows that although there is a slight forward movement in negative x direction, this is a negligible contribution to the total deflection, which essentially overlaps with the vertical deflection. A scaling factor of 5 is applied to the deflection for visibility. The maximum total deflection (horizontal and vertical component) at the wingtip

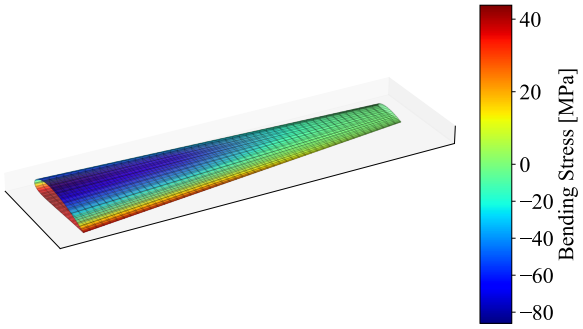

Figure 9.6: Maximum tensile and compressive bending stress along the span.

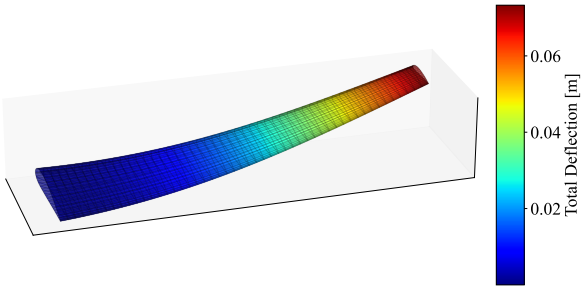

Figure 9.7: Wing deflection.

The maximum shear stress along the span is shown in Figure 9.9, for a gust load of 6 and a torque applied at the boom location due to a control force at the elevator. As expected, there is a large peak in shear stresses at $0.75\,\mathrm{m}$. Figure 9.10 shows the internal shear stresses. The highest shear stress is experienced at the leading edge segment, at $27.6\,\mathrm{MPa}$. Although closer to failure than the bending stresses, the shear stresses are still below failure (see Table 9.4). Recall that a 1.2 safety factor is applied on all forces and moments, and a 0.8 knockdown factor on material properties, so no measures have to be taken.

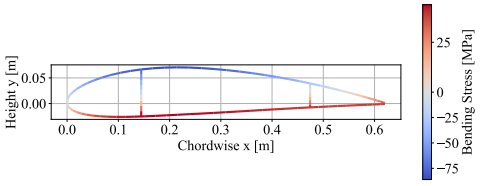

Figure 9.8: Bending stresses at root.

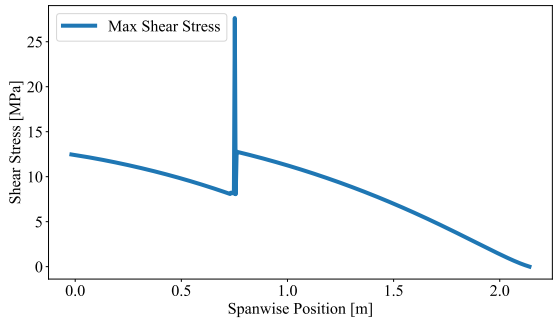

Figure 9.9: Maximum shear stress along the span.

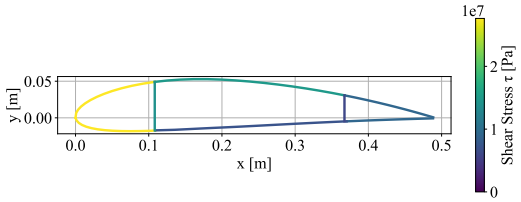

Figure 9.10: Internal shear stress distribution.

The limiting case for the wingbox is buckling. Without any stringers, the critical buckling stress is 1.0 MPa, due to the low Poisson ratio and thin skin. For σ_{cr} to be below the highest compressive stress reached, 9 stringers are required in total to have $\sigma_{cr} = 103.1$ MPa.

9.6.Manufacturing, Assembly and Integration Plan

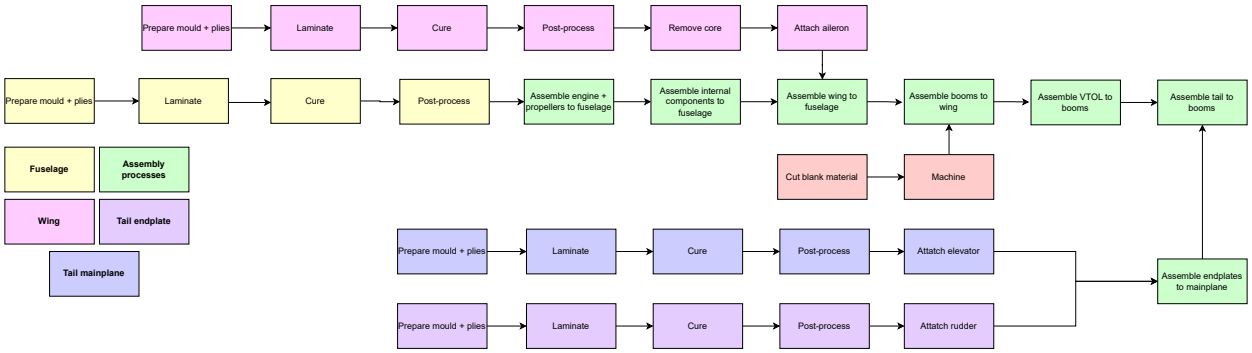

Figure 9.11: Production and assembly plan

For the production and assembly of the UAV, the system is split up into different subassemblies: fuselage, wing, booms and tail. The structure of the fuselage, wing, and tail are all laminated. First, the mould has to be prepared (cleaning, afterwards applying sealing and release agent) and the prepreg roll has to be taken out of the freezer to cut the plies for laminating. During laminating, each layer is applied onto the mould with sufficient overlap between plies, occasionally performing a debulk. If required, inserts are laminated in during this stage of the process. The curing process includes vacuum bagging and the entire curing cycle with cool down time. In post-processing, holes are drilled and frayed ends are removed. Note that for the wingbox, as it is a hollow structure, the core needs to be removed (for example a dissolvable foam or metal with a low melting temperature). In the timeline the fuselage is the first part that has to be finished, as this is where everything is assembled onto. The engine and propellers are the first components to be assembled to the fuselage. Next are all other internal components, such as the sensor, fuel tank, etc. After that first the wing is assembled to the fuselage. To the wing the booms are attached, which are first machined (for example on a lathe to create the hollow cilinder with the desirable dimensions). The VTOL propellers are then attached to the booms. Finally, the tail (with the endplate and mainplane laminated in advance and then assembled together) is attached to the booms. This process is shown in Figure 9.11. Note that in parallel to all of this is the process of machining brackets for attachment, which is not shown.

The wing shall be detachable, bolted to the fuselage with redundant bolts to specification torque with a positive locking mechanism. The booms shall be bolted to the wing. This is accounted for in design where it was confirmed the wing would not need to be split into multiple sections for operations. Further analysis of loading cycles must be performed, where more complex locking mechanisms may be used to reduce stress concentration, eliminate need for locking devices and streamline disassembly.

9.6.1.Manufacturing and Assembly Costs

To estimate costs of manufactured items a simple method combining mass and processing time estimate was employed. A price of €12 per kg for aerospace grade aluminium was considered[7] and a price of €94 per kg for CFRP composite[8].

[7]https://www.customproc.com/aluminium-alloy-7075-price-guide/ Accessed 17/06/2025

[8]https://carbonfibergear.com/blogs/carbonfiber/carbon-fiber-vs-aluminum?srsltid=AfmBOoqj7EzakUDc_LDKn15xueENHYhhtu7I04xBtUx3ByWCvMykmEL Accessed 17/06/2025

Each process time is given an estimate based on team member experience, summarized in Table 9.7. A price per hour of machine shop time was assume at €100 per hour, with a 20% contingency to €120 per hour manufacturing time to cover personnel and costs of machinery. In addition a 30% cost margin is given for specification price when broken down in cost section. In practice, as a high volume of aircraft with a series production of approximately 1000 aircraft will be built[9], the learning factor will mean first unit costs will be higher, and final units will be lower cost.

Table 9.7: Bill of Materials for UAV structure

Item	Unit Weight [kg]	Time [h])	Unit Cost [€]	Quantity	Total Cost (€)	Total Weight
Wing Spar	1	2	333.6	4	1334	4
Wing Skin	1.6	4	629.76	2	1259	3.2
Boom	2.7	6	752.4	2	1504	5.4
Fuselage	2.6	5	843.36	1	843	2.6
Engine Mount	0.5	2	246	1	246	0.5
Horizontal Stab	0.5	5	606	1	606	0.5
Vert Stabs	1	5	612	2	1224	2
Ailerons	0.1	1	121.2	2	242.4	0.2
Wing Bracket	1	4	492	1	492	1
General Bolts	0	0	0.5	50	25	0
Fuel Tank	1	2	252	1	252	1
Water Tank	0.5	4	486	1	486	0.5
TOTAL					**8515**	**21.4**

Assembly Cost
The estimate of assembly cost is as follows based on the team experience. 3 people will work for 1 working week of 40 hours, using the cost of €120 per hour from the manufacturing estimation. This results in an assembly cost of €14 400, and with a 30% margin applied this results in a final estimated manufacturing cost of €19 000. This will include all wiring, structural assembly, loading software and adding purchased subsystems.

9.6.2.Sensitivity
The structure of the booms is highly sensitive to the length as the bending deflection and reduction in natural frequency is significantly reduced. As such the design of booms was iteratively reduce to the 2.7m length in correspondence with control team and confirmation of clearance for propellers.

Table 9.8: Airframe compliance matrix.

ID	Verification Method	Status	Value
REQ-UAV-STRUCT-01	Analysis/Test	Preliminary yes	-
REQ-UAV-STRUCT-02	Inspection	Yes	-
REQ-UAV-STRUCT-03	Test	TBD	-
REQ-UAV-STRUCT-04	Inspection	TBD	-
REQ-UAV-STRUCT-05	Inspection	Yes	-
REQ-UAV-STRUCT-06	Analysis/Test	Preliminary yes	$153\,^{\circ}\mathrm{C}$
REQ-UAV-STRUCT-07	Analysis	TBD	TBD% recyclable
REQ-UAV-STRUCT-08	Analysis/Test	Preliminary yes	-
REQ-UAV-STRUCT-09	Analysis	Yes	$< 0.3^{\circ}$
REQ-UAV-STRUCT-10	Analysis	Yes	$< 21.4\,\mathrm{kg}$
REQ-UAV-STRUCT-11	Cost Analysis	Yes	$<$ €8 500
REQ-UAV-STRUCT-12	Analysis/Test	Yes	$N = 6$
REQ-UAV-STRUCT-13	Analysis	TBD	TBD
REQ-UAV-STRUCT-14	Inspection	Yes	-
REQ-UAV-STRUCT-15	Inspection	Yes	-

9.7.Sustainability
The initial target for recyclable materials was optimistically 80% of OEW. It was attempted to design with aluminium for recyclibility, this was however unfeasible for the wingbox. Using carbon fibre for the wingbox, fuselage, and empen-

[9] 35 UAVs, for 30 customers.

nage, the estimate is 10.8kg of non-recyclable material out of the total structure budget of 22.24kg, approximately 50% recyclability.

9.8.Structural Verification & Validation

The verification and validation of the structural design includes the compliance matrix that can be seen in Table 9.8, methodology for code V&V and sensitivity.

Code verification is performed manually by plotting the graphs of load distribution and shear and bending moment diagrams and confirming by inspection their validity. Moments and forces at unsupported end of beams must be 0 unless a load or moment is applied. The direction of the gradient is confirmed to be in the correct direction. Large load discontinuities are observed at application of forces that coincide with correct placement. Forces and force distributions are confirmed to be acting in the correct directions.

Throughout the code specific assertions are added to confirm the validity of inputs. Instead of unit tests, this improved iterability as feedback on incorrect configurations is immediately delivered to the user. Unit tests are performed for simple cases for beam sizing by specifying a constant uniform load and confirming the suggested beam is able to handle the specified load in bending and shear.

9.9.Structural Recommendations

Due to time constraints for the aircraft system design in relation to the total project timeline, the analysis should be expanded beyond the current major sizing parameters to include comprehensive sensitivity analysis for fuselage mass and material selection. While wing, boom, and fuselage sections have been determined to have detachable assemblies, the disassembly process requires further detailed design to ensure efficient maintenance and end-of-life processing. Additionally, recyclability requirements must be addressed with close monitoring of associated risks throughout the design and operational phases.

Temperature effects and heat absorption times should be analysed in greater detail to enhance thermal protection and operational reliability. Investigation of heat-resistant coatings to reduce absorptivity of critical materials is recommended to mitigate thermal loading on critical components during operation. In addition effects of thermal expansion on structures should be at least tested to confirm correct behaviour, despite initial calculations showing minimal percentage expansion.

The current design of the aircraft booms allows for significant deflection of the empennage with respect to the wing and fuselage, and the hollow circular cross-section is not optimal given that the design is stiffness-limited. Controllability analysis should be conducted to assess the effect of tail boom oscillations and pitch-up manoeuvrer characteristics on flight dynamics. Implementation of notch filters for structural resonance frequencies in the flight control system should be considered to maintain stability and control authority.

For the wingbox, the next step of the design would be to perform FEA, e.g. using Hypermesh, as the assumptions made on composites and taper can have a significant impact on the structure. Moreover, a non-linear FEA would be useful to analyse the buckling behaviour of the composite skin. To solve the problem of buckling, a more efficient method than attaching 9 stringers, could be to locally change the number of stringers (more at the root, and less at the tip) or have a foam or honeycomb core, thus increasing the thickness (which cannot be accounted for in the current method assuming a single, isotropic material). Performing proper lay-up design can greatly increase stiffness and reduce mass, for instance by using unidirectional fibres along the wingspan. Finally, a dynamic analysis could provide accurate information on natural frequencies and structural resonance.

Further detailed component design development is required for motor mounting systems and associated wiring cutouts to ensure robust integration and maintenance accessibility. Shock loading analysis, particularly for landing scenarios, should be completed to verify structural integrity under operational loads. Fatigue analysis should be conducted with integration of fatigue monitoring into the maintenance plan to ensure long-term structural reliability and operational safety.

10 Further Aerodynamic Analysis

To verify and refine the aerodynamic characteristics of the wing at a cruise angle of attack of 7.45, a higher-fidelity CFD study is conducted using ANSYS Fluent, a finite volume solver. This supplements the preliminary analysis performed in XFLR5 in Section 11.6 and the Class II estimations in Section 7.3. The CFD analysis offers a more realistic insight into the 3D aerodynamic characteristics of the wing.

10.1.Meshing Strategy

To accurately simulate the airflow around the wing while maintaining computational efficiency, a hybrid meshing approach is used. The fluid domain was defined as a rectangular enclosure around the wing, with the boundaries positioned sufficiently far from the geometry to minimise any influence of the boundary conditions on the flow solution. The distances from the origin (assumed at the wing root leading edge) to each domain boundary are: +x = 7c, -x = 25c, +y = 15c, -y = 0, +z = -z = 10c with c being the mean aerodynamic chord.

A finer block is defined around the wing as a body of influence to increase mesh density in the region of interest. This body extends: +x = 0.82m, -x = 0.3m, +y = 2.82m, -y = 0m, +z = -z = 0.35m. This region ensures finer mesh control around the wing, where large pressure gradients and flow separation are expected.

To resolve the boundary layer near the wing surface, inflation layers were applied. These are essential for accurately capturing the near-wall flow physics. The turbulence model employed in this study is the k-ω Shear Stress Transport (SST) model, which incorporates enhanced wall functions. For this wall treatment to function correctly, the y^+ must be below 2 (for resolving the viscous sublayer) or above 30 (for the log-law region) to be able to accurately model the shear stresses in the viscous sublayer[1] [2]. y^+ values in between fall in the buffer region where the wall functions are unreliable. Using Cadence's boundary layer tool[3] for y^+ of 100, a first cell height of 0.001354 m is required for the inflation layer. Equation 10.1 is used to estimate the thickness δ of the boundary layer for a turbulent flow[4]. It is found that 7 inflation layers are needed in the simulation to capture this boundary layer height using Equation 10.2, where g is the growth factor of 1.25, N is the amount of inflation layers, and the total and first layer thickness thicknesses are obtained from previously.

$$\delta = \frac{0.37x}{Re^{0.2}} \tag{10.1}$$

$$\delta = \delta_{1st,layer} \cdot \frac{1 - g^{N+1}}{1 - g} \tag{10.2}$$

The mesh was made following ANSYS Meshing guidelines, for this it needs to have a skewness < 0.75, orthogonality > 0.5, and element quality > 0.3[5]. Mesh refinements are applied to regions where the computational cells do not meet the required accuracy. The final cell sizes used are summarized in Table 10.1 and the final mesh displayed in Figure 10.1.

Table 10.1: Mesh sizing in different regions.

Region	Body of influence	Wing surface edge	Root & tip edge	Leading layer	Inflation
Size [m]	0.075	0.0075	0.01	0.0035	0.001354

The resulting mesh statistics are:

- **Skewness:** average = 0.238, standard deviation = 0.144
- **Orthogonality:** average = 0.762, standard deviation = 0.143
- **Element quality:** average = 0.762, standard deviation = 0.143
- **Number of elements:** 1 354 168

These values indicate a high-quality mesh, while keeping computational cost within reasonable limits.

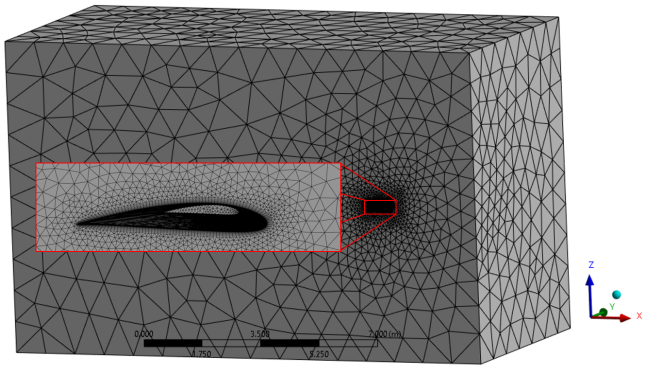

Figure 10.1: Mesh with zoomed-in view.

[1] See: https://ansyshelp.ansys.com/public/account/secured?returnurl=///Views/Secured/corp/v251/en/flu_th/section_kbf_dl4_vvb.html. Accessed 17-06-2025.

[2] See: https://www.youtube.com/watch?v=h5OiFpu0L4M. Accessed 17-06-2025

[3] See: https://www.cadence.com/en_US/home/tools/system-analysis/computational-fluid-dynamics/y-plus.html. Accessed 15-06-2025

[4] See: https://resources.system-analysis.cadence.com/blog/2023-computing-boundary-layer-thickness-in-cfd-analysis. Accessed 23-06-2025.

[5] See: https://ansyshelp.ansys.com/public/account/secured?returnurl=/Views/Secured/corp/v251/en/flu_ug/tgd_user_report.html. Accessed 17-05-2025.

Attention does have to be paid around the wing and inflation layers, which were usually the areas where the mesh quality was sub-optimal.

10.2.Setup

To solve the Reynolds-Averaged Navier–Stokes (RANS) equations, the k-ω SST turbulence model is chosen due to its proven accuracy and robustness for external aerodynamic flows. It combines the strengths of two turbulence models: k-ω near the walls for better boundary resolution and k-ε in the outer region such that it is less sensitive to inlet conditions[6] [7].

For the boundary conditions, the -x and +z face has been set as outlet, -y is set as symmetry plane, and the rest of the faces are set as inlet with the wind coming in at an AoA of 7.45° for cruise. This is done by dividing the incoming flow into a component $V_x = \cos(7.45°)$, $V_z = \sin(7.45°)$.

The solver is set to pressure-based and uses the SIMPLE scheme, segregated flow solvers are known for their stability. It can handle a range of different flow conditions and is not as sensitive to small changes in the input parameters as other numerical methods. However, segregated flow solvers can suffer from issues of slow convergence in certain cases. This is particularly true for problems that involve complex geometries such as turbulence, heat transfer or multiphase flows[8]. The SIMPLE scheme solves the incompressible Navier-Stokes[9], suitable for the cruise conditions which are at M=0.073.

Table 10.2: Comparison C_L and C_D from different CFD tools.

Tool	ANSYS Fluent	XFLR5	Class II estimations
C_L	0.8472	1.0126	0.9756
C_D	0.0495	0.0409	0.0429
L/D	17.1	24.8	22.8

10.3.Results & Discussion

The wing lift and drag coefficient of the ANSYS Fluent simulation are displayed in Table 10.2 as well of XFLR5 and the Class II estimations for comparison at a cruise angle of attack of 7.45°.

XFLR5—using the vortex lattice method—overestimates the lift and underestimates the drag. This is because it interpolates 2D parasitic drag data from local wing lift to obtain 3D viscous drag, thus not fully taking into account cross-flow or other 3D aerodynamic phenomena. It also assumes the wake as a straight extension of flat panels, resulting in overestimating the lift and vortex strength . This corresponds with findings of Deperrois[10] [11] and Prieto [23].

The Class II estimation method is a semi-empirical approach used to estimate the initial aerodynamic characteristics of an aircraft during the preliminary design phase and therefore cannot be fully trusted for detailed design. It combines simplified aerodynamic theory with empirical correction factors, allowing quick and reasonably accurate predictions based on basic geometric inputs and historical data. These estimates can be refined as more detailed information becomes available about the UAV's components, configuration, and operating conditions.

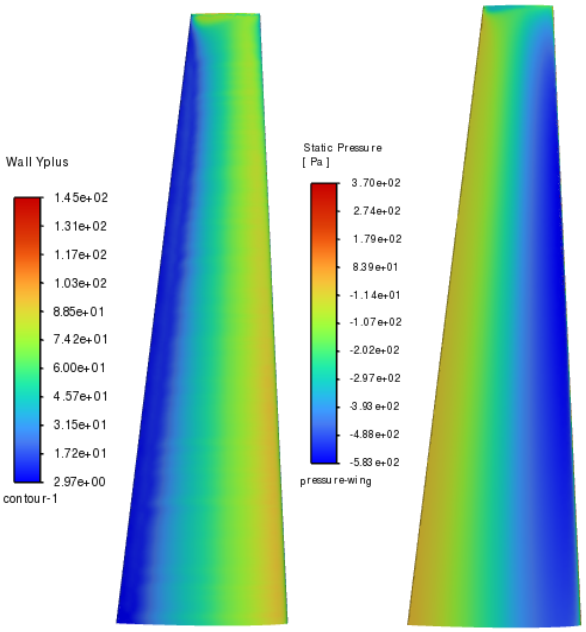

(a) y^+ values. **(b)** Pressure distribution.

Figure 10.2: Contours on wing top wing surface.

ANSYS Fluent predicted a lower lift and higher drag coefficient than both XFLR5 and the Class II method. This can be attributed to the following:

Firstly, the k-ω SST turbulence model assumes the flow is fully turbulent from the leading edge. This typically leads to reduced suction peak and consequently lower lift as well as an overestimated drag [24].

Secondly, part of the discrepancy is likely due to meshing irregularities, particularly in the inflation layer. As shown in Figure 10.2a, the computed wall y^+ values vary significantly, ranging from 2.97 at the trailing edge to 140 near the leading edge. As discussed in Section 10.1, values within the buffer region ($2<y^+<30$) are suboptimal for wall functions, most of these values are only at the trailing edge. Enhanced wall functions are not reliable in this range and may lead to

[6] See: https://turbmodels.larc.nasa.gov/sst.html. Accessed 17-06-2025.
[7] See: https://www.youtube.com/watch?v=myv-ityFnS4. Accessed 17-06-2025.
[8] See: https://www.resolvedanalytics.com/cfd/coupled-vs-segregated-cfd-flow-solvers. Accessed 17-06-2025.
[9] See: https://www.youtube.com/watch?v=OOILoJ1zuiw. Accessed 17-06-2025.
[10] See: http://www.xflr5.tech/docs/Part%20IV:%20Limitations.pdf. Accessed 17-06-2025.
[11] See: http://www.xflr5.tech/docs/Results_vs_Prediction.pdf. Accessed 17-06-2025.

inaccuracies in predicting velocity gradients and shear stress near the wall. To improve the accuracy of the simulation, the mesh should be refined to ensure that the entire wing surface falls either within the viscous sublayer (y^+<2) or the log-layer (y^+>30). Doing so would allow the turbulence model to better resolve boundary layer behaviour, leading to more accurate predictions of lift and drag.

Despite the noted discrepancies, ANSYS Fluent still provides accurate results due to its high-fidelity nature. As shown in Table 10.2, the lift-to-drag ratio at the cruise angle of attack of 7.45° is lower compared to other methods. This implies that, in reality, the UAV would need to operate at a higher angle of attack to generate the required lift for steady-level flight.

10.4.Aerodynamics Verification

Verification needs to be performed on the mesh to make sure that the solution is not dependent on the meshing step and remains within an acceptable margin upon refinement. This is done by performing a grid convergence analysis. The grid convergence index (GCI)—based on the Richardson extrapolation—should be within 1-5% for detailed studies and within 5-10% for preliminary or parametric studies[12]. For this at least three refinements are necessary, one doubling and one halving the number of cells w.r.t. the previous mesh. The most relevant variables, the lift and drag coefficient, are evaluated over the different meshes to grid convergence. The grid convergence index can be calculated using Equation 10.3 to Equation 10.6, with f_1, f_2 and f_3 being the three refinements from finest to coarsest with N being the number of elements and D the dimensionality (3 in this case)[13]:

$$r = \left(\frac{N_{coarse}}{N_{fine}}\right)^{D}, \tag{10.3}$$

$$p = \frac{\ln(\frac{f_3 - f_2}{f_2 - f_1})}{\ln(r)}, \tag{10.4}$$

$$E = \frac{f_2 - f_1}{1 - r^p}, \tag{10.5}$$

$$GCI = 1.25 \cdot |E|. \tag{10.6}$$

To double the mesh size, the volume halves, so the element length for all areas decrease by $\sqrt[3]{2} \approx 1.26$. The ratio of the number of elements will not be exactly two due to the use of an unstructured grid. Table 10.3 shows the total number of elements, and values of C_L and C_D.

Using Equation 10.3 to Equation 10.6, a GCI of 5.3% is found for both C_L and C_D, thus grid convergence is achieved.

Additionally, the inlet distance was doubled to assess the sensitivity of the results to the boundary condition placement. The resulting variation in C_L and C_D was only 0.59%, indicating that the simulation is sufficiently independent of the inlet boundary location.

Table 10.3: Iteration results for grid convergence simulations.

Mesh	1	2	3
Number of elements	2 674 313	1 354 168	674 190
C_L	0.8265	0.8479	0.8645
C_D	0.0480	0.0495	0.0509
L/D	17.2	17.1	17.0

10.5.Aerodynamics Validatio

To further validate, the results can be compared with experimental data. Carter [25] performed a test in the Langley wind tunnel on an unswept, untapered wing with a continuous NACA 4415 profile, aspect ratio of 6, and chord of 0.2032 m. The chordwise pressure distribution was measured at 25% wingspan at a dynamic pressure of 420 N·m^{-2} and angle of attack of 7.15°. Figure 10.3 plots the experimental data as well as the Cp distribution of ANSYS Fluent at 0.551 25 m or 25% wingspan. It can be seen that the general shape is similar, with the suction peak and overall Cp on the upper surface being more negative in the wind tunnel test.

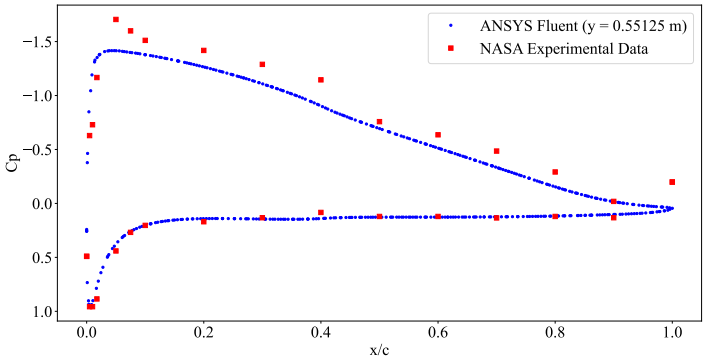

Figure 10.3: Cp distribution comparison with experimental data.

This can be attributed to ANSYS underestimating lift and the suction peak due to the turbulence model used as discussed before, but also the different conditions in which test was performed. The free stream dynamic pressure and Reynolds number (based on C_{mac}) of the wind tunnel was 420 N·m^{-2} and 900 000 while Phoenix flies at 383 N·m^{-2} and 800 000. Additionaly, the UAV wing features a different planform, one that is tapered, whereas Carter's model assumes a rectangular planform with no taper. As noted by Guzelbey [26], tapering typically reduces the lift generated in the inboard 25% of

[12] See: https://cfd.university/blog/how-to-manage-uncertainty-in-cfd-the-grid-convergence-index/aioseo-how-to-calculate-the-grid-convergence-index. Accessed 17-06-2025.

[13] See: https://www.grc.nasa.gov/WWW/wind/valid/tutorial/spatconv.html. Accessed 17-06-2025.

the wing span, due to changes in chord distribution and local Reynolds number effects. In addition, the UAV does not maintain a constant NACA 4415 airfoil across the span, instead the airfoil gradually transitions to a NACA 4412 toward the wingtip. Due to the geometric and aerodynamic differences between the models, the validation results should not be interpreted as a precise benchmark. However, it does provide a useful sanity check, offering confidence that the simulation captures the correct order of magnitude and general aerodynamic trends.

10.6.Aerodynamics Recommendations

To improve the accuracy of the simulation results, it is recommended to further amend the mesh near the trailing such that the y^+ values remain consistently between 30 and 300. This would enable better resolution of the log-law layer using the enhanced wall functions of the k-ω SST model, ensuring more accurate prediction of near-wall flow behaviour, and consequently more reliable estimates of lift and drag.

It can also be observed that different lift coefficients are obtained across the tools, despite all simulations being conducted at the same cruise angle of attack of 7.45°. In future analyses, it is recommended to match the target lift coefficient for cruise conditions instead of fixing the angle of attack. This approach would provide a more consistent basis for comparison between different tools and methods. Nonetheless, the current results still offer valuable insights into 3D aerodynamic effects on the aerodynamic coefficients, which are captured more realistically in the higher-fidelity CFD simulation.

While the advantages and disadvantages of the used tools—ANSYS Fluent, XFLR5, and Class II estimation— and difference of coefficients have been discussed, the results of ANSYS should be used for future aerodynamic development of the UAV, serving as a good stepping stone. This is due to the high fidelity nature of the CFD simulation. For example, it is important to consider the impact of the boom ahead of the wing. This would introduce significant flow disturbances, including wake and turbulence, which would reduce lift and increase drag. Including this geometry in future CFD studies would provide a more realistic assessment of the aircraft's aerodynamic performance and help guide design decisions to mitigate adverse effects.

11 Stability & Control

This chapter concerns the stability and controllability of the aircraft during each design stage. To analyse the objectives for the subsystem, a functional analysis for the stability and control subsystem alongside the subsystem requirements is provided in Section 11.1. Next, as the empennage directly influences the stability and control performance of the aircraft, its trade-off alongside the airfoil selection is discussed in Section 11.2 and Section 11.3, respectively. A discussion of the component positioning with the centre of gravity range is given in Section 11.4. Moreover, the tail and control surface sizing is performed in Section 11.6. After having positioned and sized the components, the dynamic and static stability will be analysed in Section 11.7 and Section 11.8. Moreover, the stability and controllability of the VTOL system is elaborated on in Section 11.9. The stability and control system's sensitivity is elaborated on in Section 11.10 to identify the stability of the obtained solution. Next, a verification and validation is performed for the subsystem in Section 11.11. Lastly, further recommendations are given in Section 11.12

11.1.Stability & Control Functional Analysis and Requirements

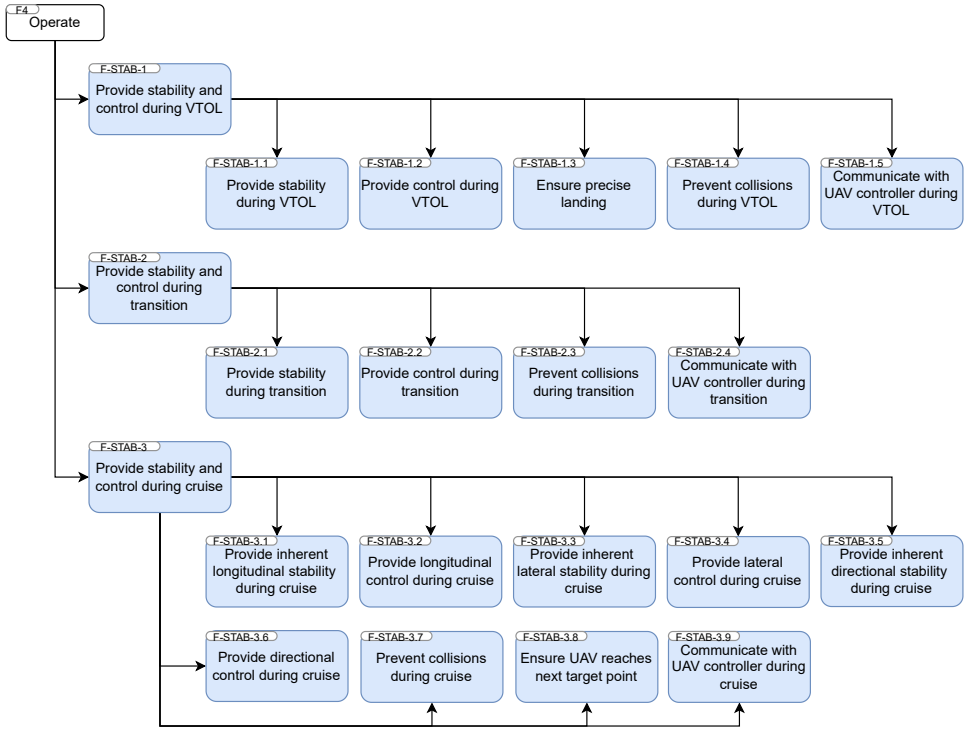

Figure 11.1: Functional breakdown of the stability and control subsystem.

To design the stability and control system of the UAVs, a functional analysis is provided. This describes the required functions that need to be performed by the subsystem during the operational phases of the mission. For this, the mission is divided into the vertical take-off and landing phase, cruise, including manoeuvres to stay on the optimal path and perform the suppression, and the transition between cruise and VTOL. While stability during cruise can be achieved by designing the aircraft to be inherently stable, a flight controller is required to control the aircraft during VTOL, manoeuvres and severe weather conditions. To actively control the UAV, the VTOL system and control surfaces can be used. The functional diagram is depicted in Figure 11.1.

The stability and control subsystem requirements provide a guideline during the design process of the stability and control subsystem. These are defined such that the UAV is able to perform the mission if the subsystem complies with them. The most demanding part of the mission is suppression, as will be explained in Chapter 16, and thus the values present in the requirements are obtained from there. In Table 11.1 these requirements are defined while also including the empennage requirements, as it drives the pitch and yaw manoeuvrability and stability of the UAV.

Table 11.1: Requirements for the stability and control subsystem.

ID	Requirement Description
REQ-UAV-EMP-STR-1	The empennage shall be able to withstand a maximum load factor of 6 without fracture.
REQ-UAV-EMP-STR-2	The empennage shall be able to withstand a maximum load factor of 4 without yielding.
REQ-UAV-EMP-STR-3	The empennage shall be able to deflect by at least 20 mm without fracturing.
REQ-UAV-EMP-STR-4	The empennage shall be able to deflect by at least 10 mm without yielding.
REQ-UAV-EMP-STR-5	The empennage shall have a maximum mass of 3 kg.
REQ-UAV-EMP-STR-6	The empennage shall withstand 3000 flight cycles without failure.
REQ-UAV-EMP-STR-7	The empennage shall be able to operate within a temperature range of -20 to 100°C.
REQ-UAV-EMP-AER-1	The empennage shall provide a minimum lift to drag ratio of 5.
REQ-UAV-EMP-AER-2	The empennage stall speed shall be lower than the wing stall speed.
REQ-UAV-EMP-AER-3	The empennage stall angle of attack shall be higher than the wing stall angle of attack.
REQ-UAV-SAC-1	The UAV shall have a flight control system.
REQ-UAV-SAC-2	The UAV shall be able to autonomously perform the mission.
REQ-UAV-SAC-3	The UAV shall be in equilibrium when on ground.
REQ-UAV-SAC-4	The UAV shall be longitudinally, directionally and laterally statically stable during all operations.
REQ-UAV-SAC-5	The UAV shall be dynamically stable.
REQ-UAV-SAC-6	The UAV shall be controllable about all axis.
REQ-UAV-SAC-7	The UAV shall be able to roll 60° in 1.3 seconds during cruise.
REQ-UAV-SAC-8	The UAV shall have a maximum pitch acceleration of at least 5 rad/s^2 during cruise.
REQ-UAV-SAC-9	The UAV shall have a maximum yaw acceleration of at least 5 rad/s^2 during cruise.
REQ-UAV-SAC-10	The UAV shall have a maximum pitch acceleration of at least 15 rad/s^2 during VTOL.
REQ-UAV-SAC-11	The UAV shall have a maximum roll acceleration of at least 15 rad/s^2 during VTOL.
REQ-UAV-SAC-12	The UAV shall have a maximum yaw acceleration of at least 5 rad/s^2 during VTOL.
REQ-UAV-SAC-13	The UAV shall be able to maintain attitude when experiencing cross-winds of up to 44.44 m/s.

11.2.Empennage Configuration Trade-off

The empenage configuration needs to be traded off to allow the best compromise between flight control and stability and operations and ground support as well as mission execution such as suppression and landing.

11.2.1.Determining Trade-Off Criteria, Weights, and Scoring

After reviewing the requirements defined in Section 5.4, the following trade-off criteria were chosen.

- **Risk** – The UAV must maintain stability and control even during partial system failures. Designs with coupled surfaces may pose higher risks than those with fully independent surfaces. With this said, evaluated under risk is the redundancy and the complexity of the system. The complexity may also be seen as the cost of the system, as a higher complexity results in higher development and maintenance costs.
- **Mass** – The structural weight of the empennage components need to be minimised, including mounting structures, boom structures, and actuators.
- **Sustainability** – This criterion assesses the aerodynamic efficiency of the empennage in terms of the amount of drag it creates.
- **Controllability** – Controllability encompasses flight dynamics characteristics such as yaw-roll coupling and deep stall (turbulent flow from wings and the engine interacts with tails).

Figure 11.2 shows the requirements represented by each criterion.

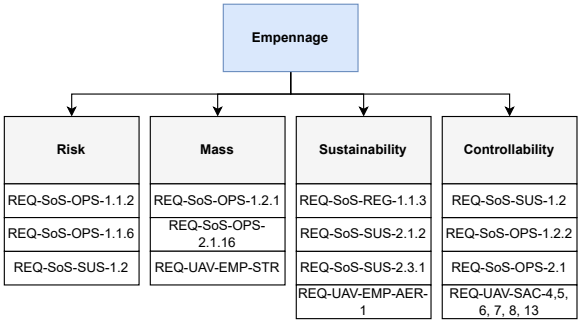

Figure 11.2: Criteria for empennage trade-off selection.

Table 11.2: Weight distribution matrix for empennage trade-off criteria (0 = less important, 1 = equally important, 2 = more important).

Comparison Criteria	Risk	Mass	Sustainability	Controllability
Risk	x	0	0	0
Mass	2	x	1	0
Sustainability	2	1	x	0
Controllability	2	2	2	x
Total	6	3	3	0
Final Weight	**0.3**	**0.25**	**0.25**	**0.2**

Table 11.2 was used to find the weights of all criteria. Table 11.3 shows how the scoring is given to each criterion for each design option.

Table 11.3: Scoring rubric for empennage trade-off criteria.

Criteria	1 - Critical Concern	2 - Major Deficiency	3 - Needs Improvement	4 - Acceptable	5 - Good Performance	6 - Excellent
Risk	Design is too complex to control. There is too much coupling between yaw and pitch.	Design has a very high complexity. There is very significant coupling between yaw and pitch.	Design has high complexity. There is significant coupling between yaw and pitch.	Design has medium complexity. There is no coupling between yaw and pitch.	Design has low complexity. There is no coupling between yaw and pitch.	Design has very low complexity. There is no coupling between yaw and pitch.
Mass	Impossible to meet mass requirements	Mass meets allocated budget at extensive detriment to the mission	Mass meets allocated budget at acceptable compromise to performance	Mass meets allocated budget with minimal compromise to performance	Mass meets allocated budget	Mass is below the allocated budget, allowing for further performance investments
Sustainability	Fuel efficiency is too low, leading to an unacceptable range.	Fuel efficiency is very low, leading to a very low range.	Fuel efficiency is low, leading to a low range.	Fuel efficiency is medium, leading to a medium range.	Fuel efficiency is high, leading to a high range.	Fuel efficiency is very high, leading to a very high range.
Controllability	Design is non-manoeuvrable	Design has very low manoeuvrability	Design has low manoeuvrability	Design has medium manoeuvrability	Design has high manoeuvrability	Design has very high manoeuvrability

11.2.2.Design Options Considered

It was decided that a single pusher engine is needed as camera clearance is needed at the front of the UAV. This makes the twin-boom configuration more attractive than its single-boom counterpart.

However, twin-boom configurations have high drag, so, to determine which option is best, the C_{D_0} of the single and twin-boom configuration is calculated based on the Class II estimations performed in. The single-boom configuration is where the fuselage extends until the empennage and the engine is placed behind the tail. In this configuration, two short booms, mounted on the wing, are still required for carrying the VTOL propellers. The twin-boom configuration has a short fuselage and two long booms, mounted on the wing, that extend backward to carry the empennage. The C_{D_0} estimates can be seen in Table 11.4. These conclude that there is a C_{D0} difference of 0.0013 between both configurations, which translates into an added drag of $0.9\,\mathrm{N}$, and an added power of $22.4\,\mathrm{W}$ at a speed of $25\,\mathrm{m{\cdot}s^{-1}}$. Although this is still a Class II estimation, it shows that there is only a slight difference in drag between the single-boom and twin-boom configurations. Seeing that the single-boom configuration results in a much more complex design due to having the empennage and main engine in the same location, it was decided that the final design will be twin-boom. Placing the main engine next to the empennage would also result in a rear shift of the centre of gravity, destabilising the UAV, and there would be added complexity for embedding the engine in the tail as well as the supporting systems such as fuel lines. Having a twin-boom configuration is also beneficial for packing the UAVs in the base station, as the booms may be disassembled, reducing the space occupied by a UAV.

Table 11.4: Comparison of zero-lift drag between single-boom and twin-boom configurations.

	Single-boom	Twin-boom
$C_{D_{0,\text{fuselage}}}$	0.0057	0.0047
$C_{D_{0,\text{booms}}}$	0.0032	0.0056
$C_{D_{0,\text{booms+fuselage}}}$	0.0089	0.0103

The empennage options considered for a twin-boom configuration are:

- **Inverted U-tail** – Two vertical tails that extend above the booms. The horizontal tail is placed between the two vertical tails, at their top ends.
- **U-tail** – Two vertical tails that extend below the booms, acting as landing gear. The horizontal tail is placed between the two vertical tails, slightly above their bottom ends for ground clearance.
- **Inverted V-tail** – Two diagonal tails that extend above the booms and connect at their top ends.
- **V-tail** – Two diagonal tails that extend below the booms and connect at their bottom ends. The joint at the bottom is used as landing gear.

An option where the horizontal tail is placed inside the propeller wash is not considered, as the vortices generated by the tip of the propeller blades would induce vibrations on the tail structure [11]. This would then induce vibrations in the entire aircraft, reducing the quality of the images taken by the camera.

11.2.3.Trade-Off Summary Table

Table 11.5 shows the trade-off for the empennage configuration.

Table 11.5: Trade-off table for empennage configuration.

Empennage Configuration	Risk (0.3)	Mass (0.25)	Sustainability (0.25)	Controllability (0.2)
Inverted U-tail	Same complexity as conventional tail. Two vertical tails so added redundancy. [Blue, 6]	Vertical tail sweep allows for a longer horizontal tail arm, decreasing the size of the horizontal tail. But vertical tails must be stronger to carry load from horizontal tail [27]. Also may require vortilons to avoid deep stall [27]. Two vertical tails means added mass. [Orange, 3]	Low induced drag due to having the vertical tails act as winglets that increase the effective aspect ratio of the horizontal tail [27]. The horizontal tail has the same effect on the vertical tails. Vertical tails outside fuselage wake. However, two vertical tails so higher friction drag. [Green, 4]	Turbulent air from wing on tail at high angles of attack leads to deep stall [27]. But best stability and manoeuvrability characteristics [28]. [Green, 4]
U-tail	Same complexity as conventional tail. Two vertical tails so added redundancy. [Blue, 6]	Vertical tail sweep allows for a longer horizontal tail arm, decreasing the size of the horizontal tail. Tail can be used as landing gear. But vertical tails must be stronger to carry load from horizontal tail [27]. Two vertical tails means added mass. [Green, 4]	Low induced drag due to having the vertical tails act as winglets that increase the effective aspect ratio of the horizontal tail [27]. The horizontal tail has the same effect on the vertical tails. Vertical tails outside fuselage wake. No rear landing gear so less drag. However, two vertical tails so higher drag. [Green, 5]	Positive yaw-roll effect, and best stability and manoeuvrability characteristics [28]. [Blue, 6]
Inverted V-tail	Complex control system due to coupling between pitch, roll, and yaw [27]. Same surface for pitch and yaw, so if it fails, controllability is lost in both axes. [Orange, 3]	Only two surfaces so lower mass. [Green, 4]	Low induced drag due to having higher aspect ratio [27]. Tail outside wing wake. [Green, 5]	Adverse yaw-roll effect [27] and less stability and manoeuvrability [28]. [Orange, 3]
V-tail	Complex control system due to coupling between pitch, roll, and yaw [27]. Same surface for pitch and yaw, so if it fails, controllability is lost in both axes. [Orange, 3]	Only two surfaces so lower mass, and tail can be used as landing gear. [Green, 5]	Low induced drag due to having higher aspect ratio [27]. Tail outside wing wake. No rear landing gear so less drag. [Blue, 6]	Positive yaw-roll effect [27], but less stability and manoeuvrability [28] [Green, 4]

This produces the following final scores, shown in Table 11.11.

Table 11.6: Resulting scores for empennage trade-off.

Option	Inverted U-tail	U-tail	Inverted V-tail	V-tail
Score (weighted)	4.35	5.25	3.75	4.45

As shown by the scores, the highest-scoring option is the U-tail. The V-tail has a close score due to its high fuel efficiency, but that does not compensate for its increased complexity and decreased controllability.

11.2.4.Sensitivity Analysis

To ensure that the U-tail may be chosen as the final empennage design, a sensitivity analysis is performed, which can be seen in Table 11.7. A description of what the numbers in this table represent is shown in Chapter 6.

Table 11.7: Sensitivity analysis of the empennage trade-off.

Option	Type	Risk	Mass	Sustainability	Controllability
Weight	Value	0.3	0.25	0.25	0.2
	Delta	-0.25	0.35	0.35	N/A
Inverted U-tail	Value	6	3	4	4
	Delta	3	4	4	5
U-tail	Value	6	4	5	6
	Delta	-3	-3	-3	-4
Inverted V-tail	Value	3	4	5	3
	Delta	5	6	6	8
V-tail	Value	3	5	6	4
	Delta	3	3	3	4

It is clear that large changes in weights or scores are required in order for a new choice to appear as the primary contender. Uncertainties in the scoring can not cause a change in design configuration, and so the final choice is reliable.

11.3.Empennage Airfoil Selection

In Table 11.5 it was determined that the empennage will be a U-tail, that also serves as a landing gear. The airfoil for the horizontal and vertical tail can now be chosen, the aerodynamic analysis will be done in XFLR5 at cruise conditions with a Reynolds number of 340 000 based on a 0.2 metre chord length.

11.3.1.Determining Trade-Off Criteria, Weights, and Scoring

- C_{l_α} – The slope of the lift curve is important in the context of static stability and control effectiveness. A high C_{l_α} means that for a small change of AoA of the control surface will give the same lift force. This also makes empennage more responsive to smaller inputs. It decreases required tail size and increases efficiency by reducing drag [29].
- $C_{d_{cr}}$ – This reflects the airfoil's ability to minimise drag during cruise. Lower drag leads to better fuel efficiency and higher cruise speed for the same power.
- **Stall AoA** – The empennage also needs a large range of usable AoA, such that the control surfaces can be used more extremely without stalling. Thus is it beneficial to have a large stall angle [29].
- **t/c** – This criterion is only used for the vertical tail, since it will act as a landing gear it needs to have a big enough thickness such that it will not buckle. The thickness-to-chord ratio is not considered for the horizontal tail.

Table 11.8: Weight distribution matrix for empennage airfoil trade-off (0 = less important, 1 = equally important, 2 = more important).

Comparison Criteria	C_{l_α}	$C_{d_{\text{cruise}}}$	Stall AoA	t/c
High C_l Slope	X	2	2	1
C_d at Cruise	0	X	1	0
Stall AoA	0	1	X	0
t/c	1	2	2	X
Total	1	5	5	1
Final Weight	**0.1**	**0.4**	**0.4**	**0.1**

The weights per criterion for the vertical tail are given in Table 11.8, however the horizontal tail does not consider t/c. When removing this criterion, the weight distribution is: 0.1, 0.45, 0.45 and for the trade-off these weights are displayed as: criterion (vertical weight | horizontal weight).

11.3.2.Design Options Considered

Airfoil National Advisory Committee for Aeronautic (NACA) 0009, 0012, 0015, 23012 inverted, and BAC317 have been selected for the empennage based on common use and recommendations made by Torenbeek [29]. During the trade-off, only the symmetrical airfoils will be considered for the vertical tail, since no lift is required at zero AoA.

11.3.3.Trade-Off Summary Table

The values and characteristics for each criteria are displayed in Table 11.9, scored in Table 11.10. With the final result per airfoil is given in Table 11.11.

Table 11.9: Comparison of symmetric airfoil design options. The bars are indicating the magnitude of the value.

Design Option	C_{l_α} (0.1 | 0.1)	$C_{d_{\text{cruise}}}$ (0.4 | 0.45)	Stall AoA (0.4 | 0.45)	t/c (0.1 | 0)
BAC 317	0.1076	0.0053	14	11.3
NACA 0009	0.1214	0.0044	10	9.0
NACA 0012	0.1135	0.0055	15	12.0
NACA 0015	0.1067	0.0065	14.5	15.0
23012 inverted	0.1020	0.0060	8.5	12.0

Table 11.10: Trade-off table for symmetric and inverted airfoil options.

Airfoil	C_{l_α} (0.1 | 0.1)	$C_{d_{\text{cruise}}}$ (0.4 | 0.45)	Stall AoA (0.4 | 0.45)	t/c (0.1 | 0)
BAC 317	4	4	5	4
NACA 0009	6	6	2	3
NACA 0012	5	4	6	4
NACA 0015	4	2	5	6
NACA 23012 inverted	3	3	1	4

Table 11.11: Resulting scores for empennage airfoil trade-off.

Option	BAC 317	NACA 0009	NACA 0012	NACA 0015	NACA 23012 inverted
Score (weighted) vertical tail	/	4.1	4.9	3.8	/
Score (weighted) horizontal tail	4.45	4.2	5.0	3.55	2.1

11.3.4.Sensitivity Analysis

With the trade-off conducted, a sensitivity analysis is in order. This allows for a quantification of the importance of each criterion in assessing the final chosen option, as well as the variance in results given a shift in this quantification. Both these analyses are combined into Table 11.12 to show all the results. All deltas that show a sensitive weight or score (less than 2 or 0.2 for scores or weights, respectively) are highlighted in yellow.

Table 11.12: Sensitivity analysis of empenneage airfoil trade-off.

Option	Type	C_{l_α}	$C_{d_{\text{cruise}}}$	Stall AoA	t/c
Weight	Value	0.1	0.4	0.4	0.1
	Delta	0.4	0.15	-0.15	0.35
BAC 317	Value	4	4	5	4
	Delta	5	1	1	5
NACA 0009	Value	6	6	2	3
	Delta	8	2	2	8
NACA 0012	Value	5	4	6	4
	Delta	-5	-1	-1	-5
NACA 0015	Value	4	2	5	6
	Delta	11	3	3	11
23012 inverted	Value	3	3	1	4
	Delta	26	7	7	26

It is clear that BAC 317, NACA 0019 and NACA 0012 are all closely contested options as small variances in their scores for drag and stall characteristics cause them to come out as the chosen option instead. This highlights that while the NACA 0012 is the most valued airfoil, it only marginally edges out a few other choices; nonetheless, NACA 0012 is still retained due to the trade-off being done based on numerical values and not qualitatively. Furthermore, the weights of these two criteria also largely affect the outcome given a slight change. Therefore, it can be concluded that the drag and stall characteristics of these airfoils closely match each other in terms of their effect on their attractiveness in the empennage design.

11.4.Component Positioning

The component positioning includes the determination of the location of the components to ensure the overall design is physically feasible, while considering the centre of gravity range. The component positioning strongly relies on the analysis performed in previous steps and is an iterative process as it determines the stability and controllability characteristics of the UAV. In the most recent iteration step, the parameters in Table 11.13 have iteratively been updated and will be used for the following chapters.

Table 11.13: Summary of values after final iteration.

ID	Value	Unit	ID	Value	Unit
MTOW	64.64	kg	W_{Fuel}	5.28	kg
W_{OE}	44.6	kg	S	1.87	m^2
b	4.32	m	Range	350	km
W_{PLD}	15.91	kg	V_{cr}	25.9	m/s
$V_{H_{max}}$	33	m/s	$C_{L_{cr}}$	1.06	-
$C_{D_{cr}}$	0.04	-	L/D_{cruise}	11.7	-

Using the results from previous design steps combined with a visual analysis in CATIA, the operational empty weight components were carefully placed while trying to keep enough space close to the centre of gravity, as the fuel tank and the suppressant payload might change the centre of gravity location significantly during the flight, if positioned inappropriately. In addition, the fuel and suppressant take will be placed on top of each other, allowing their centre of gravity positions to be the same. To position the operational empty weight components, the subsystems were divided into a wing and fuselage group. This allocation is provided in Table 11.14, where the fuselage group components' centre of gravity is measured from the nose of the UAV, while that of the wing group is measured from the leading edge of the mean aerodynamic chord.

Important to note is also that the VTOL system will as well be centred around the operational empty weight location as it allows for the most efficient and stable flight during vertical take-off and landing.

Table 11.14: Masses and centre of gravity locations of UAV components.

Group	Component	Mass [kg]	CG Location [m]
Fuselage	Engine	3.03	1.572
	Fuselage + half paint	3.02	0.597
	Hardware	3.40	0.315
	Surveillance payload	0.91	0.060
	Landing gear	0.80	0.674
	Battery (VTOL)	10.80	0.450
	Fuselage group	21.96	0.596
Wing	Wing + half paint	6.58	0.188
	Booms	5.40	0.467
	Empennage	1.17	1.700
	VTOL system	9.25	0.118
	Wing group	22.40	0.305
Operational empty weight components		44.36	0.788
Removable components	Fuel	5.28	0.788
	Suppression payload	15	0.788
Maximum take-off weight components		64.64	0.788

To relate the position of the fuselage and wing group, a position of the operational empty weight with respect to the wing must be chosen. For that, the operational empty weight is positioned at 0.25 of the mean aerodynamic chord of the wing, which lies well within the range suggested by R. Vos [30] of 0.15 and 0.3. Using this estimate, combined with the centre of gravity location of the subcomponents and the formula provided in Equation 11.1 the position of the leading edge of the mean aerodynamic chord X_{LEMAC} can be determined.

$$X_{\text{LEMAC}} = X_{\text{FSG}} + \bar{c}\left[\left(\frac{x}{\bar{c}}\right)_{\text{WCG}} \frac{M_W}{M_F} - \left(\frac{x}{\bar{c}}\right)_{\text{OEWCG}} \left(1 + \frac{M_W}{M_F}\right)\right] \tag{11.1}$$

Here, X_{FCG} is the fuselage group centre of gravity, $\bar{c} = 0.47\,\text{m}$ is the mean aerodynamic chord of the wing and $\left(\frac{x}{\bar{c}}\right)_{WCG}$ and $\left(\frac{x}{\bar{c}}\right)_{OEWCG}$ the wing and operational empty weight position with respect to the mean aerodynamic chord, respectively. Furthermore, M_W and M_F correspond to the total mass of the fuselage. The obtained X_{LEMAC} position is found to be at $0.67\,\text{m}$ and allows to obtain the operational empty weight position $X_{CG_{OEW}} = 0.788\,\text{m}$ from the nose using Equation 11.2.

$$X_{\text{CG}_{\text{OEW}}} = X_{\text{LEMAC}} + \left(\frac{x}{\bar{c}}\right)_{\text{OEWCG}} \bar{c} \tag{11.2}$$

Following the approach of iteratively positioning the components, while leaving enough space for the fuel and suppression payload, it was possible to position the removable components at the same location as the operational empty weight. This is shown in the removable component row in Table 11.14. Furthermore, the maximum take-off weight is shown with the centre of gravity location positioned on top of the operational empty weight. Furthermore, anti-sloshing vanes are used to reduce the centre of gravity shift to a minimum during operations. A picture of the component positioning is provided in Figure 11.3. In addition to this, the centre of gravity range is also analysed using a loading diagram. This is plotted in Figure 11.4, where the operational empty weight is the lowest point and the fuel and payload weights are added after each other to analyse the minimum and maximum possible centre of gravity location during operations. As these could be positioned at the operational empty weight centre of gravity, the discussed lines are purely vertical, not shifting the MTOW centre of gravity position. Accounting for uncertainty in the design, a 2% margin is applied. Furthermore, in Figure 11.4 the final range is provided, showing the change during operations.

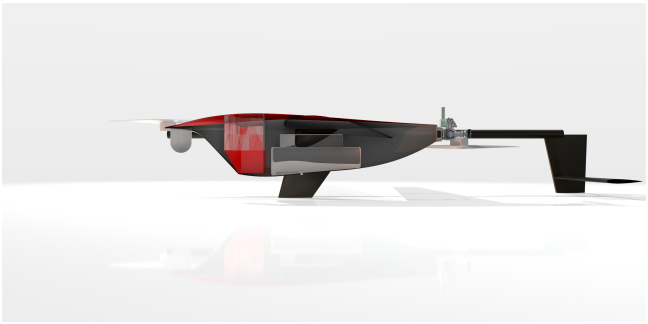

Figure 11.3: Fuselage component side view.

Parameter	CG from x_{LEMAC} [%MAC]
OEW CG	25.0%
Min CG + 2% Margin	23.0%
Max CG + 2% Margin	27.0%

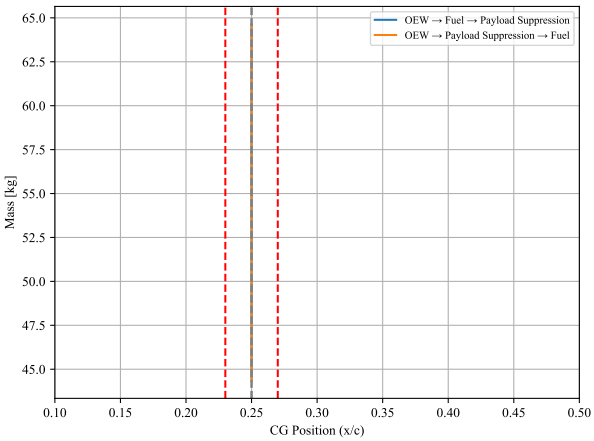

Figure 11.4: Loading diagram describing the centre of gravity location shift when adding the removable components in variable order.

11.5.Tail Sizing

This section discusses the tail sizing of the UAV. This includes the vertical tail and the horizontal tail which must be designed appropriately to be able to control and stabilise the aircraft.

11.5.1.Preliminary Tail Sizing

Empennage planform design is the next step, as it determines the basic dimensions of the tail. The sizing is performed following the tail volume method for single propeller aircraft described by Roskam [11]. Based on reference aircraft, a horizontal tail volume $\bar{V}_h$ of 0.667 and vertical tail volume $\bar{V}_v$ of 0.0436 is found. The respective surface areas can be calculated using Equation 11.3 and Equation 11.4:

$$S_h = \frac{\bar{V}_h S \bar{c}}{X_h - X_{\text{aft,cg}}}, \qquad (11.3) \qquad S_v = \frac{\bar{V}_v S b}{X_v - X_{\text{aft,cg}}}. \qquad (11.4)$$

During the calculations for the vertical tail, $S_v/2$ will be used as surface area, since a U-tail configuration was chosen in Section 11.2, where the vertical tail is divided into two surfaces.

A separate parameter to consider is the sweep of the wing. Sweep is used mainly as a way to delay drag divergence at higher Mach number, and to improve stability [1]. Nevertheless, the expected Mach number is much lower than when drag divergence is to be expected in accordance with ASM-MIS-05; as such, the quarter-chord sweep for both tails is $\Lambda_{0.25c} = 0$.

The U-configuration empennage makes it that the span of the horizontal tail is the same as the distance between the two booms $1.52\,\text{m}$. Additionally, the tip and chord are the same length since the horizontal tail will have a rectangular planform, so the chord can be determined by dividing S_h by b_h. The tip of the vertical tail has to be the same length as the chord of the horizontal tail since they will be placed on top of each other. The span of the vertical tail b_V is fixed by the height of the booms to the ground 376 mm. The root chord c_r for the vertical tail can be found using Equation 11.5:

$$c_r = \frac{c_t}{\lambda}, \qquad (11.5), \text{ with} \qquad \lambda = \frac{c_t b_V}{2S - c_t b_V}. \qquad (11.6)$$

The final values of the vertical tail are displayed in Table 11.15, the horizontal tail needs additional analysis for stability.

[1] See: https://www.boldmethod.com/learn-to-fly/aerodynamics/straight-tail-vs-swept/?text=A%20Swept%20Tail%20Flies%20Like%20A%20Swept%20Wing&text= Accessed 06-06-2025

Table 11.15: Vertical tailplane geometric parameters.

Parameter	Symbol	Value	Unit
Vertical tail root chord	c_v	0.25	m
Vertical tail span	b_v	0.40	m
Vertical tail area (total)	S_v	0.20	m^2
Vertical tail aspect ratio	A_v	1.60	–
Quarter-chord sweep angle	$\Lambda_{0.25,v}$	0	rad
Vertical tail taper ratio	λ_v	0.82	–

11.5.2.Scissor Plot

Table 11.16: Scissor plot input parameters.

Parameter	Symbol	Value	Unit
Wing lift curve slope	$C_{L_{\alpha_w}}$	5.20	1/rad
Tailplane aspect ratio	A_h	7.60	–
Taper ratio	λ	0.4	–
Fuselage width	b_f	0.31	m
Fuselage height	h_f	0.343	m
Fuselage length	l_f	1.492	m
Geometric wing chord	c_g	0.442	m
Wing root chord	C_r	0.617	m
Tail moment arm	l_h	1.7	m
Tail velocity ratio	$\frac{V_h}{V}$	1.0	–
Sweep angle at 25% chord	$\Lambda_{0.25}$	0	deg
Tail sweep angle at 50% chord	$\Lambda_{0.5_h}$	0	deg
Prandtl-Glauert compressibility factor	β	0.887	–
Zero-lift moment coefficient of airfoil	$c_{m_{0,\text{airfoil}}}$	-0.105	–
Lift coefficient at $\alpha = 0^\circ$	C_{L_0}	0.38	–
Maximum lift coefficient of the wing	$C_{L_{\text{max}}}$	1.539	–

During cruise condition, the horizontal tail must provide stability and controllability to the UAV, allowing it to operate as desired. The analysis underlying the sizing is the scissor plot [31], which consists of a stability and controllability line and the CG position range obtained from the loading diagram given in Figure 11.4. The functions for the stability and ccontrollability line are presented in Equation 11.7 and Equation 11.8, respectively and can be used to optimise the tail size. Both formulas have $\bar{x}_{cg}$ as the independent variable and are discussed successively.

$$\frac{S_h}{S} = \frac{1}{\frac{C_{L_{\alpha_h}}}{C_{L_{\alpha_{A-h}}}}\left(1-\frac{\partial\epsilon}{\partial\alpha}\right)\frac{l_h}{\bar{c}}\left(\frac{V_h}{V}\right)^2}\bar{x}_{cg} - \frac{\bar{x}_{ac}-0.05}{\frac{C_{L_{\alpha_h}}}{C_{L_{\alpha_{A-h}}}}\left(1-\frac{\partial\epsilon}{\partial\alpha}\right)\frac{l_h}{\bar{c}}\left(\frac{V_h}{V}\right)^2} \tag{11.7}$$

$$\frac{S_h}{S} = \frac{1}{\frac{C_{L_h}}{C_{L_{A-h}}}\frac{l_h}{\bar{c}}\left(\frac{V_h}{V}\right)^2}\bar{x}_{cg} + \frac{\frac{C_{m_{ac}}}{C_{L_{A-h}}}-\bar{x}_{ac}}{C_{L_{A-h}}\frac{l_h}{\bar{c}}\left(\frac{V_h}{V}\right)^2} \tag{11.8}$$

Starting with the stability line, the downwash gradient $\frac{\partial\epsilon}{\partial\alpha}$ can be obtained using Equation 11.6.2. The lift gradient coefficients of the tail and the tailless aircraft $C_{L\alpha_h}$ and $C_{L\alpha_{A-h}}$ are calculated using the DATCOM [31] method given by Equation 11.10 and Equation 11.11 respectively. In Equation 11.11 the lift gradient of the wing $C_{L_{\alpha_w}}$ has been obtained from the aerodynamic analysis and is given alongside the remaining input parameters in Table 11.16. S_{net} can be calculated using Equation 11.12 and corresponds to the wing surface area excluding the projected fuselage area.

$$\frac{\partial\epsilon}{\partial\alpha} = \frac{2C_{L_{\alpha_w}}}{\pi A} \tag{11.9}$$

$$C_{L_{\alpha_h}} = \frac{2\pi A_h}{2+\sqrt{4+\left(\frac{A_h\beta}{0.95}\right)^2\left(1+\frac{\tan^2\left(\Lambda_{0.5_h}\right)}{\beta^2}\right)}} \tag{11.10}$$

$$C_{L_{\alpha_{A-h}}} = C_{L_{\alpha_w}}\left(1+2.15\frac{b_f}{b}\right)\frac{S_{\text{net}}}{S}+\frac{\pi}{2}\frac{b_f^2}{S} \tag{11.11}$$

$$S_{net} = S - b_f c_r \tag{11.12}$$

The aerodynamic centre location $\bar{x}_{ac}$ of the tailless aircraft is determined by accounting for the contributions of the wing, fuselage and the nacelles as described in Equation 11.13. While the aerodynamic centre of the wing can be found from Figure 11.5 to be at the quarter chord, the fuselage consists of a stabilizing and destabilizing contribution as shown in Equation 11.14. These are calculated using Equation 11.15 and Equation 11.16. Lastly, the engine contribution can be neglected as the UAV has a single propeller with the engine at the back of the fuselage.

$$\bar{x}_{ac} = \frac{x_{ac}}{\bar{c}} = \frac{x_{ac_w}}{\bar{c}} + \frac{x_{ac_f}}{\bar{c}} + \frac{x_{ac_n}}{\bar{c}} \tag{11.13}$$

$$\frac{x_{ac_f}}{\bar{c}} = \frac{x_{ac_{f_1}}}{\bar{c}} + \frac{x_{ac_{f_2}}}{\bar{c}} \tag{11.14}$$

$$\frac{x_{ac_{f_1}}}{\bar{c}} = -\frac{1.8}{C_{L_{\alpha_{A-h}}}} \frac{b_f h_f l_f}{S\bar{c}} \tag{11.15}$$

$$\frac{x_{ac_{f_2}}}{\bar{c}} = \frac{0.273}{1+\lambda} \frac{b_f c_g (b - b_f)}{\bar{c}^2 (b + 2.15 b_f)} \tan(\Lambda_{0.25}) \tag{11.16}$$

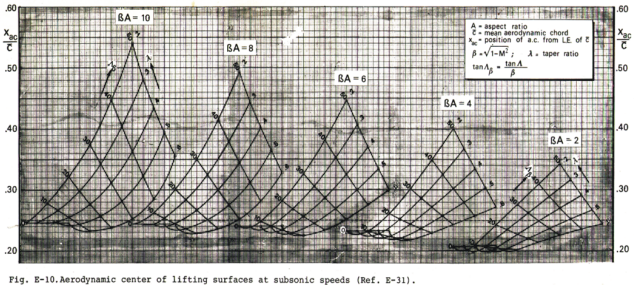

Fig. E-10. Aerodynamic center of lifting surfaces at subsonic speeds (Ref. E-31).

Figure 11.5: Wing aerodynamic centre location with respect to the UAV speed, taper ratio and sweep [29].

Moving on to the controllability line of the scissor plot, the tail lift coefficient C_{L_h} can be estimated using Equation 11.17, which is valid for fixed tails. The tailless aircraft lift coefficient $C_{L_{A-h}}$ is obtained by assuming it to be equivalent to the maximum lift coefficient of the wing, $C_{L_{max}}$ and is provided in the input table. This leaves only $C_{m_{ac}}$, which consists of a contribution of the wing, potential flaps, the fuselage and nacelles as shown in Equation 11.18. As the VTOL UAV does have flaps and nacelles outside the fuselage, only the wing and fuselage contribution need to be taken into account. The wing contribution is given by Equation 11.19 and relies on the zero lift moment coefficient of the airfoil that is obtained from XFLR5 and provided in Table 11.16. Lastly, the fuselage contribution follows from Equation 11.20, where again XFLR5 is employed to obtain the lift coefficient at an angle of attack of 0°. The resulting values are compiled in Table 11.17.

$$C_{L_h} = -0.35 A_h^{1/3}. \tag{11.17}$$

$$C_{m_{ac}} = C_{m_{ac_w}} + \Delta_f C_{m_{ac}} + \Delta_{\text{fus}} C_{m_{ac}} + \Delta_{\text{nac}} C_{m_{ac}} \tag{11.18}$$

$$C_{m_{ac_w}} = c_{m_{0,\text{airfoil}}} \frac{A \cos^2 \Lambda_{0.25}}{A + 2\cos \Lambda_{0.25}} \tag{11.19}$$

$$\Delta_{fus} C_{m_{ac}} = -1.8 \left(1 - \frac{2.5 b_f}{l_f}\right) \frac{\pi b_f h_f l_f}{4 S \bar{c}} \frac{C_{L_0}}{C_{L_{\alpha_{A-h}}}} \tag{11.20}$$

Table 11.17: Calculated parameters for scissor plot analysis.

Parameter	Symbol	Value	Unit
Downwash gradient	$\frac{\partial \epsilon}{\partial \alpha}$	0.314	–
Tail lift curve slope	$C_{L_{\alpha_h}}$	3.117	1/rad
Tailless lift curve slope	$C_{L_{\alpha_{A-h}}}$	5.196	1/rad
Net wing surface area	S_{net}	1.68	m^2
Aerodynamic centre of tailless aircraft	$\bar{x}_{ac}$	0.19	–
Wing aerodynamic centre	$\bar{x}_{ac_w}$	0.25	–
Fuselage aerodynamic centre 1	$\bar{x}_{ac_{f_1}}$	-0.06	–
Fuselage aerodynamic centre 2	$\bar{x}_{ac_{f_2}}$	0	–
Moment coefficient about ac	$C_{m_{ac}}$	-0.097	–
Wing moment coefficient about ac	$C_{m_{ac_w}}$	-0.088	–
Fuselage moment contribution	$\Delta_{\text{fus}} C_{m_{ac}}$	-0.009	–

With these results the scissor plot can be constructed for the design to analyse whether the stability and controllability is ensured during all conditions. For the construction of the stability line, a margin of 5% is added to guarantee stability of the aircraft. The scissor plot for the design can be found in Figure 11.6a.

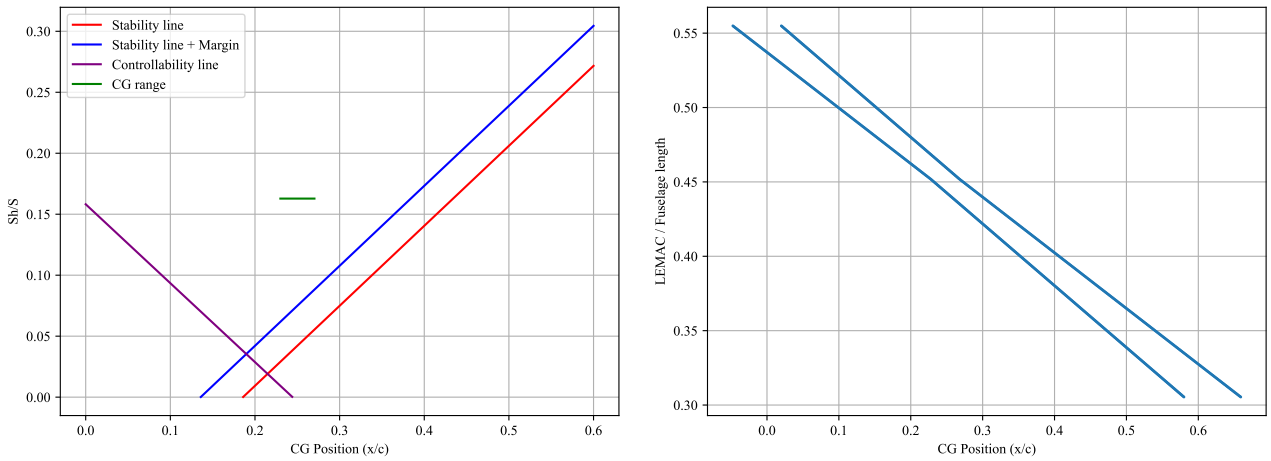

(a) Scissor plot describing the stability and controllability characteristics of the UAV.

(b) Centre of gravity range for different wing positions.

Figure 11.6: UAV stability and centre of gravity range.

The green line indicates the CG range during operations and lies well within the controllable and stable regime. To further analyse the design the operational empty weight location with respect to the wing and the horizontal tail area can be varied, determining the optimal combination for which the minimum and the and maximum CG range locations intersect with the controllability and stability line, respectively. This analysis is done using Figure 11.6b in combination with the scissor plot. However, after optimising the values, it has been found that the horizontal tail design is rather driven by the manufacturability and structural integrity as the low tail surface area would result in a horizontal tail chord of less than $5\,\mathrm{cm}$ and would make the implementation of control surfaces unfeasible. Thus, under compliance with the structural and physical constraints, the horizontal tail dimensions found in Table 11.18 will provide the desired properties during all mission phases.

Table 11.18: Horizontal tailplane geometric parameters.

Parameter	Symbol	Value	Unit
Horizontal tail chord	c_h	0.20	m
Horizontal tail span	b_h	1.52	m
Horizontal tail area	S_h	0.304	m^2
Horizontal tail aspect ratio	A_h	7.6	–
Quarter-chord sweep angle	$\Lambda_{0.25,h}$	0	rad
Horizontal tail taper ratio	λ_h	1.0	–

11.6.Control Surface Sizing

With the planform of the wing fully sized and the airfoil selected, the components residing on top can be sized. This concerns the control surfaces as well as the high-lift devices (HLDs). HLDs are not required as VTOL is the means by which the aircraft will take-off. The control surface sizing strongly depends on the sizing of the wing as well as the horizontal and vertical tail. The sizing will be done by using a combination of statistical values, design formulas and the subsystem requirements.

11.6.1.Aileron Sizing

Aileron sizing is conducted using the method defined by Raymer [15]. Its input parameters can be seen in Table 11.19.

Table 11.19: Aileron input parameters.

Parameter	Symbol	Value	Unit
Airfoil lift curve slope	$c_{l\alpha}$	5.91	1/rad
Root chord	C_r	0.617	m
Tip chord	C_t	0.247	m
Airfoil parasitic drag coefficient	c_{d_0}	0.008	–
Aileron chord ratio	-	0.15	-
Cruise velocity	V_{cruise}	25.9	m/s

The airfoil's lift curve slope and parasitic drag coefficient were obtained using an airfoil analysis in XFLR5. Sizing the aileron stems from a roll rate (p) requirement. This is derived as an unmanned equivalent to the Class I aircraft type roll rate requirement found in the MIL-F-8785B Specification [32] to be 60 degrees in 1.3 seconds (46.2 deg/s). This is achieved with a certain aileron length, width, and deflection angle. Its formula Equation 11.21 is retrieved from Raymer [15], where the control derivatives are given by the following integrals in Equation 11.22 and Equation 11.23:

$$p = -\frac{C_{l_{\delta a}}}{C_{l_P}} \delta a \left(\frac{2V}{b}\right), \tag{11.21}$$

$$C_{l_{\delta a}} = \frac{2c_{l\alpha}\tau}{Sb} \int_{b_1}^{b_2} c(y)\, y\, dy, \tag{11.22}$$

$$C_{l_P} = -\frac{4(c_{l\alpha} + c_{d_0})}{Sb^2} \int_0^{b/2} y^2\, c(y)\, dy. \tag{11.23}$$

Here, τ is the aileron-effectiveness factor, derived from the aileron chord ratio; this leads to $\tau = 0.35$ according to M. H. Sadraey [33]. Finally the integrals contain the width of the ailerons as its bounds b_1 and b_2, these stem from the statistical norm that Raymer developed [15]. With the above parameters determined, the deflection angle of the aileron can be determined which suffices the roll requirement. To achieve a 46.2 deg/s roll, a deflection angle of 12.72 degrees is required. Since this value is well within the margin typically seen, a value of 15 is taken such that the roll performance of the aircraft is improved. This corresponds to a roll rate of 54.5 deg/s. The final parameters of the ailerons can be seen in Table 11.20.

Table 11.20: Final aileron parameters.

Parameter	Symbol	Value	Unit
Aileron span (each)	b_a	0.86	m
Aileron mean aerodynamic chord	c_a	0.07	m
Aileron surface area (each)	S_a	0.06	m^2
Max aileron deflection (up and down)	δ_a	20	deg
Aileron half-span inner limit	$b1$	50	%
Aileron half-span outer limit	$b2$	90	%

11.6.2.Elevator Sizing

The elevator sizing is based on a design approach by M. H. Sadraey [33]. The elevator needs to be designed to stabilise the aircraft during cruise condition and allow pitch manoeuvrability during climb and decent. To ensure that the required pitch acceleration can be provided, the elevator chord can be chosen based on the angle of attack efficiency from Figure 11.7. The input parameters are compiled in Table 11.21, where the geometry parameters are estimated with Figure 11.8. The elevator angle of attack efficiency τ_e can be calculated using Equation 11.25, where α_h can be found with Equation 11.24 using the input parameters, Equation 11.26, Equation 11.27 and Equation 11.28.

Table 11.21: Elevator input parameters.

Parameter	Symbol	Value	Unit
Angle of attack	α	0.237	rad
Tailplane incidence angle	i_h	0.123	rad
Wing lift coefficient	C_{L_w}	1.54	–
Tail lift coefficient gradient	$C_{L_{\alpha_h}}$	3.117	–
Max elevator deflection	$\delta_{e_{\max}}$	20	deg
Min elevator deflection	$\delta_{e_{\min}}$	-25	deg
Tailplane lift curve slope	$C_{L_{\alpha_w}}$	4.938	1/rad
Tailplane lift coefficient	C_{L_h}	-0.69	–
Tail dynamic pressure ratio	η_h	1	–
Tail moment arm	l_h	1.7	m
Tailplane surface area	S_h	0.30	m^2
Elevator span ratio	$\frac{b_e}{b_h}$	0.8	–
Air density	ρ	1.225	kg/m^3
Moment of inertia (pitch)	I_{yy}	8.88	kgm^2

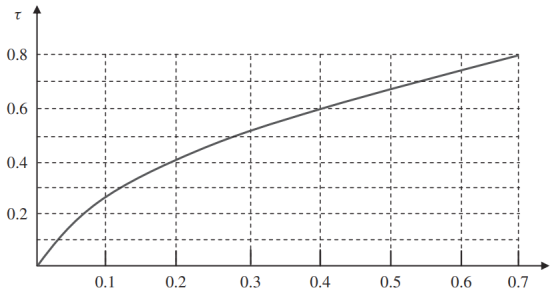

Figure 11.7: Angle of attack efficiency to chord ratio table [33].

Control surface	Elevator	Aileron	Rudder
Control surface area/lifting surface area	$S_E/S_h = 0.15–0.4$	$S_A/S = 0.03–0.12$	$S_R/S_V = 0.15–0.35$
Control surface span/lifting surface span	$b_E/b_h = 0.8–1$	$b_A/b = 0.2–0.40$	$b_R/b_V = 0.7–1$
Control surface chord/lifting surface chord	$C_E/C_h = 0.2–0.4$	$C_A/C = 0.15–0.3$	$C_R/C_V = 0.15–0.4$
Control surface maximum deflection (negative)	−25 deg (up)	25 deg (up)	−30 deg (right)
Control surface maximum deflection (positive)	+20 deg (down)	20 deg (down)	+30 deg (left)

Figure 11.8: Statistical dimensions of ailerons, elevators and rudders [33].

$$\alpha_h = \alpha + i_h - \epsilon \tag{11.24}$$

$$\tau_e = \frac{\alpha_h + \frac{C_{L_h}}{C_{L_{\alpha_h}}}}{\delta_{e_{min}}} \tag{11.25}$$

$$\epsilon = \epsilon_0 + \frac{\partial \epsilon}{\partial \alpha}\alpha \tag{11.26}$$

$$\epsilon_0 = \frac{2C_{L_w}}{\pi A} \tag{11.27}$$

$$\frac{\partial \epsilon}{\partial \alpha} = \frac{2C_{L_{\alpha_w}}}{\pi A} \tag{11.28}$$

The calculation results in an angle of attack efficiency τ_h of 0.64, which leads to an elevator chord ratio c_e/c_h of 0.44. To evaluate the compliance with the acceleration requirement, the pitch moment coefficient with can be calculated from Equation 11.29. From this, the maximum achievable pitch moment can be obtained using Equation 11.31, which in Equation 11.30 combined with the mass moment of inertia I_{yy} gives the angular pitch acceleration.

$$C_{m_{\delta e}} = -C_{L_{\alpha_h}} \eta_h \frac{l_h S_h}{S C_{\text{MAC}}} \frac{b_e}{b_h} \tau_h \tag{11.29}$$

$$\dot{q}_{max} = \frac{M_{e_{\text{max}}}}{I_{yy}} \tag{11.30}$$

$$M_{e_{max}} = \frac{1}{2}\rho V_{cruise}^2 S C_{MAC} C_{m_{\delta e}} \delta e_{min} \tag{11.31}$$

As a result, an angular pitch acceleration of $\dot{q}_{n_{max}} = 16.6\,\text{rad}\cdot\text{s}^{-2}$ can be achieved during cruise conditions and confirms compliance with the requirements and functionality of the design. The final elevator design parameters are provided in Table 11.22.

Table 11.22: Final elevator parameters.

Parameter	Symbol	Value	Unit
Elevator span	b_e	1.22	m
Elevator mean aerodynamic chord	c_e	0.09	m
Elevator surface area	S_e	0.107	m^2
Max elevator deflection	δe_{max}	20	deg
Min elevator deflection	δe_{min}	-25	deg

11.6.3.Rudder Sizing

Similarly to the elevator design, the rudder sizing is performed using the method provided by M. H. Sadraey [33]. Just as for the vertical tail design, the dimensions of the rudder can be obtained by analysing the critical mission design phase. Since the goal is to be able to operate in strong winds of up to $160\,\text{km}\cdot\text{h}^{-1}$ during the suppression phase, cross-winds are expected to be the driving factor. The general approach relies on choosing dimensions from statistical data given in Figure 11.8 and proving that these dimensions provide the required performance. The parameters in Table 11.23 are used as input to obtain the maximum required deflection angle of the rudder from the system of two non-linear equations provided in Equation 11.32 and Equation 11.33 with $\delta_{r_{req}}$ and σ as independent variables.

Table 11.23: Rudder input parameters.

Parameter	Symbol	Value	Unit
Rudder span ratio	$\frac{b_R}{b_V}$	1.0	–
Rudder chord ratio	$\frac{c_R}{c_V}$	0.4	–
Max rudder deflection	$\delta r_{\max}$	30	deg
Air density	ρ	1.225	kg/m^3
Cross-wind velocity	V_{cross}	44.44	m/s
Cruise velocity	V_{cruise}	25.9	m/s
Dive velocity	V_{dive}	36.2	m/s
Vertical tail span	b_V	0.4	m
Vertical tail chord	c_V	0.25	m
Side drag coefficient	C_{D_y}	0.5	–
Fuselage length	l_f	1.492	m
Fuselage height	h_f	0.343	m
OEW CG location	$X_{\text{cg,OEW}}$	0.788	m
Vertical tail moment arm	l_V	1.70	m
Vertical tail lift curve slope	$C_{L_{\alpha_V}}$	3.117	1/rad
Side wash gradient	$\frac{d\sigma}{d\beta}$	0	–
Dynamic pressure ratio	η_V	1	–
Fuselage correction factor 1	K_{f1}	0.7	–
Fuselage correction factor 2	K_{f2}	1.4	–
Moment of inertia (yaw)	I_{zz}	15.488	kgm^2

$$\frac{1}{2}\rho V_{\text{tot}}^2 Sb(C_{n_\beta}(\beta-\sigma)+C_{n_{\delta r}}\delta r_{\text{req}})+F_w d_c\cos\sigma=0 \tag{11.32}$$

$$\frac{1}{2}\rho V_{\text{tot}}^2 S(C_{y_\beta}(\beta-\sigma)+C_{y_{\delta r}}\delta r_{\text{req}})=\frac{1}{2}\rho V_{\text{cross}}^2 S_S C_{D_y} \tag{11.33}$$

To solve the system of equations, several additional parameters need to be determined. First, the total velocity V_{tot} and the side slip angle β, resulting from the combination of cross-wind under an angle of 90° and the dive speed used during suppression, are obtained with Equation 11.34 and Equation 11.35. Next, the projected horizontal surface area S_S is calculated using Equation 11.36, which consists of a conservative contribution of the projected fuselage area and vertical tail area and serves as an input for aircraft side force F_w that is calculated using Equation 11.37. Furthermore, x_{ca}, representing the centre of the aircraft is obtained in Equation 11.38 to determine its distance to the centre of gravity of the UAV d_c. The remaining inputs are the four stability derivatives C_{n_β}, C_{y_β}, $C_{n_{\delta r}}$, $C_{y_{\delta r}}$ calculated in Equation 11.40, Equation 11.41, Equation 11.42 and Equation 11.43, respectively, and the angle of attack effectiveness of the rudder that can be obtained from Figure 11.7.

$$V_{\text{tot}}=\sqrt{V_{\text{cross}}^2+V_{\text{dive}}^2} \tag{11.34}$$

$$\beta=\arctan\left(\frac{V_{\text{cross}}}{V_{\text{dive}}}\right) \tag{11.35}$$

$$S_S=l_f h_f+2c_V b_V \tag{11.36}$$

$$F_w=\frac{1}{2}\rho V_{\text{cross}}^2 S_S C_{D_y} \tag{11.37}$$

$$x_{ca}=\frac{l_f h_f \frac{l_f}{2}+2c_V b_V(X_{\text{cg,OEW}}+l_V)}{l_f h_f+2c_V b_V} \tag{11.38}$$

$$d_c=x_{ca}-X_{\text{cg,OEW}} \tag{11.39}$$

$$C_{n_\beta}=K_{f1}C_{L_{\alpha_V}}\left(1-\frac{d\sigma}{d\beta}\right)\eta_V\frac{l_V 2c_V b_V}{bS} \tag{11.40}$$

$$C_{Y_\beta}=-K_{f2}C_{L_{\alpha_V}}\left(1-\frac{d\sigma}{d\beta}\right)\eta_V\frac{2c_V b_V}{S} \tag{11.41}$$

$$C_{n_{\delta r}}=-C_{L_{\alpha_V}}\frac{l_V 2c_V b_V}{bS}\eta_V\tau_r\frac{b_R}{b_V} \tag{11.42}$$

$$C_{Y_{\delta r}}=C_{L_{\alpha_V}}\eta_V\tau_r\frac{b_R}{b_V}\frac{2c_V b_V}{S} \tag{11.43}$$

From the system of equations, a required elevator deflection of 29.0° is obtained, indicating that the maximum deflection of 30° will be sufficient during all mission phases. To further determine the adherence to the requirements, the angular yaw acceleration will be analysed in the following. Using the input parameters, the maximum achievable moment provided by the rudder will be calculated in Equation 11.44. With this, the angular yaw acceleration $\dot{r}_{n_{max}}$ is found to be $8.8\,\text{rad}\cdot\text{s}^{-2}$

during cruise conditions by using Equation 11.45. This shows that the rudder is able to perform the desired manoeuvres. The relevant rudder parameters can be found in Table 11.24

$$N_{r_{\max}} = \frac{1}{2}\rho V_{\text{cruise}}^2 S b C_{n_{\delta r}} \delta_{r_{\max}} \tag{11.44}$$

$$\dot{r}_{n_{\max}} = \frac{N_{r_{\max}}}{I_{zz}} \tag{11.45}$$

Table 11.24: Final rudder parameters.

Parameter	Symbol	Value	Unit
Rudder span	b_R	0.4	m
Rudder mean aerodynamic chord	c_R	0.075	m
Rudder surface area	S_R	0.03	m^2
Max rudder deflection	$\delta_{r_{\max}}$	30	deg
Min rudder deflection	$\delta_{r_{\max}}$	-30	deg

11.7.Dynamic Stability

The dynamic stability characteristics of the UAV are assessed using XFLR5, which allows for a stability analysis of an aircraft given its wing and tail planform sizes as well as the distribution of each component's weights. The model geometry parameters are listed in Table 11.25. XFLR5 is well suited to analyses at low Reynolds numbers as the model primarily considers viscous forces, and only partially simulates laminar separation bubbles; this goes against the conditions expected. With the cruise velocity established at $V_{\text{cruise}} = 25.9$ m/s, a characteristic length of $c_{mac} = 0.459$ m (the mean aerodynamic chord, established in the Midterm Report), and using the fluid characteristics of air at sea level, a Reynolds number around 800 000 is obtained. This is considerably higher; nevertheless, a stability analysis is still useful in gaining an understanding of how the aircraft behaves. The analysis focuses on the aircraft's response to small perturbations to its pitch, roll, and yaw in trimmed flight, examining both longitudinal and lateral-directional dynamic eigenmotions.

Table 11.25: XFLR5 Model Geometry.

Lifting Surfaces	Panels in X	X-distribution	Panels in Y	Y-distribution	VLM Panels	3D panels
Main Wing	20	Cosine	40	Uniform	800	1620
Horizontal Tail	5	Cosine	25	Uniform	250	510
Vertical Fins	15	Cosine	25	Uniform	375	780

The geometry of the aircraft's wing, horizontal tail, and vertical fins were modelled using the previously determined airfoil sections and planform parameters. The analysis was conducted under steady-level flight conditions at cruise, and the CG location was computed by incorporating the masses and locations of every other subsystem, taken from the results of the Class II weight estimation. This also provides the software with the moments of inertia of the aircraft. The dynamic stability analysis is thus performed, providing the time evolution of the aircraft's state variables for all dynamic stability modes, which include five characteristic eigenmotions: Short-Period, Phugoid, Aperiodic Roll, Dutch Roll, and Spiral Roll.

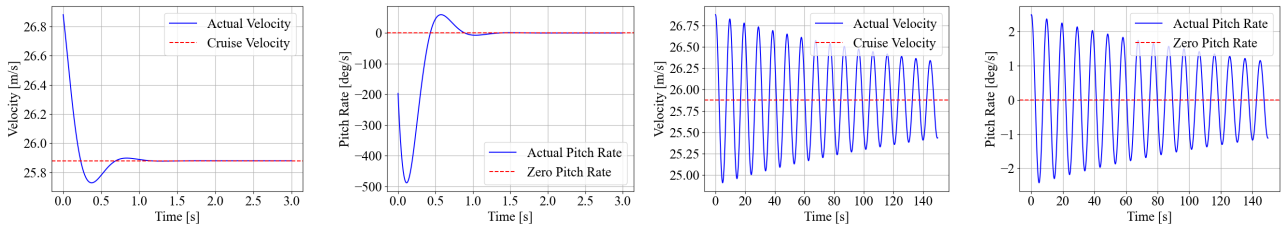

Figure 11.9: Velocity and pitch rate responses in a short period, and phugoid.

Figure 11.9 depicts the short period and phugoid response of the UAV in terms of its velocity and pitch rate change over time. It's clear that a highly damped response exists for short period; the aircraft returns to its stable configuration within 1.5 seconds. One noteworthy observation to make is that the pitch rate briefly jumps to -500 deg/s, before immediately damping to 0. Although an exceedingly high value, this may stem from an uncertainty in XFLR5's modelling method. Nevertheless, the main takeaway is the stable short period motion depicted. Similarly, the phugoid response has a stable response with high periodicity which can be seen, albeit with an extended amount of time to dampen (its half-amplitude

time is quite long, refer to Table 11.26). On the other hand, the deviations in velocity and pitch rate are relatively low, as is to be expected. With a designated controller, these fluctuations can be well-managed to dampen much quicker.

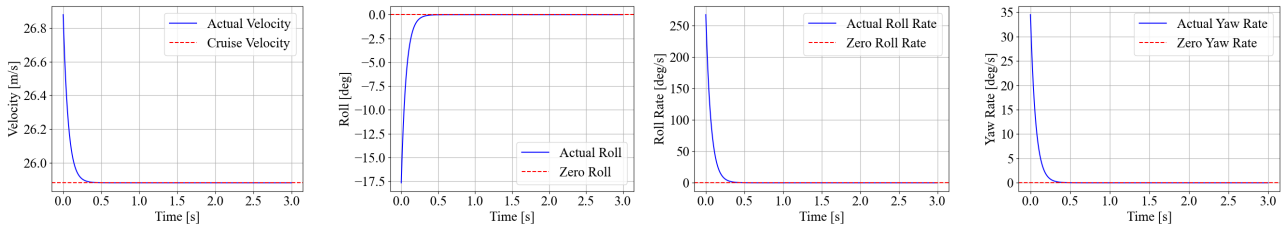

Figure 11.10: Velocity, roll, roll rate and raw rate responses in an aperiodic roll.

With the longitudinal modes covered, the lateral-directional modes can be analysed next. Figure 11.10 presents the velocity, roll, roll rate, and yaw rate response of the UAV in an aperiodic roll. Aperiodic roll does not consist of any oscillations, which is confirmed by the response which exponentially returns to the cruise setting of the aircraft. The UAV appears to posses a high roll damping phenomenon, a benefit for dynamic stability. Again, it is important to note that the roll rate contains very high values initially, which can be attributed to the analysis of a small lightweight aircraft in a simplified model such as XFLR5.

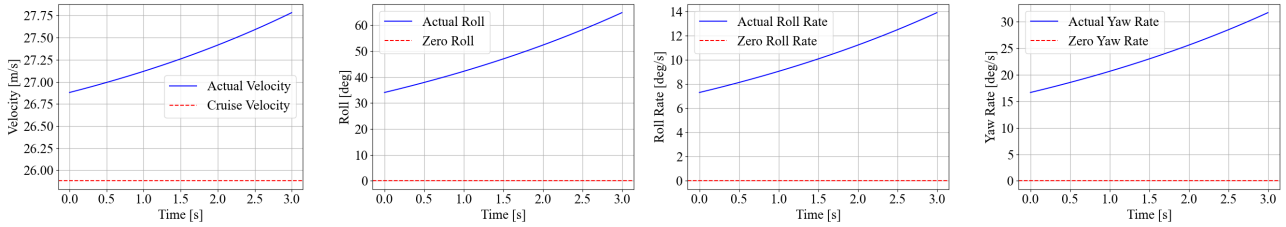

Figure 11.11: Velocity, roll, roll rate and yaw rate responses in a spiral roll.

Next, the spiral characteristics can be seen in Figure 11.11, with the same listed variables being plotted as for aperiodic roll. The response visible is clearly divergent, and over time the aircraft will continue to bank and lose altitude. This also appears to be at a high divergence rate, which is also concerning. In general, aircraft exhibit divergent spiral roll characteristics according to Sadraey [33] and so no requirements are placed on this ability. Nonetheless, this extent is unacceptable and must be improved upon; recommendations are asserted in Section 11.12.

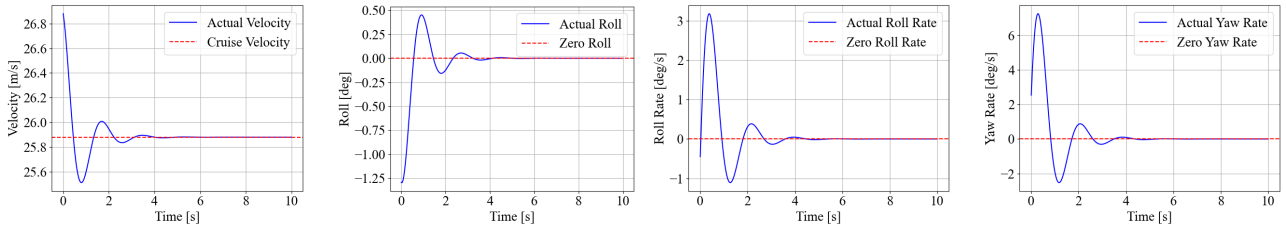

Figure 11.12: Velocity, roll, roll rate and yaw rate responses in a Dutch roll.

Finally, the dutch roll is exhibited in Figure 11.12. This does show converging behaviour with a low half-amplitude time and reasonable deviation values. The results of the dynamic stability analysis for the longitudinal and lateral-directional eigenmotions can be seen in Table 11.26 and Table 11.27, respectively. Mohammed. H. Sadraey [33] provides figures for what damping ratios are acceptable. Two eigenmotions create cause for concern: the phugoid exhibits a damping ratio of 0.00814, which classifies it as a ”Level 2 - Adequate” response, which could be improved. The other is the Spiral Roll, which is imposed with a requirement for the minimum time it must endure for the amplitude of the response to double (assuming a divergent response in the first place). The lowest tier response ”Level 3” requires a 4 second half-amplitude time, while Phoenix takes only 3.23 seconds; this is an unacceptable rate as described earlier. As this is the preliminary design phase, the future process requires an iteration of the fundamental design of the aircraft in which either the dihedral or sweep of the wing is increased. This is further explained in Section 11.12.

Below, Table 11.26 and Table 11.27 show the eigenvalues, half-amplitude time, period, undamped natural frequency, and damping ratio defining all of the responses. These were obtained from the graphs above.

Table 11.26: Longitudinal eigenmotion values.

Short Period				**Phugoid**			
Parameter	**Symbol**	**Value**	**Unit**	**Parameter**	**Symbol**	**Value**	**Unit**
Eigenvalue(s)	λ	-4.57 $\pm$ 6.83 j	-	Eigenvalue(s)	λ	-0.0053 $\pm$ 0.651 j	-
Half-Amplitude Time	$T_{\frac{1}{2}}$	0.152	s	Half-Amplitude Time	$T_{\frac{1}{2}}$	131.	s
Period	P	0.920	s	Period	P	9.65	s
Undamped Natural Frequency	ω_0	8.22	Hz	Undamped Natural Frequency	ω_0	0.651	Hz
Damping Ratio	ζ	0.556	-	Damping Ratio	ζ	0.00814	-

Table 11.27: Lateral-Directional eigenmotion values.

Aperiodic Roll				**Dutch Roll**			
Parameter	**Symbol**	**Value**	**Unit**	**Parameter**	**Symbol**	**Value**	**Unit**
Eigenvalue(s)	λ	-15.1	-	Eigenvalue(s)	λ	-1.19 $\pm$ 3.53 j	-
Half-Amplitude Time	$T_{\frac{1}{2}}$	0.0459	s	Half-Amplitude Time	$T_{\frac{1}{2}}$	0.582	s
Spiral Roll				Period	P	1.78	s
Eigenvalue(s)	λ	0.2147	-	Undamped Natural Frequency	ω_0	3.73	Hz
Half-Amplitude Time	$T_{\frac{1}{2}}$	-3.23	s	Damping Ratio	ζ	0.318	-

11.8.Static Stability

Static stability refers to the initial tendency of an aircraft to return to its original equilibrium state following a small disturbance, without looking at the time history of motion. This analysis uses key aerodynamic stability derivatives that were computed throughout the sizing of the control surfaces to evaluate the UAV's inherent stability characteristics in pitch, yaw, and roll axes, and it serves as a comparison with the results of the dynamic stability analysis.

The dynamic stability analysis resulted in that the spiral roll mode was unstable. This can be attributed to a certain combination of stability derivatives shown in Figure 11.13. The lateral stability diagram highlights that spiral stability is characterised by a low, positive C_{n_β}, and a highly negative C_{l_β}. From the calculated values, it is clear that C_{n_β} is quite low which is beneficial. This implies that the divergent spiral mode is caused by a low magnitude (and possibly positive) C_{l_β}. The effect of sideslip on the rolling moment can be adjusted by fine-tuning the dihedral on the main wing.

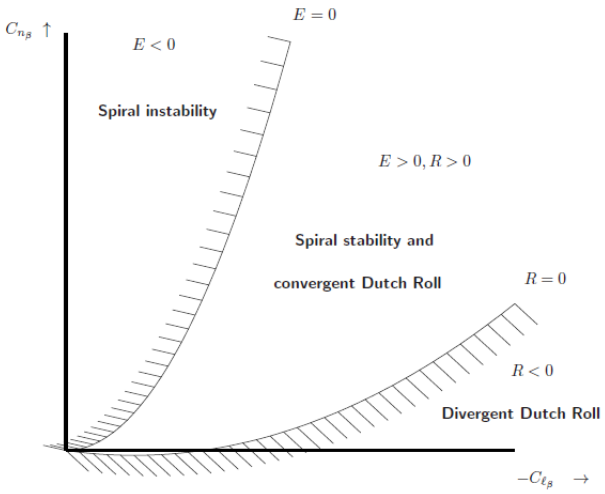

Figure 11.13: Lateral stability diagram [34]

C_{l_p} = -0.775 (taken from Equation 11.23): A negative effect of rolling velocity on roll moment confirms that the aircraft generates a restoring rolling moment when subjected to a roll rate. This damping effect makes sure that perturbations in roll do not grow, which indicates to stable roll behaviour. This is consistent with the fast, convergent roll mode identified in the dynamic analysis.

C_{Y_β} = -0.467 (taken from Equation 11.41): This indicates that a side slip to the right generates a side force to the left, opposing the disturbance. This derivative contributes to directional stability and influences the dutch roll and spiral modes.

C_{n_β} = 0.091 (taken from Equation 11.40): Positive C_{n_β} shows that the aircraft generates a yawing moment that opposes a side slip, meaning positive static directional stability. While this value is positive, it is relatively small in magnitude, and so this suggests that yaw stability exists but may be marginal. This aligns with the observation that the spiral mode is divergent, which is common for light UAVs with relatively small vertical tails.

11.9.VTOL System

The VTOL system must provide the UAV with the capability to provide thrust during the take-off and landing but more importantly for the control subsystem, allow the UAV to stay stable and controllable during the the take-off, landing and transition phase. These properties will be analysed in the following.

From the arrangement provided in Chapter 8 combined with the positioning selected in Section 11.4 the UAV is automatically stabile for an equally divided thrust of all propellers. To not start yawing, however, the same amount of propellers is required to rotate clockwise as anticlockwise, as otherwise a moment will be induced to the system. During strong wind conditions or unexpected events, the flight controller automatically adjusts the provided thrust per propeller to keep the aircraft stable.

To study manoeuvrability of the VTOL system, the overall approach to achieve pitch, roll and yaw motion must be understood. For this, the arrangement of the propellers as well as their rotation direction and speed are relevant. To pitch the aircraft, the two front propellers need to rotate at a different angular velocity than the aft propellers, while the propellers with the same speed need to rotate in counteracting directions. Similarly, the aircraft can roll by having the propellers on the left and right side of the UAV rotating at a different velocities. Again the motors with the same angular speed are required to spin in counteracting directions to not induce yawing moments. Lastly, yawing can be achieved by spinning the propellers on one diagonal with a different speed than the propellers at the other diagonal. This does not rotate the UAV with respect to the pitch and roll axis but only induces a moment about the yaw axis. A visualisation of the manoeuvres is provided in Figure 11.14.

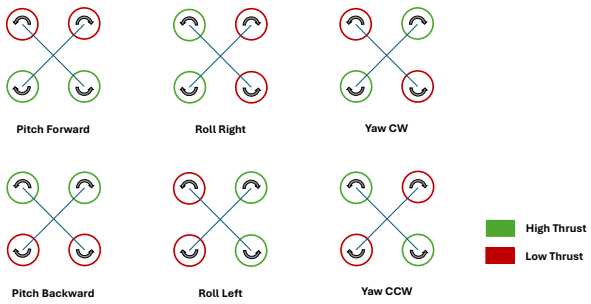

Figure 11.14: UAV control mechanisms. CW: Clockwise, CCW: Counter-clockwise.

After understanding the rotation mechanisms, the achievable angular roll, pitch and yaw accelerations p_{max}, q_{max}, r_{max} can be obtained using Equation 11.46, Equation 11.47 and Equation 11.48. Here, L_{max}, M_{max} and N_{max} correspond to the moments provided by the thrust and I_{xx} =6.774 kg·m^2, I_{yy} = 8.877 kg·m^2, I_{zz} = 15.488 kg·m^2 to the mass moments of inertia. The maximum moments can be achieved by considering the higher velocity propellers to be spinning at maximum rate, while the other two propellers stay stationary for each manoeuvre, respectively. The moments for the pitch and roll manoeuvre are therefore calculated from using Equation 11.49 and Equation 11.50, where d is the lateral and e the longitudinal distance between the propellers and the centre of gravity. Moreover, the yaw moment can be obtained using Equation 11.51, where P is the power of the two propellers running at maximum speed an ω is the angular velocity of the propellers.

$$\dot{p}_{max} = \frac{L_{max}}{I_{xx}} \quad (11.46) \qquad \dot{q}_{max} = \frac{M_{max}}{I_{yy}} \quad (11.47) \qquad \dot{r}_{max} = \frac{N_{max}}{I_{zz}} \quad (11.48)$$

$$L_{max} = \frac{1.5MTOWgd}{2} \quad (11.49) \qquad M_{max} = \frac{1.5MTOWge}{2} \quad (11.50) \qquad N_{max} = \frac{P}{\omega} \quad (11.51)$$

With a lateral distance of 0.76 m, a longitudinal distance of 1 m, a maximum power of 8000 m per propeller, leading to an rpm of 5300 rpm. Inserting these values, an angular roll, pitch and yaw acceleration of 53.4 rad·s^{-2}, 54.2 rad·s^{-2} and 11.7 rad·s^{-2} is found. This complies with the provided requirements and confirms the functionality of the design.

11.10.Stability & Control Sensitivity

For the stability and control subsystem, a sensitivity analysis of the most relevant analyses is performed to identify how the output varies for specified input changes. In this chapter the analysis has been performed for the centre of gravity position range in Subsection 11.10.1 as it is deemed as one of the most crucial output, driving a variety of subsystems and the mission performance as well as for the dynamic stability analysis in Subsection 11.10.2 due to its importance for the stability of the system during all mission phases. Following the results of the scissor plot it is found that no sensitivity analysis is required due to the strongly stable and controllable characteristics of the horizontal tail. Furthermore, the control surfaces have been designed with a margin with respect to the requirements, taking into account uncertainties of the input parameters, and do not require a sensitivity analysis.

11.10.1.Centre of Gravity Range Sensitivity Study

To investigate the change of the centre of gravity range when loading the aircraft for specified input parameter variations, a sensitivity analysis is provided. This evaluation consists of altering the weight of the heaviest components that are not directly located at the centre of gravity and a variation of the centre of gravity location of the heaviest components and the operational empty weight location with respect to the wing. These parameter changes have been chosen as they are

expected to have the most critical impact on the design. For the purpose of this sensitivity analysis it was decided to vary the parameters by 10% of their default values. By visual analysis of Table 11.28 and Table 11.29 it can be found that the computation is not sensitive to weight variations. However, changes of the centre of gravity location of the most impactful components, particularly of the suppression payload, might have a significant influence on the centre of gravity range of the UAV. Also the operational empty weight location with respect to the wing positions drives the design. However, while the suppression payload increases the range, the operational empty weight location primarily shifts the position forward or aft and is more desirable. To ensure that CG changes in the suppression payload are minimised, anti-sloshing vanes are used along a margin of 2% that is added to the centre of gravity range, providing additional design certainty.

Table 11.28: Change of CG range for a weight variation of 10% for the three heaviest components not positioned at the CG

Variation Parameter	Min CG (%)	Max CG (%)
Wing +10%	-0.57	0
Wing -10%	0	+0.49
VTOL Battery +10%	0	+3.85
VTOL Battery -10%	-5.16	0
Booms +10%	-2.48	0
Booms -10%	0	+2.15

Table 11.29: Change in CG range for a CG variation of 10% for the three heaviest components and the OEW location with respect to the wing

Variation Parameter	Min CG (%)	Max CG (%)
Suppression Payload +10%	0	+15.69
Suppression Payload -10%	-18.42	0
VTOL Battery +10%	-6.42	0
VTOL Battery -10%	0	+5.47
VTOL System +10%	-1.44	0
VTOL System -10%	0	+1.22
$\left(\frac{x}{C_{\text{mac}}}\right)_{\text{OEW}}$ +10%	+10.87	+10.28
$\left(\frac{x}{C_{\text{mac}}}\right)_{\text{OEW}}$ -10%	-12.07	-9.26

11.10.2.Dynamic Stability Sensitivity Study

For the dynamic stability a sensitivity analysis was conducted to evaluate the impact of changing geometric parameters or configuration changes on the aircraft's dynamic stability modes. Specifically, variations of $\pm 10\%$ in tail moment arm length, tail area, and CG location, as well as $\pm 1°$ changes in wing dihedral angle, were simulated in XFLR5. The resulting changes in eigenvalues are then given in terms of percentage change to see which effects had the greatest impact and their significance. Results in Table 11.30 and Table 11.31 show that the short period and Dutch roll modes were relatively insensitive to the tested changes, with eigenvalue magnitude variations generally remaining within $\pm 2.5\%$. The phugoid mode exhibited the lowest sensitivity, with variations in damping and frequency below $\pm 2\%$, consistent with its weakly damped nature. Aperiodic roll and spiral modes were more responsive, particularly to dihedral angle and tail moment arm modifications. Notably, spiral mode eigenvalues changed by up to $\pm 12.4\%$ and -11.0%, showing a stronger dependence on lateral stability geometry. These results reaffirm that the UAV's dynamic stability is robust against moderate design perturbations, with the exception of the spiral mode, which requires closer attention during lateral-directional stability tuning and a change in order to retain an acceptable stability performance.

Table 11.30: Eigenvalue Sensitivity Analysis (Complex Eigenvalues Combined)

Parameter	Value	Short Period	Phugoid	Aperiodic Roll	Dutch Roll	Spiral Roll
Tail moment arm	+10%	$-4.8243 \pm 6.4794j$	$-0.0065 \pm 0.6574j$	-14.7039	$-1.2856 \pm 3.5101j$	0.2293
	-10%	$-4.2943 \pm 7.1845j$	$-0.0042 \pm 0.6400j$	-15.7023	$-1.0756 \pm 3.5407j$	0.1977
Tail area	+10%	$-4.3463 \pm 6.7559j$	$-0.0045 \pm 0.6412j$	-15.4309	$-1.1327 \pm 3.4991j$	0.2047
	-10%	$-4.7888 \pm 6.8943j$	$-0.0061 \pm 0.6583j$	-14.8980	$-1.2314 \pm 3.5561j$	0.2232
CG	+10%	$-4.6236 \pm 6.9399j$	$-0.0053 \pm 0.6464j$	-15.2910	$-1.1794 \pm 3.5627j$	0.2102
	-10%	$-4.5246 \pm 6.7461j$	$-0.0054 \pm 0.6539j$	-15.0174	$-1.1897 \pm 3.5038j$	0.2182
Dihedral	+1°	$-4.5970 \pm 6.9623j$	$-0.0053 \pm 0.6482j$	-15.3064	$-1.1454 \pm 3.5553j$	0.1910
	-1°	$-4.5138 \pm 6.6532j$	$-0.0054 \pm 0.6546j$	-14.9406	$-1.2195 \pm 3.5001j$	0.2413

Table 11.31: Percentage Change in Eigenvalue Magnitudes Relative to Baseline

Parameter	Short Period (%)	Phugoid (%)	Aperiodic Roll (%)	Spiral Roll (%)	Dutch Roll (%)
Tail moment arm +10%	-1.70	0.98	-2.62	6.80	0.35
Tail moment arm -10%	1.85	-1.69	3.99	-7.92	-0.66
Tail area +10%	-2.25	-1.51	2.19	-4.66	-1.27
Tail area -10%	2.15	1.12	-1.34	3.96	1.02
CG +10%	1.47	-0.71	1.26	-2.10	0.74
CG -10%	-1.16	0.45	-0.55	1.63	-0.67
Dihedral +1°	1.52	-0.43	1.37	-11.04	0.27
Dihedral -1°	-2.17	0.55	-1.06	12.39	-0.50

11.11.Stability & Control Verification & Validation

This section discusses the verification and validation of the stability and control analysis performed in this chapter. The structure provided in Chapter 5 will be used as a guideline. The section will first go into detail on how the unit testing is performed in Subsection 11.11.1 and then discuss in Subsection 11.11.2 how the overall system is analysed. After certifying the overall functionality, the results will be validated in Subsection 11.11.3. Lastly, the compliance matrix is provided in Subsection 11.11.4, showing to what extent the subsystem requirements are met.

11.11.1.Unit Testing

For unit testing, the code has been verified constantly by asserting that the relevant results lie within a sensible range. For long formulas, a hand calculation was performed and compared using simplified input values. Furthermore, if values were stored in a list or matrix, the shape has been verified, given the dimensions. In addition, the debugging tool was used to keep track of results in between lines. Lastly, for parameters like the stability derivatives, it was checked whether those have the correct sign. After unit testing, a total coverage of 98 % has been attained for the stability and control subsystem code.

11.11.2.System Testing

System testing was one of the major methods for verifying the results. For the component positioning, the code has been verified using the graphs and observing whether the results behave as expected. Furthermore, while performing the sensitivity analysis, it was visually observed whether the input parameters have the correct influence on the new CG range. The scissor plot has been verified by analysing the overall shape as well as the scale of the numbers and the slopes. Here, it was crucial to see that the stability line has a positive and the controllability line a negative gradient, while crossing the x-axis at x_{ac} and $x_{ac} - C_{m_{ac}}/C_{L_{ac}}$, respectively. Moreover, it was checked whether the CG range obtained from the CG range plot translates correctly. For the control surfaces and the VTOL analysis, the reasonableness of the results could be verified by comparing the achievable performance to the requirements. To verify the results from the static and dynamic stability analysis, the calculated stability coefficients are compared to the coefficients that would lead to the behaviour and magnitude of the eigenmotions obtained from XFLR5. Additionally, while performing the sensitivity analysis, input changes in XFLR5 were found to give the expected response in the output.

11.11.3.Validation

For the validation of the feasibility of the component positioning, the CATIA model was employed, which allowed direct visual validation, certifying that the components can be stored in the planned manner. The scissor plot outcome could be validated by comparing the UAV tail area to the wing surface area ratio with typical ratios found in other UAV systems. The size of the control surfaces was compared to the commonly used values presented by Sadreay [33]. It is planned to further validate the aircraft's CG location and stability and controllability behaviour ones a prototype is build. For stability and controllability analysis this is inevitable, as accurate stability derivatives can only be obtained from testing.

11.11.4.Compliance Matrix

With the stability analysis complete, the compliance of the aircraft to its stability requirements is assessed in Table 11.32.

Table 11.32: Compliance matrix for empennage / Stability & Control subsystem.

ID	Verification Method	Status	Value
REQ-UAV-EMP-STR-1	Analysis	TBD	-
REQ-UAV-EMP-STR-2	Analysis	TBD	-
REQ-UAV-EMP-STR-3	Analysis	TBD	-
REQ-UAV-EMP-STR-4	Analysis	TBD	-
REQ-UAV-EMP-STR-5	Analysis	Yes	1.17
REQ-UAV-EMP-STR-6	Analysis	TBD	-
REQ-UAV-EMP-STR-7	Analysis	Yes	-
REQ-UAV-EMP-AER-1	Analysis	Preliminary Yes	-
REQ-UAV-EMP-AER-2	Analysis	Yes	-
REQ-UAV-EMP-AER-3	Analysis	Yes	-
REQ-UAV-SAC-1	Inspection	Yes	-
REQ-UAV-SAC-2	Analysis	TBD	-
REQ-UAV-SAC-3	Analysis	Yes	-
REQ-UAV-SAC-4	Analysis	Yes	-
REQ-UAV-SAC-5	Analysis	Yes	-
REQ-UAV-SAC-6	Analysis	Yes	-
REQ-UAV-SAC-7	Analysis	Yes	-
REQ-UAV-SAC-8	Analysis	Yes	$17.4\,\mathrm{rad{\cdot}s^{-2}}$
REQ-UAV-SAC-9	Analysis	Yes	$8.6\,\mathrm{rad{\cdot}s^{-2}}$
REQ-UAV-SAC-10	Analysis	Yes	$54.2\,\mathrm{rad{\cdot}s^{-2}}$
REQ-UAV-SAC-11	Analysis	Yes	$53.4\,\mathrm{rad{\cdot}s^{-2}}$
REQ-UAV-SAC-12	Analysis	Yes	$11.7\,\mathrm{rad{\cdot}s^{-2}}$
REQ-UAV-SAC-13	Analysis	Yes	-

11.12.Stability & Control Recommendations

For future work, it is recommended to perform further analysis on the stability derivatives as these define whether the UAV is inherently statically stable. Additionally, it is recommended to analyse the interaction of the flight controller and the stability and control subsystem. This relates specifically to autonomous control during VTOL and transition, but also to the use of control surfaces to perform the desired manoeuvres during cruise. Lastly, the VTOL system's response to a propeller failure could be investigated.

Given the trade-off between structural redesign cost and control system complexity, it is recommended to first implement modest aerodynamic refinements to improve the spiral roll behaviour: this can be achieved with an increase in dihedral which allows the lower wing to induce a rolling moment returning the aircraft back to a neutral state. Another method is to increase the vertical tail area, as this increases the aircraft's resistance to sideslip. This should be followed by the integration of a feedback control loop; this can be achieved with a Proportional-Integral-Derivative (PID) controller or a Linear Quadratic Regulator (LQR), which incorporates information of the whole state for scenarios including coupled lateral-directional modes as has been shown by Chrif et al. [35].

12 Flight Performance

This chapter details the performance characteristics of the fixed-wing UAV in the context of surveillance and suppression of wildfires. Its climb, turn, cruise, emissions, and noise performance will be studied and presented. This is preceded by a requirement analysis, and the end includes verification and validation of the results along with recommendations.

12.1.Flight Performance Requirement Analysis

Table 12.1 presents the requirements that are to be followed for the performance of the aircraft, in order for the surveillance and suppression mission to be conducted. These stem from the user requirements; for instance, requirement USR-PERF-001 defines the area that must be covered, which leads to a range requirement for the aircraft to adhere to.

Table 12.1: Requirements for the performance of the aircraft, relating to the user requirements.

ID	Requirement
REQ-UAV-FP-01	The aircraft must be capable of reaching the mission range of 350km
REQ-UAV-FP-02	The aircraft must be capable of climbing at the designed RoC of 2 m/s
REQ-UAV-FP-03	The aircraft must be able to complete a rate 2 turn
REQ-UAV-PROP-11	The propulsion system shall produce at most 84 dB effective percieved noise when operating & the FireFlight mission in cruise
REQ-UAV-PROP-12	The propulsion system shall produce at most 86 dB effective percieved noise when operating & the FireFlight mission in take-off
REQ-UAV-PROP-13	The propulsion system shall produce at most 89 dB effective percieved noise when operating & the FireFlight mission on approach

12.2.Climb & Descent Performance

Horizontal climb performance is a critical aspect of the aircraft's abilities, particularly for wildfire surveillance and suppression where ascent to operational altitude influences its response time and improves coverage efficiency. The horizontal climb capability of the UAV is determined by the available excess power compared to the required power due to drag. The rate of climb (RoC), is defined as the vertical component of the aircraft's velocity during a steady climb and is given by:

$$RoC = \frac{P_{\text{excess}}}{W} = \frac{P_a - P_r}{W}. \tag{12.1}$$

$$P_r = D \cdot V = \frac{1}{2} C_{D_0} \rho S V^3 + \frac{2W^2}{\pi A e} \frac{1}{V} \tag{12.2}$$

This equation is taken from Raymer [15], where: P_a is the available power from the propulsion system, P_r is the required power to maintain steady level flight at the climb airspeed, W is the aircraft weight (in Newtons). For this UAV, climb is powered by a piston engine + propeller configuration, where the available power decreases with altitude due to engine and propeller efficiency losses. The climb performance is therefore evaluated at sea level (worst-case weight) and at maximum take-off weight. This is deemed sufficiently accurate as well due to the low flight operations of the drone (cruise altitude of 450 m).

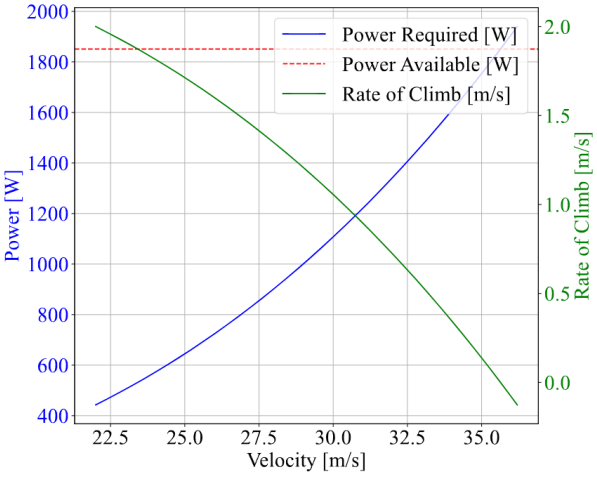

Figure 12.1: Climb Performance Diagram.

The propeller available power is also dependent on the rate at which the engine is ran at and the derived efficiency it provides. Subsection 8.3.3 describes the variation of propeller efficiency over the advance ratio. Using these results, the available power of the propeller can be sized based on how much is required to meet the climb requirements as well as optimised for maximum efficiency. The required power P_r at the climb airspeed is estimated using drag and velocity data from the performance model. Therefore, both powers can be graphed to find the maximum difference for maximum climb performance. This can be seen above in Figure 12.1. Two things of note: the power has been graphed over the velocity range of the aircraft from stall speed to dive speed, with an additional 1.1 safety factor imposed to ensure the aircraft has a margin when climbing; the corresponding climb rate is also plotted. By finding the minimum required power, the power available required to suffice the 2 m/s climb requirement can be obtained, which informs the propulsion system on how efficient it must run to provide this climb value. Looking at the graph, it is clear that minimum power is achieved at minimum velocity. This corresponds to a P_r value of 461.74 W at a velocity of 22 m/s. With a climb rate of 2 m/s, the

available power comes out to be 1872.80 W, which can be extracted from the propeller at an efficiency of 0.635 according to Figure 8.3.

Descent performance is found in a similar manner but with the power available being in excess. A theoretical maximum descent rate can be found by terminating the horizontal engine and diving down. A dive speed of $V_{\text{dive}} = 36.20$ m/s leads to a $P_r = 1939.71$ W and a $RoD = 2.78$ m/s. However, for a controlled descent where the engine is not turned off, a shallower descent rate can be chosen for return to the ground station. With a 0.95 value applied to the dive speed ($V_{\text{descent}} = 34.0765$ m/s), the required power is 1677.50 W. Assuming the propeller is provided power at its maximum efficiency rating, 1276 W, a descent rate of 0.565 m/s is obtained. This is the descent rate for which the aircraft performs at its most efficient power levels.

12.3.Turning Performance

Turning performance is a key factor in the manoeuvrability and operational agility of a UAV, particularly for its mission where it requires tight loitering over wildfire risk areas and rapid path adjustments when fire is detected. The turning capability of the UAV is dependent on the bank angle and load factor the aircraft will experience. A value of $25°$ value is imposed as a hard lower limit by the International Civil Aviation Organisation (ICAO) [1]. In a steady, coordinated level turn, the bank angle can be used to compute the load factor sustained throughout the turn in Equation 12.3.

$$n = \frac{1}{\cos\phi} \quad (12.3) \qquad V_{\text{stall, turn}} = V_{\text{stall}} \cdot \sqrt{n} \quad (12.4) \qquad \omega = \frac{g \cdot \tan\phi}{V}, \qquad R = \frac{V^2}{g \cdot \tan\phi} \quad (12.5)$$

During the suppression phase of flight, Phoenix will be flying at dive speed towards the fire. This corresponds to a load factor of n = 3.5, and a bank angle of $73°$. Since this is the maximum angle the aircraft may experience, a safety margin is applied and the suppression bank angle is maintained at $70°$. However, during cruise a shallower angle is produced as the maximum load factor of the aircraft experiences is lower; this stems from a the lower speed of flight. With a maximum cruise speed of 30 m/s, a bank angle of $66°$ is available to support the need of collision avoidance. Finally, for typical cruise turn performance such as during the surveillance phase of flight, the bank angle is maintained at $30°$. The following results in the text are presented for the normal cruise setting.

Table 12.2: Results of turning performance.

Velocity (m/s)	Bank Angle (°)	Load Factor	Turn Rate (°/s)	Turn Radius (m)
23.64	30	1.15	13.72	98.71
30	66	2.46	42.07	40.86
36	70	2.92	42.88	48.10

With a $30°$ bank angle, a load factor of 1.15 is experienced. During a turn, the aircraft's lift is partially used to provide the lateral centripetal force required to sustain the turn, while still maintaining a vertical equilibrium to stay in steady flight. This increases the lift required before stall occurs, and hence the stall speed. This effect can be calculated as follows in Equation 12.4. This provides a value of 21.49 m/s for the turn stall speed. Assuming again a safety factor of 1.1, this means the aircraft shall fly at 23.64 m/s. With the turn velocity computed, the turn rate ω and turn radius R are given by Equation 12.5. Thus, it follows that the corresponding turn rate is 13.72 deg/s and a turn radius of 98.71 m. The turn rate is classified as a rate 3 turn according to the FAA guidelines [36].

12.4.Cruise Performance

Cruise performance is another important parameter as it is the UAV's primary phase of flight. Its ability to efficiently cover ground over extended distances while maintaining stable flight conditions is vital for its operations. The cruise condition is defined as steady, level, unaccelerated flight, where the thrust equals drag and lift equals weight. The drag force is given below in Equation 12.6:

$$D = C_{D_0}\frac{1}{2}\rho V^2 S + \frac{2W^2}{\pi A e}\frac{1}{V^2} \quad (12.6) \qquad R_{\text{max}} \Rightarrow \left(\frac{V}{FF}\right)_{\text{max}} \Rightarrow (D)_{\text{min}} \quad (12.7)$$

$$(D)_{\text{min}} = (D)_{\text{min}} \cdot \frac{L}{L} = \left(\frac{D}{L}\right)_{\text{min}} \cdot W = \frac{W}{\left(\frac{C_L}{C_D}\right)_{\text{max}}} \quad (12.8)$$

The thrust is also computed, simply from the fixed power available of the propeller divided by the velocity. The cruise performance diagram can be seen in Figure 12.2. According to Varriale [37], the optimum cruise condition is found at the velocity at which the drag of the aircraft is minimised as in Equation 12.7; this also corresponds to the condition at which the lift-to-drag ratio is maximised as in Equation 12.8. The cruise velocity is defined to be 25.9 m/s where the drag is at its minimum. Finally, the actual range of the aircraft can be computed by using the Breguet range equation.

[1] See: https://skybrary.aero/articles/rate-turn. Accessed 15-06-2025.

This requires the brake-specific fuel consumption of the DLE60 engine, which can be computed from its fuel consumption and power output. The fuel consumption was found to be 1.5 L/hr. Combined with the density of gasoline ($\rho = 0.7429$ kg/m^2), the fuel flow in kg may be computed in Equation 12.9. The lift & drag coefficient for the state of minimum drag can be calculated with Equation 12.10 & Equation 12.11, taken from [37]. The weights uses the MTOW & total fuel weight; while this is an overestimation of the range as it does not consider the climb & descent phases of the mission profile, these phases are considered to be negligible with respect to the duration of the cruise phase and as such as deemed valid. With the fuel consumption computed, the final range of the aircraft can be computed using Equation 12.12; this comes out to be 479.303 km. This value far exceeds the mission range of 350 km, which is favourable for the operation of the aircraft. The parameters for the range equation can be seen in Table 12.3.

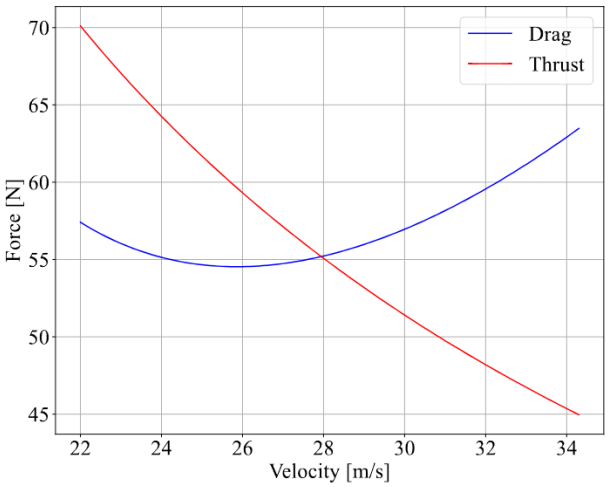

Figure 12.2: Cruise Performance Diagram.

$$c_p = \frac{FF}{P_{sh}} = \frac{FC \cdot \rho}{P_{sh}} \tag{12.9}$$

$$(C_L)_{D_{\min}} = \sqrt{\pi A e C_{D0}} \tag{12.10}$$

$$(C_D)_{D_{\min}} = 2C_{D0} \tag{12.11}$$

$$R = \frac{\eta}{g \cdot c_p} \frac{C_L}{C_D} \log \frac{W_i}{W_f} \tag{12.12}$$

Table 12.3: Inputs for Breguet Equation.

Parameter	Symbol	Value	Unit
Fuel Consumption	FC	1.5	L/hr
Shaft Power	P_{sh}	2200	W
Propulsion Coefficient	c_p	$1.41 \cdot 10^{-7}$	s^2/m^2
Propeller Efficiency	η	0.701	-
Lift Coefficient	C_L	0.921	-
Drag Coefficient	C_D	0.0713	-
Initial Weight	W_i	71.8	kg
Final Weight	W_f	66.7	kg

12.5.Emission Performance

Emission performance is the final performance metric analysed, with an emphasis placed on the sustainable operation of the aircraft. This is particularly important for the mission near sensitive environments such as forests and national parks. This section estimates the emissions produced by the UAV's piston engine during cruise, looking at pollutants in the form of carbon dioxide (CO_2), carbon monoxide (CO), unburned hydrocarbons (HC), and nitrogen oxides (NO_x).

Firstly, the fuel flow of the aircraft can be found as it was calculated in Section 12.4: FF = 1.114 kg/hr. Based on how much fuel is burnt and the amount of a given pollutant is produced per kilo of fuel, the overall pollutant production of the aircraft over its mission can be calculated.

The emission indices of these four types of pollutants were studied by Camilleri et al. [38], which can be found in Table 12.4. As a verification of these values, the emission index of CO_2 can also be calculated. Although gasoline is a mixture of multiple hydrocarbons in reality, octane is a reasonable appraisal. Based on the chemical equation in Equation 12.13, the following calculation in Equation 12.14 can be made for the emission index:

$$C_8H_{18} + 12.5O_2 \rightarrow 8CO_2 + 9H_2O \tag{12.13}$$

$$EI_{CO_2} = \frac{8 \cdot (12 + 16 \cdot 2)}{12 \cdot 8 + 18 \cdot 1} = 3.09\text{kg/kg} \tag{12.14}$$

Table 12.4: Emission indices.

Pollutant	Emission Index	Unit
CO_2	3169	g/kg
CO	240	g/hp/hr
HC	4	g/hp/hr
NO_x	4	g/hp/hr

Table 12.5: Overall pollutant emissions per mission & per lifecycle.

Pollutant	Single Mission Mass Expelled (kg)	Total Lifecycle Mass Expelled (10^3 kg)
CO_2	15.78	3280.5
CO	3.16	657.8
HC	0.0527	11.0
NO_x	0.0527	11.0

Comparing the values (3.169 vs. 3.09 kg/kg), the emission indices can be considered accurate for this preliminary estimation. With these emission indices, the amount of pollutant released by a single UAV over the course of one mission can be extracted, either through total fuel consumed or amount of power generated and total time in the air:

$$\dot{m}_{Pollutant} = EI_{fuel} \cdot m_{fuel} \quad (12.15) \qquad \dot{m}_{Pollutant} = EI_{power} \cdot P_{sh} \cdot T \quad (12.16)$$

Based on the mission range and cruise velocity, the time spent cruising in the air can be given as 3.76 hr. Using this value, the emissions for a single mission can be calculated in Table 12.5, along with the emissions for the total lifecycle of the whole system. This takes all 35 drones into account, over a 20 year lifespan assuming each drone has an effective deployment time of 10.9 hours per day and 4 months a year.

12.6.Noise Performance

An important parameter of the aircraft to consider is the noise produced throughout its operation. From an environmental standpoint, disruptions can be caused to populations and wildlife in wildfire-prone regions. This is a factor to be considered in the environmental effects that the FireFlight aircraft presents, and so it must abide with the regulations set by EASA. According to Roskam et al. [11], propeller noise is the dominant contributor for propeller-driven aircraft, exceeding both engine and aerodynamic sources. As such, this analysis focuses solely on the propeller and uses three sound metrics for quantification.

The Sound Pressure Level (SPL), written in dB, measures the acoustic pressure variation at a receiver, based on some emitter (in this case the propeller of the aircraft). It is a measure of the sound power but is also influenced by propagation distance, atmospheric absorption, ground reflection, and directivity. This value is often ”A-weighted”; this accounts for the fact that human ears discern varying frequencies differently and perceive them to have different loudness levels. A-weighting corrects the frequency response so that ones with less impact to human ears are given less weight and vice versa.

Sound Power Level (PWL) on the other hand, quantifies the total acoustic energy emitted by a source per unit time, regardless of what the environment surrounding the source is. It is an intrinsic property of the noise source, independent of distance or propagation effects.

Finally, the Effective Perceived Noise Level (EPNL), using EPNdB units, is a special regulatory metric used to assess the annoyance potential of noise. It uses A-weighted SPL values, distributed over a spectral shape (specifically in 24 one-third octave bands). These are then converted to a Tone Corrected Perceived Noise Level which are then logarithmically summed to an EPNL figure. While EPNL and A-weighted SPL both account for human ear loudness perception, EPNL employs more sophisticated tone correction factors and is therefore more accurate for certification purposed; as such, it is the metric used by EASA in accrediting an aircraft.

EASA Regulation (EU) 2018/1139, Article 9(2), Annex III [39] indicates the technical specifications on noise levels for VTOL lightweight aircraft. These requirements are specified in EPNL, which have also been implemented in the propulsion system requirements in REQ-UAV-PROP-11, 12, & 13. Guidelines on obtaining these values are also presented, however, the specified analysis is outside of the scope of this project. Alternatively, Roskam et al. [11, p. 317–318] provides an empirical method for computing EPNL values of aircraft, which suffices as a preliminary estimate for noise performance. It should be noted, however, that Roskam’s method is better suited for larger manned propeller aircraft and as such, some extrapolations were needed to find values applicable to a smaller MTOW aircraft. Engine noise is considered to be included in the outputted values as test data was used for this empirical method. Table 12.6 & Table 12.7 provide the input values for this analysis.

Table 12.6: Cruise input parameters.

Parameter	Symbol	Value	Unit
Propeller rotational velocity	n	4000	rpm
Propeller diameter	D	0.610	m
Power available	P_a	1542	W
Blade count	-	2	–
Distance from propeller	-	30	m
Azimuth angle	θ	90	deg
Propeller count	-	1	-

Table 12.7: Take-off/approach input parameters.

Parameter	Symbol	Value	Unit
Propeller rotational velocity	n	5000	rpm
Propeller diameter	D	0.810	m
Power available	P_a	4500	W
Blade count	-	2	–
Distance from propeller	-	50	m
Azimuth angle	θ	45	deg
Propeller count	-	4	-

The cruise and take-off/approach phases are all looked at separately on account of their guidelines being different as well as the use of two separate propulsions systems with different propeller tip speeds, number of blades, etc. Firstly, the overall sound pressure (OSPL) is estimated using contributions from five components and are summed together:

- Partial Noise FL1: Based on the propeller Mach number and the input power
- Partial Noise FL2: Based on the number of blades and size of each propeller
- Partial Noise FL3: Considers atmospheric and distance effects
- Directivity Index: Adjusts for the angle at which the line of sight between the receiver to the propeller is with respect to the propeller centreline
- Correction NC: takes the number of propellers into account

This is followed by an adjustment to find the Perceived Noise Level (PNL) to account for the human ear frequency response. Finally, converting from PNL to EPNL is based on the phase of flight: cruise (-2dB), take-off (-4dB), or approach (-2dB).

With the analysis run, the results of the noise prediction can be seen in Table 12.8 and Table 12.9. Looking at the results, it appears that the aircraft adheres to the imposed regulations throughout all phases of flight. The cruise phase of the flight profile has a much lower noise level compared to the take-off and approach phases. Meanwhile, the latter phases draw much closer towards the required limit.

Table 12.8: Cruise noise.

Noise Parameter	Value	Units
EASA Maximum EPNL	85	dB
Partial Noise FL1	39	dB
Partial Noise FL2	21	dB
Partial Noise FL3	14	dB
Directivity Index	0	dB
NC	0	dB
OSPL	74	dB
ΔPNL	0	dB
PNL	74	dB
Calculated EPNL	**72**	dB

Table 12.9: Approach noise.

Noise Parameter	Value - Take-off	Value - Approach	Units
EASA Maximum EPNL	86	89	dB
Partial Noise FL1	54		dB
Partial Noise FL2	18		dB
Partial Noise FL3	10		dB
Directivity Index	-3		dB
NC	6		dB
OSPL	85		dB
ΔPNL	3		dB
PNL	88		dB
Calculated EPNL	**84**	**86**	dB

12.7.Flight Performance Verification & Validation

The final compliance of the aircraft to the requirements of flight performance is presented in Table 12.10.

Table 12.10: Compliance matrix for flight performance requirements.

ID	Verification Method	Status
REQ-UAV-FP-01	Analysis	Preliminary yes
REQ-UAV-FP-02	Analysis	Preliminary yes
REQ-UAV-FP-03	Analysis	Preliminary yes
REQ-UAV-PROP-11	Analysis	Preliminary yes
REQ-UAV-PROP-12	Analysis	Preliminary yes
REQ-UAV-PROP-13	Analysis	Preliminary yes

Furthermore, unit tests and system tests were conducted on the code used to execute the calculations for the performance analysis. To ensure reliability and accuracy of the estimation module, `pytest` was employed in a structured testing process for both unit and system testing. Unit tests were developed for individual functions within the class. These tests verify that each equation returns mathematically consistent and reasonable results as expected. A coverage result of 100% was obtained, highlighting that the unit tests fully screen the code.

12.8.Flight Performance Recommendations

For flight performance metrics, it is highly recommended to update the results of the aircraft's abilities with physical testing. This includes short-term flight tests of climb, cruise, and noise performance, as well as long-term analyses of emissions produced over missions in the expected environment. While the noise results provide a preliminary result and confirmation that the propulsion system meets the EASA requirements, a comprehensive test must be conducted with the manufactured components to confirm adherence; this will be conducted in the post-DSE testing phase.

13 Embedded Systems

This chapter defines the embedded systems architecture onboard the UAV. It outlines a functional and requirement analysis, as well as the hardware layout, communication architecture, and complete mission data flow. The physical interfacing and information exchange across system elements are emphasised.

13.1.Embedded Systems Functional Analysis and Requirements

The functional analysis for embedded systems is provided in Figure 13.1.

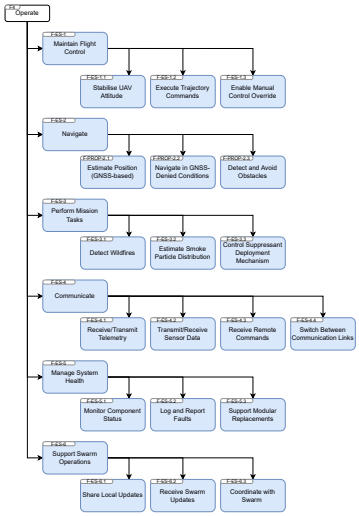

Figure 13.1: Embedded systems functional analysis.

Embedded systems requirements are presented in Table 13.1.

Table 13.1: UAV embedded systems requirements.

ID	Requirement
REQ-UAV-ES-FL-1	The UAV embedded systems (ES) shall autonomously perform flight stabilisation/control across all flight regimes.
REQ-UAV-ES-FL-2	The UAV ES shall provide navigation capabilities in GNSS-based environments.
REQ-UAV-ES-FL-3	The UAV ES shall provide navigation capabilities in GNSS-denied environments.
REQ-UAV-ES-FL-4	The UAV ES shall monitor UAV state telemetry.
REQ-UAV-ES-FL-5	The UAV ES shall support manual override of flight control.
REQ-UAV-ES-SUP-1	The UAV ES shall control mechanical actuation of suppressant release mechanism.
REQ-UAV-ES-SENS-1	The UAV ES shall autonomously detect wildfires.
REQ-UAV-ES-SENS-2	The UAV ES shall detect smoke within field of view.
REQ-UAV-ES-SENS-3	The UAV ES shall detect potential collisions.
REQ-UAV-ES-COM-1	The UAV ES shall support communication with the ground control station (GCS).
REQ-UAV-ES-COM-2	The UAV ES shall support communication with other swarm UAVs.
REQ-UAV-ES-COM-3	The UAV ES shall support beyond-visual-line-of-sight (BVLOS) communication.
REQ-UAV-ES-COM-4	The UAV ES shall support communication link redundancy.
REQ-UAV-ES-COM-5	The UAV ES shall switch to alternative communication link upon primary link failure.
REQ-UAV-ES-COM-6	The UAV ES shall allow over-the-air updates to mission parameters.
REQ-UAV-ES-COM-7	The UAV ES shall support secure, encrypted communication links.
REQ-UAV-ES-INT-1	The UAV ES shall log system-level faults during operation.
REQ-UAV-ES-INT-2	The UAV ES shall support swarm operations.
REQ-UAV-ES-INT-3	The UAV ES shall support modular component replacement.

13.2.Onboard Hardware Layout

The hardware block diagram (HWBD) in Figure 13.2 illustrates the layout of the hardware components onboard the UAV system. The architecture is divided into five tightly integrated domains: sensing, computing, communication, power

distribution, and actuation.

In addition, the preliminary hardware component list presented in the Midterm Report is expanded upon and rectified at this stage. Table 13.2 provides an overview of all commercial off-the-shelf (COTS) components onboard the UAV. All technical specifications and characteristics alluded to in subsequent descriptions of components/connections in the HWBD are in alignment with the specifications of the respective COTS hardware component in Table 13.2.

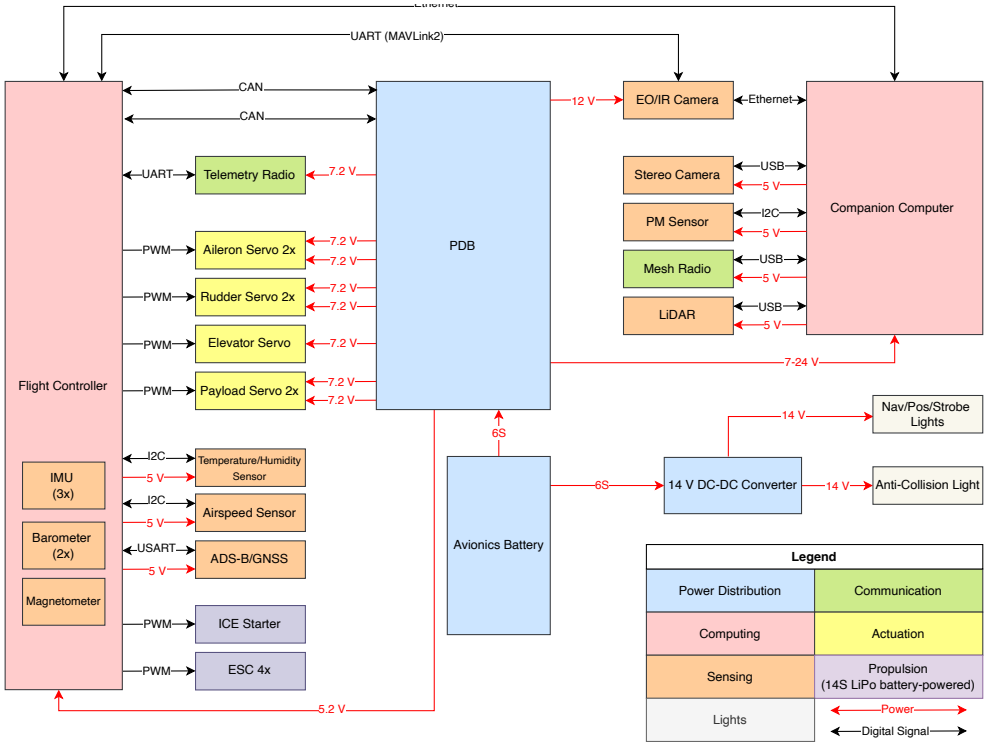

Figure 13.2: Hardware (and electrical) block diagram.

Table 13.2: Onboard hardware overview.

Component	Quantity	Dimensions [mm]	Mass [g]	Power [W]	Price [€]
SYK-30 AI EO/IR Gimbal Camera	1	122×128×198	880	30	10000
SF45/B (50 m) Scanning LiDAR (2D)	1	51×48×44	58	1.7	449
SPS30 PM Sensor	1	41×41×12	26	0.4	36.27
TFHT01 Humidity and Temperature Sensor	1	30×15×6.5	2	0.5	81
D450 Stereo Camera	1	119.9×17.4×10.53	30	0.65	184
PX4 Digital Airspeed Sensor	1	17.4×12.4×11.7	20	0.1	80
Pixhawk Jetson Baseboard	1	126×80×38.6	203.2	25	369
DroneV GS Nav/Strobe/Pos Lights	3	75.5×21.1×18.9	30	2.8	659
RedBaron Mini NXT Anti-Collision Light	1	58×58×33.8	70	28	263
CUAV CAN Power Distribution Board	1	128×100×12	200	N.A.	483
SiK Telemetry Radio 1 W	1	66.5×32×16.5	67	5	205
RM-1700-22M4 Mesh Radio	1	46×51×6.5	36.5	8	1590.15
LM252 RP SMA Antenna 5dBi	1	200×13.7×13.7	30	N.A.	3.96
TR-1A ADS-B + GNSS	1	35×25×8.5	14	0.7	950
JX CLS-HV7332MG HV Servos	7	40.5×20.5×36	73	36.9	50
Total			**2237.7**	**366.49**	**15609.52**

13.2.1.Computing

The computing domain is comprised of the two onboard processing units serving as low- and high-level computers – the flight controller (autopilot) and companion computer, respectively.

Pixhawk Jetson Baseboard An integrated autopilot and companion computer platform combining a Pixhawk 6X Pro

flight controller with an NVIDIA Jetson Orin NX 16GB module is selected as UAV computing hardware. The Pixhawk executes real-time flight control tasks, while the Jetson handles high-level onboard mission-specific computations.

The two modules are mounted on a baseboard which supports an Ethernet, UART, and CAN communication protocols between them; Ethernet is chosen. The baseboard provides multiple interfaces with both computing elements, enabling the simultaneous integration of all peripherals required for the mission (sensors, radios, etc.). The block diagram in Figure 13.3 provides an overview of the available communication interfaces between the computers and any devices that add functionality when connected to the Pixhawk Jetson Baseboard Bundle on the respective ports; such devices are referred to as peripherals. The block diagram in Figure 13.4 outlines the power pathways from primary input sources to each of the two onboard modules and the peripheral ports. Peripherals whose supply current and voltage specifications are supported by the integrated power distribution architecture of the baseboard will not require an additional connection to an external power source.

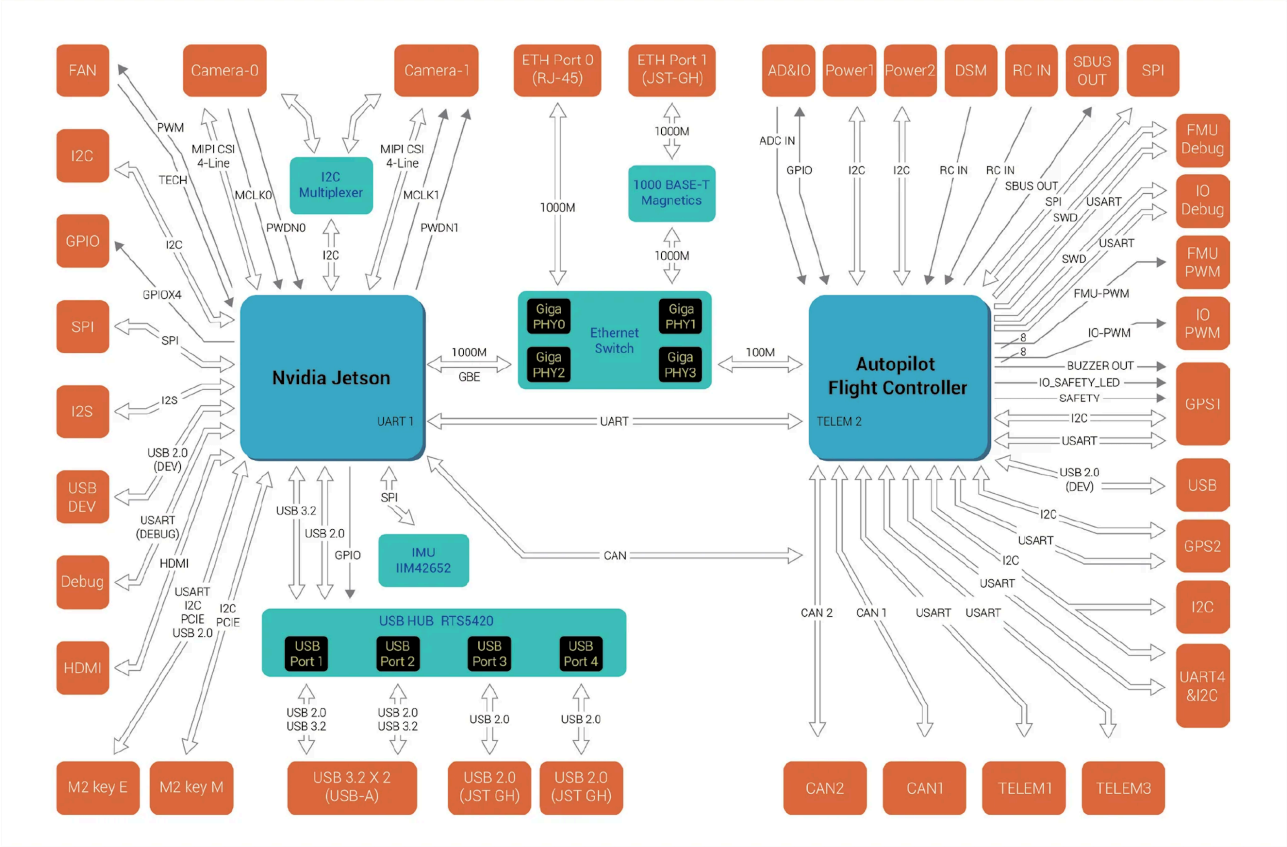

Figure 13.3: Pixhawk Jetson Baseboard Bundle peripherals block diagram[1]. Modules are represented in dark blue; internal connectors in turquoise; and peripheral connectors in orange.

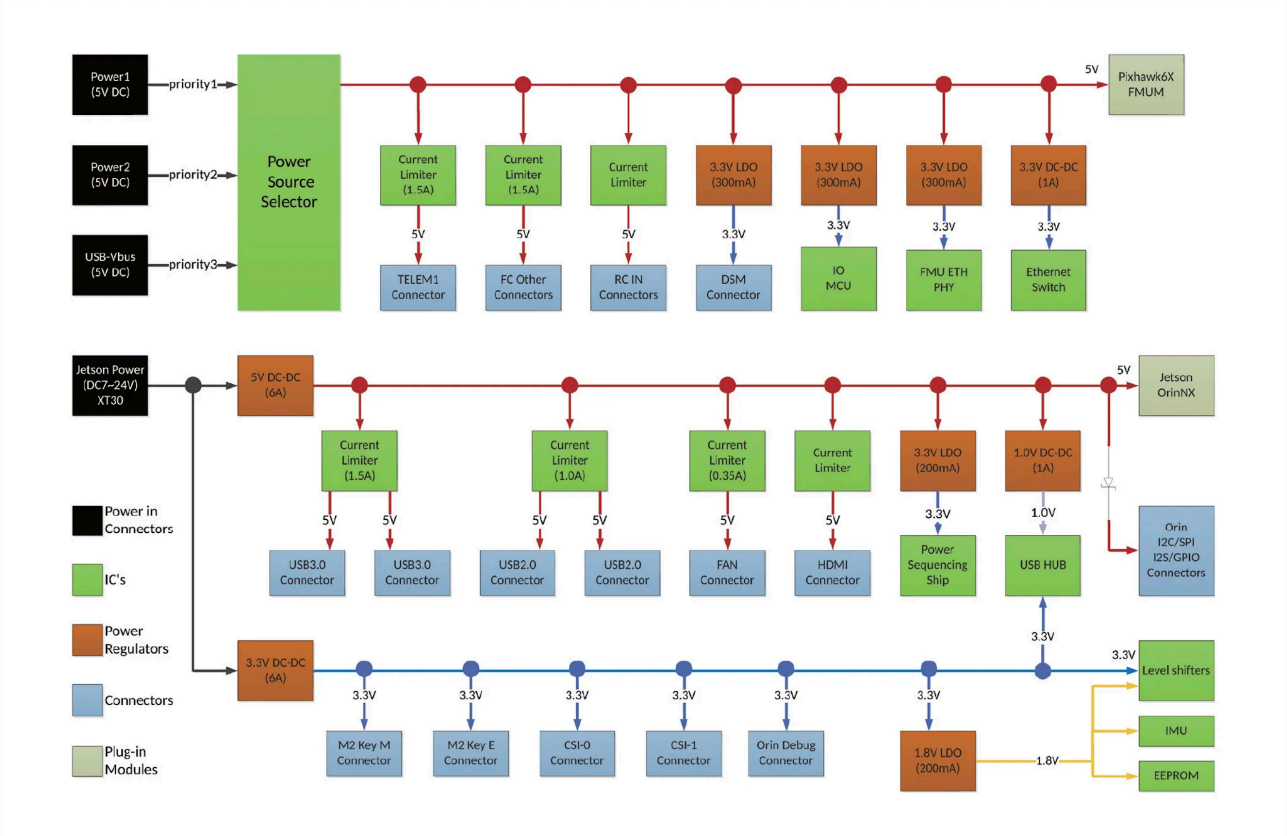

Figure 13.4: Pixhawk Jetson Baseboard Bundle peripherals block diagram[2]. Legend in image.

As the hardware components are presented, so shall their interfaces with precisely either the flight controller or companion computer.

13.2.2.Power Distribution

The power distribution domain manages power from the UAV's dedicated avionics battery and allocates it to all onboard hardware components; this excludes electronic speed controllers (4x), electric motors (4x), and engine starter, which are powered by a separate 14S LiPo battery (see Chapter 8). The domain consists of the 6S (22 V) LiPo battery for avionics, as well as a power distribution board (PDB).

Power Distribution Board (CUAV CAN PDB[3]) Power distribution board routes power from the 6S battery. Integrated DC-DC converters step down battery voltage (14–62 V supported) to regulated 5 V (avionics), 7.2 V (servos), and 12 V (EO/IR gimbal) via independent rails. The board includes 14 servo signal + power outputs, I2C (3x), UART (5x), CAN (2x), USB-C (1x), among other ports. It transmits voltage, current, power, and temperature data to the flight controller via CAN using the DroneCAN protocol.

13.2.3.Sensing

The sensing domain comprises a set of flight state and payload (mission-specific) sensors; it is tasked with providing the onboard computers with real-time data for state estimations, control, and higher-level mission planning. Included are both internal flight controller sensors (IMUs, barometers, and magnetometer) and external navigation and perception sensors.

Inertial Measurement Unit (IMU) Three redundant IMUs are integrated into the flight controller; these use inertial sensors three sets of 3-axis accelerometer/gyroscope sensor modules (ICM-45686[4]) to measure the acceleration and angular rate (roll, pitch, yaw) of the UAV [40]. Redundant IMU data is automatically compared by the flight controller for the purpose of fault detection.

Barometer Two barometric pressure sensors (ICP-20100[5] and BMP388[6]) integrated into the flight controller measure atmospheric pressure to estimate altitude. Redundant barometer data is automatically compared by the flight controller for the purpose of fault detection.

[3]See: https://doc.cuav.net/power-module/can-pdb/en/. Accessed: 17-06-2025.
[4]See: https://invensense.tdk.com/products/motion-tracking/6-axis/icm-45686/. Accessed: 17-06-2025.
[5]See: https://invensense.tdk.com/products/smartpressure/icp-20100/. Accessed: 17-06-2025.
[6]See: https://www.bosch-sensortec.com/products/environmental-sensors/pressure-sensors/bmp388/. Accessed: 17-06-2025.

Magnetometer A single 3-axis digital geomagnetic sensor (BMM150[7]) integrated into the flight controller measures the Earth's magnetic field and provides absolute spatial orientation and motion vectors, i.e., UAV heading information with respect to the magnetic North.

The flight controller fuses data from the integrated sensors to attain accurate flight state estimations.

ADS-B Transceiver with GNSS Receiver An ADS-B transceiver unit equipped with a multi-GNSS receiver and pressure sensors provides air traffic awareness and global navigation. Both ADS-B IN/OUT supported at $1090\,\mathrm{MHz}$ with configurable transmit power (0.25, 0.5, or 1 W) for the broadcasting the UAVs own position and localising other aircraft.

The GNSS + ADS-B module is mounted flush on top of the fuselage such that the antennas point upwards, maximising satellite and air traffic signal reception.

Interfaces with the flight controller via a serial USART (UART) using the TELEM3 port; 3D position and air traffic telemetry is transmitted through the MAVLink communication protocol. The $5\,\mathrm{V}$ supply voltage required by the component is provided through the flight controller TELEM3 port itself, such that no additional power connections are necessary.

Airspeed Sensor Modular airspeed sensing unit consisting of pitot tube, rubber tubing, a cable, and the digital pressure sensor itself (MS5525DSO[8]). Measures static and dynamic pressure used to compute airspeed for the UAV. Outputs digital, temperature-compensated pressure data (using internal factory-calibrated coefficients) via a 24-bit analog-to-digital converter (ADC).

The board is housed inside the avionics bay; the pitot tube must be exposed to undisturbed airflow, with minimal sensitivity to angle-of-attack changes in the nominal range. Air hoses connecting the sensor board and pitot tube shall be routed without bending or pinching[9]. Nose mounting is standard: the tube protrudes along the longitudinal axis into clean flow, offering simple wiring and wide AoA tolerance. If infeasible, leading-edge wing mounting is used but increases wiring complexity and roll sensitivity[10]. Nose mounting is preferred and selected.

Interfaces with the flight controller via I2C using the I2C port. The $5\,\mathrm{V}$ supply voltage required by the component is provided through the flight controller I2C port itself, such that no additional power connections are necessary.

LiDAR Scanning microLiDAR for obstacle detection; operates by oscillating a single laser beam (sweep frequency up to $5\,\mathrm{Hz}$). Provides a range up to 50 metres with a customisable horizontal scanning angle of maximum $320°$.

While vision-based sensors offer some collision avoidance, their performance is limited by environmental conditions and high processing demands. Based on simulations by Portugal and Marta [41], a single front-facing LiDAR is selected for obstacle detection—ranking second-best across 40 scenarios with zero collisions. The top-performing setup used additional angled rangefinders, but this was deemed impractical due to lack of integrated COTS solutions.

Interfaces with companion computer via a USB 2.0[11] JST-GH port for both data and power ($5\,\mathrm{V}$ supply voltage).

Particulate Matter (PM) Sensor Laser-scattering particulate matter sensor measuring PM1.0, PM2.5, PM4 and PM10 concentrations (number refers to particle diameter in microns) in the 0–1000 $\mu g{\cdot}m^{-3}$ range ($\pm 5\,\mu g{\cdot}m^{-3}$).

Interfaces with the companion computer via a FTDI USB adapter[12] (USB-to-UART bridge) for initialising and communicating concentration data over UART protocol. The required $5\,\mathrm{V}$ power is supplied through the USB 2.0 JST-GH port.

Temperature and Humidity Sensor (TFHT01) Miniature digital sensor measuring ambient temperature and relative humidity, designed specifically for UAV-based atmospheric sampling. Operates in the -40–125 $°C$ temperature range ($\pm 0.1\,°C$), with accuracy degradation above $65\,°C$, and 0–100 $\%$ relative humidity range ($\pm 1.5\,\%$). While this range does not capture direct flame temperatures (not within range), the sensor is not intended for close-range fire assessment. Instead, it provides context for fire profiling and risk assessment, particularly identifying in dry hot conditions preceding or surrounding a wildfire. This also provides added input for cross-referencing/validating data from other payload sensors.

Interfaces directly with the PX4 flight controller via I2C, using a dedicated JST-GH to 4-pin DF13 adapter cable included with the unit[13]. Powered from the I2C port's $5\,\mathrm{V}$ supply rail, with an estimated draw of $10\,\mathrm{mA}$.

In accordance with manufacturer indications, the sensor is mounted on the underside of the rear fuselage, distanced from heat sources (from propulsion, for example), to ensure exposure to undisturbed ambient airflow for accurate readings. Temperature monitoring of structural elements is possible through the integration of additional sensors.

[7] See: https://www.bosch-sensortec.com/products/motion-sensors/magnetometers/bmm150/. Accessed: 17-06-2025.
[8] See: https://cdn.shopifycdn.net/s/files/1/0604/5905/7341/files/ENG_DS_MS5525DSO_D20.pdf?v=1712135249. Accessed: 05-06-2025.
[9] See: https://ardupilot.org/plane/docs/common-pitot-considerations.html. Accessed 02-06-2025.
[10] See: https://basicairdata.eu/projects/pitot-probe/pitot-manual/8mm-pitot-static-tube-esp-series-installation-and-maintenance-manual. Accessed: 02-06-2025.
[11] See: https://lightwarelidar.com/shop/sf45-b-50-m/. Accessed: 05-06-2025.
[12] See: https://sensirion.com/products/catalog/SPS30 Accessed: 05-06-2025.
[13] See: https://www.tindie.com/products/thunderfly/tfht01-aerial-drone-hygrometer-and-thermometer/. Accessed: 22-06-2025.

Electro-Optical/Infrared (EO/IR) Gimbal Camera 3-axis stabilised imaging payload featuring a 30x zoom camera and 25 mm 640x480 thermal imaging camera. Supports 1080p HD photography and recording. The imaging payload of the UAV, responsible for vision-based surveillance and detection, consists of both optical and thermal sensors integrated into a gimbal, mounted under the forward section of the fuselage – common among surveillance UAVs. This mounting configuration provides an unobstructed field of view of the mission area and lies outside the wake of propellers. The stabilisation and pointing control supported by the gimbal has the additional advantage of enabling the system to continuously observe a specific point of interest, regardless of aircraft attitude – particularly relevant during loitering and manoeuvring.

Interfaces with the Pixhawk 6X Pro flight controller through UART on the TELEM2 port to synchronise flight data for gimbal stabilisation, communicate position telemetry, and receive control commands via the MAVLink2 protocol; interfaces with the Jetson Orin companion computer via Ethernet on ETH Port 0 (RJ-45 connector) for video streaming[14]. The PDB supplies 12 V through an included power cable.

Stereo Depth Camera Stereo vision depth camera integrates a vision processor, RGB sensor (with colour image signal processing), and IMU. A pair of global shutter monochrome sensors output synchronised left-right image streams from which depth is calculated [15]. Primarily assists VTOL operations through altitude estimation; can also provide RGB sensor redundancy in case the gimbal camera is not operational. Interfaces with the companion computer for high-bandwidth data transfer (video frames) and power (5 V) via a USB 3.2 port (USB-A).

The stereo depth camera is mounted downward on the underside of the fuselage, with unobstructed ground visibility for vertical depth estimation VTOL and hover.

13.2.4.Communications

The (onboard) communications domain handles UAV–GCS and UAV–UAV data exchange. In-depth considerations regarding the complete mission communications architecture are deferred to Section 13.3.

Telemetry Radio Enables remote low-bandwidth mission telemetry monitoring and parameter updates; carries RC signals. Handles long-range, low-bandwidth telemetry between the FC and GCS. Connected via UART (TELEM1 port) and transmits MAVLink messages, along with RC signals. Operates in the 433 MHz ISM band. The selected long-range model – commercialised along with a **5dBi Antenna** – achieves ranges up to 50 km. Two-way full-duplex communication supports simultaneous telemetry transmission and RC control command reception – a useful feature case of emergency manual override. Power is supplied through a dedicated 7–28 V input (not from the TELEM1 port) from the PDB and regulated internally. Enables remote mission monitoring and parameter updates; does not carry RC signals.

The telemetry radio antenna is mounted vertically on the aft upper fuselage, distanced from other antennas to reduce RF interference.

Mesh Radio High-bandwidth dual-band mesh radio operating at 900 MHz and 2.4 GHz (configurable, latter used), used for video streaming and inter-UAV communication. Interfaces with the companion computer via Ethernet (100 Base-T) for data and the 5 V supply is provided via the USB 2.0 (JST-GH) port on the Jetson.

13.2.5.Actuation

The actuation domain executes control surface deflection and payload deployment commands issued by the flight controller. Actuators include aerodynamic control servos: elevator, rudder (2x), ailerons (2x); suppressant payload deployment servos (2x); and the starter motor for the internal combustion engine.

High-Voltage (HV) Digital Servos Seven HV servos (JX CLS-HV7332MG) are used to actuate control surfaces and payload release mechanisms. Servos receive PWM control signals from the flight controller and are powered via the PDB's high-current 7.2 V servo rail (PDB supports 14 PWM channels). The PDB can deliver up to 8 A across all outputs of the servo rail.

13.2.6.Lights

Although not referred to as a domain, it is noteworthy that the UAV is fitted with lights for navigation, position, and anti-collision purposes.

Navigation/Strobe/Position Lights Three navigation lights are mounted on the wingtips (left/right) and rear fuselage to indicate aircraft position, orientation, and direction of motion. Each module operates on a 14 V DC input. As the onboard avionics power rails do not supply 14 V directly, these lights are powered via a DC–DC converter connected to the 6S avionics battery.

Anti-Collision Light A single beacon is installed on the upper fuselage to maximise omnidirectional visibility. The 360° high-intensity LED strobe requires 12 V supply voltage; it is powered via the 12 V output from the CUAV CAN PDB. The

[14] See: https://www.foxtechfpv.com/syk-30-ai-dual-sensor.html. Accessed: 05-06-2025.
[15] See: https://store.intelrealsense.com/buy-intel-realsense-depth-camera-d455.html. Accessed: 17-06-2025.

control integration of the lights is deferred to a future design phase (and thus omitted from the HWBD), but will likely involve the use of a MOSFET-based switching circuit to enable mode toggling (ON/OFF, Navigation/Position/Strobe) based on flight controller commands.

13.3.Communications Architecture

The deployment of a swarm of up to 50 autonomous firefighting UAVs over a $400\,\mathrm{km}^2$ forested area demands a robust communication architecture. The design considerations and system components necessary to support telemetry, video streaming, manual override capability, and the transmission of outputs from GCS-based mission computing units shall be explored in detail.

13.3.1.System Overview

The mission area does not have reliable LTE (Long-Term Evolution) coverage, presumably on account of its remoteness; the use of 4G within the communication architecture is thus discarded. Instead, within the mission area, a hybrid of two radio frequency (RF) technologies form the local network; the dual-link architecture separates the communication of basic telemetry and RC override commands from mission-specific data, thus creating redundancy. Outside the mission area, remote users are connected to the on-site GCS through a satellite link.

Each UAV is equipped with a long-range, high-bandwidth mesh radio operating in a high-frequency band (RM-1700-22M4, $2.4\,\mathrm{GHz}$), typically $2.4\,\mathrm{GHz}$, $5\,\mathrm{GHz}$ or $5.8\,\mathrm{GHz}$. These frequencies support high data rates suitable for HD video streaming, as well as mission-specific sensor data, e.g., concentration data from PM sensor. This setup enables the formation of a Mobile Ad-Hoc Network (MANET), where the UAVs not only have the ability to establish a direct link with the GCS, but also relay data for each other. In the event of link loss with the GCS from blocked line-of-sight or excessive distance, the coverage is extended by forwarding traffic to other nodes; this constitutes a multi-hop wireless network. The network topology in a MANET – i.e., the arrangement of the elements in a communication network – changes dynamically with time, supporting both single- and multi-hop networks, forming unidirectional or bi-directional links[16], and adapting data routes based on a set routing protocol[17]. It is self-configured and self-healing; failure of a single node does not compromise the overall flow of information. Additionally, priority is given to critical command data over video streams, such that control responsiveness is maintained when the mesh network is under load. Swarm UAVs communicate live video feeds, detection outputs, and overall mission-specific data directly to the GCS if in range; a single-hop network topology is desirable if direct communication is feasible, as multi-hop networking introduces latency (each relay node incurs a delay) and increases energy consumption. Communication with the GCS via other UAVs is relied upon as backup when the range is insufficient; in those scenarios, multi-hop networking extends the coverage; information hops through one or more intermediate nodes until a gateway node is reached – a UAV with a direct GCS link. Multi-hoping becomes particularly relevant when the scalability of the mission area is concerned, precisely due to its ability to extend the communication range by utilising intermediate nodes to relay information. Mission-specific commands from the GCS – such as actuator commands for suppressant deployment or parameter updates – follow the reverse path.

A long-range low-frequency (sub-GHz) radio link supports the communication of flight telemetry and RC override commands over the entire mission area; it shall operate on the $433\,\mathrm{MHz}$ band (LPD433 band), in accordance with ETSI EN300 220 7.2.3 European standard[18]. While the data rates supported by sub-GHz ($\leq 1\,\mathrm{GHz}$) frequencies are lower compared to the higher frequency bands used for video streaming, these exhibit excellent obstacle penetration capability[19] (due to larger wavelength); a robust long-range link is thus established for low-level UAV telemetry and remote control commands, ensuring the operator (at GS or within mission area) still maintains an acceptable level of control over the vehicles in the event of mesh connectivity loss/degradation. The fulfilment of this capability requires each UAV to carry a long-range telemetry transceiver supporting RC commands for manual override (SiK Telemetry Radio 1 W).

Outside the mission area, the remote user is connected to the GCS through a satellite link, supported by an on-site Starlink antenna. This link supports the transmission of video feeds, sensor data, and telemetry to the user; as well as the outputs of the GCS-based mission computing unit, in the form of fire propagation predictions and path planning information. Control of swarm UAVs from remote locations is also possible through the satellite link; the 26–$36\,\mathrm{ms}$ added latency range indicated by Starlink for the Netherlands is within acceptable bounds for real-time control. In case of latency spikes, the remote user is able to revert to latency-tolerant commands, such as specifying waypoints or issuing a return-to-base directive.

13.3.2.Communications Hardware Layout

The hardware components directly involved in mission communications (mission telemetry, video, control command transmission/reception) are distributed between the UAV, GCS, and UTS. The block diagram in Figure 13.5 presents the hard-

[16] See: https://www.geeksforgeeks.org/introduction-of-mobile-ad-hoc-network-manet/. Accessed: 10-06-2025.
[17] See: https://www.geeksforgeeks.org/manet-routing-protocols/. Accessed: 10-06-2025.
[18] See: https://www.etsi.org/deliver/etsi_en/300200_300299/30022002/03.02.01_60/en_30022002v030201p.pdf. Accessed: 10-06-2025.
[19] See: https://www.flyeye.io/drone-technology-communication/. Accessed: 10-06-2025.

ware layer of the mission communications architecture connecting these three physical systems. On the UAV, two onboard radios are used: a SiK telemetry radio operating at 433 MHz and a mesh radio at 2.4 GHz. These are linked to their respective antennas via RP-SMA and MMCX-to-RP-SMA adapter connections. On the GCS side, both radio types are replicated (ground-variant of mesh radio used – RM-1700-22M4[20]) with dedicated antennas and adapters (e.g., RP-TNC to Type-N for the mesh radio) to match the physical ports of the ground equipment. Ethernet and USB connections link the radios to the GCS computer, while a Starlink satellite link (Starlink Flat High Performance Kit[21]) provides remote access for the off-site operator via VPN.

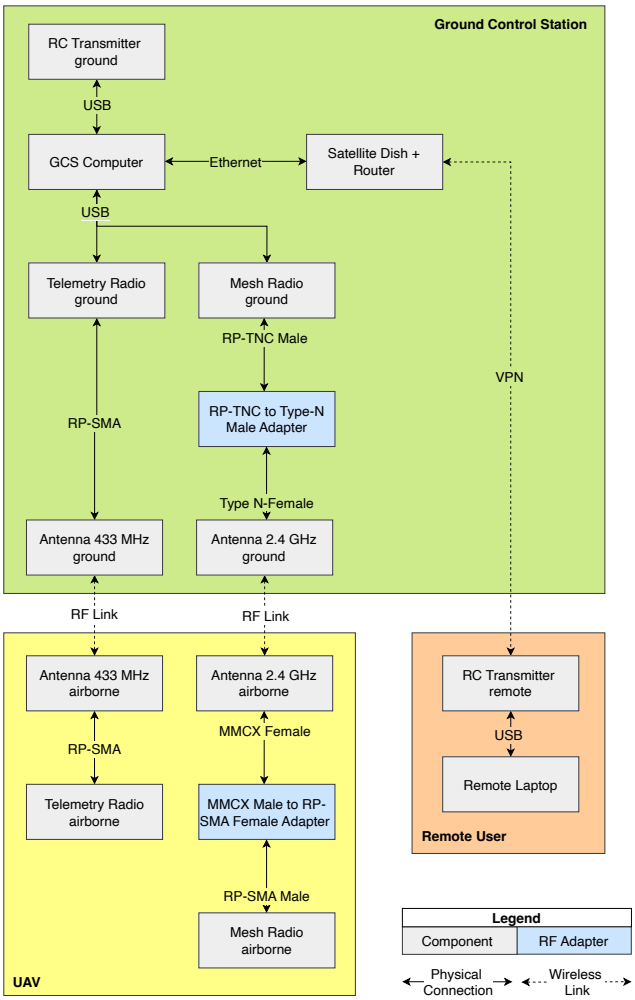

Figure 13.5: Communications hardware (electrical) block diagram

13.3.3.Data Flow

The block diagram illustrating the data flow between the three physical mission systems (UAV, GCS, remote user) is presented in Figure 13.6.

The payload sensors provide raw mission perception data. A convolutional neural network (CNN) layer processes this data onboard, producing two classes of semantically compressed outputs: perception outputs describing the UAV's surroundings, and detection outputs identifying events or entities of interest in the visual field. These outputs, together with UAV flight state sensor data (derived from the flight controller's integrated IMUs, barometers, magnetometer, and external sensors), form context for onboard planning.

The companion computer acts as the mission planning module. This module integrates onboard sensor inputs and external mission context to generate high-level flight commands. In particular, it ingests swarm coordination data, remote updates, and perception outputs to generate high-level commands, which are transmitted to the flight controller. When a fire is detected, this module can issue actuator commands to the payload actuator to release suppressant.

The flight controller executes actuator-level commands (servos, ESCs, ICE starter) based on the mission-planning logic determined by the companion computer; it also handles RC manual override commands and transmits telemetry to the GCS.

The GCS computing and communications unit receives flight telemetry, event notifications, video streams, and overall mission telemetry from the UAV and uses them to maintain situational awareness. The fire models developed are used to make predictions and generate revised mission directives. These directives may include updated flight paths, actuator parameters, or override commands, which are relayed back to the UAV.

The remote user terminal system (UTS) receives telemetry, alerts, and live video streams from the GCS; and can issue commands. These commands are processed by the GCS modelling layer, which updates the operational plan accordingly.

During nominal operation, raw sensor data and UAV flight state are processed onboard and used by the onboard mission planning module in decision-making, generating high-level commands that the flight controller executes; meanwhile, external inputs from the swarm and user shape ongoing mission decisions and can override onboard autonomous actions. This strategic planning and override authority reside in the GCS, which can supersede onboard autonomy by issuing revised objectives or updated target priorities based on system-wide context.

[20] See: https://techlibrary.doodlelabs.com/nano-oem-dual-band-mesh-rider-radio-915-mhz-and-2450-mhz-ism-bands-1. Accessed: 18-06-2025.
[21] See: https://magento-prod.kommagento.nl//pdfs/Starlink-Flat-High-Performance-Kit-Datasheet.pdf. Accessed: 18-06-2025.

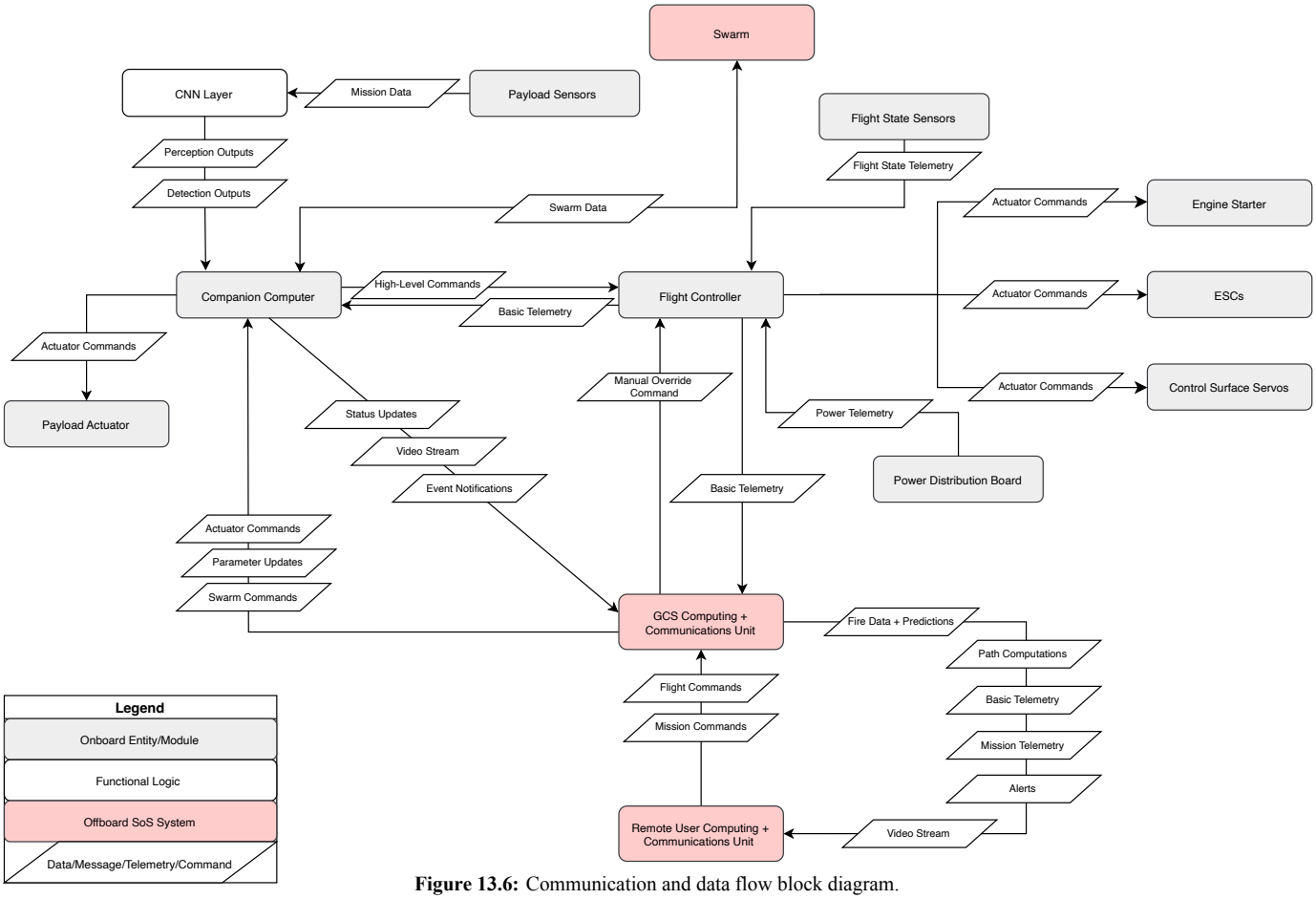

Figure 13.6: Communication and data flow block diagram.

13.4.Compliance Matrix

Table 13.3: Embedded systems requirement compliance matrix.

ID	Verification Method	Status	Justification
REQ-UAV-ES-FL-1	Demonstration	Preliminary Yes	Integration of FC & sensors complete; flight logic not yet tested
REQ-UAV-ES-FL-2	Inspection	Preliminary Yes	GNSS receiver interfaced with FC via TELEM3
REQ-UAV-ES-FL-3	Inspection	Preliminary Yes	Redundant IMUs and barometers interfaced with FC; theoretical capability exists
REQ-UAV-ES-FL-4	Demonstration	Preliminary Yes	PX4 telemetry stack defined, telemetry link configured
REQ-UAV-ES-FL-5	Demonstration	Yes	Supported by SiK telemetry link with RC passthrough
REQ-UAV-ES-SUP-1	Inspection	Yes	Servos connected via PWM to FC, PDB supports current draw
REQ-UAV-ES-SENS-1	Inspection	Preliminary Yes	CNN layer outputs described, but not implemented
REQ-UAV-ES-SENS-2	Test	Preliminary Yes	PM sensor integrated with companion; output interpreted
REQ-UAV-ES-SENS-3	Test	Preliminary Yes	LiDAR + ADS-B transceiver selected and interfaced with companion computer
REQ-UAV-ES-COM-1	Demonstration	Preliminary Yes	Telemetry link defined
REQ-UAV-ES-COM-2	Inspection	Preliminary Yes	Mesh radio integration complete, routing design pending
REQ-UAV-ES-COM-3	Inspection	Preliminary Yes	Long-range radio with antenna selected; theoretical capability exists
REQ-UAV-ES-COM-4	Inspection	Preliminary Yes	Dual-link comms defined, switching logic TBD
REQ-UAV-ES-COM-5	Inspection	TBD	Fallback mechanism not yet implemented
REQ-UAV-ES-COM-6	Demonstration	Preliminary Yes	MAVLink and GCS support over-the-air parameter updates
REQ-UAV-ES-COM-7	Inspection	Preliminary Yes	128-bit and 256-bit AES encryption supported by mesh radio
REQ-UAV-ES-INT-1	Inspection	Preliminary Yes	PX4 supports logging; usage not yet defined
REQ-UAV-ES-INT-2	Inspection	Preliminary Yes	Mesh network architecture and data flow support swarm integration
REQ-UAV-ES-INT-3	Inspection	Yes	Component wiring and interfacing kept modular (USB, UART, CAN)

13.5.Embedded Systems Recommendations

The items that follow identify areas where the design should be either verified, validated, or further development is required to progress toward implementation.

Hardware Integration Peripheral interfacing has so far been based on datasheets, interface standards, and documentation. However, theoretical compatibility does not imply functional success. The current layout likely includes mismatches, unsupported power draws, or invalid interface assumptions. Staged empirical tests are recommended: connect each peripheral to the Pixhawk Jetson Baseboard, verify data transmission, and measure voltage and current under load. These tests will expose interface failures, overdraw, and unexpected behaviour.

Software Integration The companion computer runs Linux with NVIDIA JetPack SDK[22]; the flight controller runs PX4. Their combined integration with ground control software (e.g., QGroundControl), and with mission-specific software (e.g., detection and fire propagation models), has not yet been validated. Future work must verify end-to-end compatibility—ensuring mission commands and telemetry pass correctly between Jetson, Pixhawk, and GCS.

MANET Data Routing The system relies on multi-hop mesh networking for mission-critical data. The routing behaviour under load, link degradation, or partial node failure is not yet characterised. Further design is required to define message prioritisation protocols, route selection logic, and failure fallback modes. Simulations should be conducted to assess coverage bottlenecks, worst-case latencies, and relay node requirements. A minimal framework would include: packet tagging based on criticality, dynamic gateway election based on signal strength and load, and relay node designation for operation in edge cases.

Cooling Thermal management remains undefined. No thermal modelling or component-level cooling strategies have been proposed for high-draw elements such as the Jetson, ESCs, motors, ICE, or voltage converters. Passive and active cooling concepts ought to be investigated.

Further Radio Link Design Antenna selection has not been validated beyond basic range specs. Gain, pattern, orientation, and placement effects, notable under airframe interference and during manoeuvres ought to be tested. Ground and flight tests should evaluate link stability, range, and directional sensitivity.

[22] See: https://developer.nvidia.com/embedded/jetpack. Accessed: 18-06-2025.

14 Operations and Logistics Concept

The operational design is an essential part of the project as it involves all elements of the System of Systems, in addition to the interaction with the customer and the external environment. First, the operational environment will be presented, followed by an overview of the operational concept. The UAV design for operation will then be discussed, followed by the ground station operations and design. Finally, the user experience will be discussed.

14.1.Operational Environment

The initial operating region for the SoS in The Netherlands is determined to be primarily forest on flat land with high water availability. Future operating environments determined in the market analysis may include mountainous regions. If modifications are needed to operate in more demanding environments, they will be studied and the system adapted post DSE.

14.2.Operational Concept Overview

Airspace Management

The system will operate primarily in remote, uninhabited areas with minimal air traffic, maintaining a safe distance from airports and populated regions. During regular surveillance operations, the UAVs will maintain compliance with class E airspace regulations at 150-450 m above ground level (AGL). As soon as possible after a fire is detected, in the order of minutes, it is anticipated that the relevant air traffic authorities will establish temporary restricted airspace around the fire zone, allowing for more flexible UAV operations within this designated area. All UAVs will be equipped with Automatic Dependent Surveillance-Broadcast (ADS-B) transponders and collision avoidance systems to maintain situational awareness of other aircraft that may be operating in the vicinity. The fire operations centre will maintain continuous communication with air traffic management to ensure coordination with any manned firefighting aircraft or emergency services operating in the same region. An overall picture of the system interacting with firefighting and airspace environment can be seen in Figure 14.1.

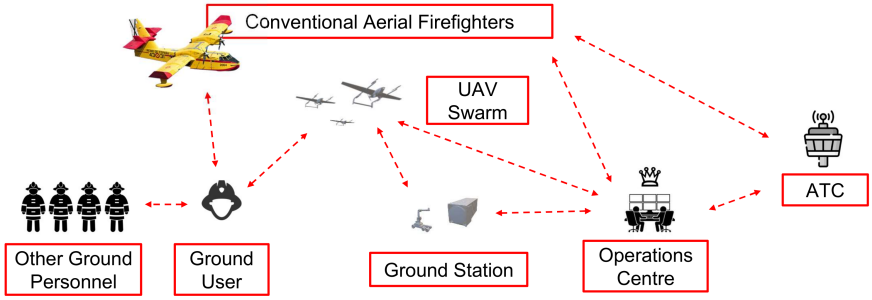

Figure 14.1: Fireflight system interaction with agents in the firefighting environment

Risk Category

The system will be operated over uninhabited areas, transporting non-dangerous payload. As such the design is aimed to fall under the 'Specific' category of operations from the European Aviation Safety Authority (EASA) [42]. Due to the approximate kinetic energy of each UAV being above 34 kJ, a dedicated SORA (Specific Operations Risk Assessment) will have to be performed.

14.3.Operational Concept Overview

This section gives an overview of the operational concept.

The missions to be accomplished by the system are three fold: surveillance, suppression and monitoring of fires. These need to integrate into current operations seamlessly. The operational concept given bellow is a result of a study of the current firefighting operations and results of the detailed design of the UAV and ground station. The outcome is a full operational scenario of how the system will fit into fire fighting operations.

The final concept for the system of systems include three main elements. The UAV, itself part of the swarm, and the ground station. In addition to this, the system of system interfaces with the firefighting organisation through a remote user interface. The UAV is a fixed wing eVTOL of single type, with a fixed surveillance camera payload and a modular payload of 15 kg. The swarm comprises of 35 drones at full capacity, which operate autonomously and are coordinated

centrally. The ground station comprises of three containers. Two containers house all needed ground station equipment, including UAVs, communication systems, water, water and fuel pumps, diesel generators, an auto-refill platform and a rover. The fuel needed for operation is brought to site and stored in a dedicated container. The operations occur in several phases, including deployment, coordination, refuelling, and suppression.

14.4.Operational Phases and Timelines

The operational phases of the SoS are described below.

14.4.1.Deployment of Ground Station

Before deploying in each area an operational plan will be created by the operating fire authority, identifying transport options, optimal location placement and alternate emergency landing zones. Water sources will be determined and accounted for accordingly. At this point all supply logistics will be set up including replenishment vehicles on standby from the operating fire department.

14.4.2.Surveillance Phase

In the surveillance phase, UAVs operate with water in the tanks and look out for starting fires. If a fire starts, the UAVs will determine the exact location of the fire and alert the system of the presence.

Camera sizing is estimated with thermal camera at 1 pixel covering $1\,\mathrm{m}^2$. This is based on the concept of a single pixel showing a detectable significant temperature difference based on fire temperature of $300\,^\circ\mathrm{C}$ [43] on a $30\,\mathrm{cm}$ x 30 area (10% of 1 pixel), including a vegetation occlusion factor of 90%, this results in detection of $100\,^\circ\mathrm{C}$, providing a difference of $5\,^\circ\mathrm{C}$ from ambient of $25\,^\circ\mathrm{C}$.

Due to the exponential decay in visibility with increased vegetation to view through [44], maximum viewing angle of 45° is feasible for direct thermal detection of fire. Scanning with shallow angle and high zoom was considered but determined infeasible if any vegetation apart from low grass is present. Based on current best thermal cameras [1], a horizontal scan width of $1280\,\mathrm{m}$ is calculated from 1280 frame width. For areas with low vegetation scan distance can be increased improving detection performance.

14.4.3.Fire Suppression Phase

In suppression mode, dedicated UAVs will be deployed either directly in the case of combined payload or from the ground station. The swarm of suppression UAVs shall fly directly towards the fire location providing no obstacles are detected.

Each UAV shall approach the fire in formation and deliver the specified payload of water of $15\,\mathrm{L}$ using a fly-by water bombing approach, from $18\,\mathrm{m}$ above the fire. The water dropping mechanism is specified in Chapter 15. After the deployment of the payload, each suppression UAV will return to the ground station to replenish water.

During the water bombing, the fire will be continuously monitored by the surveillance UAV in the corresponding area, until the system determines the fire to be extinguished. In the event that the fire increases in size beyond a predetermined metric, a warning shall be issued to the operator. The on duty operator will escalate the warning to the local fire department based on training and available data. The system shall then enter fire monitoring mode.

14.4.4.Fire Monitoring Phase

During monitoring mode, UAVs will loiter above ongoing fires. The system will relay updates on fire size, intensity and local weather conditions to the ground station and firefighters on the ground. The system can also be used to monitor an area after a fire to detect any remaining hot spots or any re-ignition.

14.4.5.Irregular Operations

Some situations require specific caution or operational limitations to be put into effect for example during adverse weather conditions or the presence of an unauthorized aircraft in the operating space. Aircraft will be designed to operate in low visibility conditions through advanced sensor suite. In addition, sensors will enable ”detect and avoid” (DAA) capabilties for obstacles including unauthorized aircraft.

14.4.6.Emergency Operations

In the event of unexpected system failure, redundant detection methods shall support the issuing of warnings to the operator. In the event that fire is detected at the ground station, the ground station shall relocate to a safe location. In the event of failure of an aircraft, it shall alert the operator and return to base if possible. If it is not possible, best attempt at landing with minimum impact will be performed, the (last known) location of the aircraft will be made available to operator, and recovery will be performed.

[1] See https://enterprise.dji.com/matrice-30/specs. Accessed 21/05/2025.

14.4.7.Maintenance Logistics and Operators

During the operation of the system both scheduled and unscheduled maintenance shall be required. A maintenance schedule shall be created for the final design of the system in compliance with EASA and National Aviation Authority (NAA) regulation. In addition, relevant pre-flight procedures and checks shall be created in order to detect potential system failures, damage, etc. before flight, and unscheduled maintenance shall be executed appropriately.

The system is designed to have multiple users connected and receiving information. Different users will have different levels of control over the system, and at least one master operator will be monitoring the system from the firefighting operational centre. There is no upper limit to the amount of users the system can accommodate. The master operator of the system shall be a dedicated person having completed a certified training to be determined from the project design, in addition to the specific technical standard (STS) remote pilot license of the NAA of the country of operation. Additional ground-staff involved shall include firefighting personnel. These shall receive a dedicated training for the operation of ground segments of the system, including basic operational procedures and maintenance activities.

14.4.8.User Experience

The user experience is a key element in making a useful and successful product. An experience has been conceptualised in order to understand what the user would need and how the user could operate and interact with the Fireflight system.

The user interface has been imagined as a portable device which could be used by users on the field or in the operational headquarters. The device has joysticks which allow for remote control of the UAVs. The main information source on the screen is a map on which various information can be displayed. The information displayed to the user depends on the operational phase. In the surveillance phase, the user sees the surveillance flight path and the UAVs, and is able to change flight paths, take direct control or access the cameras on the UAVs. In the firefighting phase, the user can see the area on fire, as well as a prediction of where the fire will spread. Additionally, the user can see ground vehicles and personnel, as well as the UAVs. This assumes that ground personnel will be equipped by GPS trackers. There is also a live feed of the ongoing fire which is displayed in a corner. In the firefighting phase, the system acts as a situational awareness tool, which should allow for better firefighting strategies and coordination.

This also allows to enhance the safety of ground personnel. Figure 14.2 depicts what the user experience could look like.

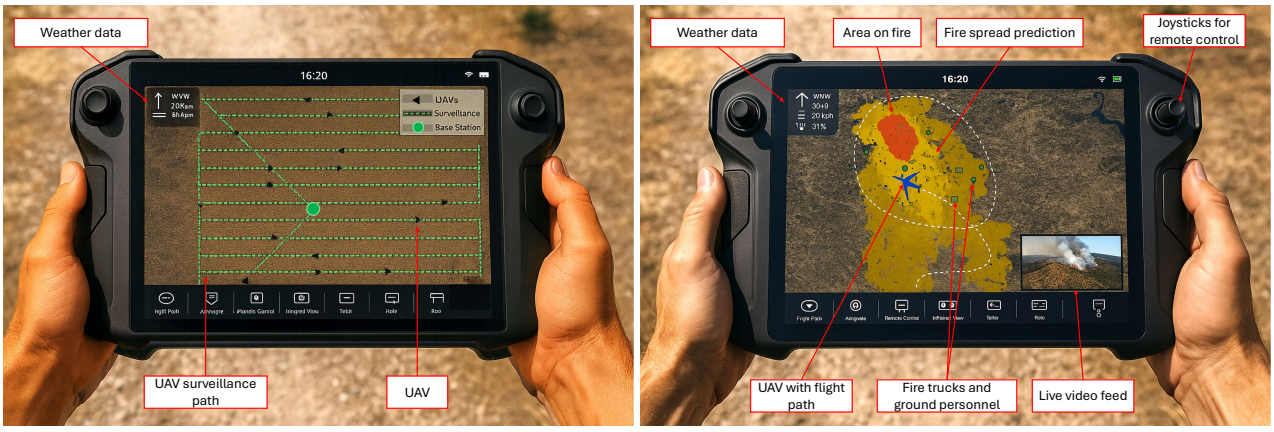

(a) Surveillance **(b)** Firefighting

Figure 14.2: Concept art for different phases of operation

14.5.UAV Design for Operations

The UAV needs to be designed to fit the operational concept. UAV design elements pertaining to the mission and operations are described bellow.

The UAV is designed to fulfil the three missions of the system, Surveillance, Suppression and Monitoring, but also is designed to meet operational constraints. The impacts of these considerations on the architecture of the UAV are detailed bellow.

Mission payloads. The payload for surveillance is an off the shelf camera and is detailed in Subsection 13.2.3. The suppression payload is an interchangeable water tank. This flexibility allows the UAV to be used for other missions and reach other markets beyond fire fighting. An obvious alternate payload is adding more fuel capacity to the aircraft. Adding an additional fuel capacity of $15\,\mathrm{L}$ would extended the range to $1400\,\mathrm{km}$. Potential other payloads for fire operations include advanced data acquisition system to assess fire risk, fire starters for tactical fires and fire extinguishing bombs and chemicals. These, and more, can be studied in more detail post DSE to assess their viability.

Figure 14.3: Concept art for the remote control of the UAV

The UAV is designed for the following sizing mission profile displayed below in Figure 14.4. This includes VTOL operations as well as cruise. This is a key component in finding fuel fractions in the Class I weight estimation.

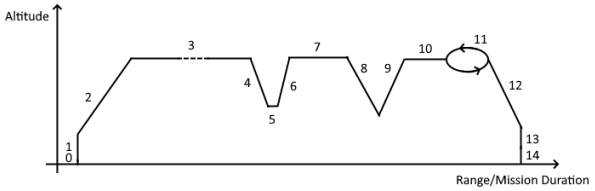

Figure 14.4: Most critical mission profile diagram. Not to scale.

0. Startup
1. Vertical take-off to 30 m
2. Climb
3. Cruise, surveillance mission segment, longest by far
4. Descent to firefight, assumed VTOL for fast altitude change
5. Firefight, assumed heavy use of VTOL propulsion
6. Climb from firefight, required to clear area for potential firefighting response
7. Return to Ground station, assumed 14.1 km, worst assumption from corner to centre of square
8. Descent for landing
9. Rejected landing, climb again
10. 20 km cruise to adjacent ground station
11. Loiter for 5 minutes to clear up alternate landing location
12. Descend to land
13. Vertical landing
14. Shutdown

The UAV is also designed for easy disassembly so it can be deployed and stored with ease. The UAV disassembles five distinct components: the fuselage, the wing, the booms and the empennage.

The battery for VTOL operations and embedded systems needs replacement for each flight as charging it would take too much time. The batteries therefore needed to be in an accessible location to be reached by an automated system. Additionally, manual operations by a human operator was also considered to ensure flexible operations. As their mass is significant, they also needed to be placed as close as possible to the desired CG location. Based on these considerations, the VTOL battery and embedded systems battery are assembled into one pack that can slide in and out from the top of the UAV. The pack is located in front of the wingbox.

The UAVs need to be refuelled each flight, and refilled with water in case of fire suppression operations. These need to be refilled within three minutes automatically. It was decided to make use of the same automated mechanised system to both refuel, refill and replace the batteries. The fuel and water lines connect using a quick disconnect coupling mechanism situated between the wingbox and the battery. The fluids flow to the tanks situated under the wingbox through pipes.

To limit the ground station footprint on the deployment zone, the UAVs are designed to be stackable. The landing gear is designed to be capable of carrying 5 UAVs. In order to have stable stacks of UAVs, a supporting structure with three poles was conceptualised. These would pass through holes in the UAV fuselage, constraining the UAVs.

14.6.Ground Station Concept and Initial Sizing

The ground station is an essential part of the system as it enables the operations of the swarm, handling the logistics of providing energy and water to the UAVs. A containerised solution has been explored to allow for easy transport and storage. An overview of ground station operations are briefly described, followed by a description of subsystems and budgeting for mass and power. Lastly, the geometry of the ground station is detailed.

14.6.1.Ground Station Operations Overview

The ground station consists of three 20 ft containers and either a generator or an array of solar panels. Two containers house the 35 UAVs, the water, generator, pumps, and the refuelling and stacking robot. The third container is a tank that stores fuel for the UAVs. Water storage and energy supply system are considered separately as they vary depending on the location of the ground station. The entire system is deployed to a suitable location by truck, and unpacked and prepared for operations manually. Once deployed, the system should ultimately operate automatically with no personnel on site. This might not be the case at first and some personnel shall be able to go on site if needed to solve problems. The system is designed to operate for four months, with 70 % capacity during the day (nine hours) and 30 % at night (fifteen hours). In reality, the number of UAVs flying at any given time will depend on the live time risk assessment of the area to be surveilled. The UAVs can operate continuously, with robots refuelling them after each flight and stacking them for storage when in reducing capacity.

14.6.2.Landing, Changing Batteries, Refuelling and Refilling

The UAVs land on one of two landing zones in reach of a robotic arm mounted on rails that carry out the battery replacement and the refuelling/refilling. The robotic arms are KUKA industrial robots, and are mounted on rails which extend from inside the container as seen in Figure 14.5a. Batteries are taken by the arm as shown in Figure 14.5b and placed in a battery rack inside the ground station, which is where the batteries are recharged. There are two batteries per UAV: one battery charges whilst the other one is used in flight. Water and fuel pumps inside the container pump fluids into flexible hoses that extend up to the end of the robotic arm. Once refuelled, the UAVs either take off or are put to storage. Bringing the UAVs to storage is done autonomously with a rover with an identical robotic arm.

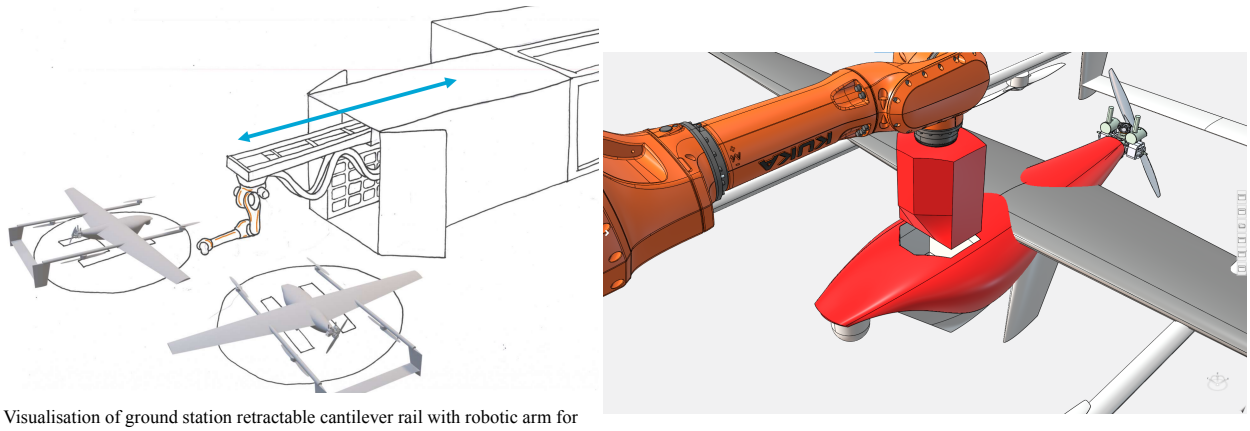

(a) Visualisation of ground station retractable cantilever rail with robotic arm for refuelling

(b) Visualisation of battery swap using CATIA

Figure 14.5: Ground station battery swap and refuelling/refilling visualisation.

14.6.3.UAV Transportation Rover

To enable the stacking of UAVs, a rover carrying the same model of KUKA robotic arm will be used. This rover is designed to operate on rough terrain, the current model having a clearance of 15. A more in depth analysis is needed to determine and quantify which terrain it can operate on. Once a UAV lands at the landing site, the rover will pick it up at its centre of gravity using the robotic arm, and place it on the closest stack with available slots. An initial model of the rover is shown in Figure 14.6.

Due to the large mass of the rover, it will consume a high amount of power, and thus a power budget must be estimated for it.

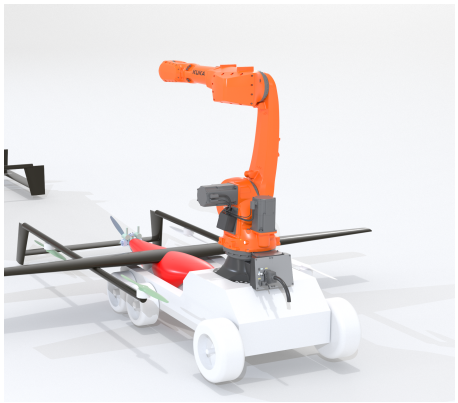

Figure 14.6: Preliminary model of rover to carry UAVs from landing site to stacks.

Starting with the total mass that the rover must carry, there is:

- UAV: $70\,\mathrm{kg}$ (rounded up and definitive)
- Robotic arm: $540\,\mathrm{kg}$ (definitive)
- Rover: $500\,\mathrm{kg}$ (taken from engineering judgement)

This sums up to a mass of $1070\,\mathrm{kg}$. To find the power required purely for accelerating the rover from stationary to a speed of $0.5\,\mathrm{m{\cdot}s^{-1}}$, which is taken based on engineering judgement and requirements, the change in kinetic energy is calculated and the time that the rover takes to accelerate is estimated. This gives a power estimate of $P_{acc} = 80W$, after adding a safety factor of 3. This is low, but the power required due to rolling resistance must also be taken into account. The total force required to overcome the rolling resistance is calculated through Equation 14.1 [45], where μ_R is the rolling resistance coefficient. The value chosen for this coefficient is 0.08, which is usually taken for medium hard soil [46], and this is necessary to enable rover operation in irregular ground.

$$F_{roll} = \mu_R mg \tag{14.1}$$

The power is calculated from this force, the speed of $0.5\,\mathrm{m{\cdot}s^{-1}}$ once again, and an efficiency of 0.6, to have a conservative estimate. This leads to $P_{roll} = 700W$, which means that the total mechanical power required is $P_{mech} = 780W$. Of course, the rover must also have onboard systems, such as embedded electronics, communication components, and sensors. To take this into account, a total budget of $P_{elec} = 150W$ is given for all electronic components that are not used for motion, which is a conservative estimate. This leads to a total power requirement for the rover of $P_{tot} = 930W$.

To ensure that the base station is able to meet this power requirement, an estimate must be made on the total amount of time that the rover will have to operate for during a single day. To obtain this, a worse case scenario of having all the UAV stacks side by side is taken. All stacks are $4.5\,\mathrm{m}$ wide to contain the entire UAV, and are $1\,\mathrm{m}$ apart. However, the first stack is $2\,\mathrm{m}$ from the landing site, to prevent collisions of UAVs in the landing phase with stacked UAVs, during conditions of high wind. Seeing that during high-risk periods, night-time operations include 11 UAVs and daytime include 24, the rover must transport a total of 26 UAVs per day. This results in a total operating time of $1200\,\mathrm{s}$, giving a total energy estimate of $500\,\mathrm{W{\cdot}h}$ per day, when rounding to the upper hundred. This finalises the power budget for the rover.

14.6.4.Self Protection Features

The ground station needs to be inaccessible to any passer by and animals as the ground station will be running autonomously without personnel on site. This will be done with metallic barriers as seen on construction sites, with signs clearly indicating the restricted area.

Additionally, the ground station needs to protect itself from fire in the event that the fire reaches it. This will be done through a sprinkler system which will allow the survival of the ground station system for 8 minutes when engulfed by flames. This was chosen based on current firefighting vehicles for ground personnel have a survivability sprinkler system that is active for 5 minutes. All UAVs are expected to flee from the ground station to a safe alternate landing zone, as specified in the operational plan. The UAVs are therefore not protected by the sprinkler system. The risk of fire arriving to the ground station will be constantly monitored, and an alert given early enough to evacuate the UAVs.

14.6.5.Water and Fuel Storage

Water and fuel storage were computed according to the design operating scenario and self protection requirements. The water storage becomes irrelevant if the ground station is placed next to a water body from which water can be pumped. Calculations for the values derived bellow are trivial.

$1000\,\mathrm{L}$ are required to sustain six hours of continuous firefighting operations for the UAVs. In addition, an estimated $1500\,\mathrm{L}$ is needed for self protection use, $500\,\mathrm{L}$ per container. This brings the total to $2500\,\mathrm{L}$ of water, over which $500\,\mathrm{L}$ are added as a safety margin. Two $1500\,\mathrm{L}$ tanks of water were chosen.

$850\,\mathrm{L}$ of unleaded petrol is needed to sustain the daily operations with the 70%/30% day/night design case. A 20 ft intermodal tank container can store $25\,000\,\mathrm{L}$, which conveniently allows for 29 days of operations. The tank can be refilled more frequently if needed by a smaller fuel truck or the entire container can be replaced monthly.

14.6.6.Mass, Cost and Footprint Budgets

The main components of the ground station were selected according to constraints given by the UAV operations. The mass, cost and footprint of these components were tracked in order to check if they stayed within the rated load of the containers, the given budget, and to track the space needed to deploy the ground station. The list of selected components can be seen in Table 14.1.

The mass budget for a container is of 30 metric tons, which is the rated capacity according to ISO. All elements of the ground station add up to less than twenty metric tons, leaving a comfortable margin.

Power needs for recharging batteries require a large array of solar panels or diesel generators. The best choice will depend on the customer, and the amount of sunlight they receive in their operating area. The decision will also depend on sustainability concerns and the allowable footprint for the ground station. The electric energy needed in a day was computed to be $231.2\,\mathrm{kW{\cdot}h}$ assuming batteries are taking off fully charged and were fully discharged at the end of a flight.

In the Netherlands, in the fire prone region considered, the area of solar panels needed would be $565\,\mathrm{m}^2$. This stems from a solar radiation of $199\,\mathrm{W/m}^2$ [2]. in summer for the region considered, a solar panel efficiency of $24\,\%$[3], and power generating time of $9\,\mathrm{h}$ per day.

Diesel generators meeting the capacity were chosen. Two Warrior $231.2\,\mathrm{kW}$ generators [4] are needed to sustain the power needs. With a tank capacity of 60L each, they have an autonomy of 1.9 days. With an additional fuel tank of $150\,\mathrm{L}$ each which can fit in the containers, they can run for a full week. These tanks therefore need to be refilled on a weekly basis unless additional external fuel storage is considered.

The cost of all chosen components was tracked in Table 14.1. The miscellaneous (Misc) item includes all elements that were not sized, including a margin for unexpected items. Fuel costs over the lifetime of the generators are also included for a fair comparison with the solar panel option. The total is summed separately between the diesel and solar power options. These amount to respectively $771\,\mathrm{k€}$ and $653\,\mathrm{k€}$.

The footprint of the deployed components was also tracked in Table 14.1. Most components in the table are inside the container and do not have a footprint. There is a large difference in total footprint between the diesel and solar option due to the area needed for solar panels.

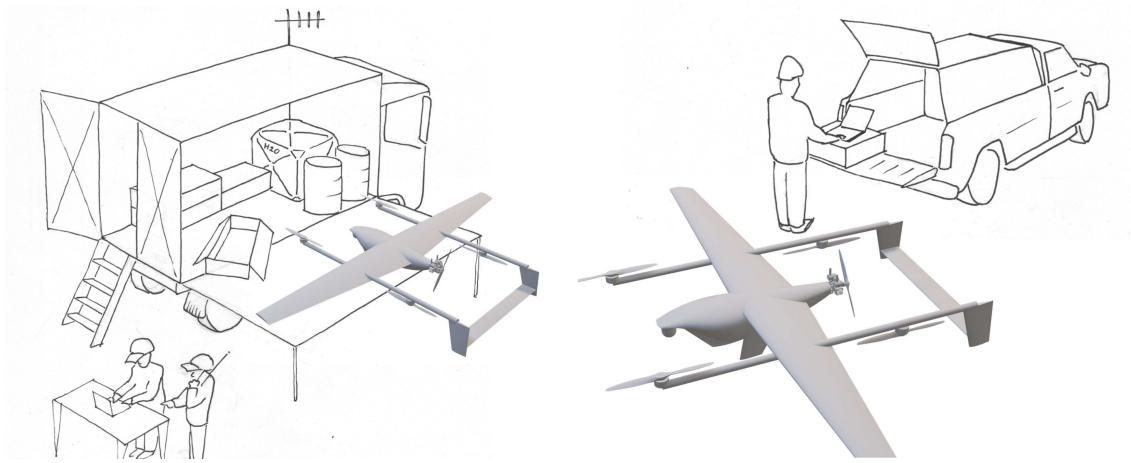

Figure 14.7: Truck and pickup based agile operations concept.

[2] See: https://www.knmi.nl/over-het-knmi/nieuws/zomer-nu-al-recordzonnig Accessed 20/06/2025.
[3] See: https://das-energy.com/storage//Datenblaetter/DE$_E$N/DAS$_E$nergy$_F$actsheet$_2$0x2$_D$E$_E$N$_2$025$_0$4$_2$5.*pdf* Accessed 20/06/2025.
[4] See: https://www.mitropower.com/nl/warrior-125-kw-125kw-295kg-68db-diesel-aggregaat.html Accessed 20/06/2025.

Table 14.1: Mass, cost and footprint budgets for the ground station.

Item / Parameter	Mass (kg)	Cost (€)	Footprint (m^2)
Budget	60 000	800 000	N/A
Total Solar	18 039	652 669	771
Total Diesel	15 570	770 534	206
20 ft standard container	3 180	10 190	14.8
20 ft standard container	3 180	10 190	14.8
UAVs	2 590	N/A	157.5
KUKA KR 70 R2100 fixed + KUKA KR C4 controller	671	53 880	inside container
KUKA KR 70 R2100 mobile + KUKA KR C4 controller	671	53 880	–
Rover	500	107 760	–
Cantilever crane	500	53 880	inside container
Storage equipment (shelves)	500	8 010	inside container
60 L/min water pump	20	880	inside container
60 L/min water pump	20	880	inside container
60 L/min water pump	20	880	inside container
5 L/min fuel pump	5	20	inside container
5 L/min fuel pump	5	20	inside container
1 500 L water tank	59	2 000	2
1 500 L water tank	59	2 000	2
3 000 L of water	3 000	N/A	inside container
Misc. (antennas, computer, cables, refuelling and other costs)	Negligible	217 556	inside container
Intermodal fuel-tank container	3 750	20 380	14.8
Power-source options			
12.5 kW Generator	295	5 990	0.023
12.5 kW Generator	295	5 990	0.023
Fuel costs, lifetime	N/A	216 147	N/A
672 × 0.8 m^2 solar panels	3 059	110 263	565

14.6.7.Ground Station Geometry and Footprint

The ground station geometry when packed is shown in Figure 14.8. The first two are used to store all the components of the system, and the third is a standard 60 ft fuel tank. In addition to the 35 UAVs, the containers contain the automated arms and rover for automated operations, the water tanks, the diesel generators and the battery rack.

Figure 14.8: Packed ground station

The full ground station footprint with solar panels is of $770\,m^2$, which reduces to $205\,m^2$ when using a generator. As the footprint of a full ground station can limit the deployable locations, agile operations is also possible for our system. Small numbers of UAVs can be operated from a truck or a pickup, as can be seen in Figure 14.7.

15 Suppression System

The suppression system is an essential element of the mission, ensuring that early stage fires can be suppressed as effectively as possible. It primarily carries 15 kg of water or other suppressant, deploying it accurately on the fire line, ensuring maximal coverage. The system's development follows a structured approach: first, the key functions and requirements are defined. Next, the water tank is addressed, including details on sealing, drop rate, and considerations for refilling and modularity. Consequently, the protocol for fire suppression - from initial detection to suppressant deployment - is outlined in detail. Lastly, the validation and verification for the suppression system as well as future recommendations are discussed.

15.1.Suppression Functional Analysis and Requirements

The functional analysis for the suppression subsystem is displayed in Figure 15.1 with requirements made in Table 15.1.

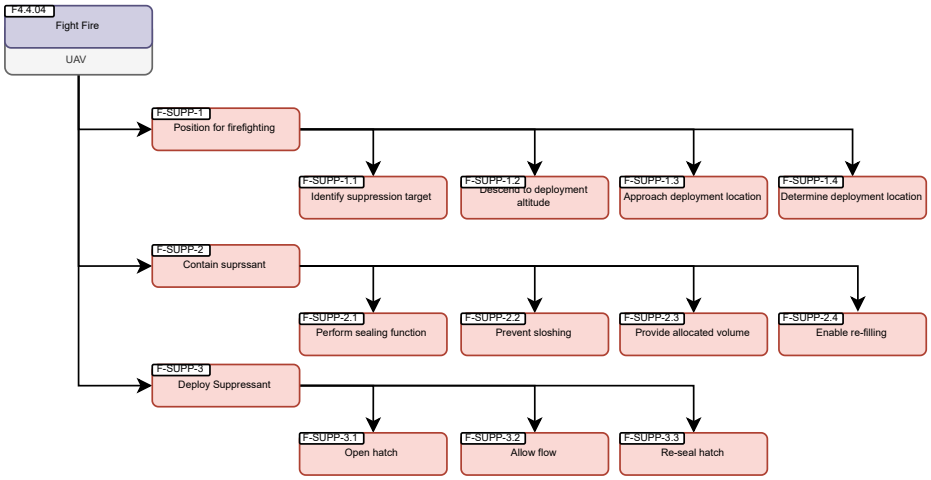

Figure 15.1: Functional Breakdown Structure for Suppression Subsystem

Table 15.1: Suppression Requirements

ID	Requirement
REQ-SUPP-01	The suppressant tank shall hold at least 15 L of suppressant
REQ-SUPP-02	The suppressant tank shall not leak significant volumes in flight
REQ-SUPP-03	The suppressant tank shall autonomously deploy suppressant
REQ-SUPP-04	The suppressant delivery system shall open with an accuracy of 0.5 s
REQ-SUPP-05	The suppressant delivery system shall deploy 60% of the tank capacity within 1 s
REQ-SUPP-06	The suppressant delivery system shall be readily inspectable
REQ-SUPP-07	The suppressant delivery system shall be readily maintainable
REQ-SUPP-08	The suppressant delivery system shall be able to re-seal after deployment
REQ-SUPP-09	The suppression tank shall weigh less than 0.5 kg
REQ-SUPP-10	The suppression tank shall not allow sloshing while executing the FireFligth mission
REQ-SUPP-11	The suppression system shall be removable by a qualified operator
REQ-SUPP-12	The suppression system shall be replaceable with system of equivalent size and weight

15.2.Water Tank

The water tank used must be lightweight, handle water and any loads and deploy water as well as be re filled. The shape is determined to be a semi cone section, seen in Figure 15.2, allowing it to fit snugly into the aerodynamic frame of the UAV, while still maintaining ample volume. The outlet port is also set on the lowest point to facilitate full emptying. Since it only needs to carry water, the internal walls can be made of

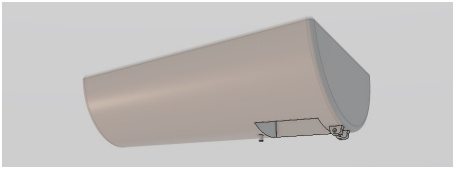

Figure 15.2: Water tank with opening.

simple PET plastic while the wall exposed to the air essentially acts as part of the fuselage and is included in fuselage analysis. Finally, two anti-sloshing vanes are included in the tank, running longitudinally, ensuring the UAV maintains stability and controllability during turns or wing gusts.

15.2.1.Sealing

Since water might be carried for a prolonged time, sealing of the water tank is essential. Since the water pressure is only hydrostatic and the liquid is non-corrosive, no high-pressure seals are required. A simple compressed rubber O-ring seal is used as it offers a long lifetime and easy maintainability. To create a sealing surface a latching mechanism is used with an external hinge as seen on Figure 15.3 to allow outwards opening.

To allow for this, a face axial seal is used. On the leading seal surface, the external hinge creates a compressive force in the x-direction, compressing the O-ring and sealing the surface. Since the flap must open outwards, the other edges must be sealed by compressing them vertically. For this, a rotary slanted latch is used as visible on the right side of Figure 15.3. It rotates a slanted surface slowly, enabling operation with a servo and applying ample compressive force for sealing. The sealing operation is first done by a second servo motor, lifting the flap with he help of air resistance, moving it close enough for the tapered edge of the latch to engage the flap. The latch then rotates, squeezing the O-rings. Note that for both the leading and other seal faces, the final compression is provided by the rotary latch. The tight compression also allows some load transfer from the external fuel tank wall to the flap, improving structural performance. The external seal and latching mechanism also allow easy inspection and maintenance. Lastly, a non-return valve is installed on the top-side of the tank on the air-facing surface to allow for air to enter the tank as the water depletes. Since the air is much less dense, this can be about 1 cm in diameter. The non-return valve is a simple mechanism that allows the air to flow in when the pressure drops but does not allow water to leak out during banking manoeuvres.

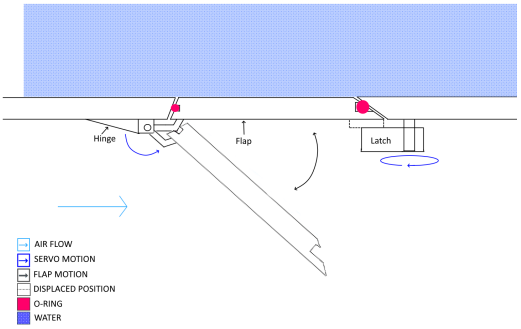

Figure 15.3: Illustration of suppressant deployment mechanism

15.2.2.Water deployment

To effectively fight fires, water must be deployed rapidly. To predict water drop rates, orifice theory is used. The back pressure is provided by the weight of the water, meaning the rate at which the suppressant drops reduces as the drop is happening. Orifice theory describes the flow rate Q as a function of orifice area A, gravity and hydrostatic head h as seen in Equation 15.1 modified for water from Reader-Harris [47]. This is valid for circular and rectangular orifices. To enable a flapped latch, a rectangular design is beneficial for sealing. The flow also depends on the discharge coefficient C_0, which takes a standard value of 0.62 for plain openings.

$$Q = C_0 A \sqrt{2gh} \tag{15.1}$$

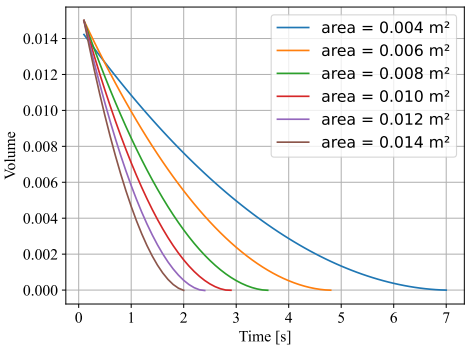

Figure 15.4: Volume vs time for different opening sizes.

As the tank volume is small, the shape contribution is minimal and a simple rectangular tank is modelled for ease of calculation. This is seen as a conservative assumption as a semi cone section design with the discharge outlet placed at its lowest point maintains a higher head, especially when the tank is almost empty. The discharge rates for different openings are seen in Figure 15.4 below.

An area of $0.012\,\mathrm{m}^2$ is chosen and a rounded rectangular opening with dimensions $0.12\,\mathrm{m}$ lengthwise and $0.10\,\mathrm{m}$ widthwise is used since the tank possesses curvature on its lower side and a narrower cutout lengthwise is preferred. This allows REQ-SUPP-07 to be met. Approximating the size from Legendre et.al. [48] and water jet approximations, the concentrated area of the water ellipse would have a major axis of $\approx 20 - 30$m, which corresponds to a fire ellipse of $\approx 150\,\mathrm{m}^2$ in area with most of the water concentrated in the final part of the ellipse.

15.2.3.Note on modularity

To enable flexible operations of the UAV swarm, a modular approach to the water tank installation is planned. This will allow the water tank payload to be replace by other payload modules. The tank may be removed by an operator, detaching it from the fuselage via a bolted interface. This ensures the outer tank shell can be aerodynamically flush and carry some structural weight. Since removing the water tank significantly weakens the fuselage, the change may only be undertaken between deployments with proper testing. Nonetheless, this is considered acceptable since the tank will practically be used for one mission during a deployment. This is subject to testing in the prototype phase, noting that if satisfactory performance cannot be obtained, other solutions are possible. These range from only allowing module switching during extensive base maintenance to making the UAV system only be delivered in a single configuration where the type of payload attachment must be specified by the client on order.

15.2.4.Suppression Procedure

Having considered the deployment of water within the UAV, the strategy for deployment can now be considered. The objective of the water deployment is to either completely suppress the fire (if possible) or delay its propagation as much as possible. Using this as the basis of suppression, the procedure can be created.

Once a fire has been detected, the UAV maps its current position to its environment and predicts its propagation direction. Then, computing its area, it determines whether it is suppressible or not. If it is, the UAV targets the centroid of the area. If not, the UAV targets the portion of the fire line that is spreading the fastest. Meanwhile, it begins its descent to an altitude of $18\,\mathrm{m}$, or $10\,\mathrm{m}$ above the tree-line (whichever is lesser), where suppression will occur. This altitude was selected based on the dive speed of the UAV ($36.4\,\mathrm{m{\cdot}s^{-1}}$ (assuming ground speed and airspeed are equivalent) and the methodology described by Legendre et al. [48] to achieve the optimal water spread over the fire of $1.6\,\mathrm{L{\cdot}m^{-1}}$ described by Bodino et al. [49]. However, these results should be treated with caution, as the assumptions in Legendre et al.'s model are derived from aerial vehicles with payloads at least an order of magnitude larger than that of the UAV, and thus may not fully reflect its dynamics. The descent should be done at dive speed (to minimise the time to reach the fire), and since the UAV is not equipped with velocity-reduction mechanism (such as airbrakes), it is assumed that the time required to decelerate to a lower velocity (e.g., stall) is longer than allowable based on fire propagation speed. The dive speed of the UAV is also similar to the speed at which most fixed-tank helicopters to drop the water [48], hence, although the vol, and consequently, the suppression drop will occur at dive speed. Throughout the dive, the UAV will turn such that it aligns its direction with the fire at least $140\,\mathrm{m}$ before arrival such that potential eigenmotions generated throughout the turn may be dissipated (for greater accuracy). This distance is based on the time it takes to dissipate 90% of the Dutch roll using the half-amplitude found in Section 11.7 of 0.582 (which yields a distance of $70.4\,\mathrm{m}$), and the horizontal distance travelled by the water between deployment and reaching the fire (based on the $18\,\mathrm{m}$ drop altitude), which is $69.7\,\mathrm{m}$.

15.3.Suppression Verification & Validation

Verification for the deployment of the suppressant payload is first performed by inspection of the graph. From Figure 15.4 it is evident that a larger opening results in faster deployment aligns with expectations. Moreover, it is observed that the deployment rate starts off fast and diminishes over time as less pressure is pushing the suppressant out of the orifice. The graph therefore seems to be performing to expectations. Unit tests are also performed the calculation results match analytical, by-hand calculations and that the plotting accurately represents the calculated data.

Finally, the requirements must be verified via a compliance matrix in Table 15.2.

Table 15.2: Compliance matrix for suppression.

ID	Method	Status	Value	Reason
REQ-SUPP-01	Analysis	Preliminary yes	15	Volume of tank
REQ-SUPP-02	Demonstration	Preliminary yes	N.A.	Seal installed
REQ-SUPP-03	Test	Preliminary yes	N.A.	Precise Servo Control
REQ-SUPP-04	Test	Preliminary yes	<0.3 sec	Precise Servo Control
REQ-SUPP-05	Test	Preliminary yes	60%	Orifice Theory
REQ-SUPP-06	Analysis	Preliminary yes	N.A.	Detachable
REQ-SUPP-07	Analysis	Preliminary yes	N.A.	Detachable
REQ-SUPP-8	Test	Preliminary yes	N.A.	Seal installed
REQ-SUPP-9	Test	Preliminary yes	N.A.	Integrated Into Fuselage
REQ-SUPP-10	Demonstration	Preliminary yes	N.A.	Anti Sloshing Vanes
REQ-SUPP-11	Analysis	Preliminary yes	N.A.	Detachable
REQ-SUPP-12	Demonstration	Preliminary yes	N.A.	Detachable

15.4.Suppression Recommendations

To efficiently implement the suppression system into the UAV and its operations, the sealing system must be tested and the O-rings must be sized, along with their groups and the deployment and retraction of the flap must be tested both in a stationary and a wind tunnel/flight test condition. The system must be fully integrated into the fuselage structure with placements of the fasteners positioned. For the system to be modular, these load paths must be further analysed and a test must be executed to verify any designs before they take flight. Another aspect to verify is that the drops are correct, as the body of work on medium-sized vehicle water suppression drops is effectively non-existent.

16 Simulation

To analyse the effectiveness of the solution, the mission needs to be simulated. This includes a simulation of fire behaviour, described in Section 16.1, of the path that the UAV will use while scanning, discussed in Section 16.2, and how the UAV will detect fire, explained in Section 16.3. Furthermore, it describes the models that were created for swarm coordination, in Section 16.4, and fire suppression, in Section 16.5. Then, the integration and the complete simulation are described in Section 16.6, and its results are shown in Section 16.7. Finally, Section 16.8, Section 16.9, and Section 16.10 describe the sensitivity analysis, verification, and validation. The chapter ends with recommendations.

16.1.Fire Simulation

The main aspect that must simulated in a fire detection and suppression mission is the fire. The fire simulation is fundamentally based on Rothermel's 1972 mathematical model for fire propagation [43]. Such a model includes various factors, hence, these must be determined and included into the fire simulation.

16.1.1.Environment Mapping

For predicting and simulating a fire, having an environment where the fire propagates is strictly necessary, as it is the environment that defines how and where the fire propagates. Note that this does not refer solely to a computer-based environment, but rather to a virtual representation of a physical space—encompassing elements such as topography, vegetation (dendrology), and weather conditions (meteorology). These elements may be derived from real-world data or artificially generated, with the fire simulation functioning equivalently in either case. This section focuses specifically on how these attributes are extracted from the physical environment.

One of the main aspects relevant to the spread rate of fires is the slope. This is because the fuel that is upslope is pre-heated and exposed to the flames of ascending fire, consequently propagating at a higher rate. To obtain the slope, satellite altitude measurements obtained using the *ridge_map* package were differentiated east-to-west and north-to-south, resulting in the slope gradient. These are then mapped to the environment and reshaped to fit the resolution.

Another essential aspect is the area's dendrology - specifically, the composition of its vegetation - as different plants have different burning characteristics. The composition is analysed by mapping the pixel colours in satellite images to fuel models. Satellite imagery is obtained using the ESA's *Sentinelsat* API, which are then reshaped to the environment resolution. Consequently, the RGB values of each grid cell are extracted and matched to the fuel type with the highest colour similarity. The colours of the fuel (or non-fuel, such as terrain) types have been defined using K-means, which was used to identify the colour ranges with the highest frequencies in the region. These colour clusters were then manually mapped to the appropriate fuel or terrain types based on flora or features that match each range.

Lastly, fire propagation is sensitive to meteorological data, including temperature, wind, and humidity. The date and time of day are also relevant. However, these are assumed to be inputs of both the environment and the meteorological data. The meteorological data is then obtained using *python_weather*.

16.1.2.Fuel Types

As previously mentioned, the basis of the fire propagation in the simulation is the 1972 Rothermel mathematical model[43]. This model contains a set of fuel types, that was later expanded upon by Scott and Burgan in 2005 [50] to include up to 256 fuel models. These are documented in great detail, and their outputs can be accessed through the United States Forest Service's BehavePlus 6 software. While the software is freely available for public use, it does not offer an interface for programmatic access.

Hence, a set of neural networks (NNs) were trained for multiple fuel models, based on data from *BehavePlus6*. The inputs of these include the wind speed, slope, and dead fuel moisture index[1], while the results included the propagation speed and the flame length. The dead fuel moisture index is obtained from a decision tree described by [43].

Each NN had a different nodal architecture based on the best results a validation set after 300 epochs. These were then trained over 3000 epochs for their respective model data. The results and errors of these are discussed in Section 16.9.

16.1.3.Fire Propagation

Lastly, the propagation speeds must be processed into an actual fire. A fire was then defined by a start point and a set of points that define the fire front. The latter get propagated in the direction opposite to the initial fire location at every step - this became the implementation of a simplified fire.

[1]Dead fuel moisture index is an index of water contents (as percentages of total weight) of dead (vegetation) fuels over different time-lags [51].

However, this is highly limited, being incapable of propagating around obstacles or propagating in different directions depending on the fuel types it interacts with, which a real fire would. Hence, the model was expanded upon in a manner analogous to the Huygens-Fresnel principle, where each point on a wave front acts as a spherical source, as shown in Figure 16.1. Therefore, the fire is now represented by a set of simplified fires, with their fire front points becoming new (simplified) fire sources after every iteration.

Although more realistic, this is highly computationally expensive, with the total number of points to propagate increasing by a factor equal to the resolution of each fire front (36 for fast simulations, 360 for accurate simulations) for every iteration step, with a very large amount of overlap. Instead, a fire grid is used, describing whether a certain grid cell is on fire or not. It then determines the perimeter areas (those that are on fire and adjacent to non-fire areas), and selects a single point within the area to become the next fire. The selection of the point may either be done at random or through some strategy.

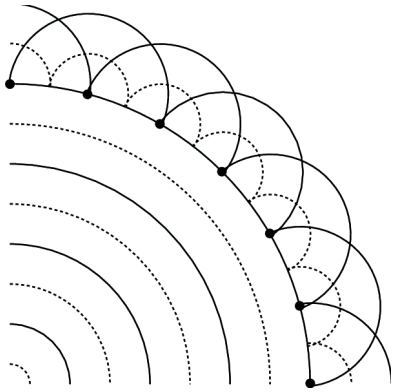

Figure 16.1: Visualisation of the Huygens-Fresnel Principle [52]

The rationale for the need of a strategy is the following. Although stochastic simulations are effectively the norm for advanced fire models due to the ability to provide probabilities on the potential of a fire spreading a certain way[53], the stochasticity of the simulation - both in the selection of points to propagate and the generation of new fires (for which the fire front may either be defined at equal angles from each other or at random) - significantly affects the results. Hence, having a deterministic simulation was deemed to be desirable for analysis, validation, and a general robustness of results. Thus, the results shown henceforth are using fires generated using uniform fire front points and a quasi-random selection strategy, which selects a point at random, yet that point will be the same for all iterations. For the generation, this effectively ensures that propagation will occur in all directions, and still maintain a degree of stochasticity through the selection of a quasi-random point.

Alternatively, other strategies are possible, such as consistently selecting the grid point furthest from the initial fire location. This strategy would accelerate fire propagation and speed up simulation convergence. However, it introduces the classic exploration–exploitation trade-off. By focusing on maximizing spread and covering as much area as possible, the model tends to produce a patchy fire with a large, irregular perimeter. This results in poorer overall coverage and slower simulation performance, as more grid locations need to be processed. Due to its inferior results and slower convergence, this approach was ultimately not used.

16.1.4.Assumptions

Throughout Section 16.1, a large number of assumptions have been made. This section serves as a brief analysis of the assumptions made, their consequent effects on the results, and a discussion the reasons why such an assumption is valid for the simulation.

Table 16.1: Assumptions of the fire model.

Assumption	Description	Effect on Results	Reason for Valid
One-to-one colour matching	Fuel models are identified solely based on colour, assuming each colour corresponds to a unique material.	In reality, multiple materials can share the same colour (one-to-many), leading to frequent misclassification.	The simulation is used over large areas, hence, the individual mislabels should average out through propagation over various fuel types.
Uniform weather	The weather (wind, temperature, and humidity) is assumed to be constant over the entire operational area.	This slightly worsens accuracy, as localized variations due to elevation (e.g., wind or shading) are neglected.	The model focuses on overall behaviour, and global results remain representative despite local inaccuracies.
Discretised values reflect continuous behaviour	The grid uses discretised values, assuming the aggregate result approximates that of continuous data.	Single iterations may deviate from true values, but over many iterations, results converge to a representative average.	The grid scale is large compared to individual cells, allowing discretisation effects to average out over time through multiple cells.
Time-independent conditions	Environmental factors (e.g., weather) are fixed for the duration of the simulation.	For long simulations, this may lead to overestimation of fire spread and area, especially for daytime fires.	Designed for FireFlight, which focuses on short-term fire detection and suppression, making time-dependence negligible.
No burn-out	Once ignited, a cell continues to burn indefinitely unless extinguished.	This overestimates the area affected, as real fires naturally burn out after a period.	For rapid-response tools like FireFlight (operating over minutes), the impact of burn-out is minimal.
Representative sample point	Fire propagation from a cell is based on a single point assumed to represent the entire cell.	If time steps are too small relative to fire speed, propagation may be underestimated. With proper scaling, it properly approximates the Huygens-Fresnel propagation.	Time steps are chosen based on grid size, ensuring an effective approximation of continuous propagation.

These simplifications enable faster simulation runtimes without significantly compromising the validity of the overall fire

behaviour predictions, especially in short-term, rapid-response applications like FireFlight.

16.2.Path Optimisation

Another essential aspect of the simulation is the routes of UAVs. The main concern is that the entire area needs to be regularly scanned and a routing strategy is required to determine how this grid would be covered. As with any region-based coverage problem, strategies/approaches differ significantly in certain properties, or, conversely, can be optimised for a particular property. This region explores how the path-determining algorithm was designed and implemented.

16.2.1.Risk Measure

For the scanning to be most effective, high-risk areas should be scanned more often than lower-risk areas. This requires an analysis of the each area's risk.

The approach taken for the risk analysis was using the propagations calculated in Section 16.1. A fundamental metric of risk was found to be the velocity squared. This is due to the fact that fire areas are elliptical[2], their areas are proportional to the propagation speed times the time since start, squared. Hence, since the time is not measurable and is effectively random, the risk can be based on the propagation speed, squared. This takes into consideration the meteorology, dendrology, and topography of the region, incorporating all into a single risk measure. The results of the risk map can be seen in Section 16.7.

Additionally, it is important to mention that the risk of the area is dynamic. Not only does it depend on the changing circumstances of the environment, but also includes the updated scans from the UAVs, which are taking images of the regions and consistently flying above them.

16.2.2.Genetic Algorithm

Generating optimal paths to achieve a particular mission is a group of problems known for having being particularly complex computation. This is as they scale poorly, and therefore require unique approaches to solve them. One such approach is genetic algorithms, which effectively reflect evolutionary processes for reaching a (near) optimal solution.

The path is encoded as a list of grid points. Grid points may be repeated, with their repetitions being proportional to the associated risk value. Since these paths are independent of range, the software computes trajectories where refuelling are necessary, and therefore implicitly incorporates the flights from and to the ground station.

With such an encoding, an initial population (first generation) is created by constructing a path of the points, randomly sorted. Then, genetic processes are performed iteratively for each generation, which consist of the following steps:

1. Assess fitnesses of all solutions in the generation
2. Select solutions to reproduce
3. Generate offspring solutions
4. Mutate offspring solutions
5. Add offspring solutions to population
6. Implement elitism: eliminate solutions with low fitness

Two key aspects of this process are worth highlighting. First, the fitness function must reflect the mission (further discussed in Subsection 16.2.3). Secondly, elitism[3] is employed to control the computational load and increase the rate of convergence.

After sufficient generations or convergence of the fitness, the result with the highest fitness is taken and set as the final path.

16.2.3.Additional Considerations

One of the main considerations with any optimisation is the fitness function that the model optimises for. Genetic algorithms are well-known for their adaptability [54], hence, any fitness function is implementable. However, it is crucial to create a fitness function that accurately represents the problem objectives. The fitness function used is defined as follows:

- Each point has a time counter.
- All points share a time threshold. If the threshold is exceed, a global penalty counter is incremented by an amount proportional to both the elapsed time.
- The total accumulated penalty is then inverted to produce the final fitness value.

[2] see: https://elmfire.io/verification/verification_01.html. Accessed 26/05/2025.

[3] In genetic algorithms, elitism is a property which eliminates poorly-performing solutions, thus, improving the average quality of solutions, and decreasing the population of a particular generation

Although the fitness function may appear unnecessarily complex, its design is essential to complete the mission successfully. A simpler metric, such as minimising total time, would not be valid. Such a metric could be exploited by the algorithm, with the multiple passes over the high-risk region being done by effectively moving to a nearby grid point and then immediately returning, thereby technically meeting the requirement of multiple visits without meaningfully re-scanning the area. Such a behaviour would result in long periods where high-risk areas are left unscanned. leaving a large gap in the scanned time. The use of a threshold avoids this exploitation by incentivise the UAV to revisit high-risk areas at more regular intervals.

An important aspect of the path is that, in practice, it will be followed by multiple UAVs. At first glance, optimizing the path for a single UAV might seem misaligned with the goal of coordinating multiple UAVs. However, this approach remains valid when the path is instead conceptualised as a sequence of smaller loops - from take-off to landing at the GS - which can be assigned to different UAVs at different times. Alternatively, it can be conceptualised as a staggered traversal of the path - with all UAVs following the same path with temporal offsets. Either of these conceptualisations is equivalent to a single UAV flying a single optimised path, with the landings included.

Lastly, it may seem that using time or distance in the fitness function is equivalent, as it is assumed that the UAV flies between points at its cruise speed. However, this is not the case as the path-determining algorithm is designed to be dynamic, finding the optimal path based on the environment conditions - in particular, the wind. Hence, although the UAV is still assumed to be flying at cruise speed (airspeed), its heading and ground speed (which is related to distance) are now adapted to navigate to the point while accounting for the wind direction. Now, the relation between time and ground speed is more complex, meaning that a fitness function based on distance may not produce the same results as one based on time. Since time is the critical factor in fire propagation, the fitness function is therefore formulated using time rather than distance.

16.2.4.Assumptions

The routing algorithm is intended to represent the optimal path in the real world, and adapt to changing circumstances. However, as with any model, certain assumptions need to be made to represent the physical environment. The main assumptions made for the path simulation are described in Table 16.2.

Table 16.2: Assumptions of the fire model.

Assumption	Description	Effect on Results	Reason for Valid
Constant cruise	The simulation assumes the UAV maintains constant cruise speed throughout the mission. This excludes VTOL, climb, and descent phases when travelling to and from the GS.	Estimated times are slight underestimations, as they do not account for slower speeds during phases other than cruise.	The take-off, climb, descent, and landing phase constitute a small fraction of the total flight time, thus, the effect will be minimal.
Instantaneous turns	The algorithm exclusively considers the time in straight flight between points, neglecting time in turns.	This will slightly underestimate the time required to move between two points, as turning time is time when the UAV is not flying directly towards the target location.	Since the UAVs have a fairly high turning rate, and operate in a large grid, the turning times are significantly smaller than the time taken during straight cruise flight.
No refuelling time	The UAV is assumed to refuel instantaneously upon reaching the GS.	Fitness values are slightly inflated, especially for less efficient paths requiring more refuelling stops.	Since the genetic algorithm generally reaches near-optimal solutions (which results in deviations from an actual optimal) and with UAV endurance exceeding $3\,\mathrm{h}$, the $5\,\mathrm{min}$ required for refuelling has minimal impact.

16.3.Fire Detection

As the main objectives of the mission are early fire detection and suppression, having a reliable detection method is essential. Due to this, FireFlight will have a redundant detection method for maximum reliability. This will be achieved by having two separate ways to detect fires. While the UAV is surveilling the area, it will use only its infrared camera for fire detection. The camera measures the temperature value at every pixel, so a simple temperature threshold can be defined, meaning that if a temperature above this value is detected, a fire is present. This temperature threshold will be determined at the operational area, by adding $5\,^{\circ}\mathrm{C}$ to the surrounding area's temperature. After detecting a fire with the infrared camera, to confirm whether a fire is indeed present, the UAV will apply a second method for confirming the presence of the fire. It will use a convolutional neural network (CNN) on images gathered from the RGB camera, and if this also identifies a fire, the UAV will alert all other UAVs of the threat.

The process of creating the CNN starts with the detection strategy, which is crucial for knowing what type of data is required. This has already been defined as using the RGB camera onboard the UAV to confirm the existence of any fires. This means that the next step is finding a dataset containing RGB images of wildfires. Fortunately, there is an existing group of researchers from the United States whose goal was to facilitate the creation of detection models to be used by wildfire surveillance UAVs. To this end, they deployed UAVs during a wildfire in Northern Arizona and collected data as both RGB and infrared images. This resulted in the generation of the three **FLAME** (Fire Luminosity Airborne-based Machine learning Evaluation) datasets [55, 56, 57]. To make the datasets easy to use for detection algorithms, the researchers also

annotated and labelled the datasets frame by frame.

These datasets were then used to write a paper detailing the development of two separate model types for fire detection [58]. This leads to the next step in the creation of the CNN, which is choosing the type of model. Shamsoshoara et al. [58] show that the two main ways of detecting a fire from an RGB image are classification and segmentation. A classification model outputs a boolean for each image, showing whether a fire is present or not. The issue with this is that the UAV would not know the precise location of the fire, only that it is inside its field of view. That is where the segmentation models come in, as they provide pixel-by-pixel classification, showing the exact location of all fires within the frame. As the present UAV requires the precise fire location to deploy the water payload and inform firefighters of the fire state, it is decided that the model used must be a segmentation model.

After choosing the model type, the exact model that will be trained must be decided upon as well. Several segmentation models exist [4], but one of the fastest computationally and easiest to implement is the U-net [59]. So, it will be used as a first attempt at creating an accurate and precise fire detection model that does not require too much computation by the UAV, which aids in reducing the power budget for the electronics. If, after developing this model, it does not achieve the accuracy and precision required by the mission, other models will be explored, such as DeepLabV3 [60]. DeepLabV3 is able to create more detailed segmentation masks of images, but is also more computationally expensive.

Everything from here onwards, which includes the technical development of the model, will be done at a later design stage. Now that a specific model has been chosen (U-net), the FLAME datasets must be pre-processed to achieve the particular format required by U-net. The data will then be divided into training, validation, and test subsets. After the first version of the model is trained, its results on the validation data will be used to choose the best-performing loss function and tune the hyper-parameters. Validation data will also be used to check whether the model is performing as intended, particularly in terms of accuracy, precision, and overfitting. After the final model tuning is completed, the model will be tested on the test data, to obtain a final accuracy result. At this point, the decision will be made on whether it is necessary to develop DeepLabV3 (or any equivalent) for greater accuracy. This concludes the development of a redundant fire detection system for FireFlight.

16.4.Swarm Coordination

In a system where several UAVs are flying in close proximity and at high speeds, an existing model for collision avoidance and proper surveillance and suppression strategies is imperative. Due to the distinctions between different mission phases, several models have been created.

Starting with the transition of take off to surveillance, collisions are avoided by having the UAV fly at a lower altitude than surveilling UAVs, until it reaches the surveillance path. The same model is applied to when the UAV must return to the ground station at the end of the mission or to refuel. To ensure that several UAVs do not attempt to land at the same time, the ground station will also act as air traffic control, communicating with UAVs to inform them of whether they may land or should loiter for a defined period of time. If several UAVs must loiter around the ground station at the same time, they will do this at different altitudes. However, this scenario will be avoided by initially deploying UAVs at different times, meaning that they will also refuel at different times.

Moving onto the coordination of UAVs while following the surveillance path, the model used is an adapted version of the Boids algorithm, developed by Craig Reynolds in 1986 [61]. While the classic Boids algorithm has three distinct rules (separation, cohesion, and alignment), the adaptation used in FireFlight only includes separation. Separation consists of ensuring that a minimum distance is kept between each UAV. In classic Boids, it works by changing the heading and speed of a UAV when it is within the minimum distance of another UAV. However, for FireFlight, this would mean that UAVs deviate from their optimal surveillance path, which is unwanted. To solve this, a second adaptation was made to the Boids algorithms, where collisions are prevented by altering only the speeds of UAVs, instead of their directions. To this end, a variable called "$change$" is created, to represent the change in speed required by the UAV to prevent a collision. When the UAV detects another UAV in front of it, it will compute its Euclidean distance from that (other) UAV, and then compute the required change in speed with Equation 16.1. In Equation 16.1, "k" is a factor to ensure that changes in speed are not too drastic, and "$separation$" is the minimum separation distance at which UAVs should fly. As this is only activated when $distance < separation$, the speed of the UAV is always reduced, which is the desired behaviour. Furthermore, a lower distance means a larger deceleration, so, if the UAV is almost colliding, it will decelerate strongly.

$$change = change - k(separation - distance) \tag{16.1}$$

This change is also computed when the UAV detects another UAV closing in from behind. However, here the first minus sign in Equation 16.1 is converted into a plus sign, to increase the speed of the UAV. Both changes are then added to find the resultant change required. The separation distance was chosen to be the length of the surveillance path divided by the number of UAVs, such that all UAVs are equally distanced. Since the swarm uses AI and surveillance data to divide itself

[4] See: https://www.superannotate.com/blog/guide-to-semantic-segmentation. Accessed: 16/06/2025.

into sub-groups of UAVs, as explained in Section 16.2, the algorithm is applied separately and with distinct separations to UAVs in different sub-groups. One aspect of this algorithm that would usually be concerning is when the path of two UAVs intersects, as here the changes in speed would be the same by both UAVs, meaning that they would still crash. However, this is not an issue for this particular system, as the path flown by all UAVs is the same, as described in Section 16.2.

When a fire starts, a UAV is only able to detect it after it reaches a size of $0.09\,\mathrm{m}^2$, due to the altitude at which the UAV is flying and the resolution of the onboard infrared camera. To account for this in the simulation, a fire is always started with that size. To enable fire detection in the simulation, an array of type boolean called "fire_present" is created, to store the positions in the surveillance path where a fire is present. Since the field of view of the UAVs is $1280\,\mathrm{m}$ by $1280\,\mathrm{m}$, when a fire is within $640\,\mathrm{m}$ of a point on the surveillance path, the index corresponding to that point is marked as "True" in "fire_present". When a UAV is reaching that point, the fire is marked as detected, and the 80% of all UAVs that are closest to the fire will fly towards it, while the remaining 20% stay in surveillance mode in case new fires arise. Having a large number of UAVs flying towards the same location greatly increases the probability of a collision, so a coordination model is required. Here, the Boids algorithm used for surveillance would be detrimental for the mission, as the UAVs should fly at maximum speed towards the fire. So, an independent model was made, also using the separation rule from the Boids algorithm, but now altering only the heading of UAVs for collision avoidance. This alters the name of the main variable "$change$" to "$steer$", representing the total rotation in heading required for a UAV. In terms of the logic of the algorithm, when the UAV is within the minimum allowed separation distance from another UAV, it will again compute its Euclidean distance. It will then calculate the difference between the positions of both UAVs, in vector form, and scale it by the distance using $diff_{sc} = diff/distance$, such that a shorter distance results in a higher heading change. "$diff_{sc}$" is then added to "$steer$", and this process is repeated for all UAVs within the minimum separation. "$steer$" is then averaged, converted into a unit vector, and later into an angle through simple trigonometry.

When a UAV reaches the fire, it will attempt suppression, and the model used for this will be explained in the next section. After suppressing, the UAV increases its altitude to cruise level, and starts circulating the fire, monitoring temperature, spread rate, location, among others. To ensure that UAVs circulating the fire do not collide with each other, the Boids adaptation used for surveillance is applied again. The adaptation is applicable here as all UAVs are also following the same path (the advancing fire line) and should not deviate from it.

16.5.Suppression Model

The procedure for deploying the water on the fire is described in Subsection 15.2.4, and a model for this is created as well. It works as follows; once a UAV is $900\,\mathrm{m}$ from the fire front, it will begin its dive from $450\,\mathrm{m}$ to $18\,\mathrm{m}$, using a negative pitch of $30°$. Once the dive is finished, the UAV will continue to fly (cruising or turning) towards the fire, with the added speed from the dive, until it is $70\,\mathrm{m}$ from it. At this point, it will deploy the water such that it hits the fire front precisely. Afterwards, the UAV will start circulating the fire, as was described in Section 16.4.

Having dropped the fire, the area suppressed is then modelled using the process described by Legendre et al. [48]. Since UAVs drop at the right location to hit the front-most area in the fire, the fire points are then moved back to the limit with the area of water hit. The area is added to a list of areas of suppressed locations, over which the fires cannot propagate. This assumption is valid for smaller fires, where the time simulated is relatively small compared to the fire it takes to evaporate the water.

16.6.Integrated Simulation

In Sections 16.1 through 16.4, an evaluation of the different aspects of the mission have been described. However, to visualise how the designed UAV behaves against all, a complete simulation needs to be devised.

16.6.1.Flight

To simulate the UAVs flight, its aerodynamic parameters have been implemented, and its equations of motion solved. To perform the mission, changing its altitude and flight direction, different flight modes have been defined. The mode of the UAV is selected by the control logic, discussed in Subsection 16.6.2.

The control modes defined include:

1. **Landed** - the UAV is grounded, refuelling and replenishing its payload.
2. **VTOL Take-off** - the UAV is rising vertically until the designated transition altitude of $30\,\mathrm{m}$. Its heading throughout the climb is directly against the wind direction[5].
3. **Transition** - Transitioning from vertical to horizontal flight, gaining velocity and lift while reducing
4. **Climb** - Climbing from VTOL take-off altitude to cruise altitude.

[5]The UAV is designed for performing VTOL into the wind, allowing the horizontal propulsion system to be used for counteracting the displacement component by the wind while simultaneously gaining an initial airspeed. This approach also reduces energy consumption for the VTOL and transition phases due to the additional lift generated.

5. **Cruise** - Cruising along pre-defined surveillance path.
6. **Turning** - Banking and changing direction towards target direction.
7. **Cruise to fire** - Cruising towards the general direction of the fire, coordinating with other UAVs through AI.
8. **Suppressing** - Attempting to suppress the fire.
9. **Circulating fire** - Once close to the fire, monitoring the fire using AI.

These change between each other based on the state of the UAV and its perceived environment. This includes everything from its location, risk maps, fire locations (if any), etc.

16.6.2.Control Logic

The mode changes are based on the control logic of the aircraft. A simplified version of the control logic is shown in Figure 16.2.

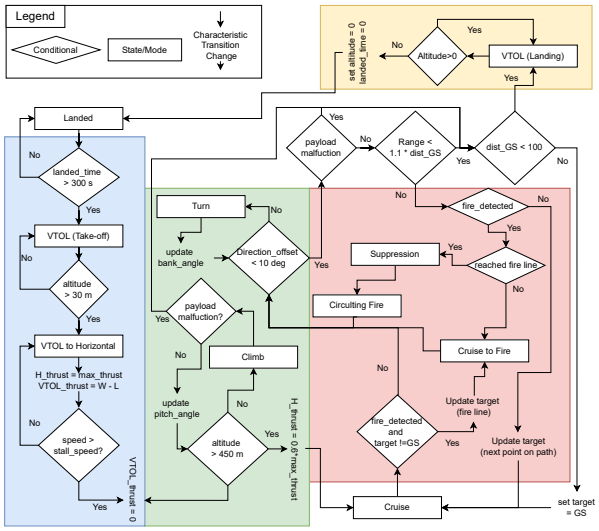

Figure 16.2: Control Logic

Note that in the diagram, the rectangular boxes are modes, rhomboidal boxes indicate decision points (that depend on the UAVs situation), and the text between transitions indicates the characteristic actions that occur within the mode transition. Within regular operations, four main phases have been identified. These include:

1. Take-off (in blue) - from the ground to effective navigational mode.
2. Navigation (in green) - conducting the two main UAV functions: quasi-straight flight and turns.
3. Firefighting (in red) - conducting firefighting operations - only set if fire is detected.
4. Landing (in yellow) - from any of the other modes down to a grounded UAV.

It is important to note that a complete flight controller has not been implemented by this stage. A rudimentary flight controller with discretised deflections and thrusts based on certain value ranges, however, a complete flight controller would be implemented in post-DSE stages.

Lastly, the conditionals ”fire suppressible” and ”payload malfunction” in Figure 16.2 require further elaboration. ”fire suppressible refers to whether the UAV is in the correct position to begin its water payload deployment phase. If so, the UAV goes into its suppression mode, where it decreases in altitude and speed and deploys its payload, as described in Subsection 15.2.4. Meanwhile, ”payload malfunction” refers to whether any critical payload has a failure, detected from one of many integrated health sensors onboard the payload subsystems. Although the UAV has redundant systems for every major subsystem, the risk of completing the mission with the redundant system alone is significantly greater, particularly if the damage was caused by high temperatures or other firefighting-relevant aspects. Thus, an order to return to the GS is automatically issued.

16.6.3.Integration

With all major aspects of the environment defined, the different simulations can be integrated in a complete simulation. A simplified flow diagram of the simulation is shown in Figure 16.3.

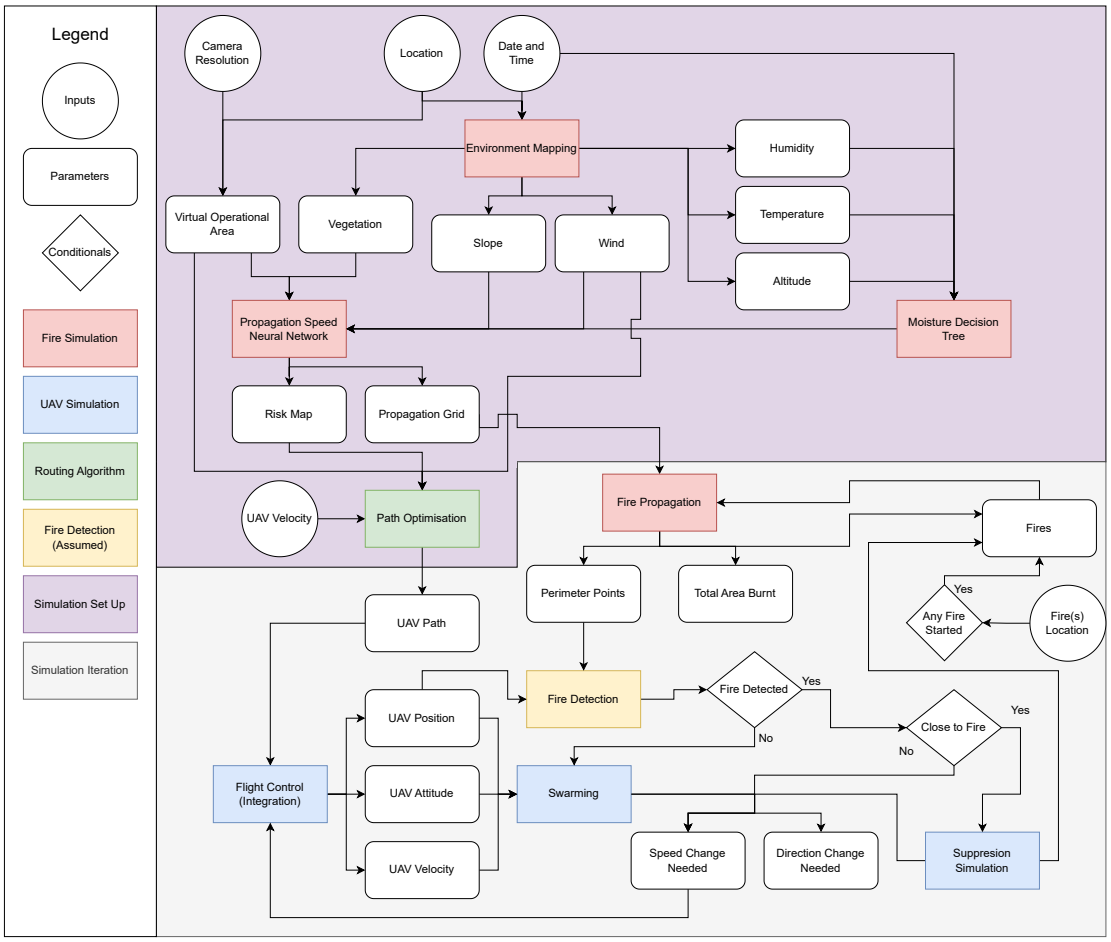

Figure 16.3: Flow diagram of the complete simulation.

Note that in Figure 16.3, the UAV Simulation ”Flight Control (Integration)” is referring to the combined simulation described in Subsection 16.6.2.

16.7.Results

Now that the implementations of the models have been described, and all models have been implemented, the results can be gathered. These will then be verified and validated in Sections 16.9 and 16.10.

Firstly, the environment mapping results for Castro Marim, Portugal, are shown in Figure 16.4 and Figure 16.5, with the former being the extracted slopes, and the later being the associated risk map for the 16th of August, 2021 (at moment of fire start). The discretised satellite image of the area is shown in Figure 16.6. The reason for the the analysis of Castro

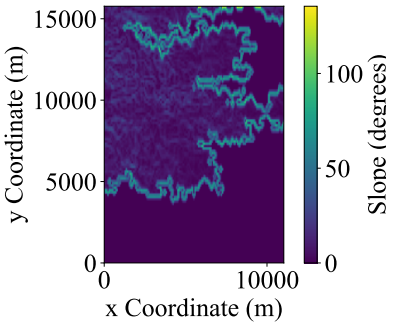

Figure 16.4: Extracted slope (magnitude) grid of Castro Marim

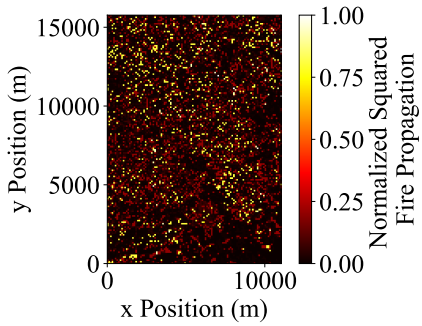

Figure 16.5: Extracted risk map of Castro Marim, Portugal, on the 16th of August, 2021.

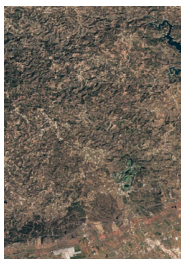

Figure 16.6: Discretised satellite image prior to the 16th of August, 2021 wildfire.

The results of the fire model are better understood when compared to the actual fire, hence, they are discussed in Section 16.10.

Then, the route to follow is then determined. Since results for large paths are highly convoluted, a low-resolution path is instead displayed for demonstration in Figure 16.7. Note that this route is for a high-speed propagation model on the top right quadrant, and a lower-speed propagation model on the remainder of the area.

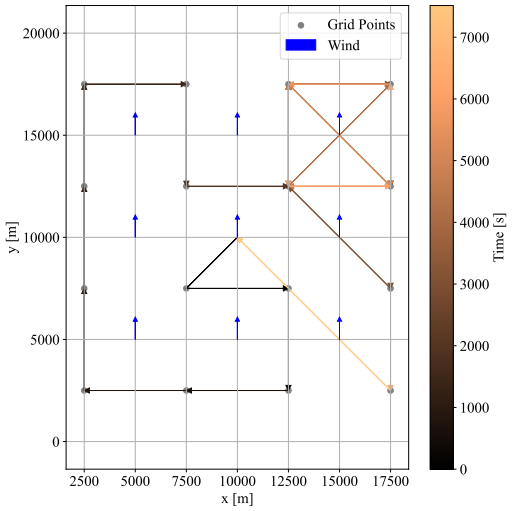

Figure 16.7: Optimal path for a $20\times20\,\mathrm{km}$ grid with a resolution of $5\,\mathrm{km}$, a $20\,\mathrm{km\cdot h^{-1}}$ wind.

Here, it is clear that the UAV makes multiple passes over the same area, and that it optimises for still scanning other areas while still returning to the high-risk area.

To show the coordination of the swarm in action, Figure 16.8a shows 24 UAVs (the number that will be used during daylight in high-alert periods) in surveillance mode, cruising along a pre-defined path; this path is the result of the routing algorithm with no wind and uniform risk. In Figure 16.8b, two UAVs detect a fire, and alert all other UAVs to fly towards the fire to suppress it. Figure 16.8c shows the UAVs that have already deployed their water payload beginning to circulate the fire. Eventually, all UAVs become coordinated with each other and thus evenly distanced, which can be seen in Figure 16.8d.

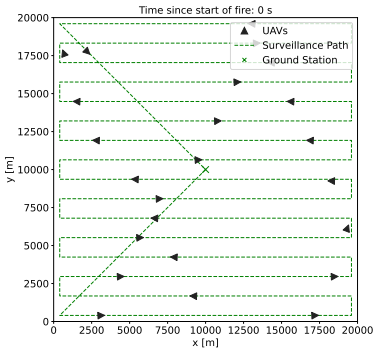

(a) Simulation of UAVs surveilling along a pre-defined path with no wind and uniform wildfire risk.

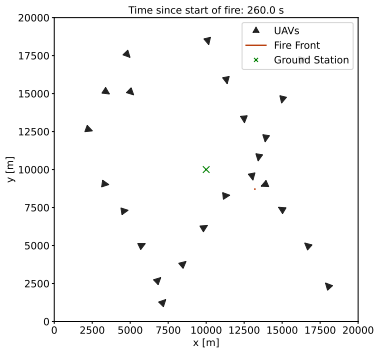

(b) Simulation where two UAVs detect a fire and all others are called to travel in the fire's direction.

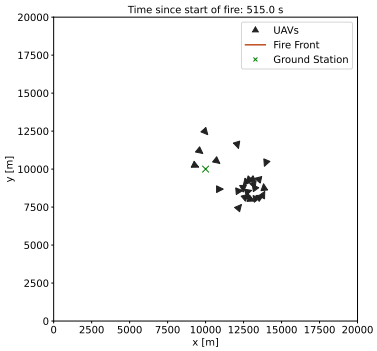

(c) Simulation of UAVs performing suppression, while others are starting fire circulation for monitoring.

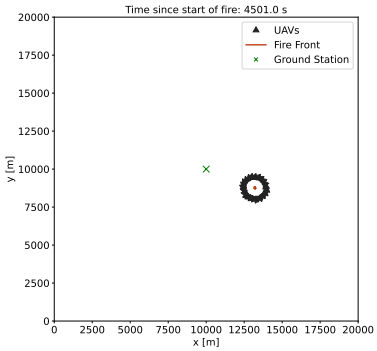

(d) Simulation of UAVs fully coordinated while circulating and monitoring an ongoing fire.

Figure 16.8: Swarm firefighting simulation.

To find the limit of the suppression capabilities of the swarm, several simulations were performed, altering the wind speed

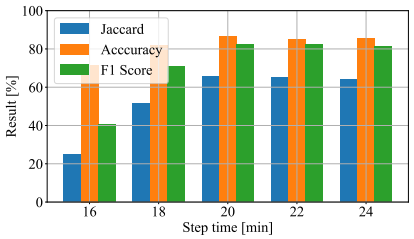

(a) Sensitivity of fire results to time steps.

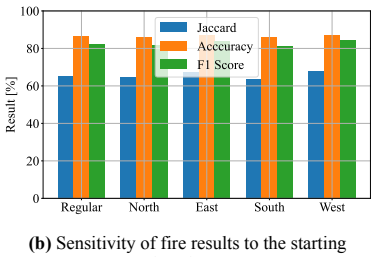

(b) Sensitivity of fire results to the starting locations.

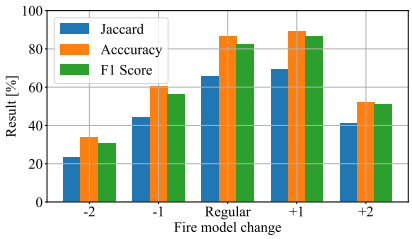

(c) Sensitivity of fire results to the colour mapping.

between them to find the maximum wind speed at which complete fire extinguishing is possible. The conditions used for these simulations were as following:

- Fire model used: Dutch forests [6]
- Number of UAVs: 24
- Fire area extinguished per UAV: $8\,\mathrm{m}^2$
- Initial fire size: $0.09\,\mathrm{m}^2$

With these conditions, the maximum wind speed possible was $7\,\mathrm{km{\cdot}h^{-1}}$. The time at which the fire was detected was $3.7\,\mathrm{min}$, and the time at which the first UAV deployed its water payload was $4.7\,\mathrm{min}$. For higher wind speeds, the wildfire is not suppressible with the conditions described above, but this does not mean that the swarm has no value. In these cases, the swarm still enables early-stage detection, which then means that firefighters can arrive while the wildfire is still small, and thus suppress it more easily.

16.8.Simulation Sensitivity Analysis

A sensitivity analysis was performed for the fire model to analyse the robustness of the results. This entails inserting a slight variation of key parameters and observing the changes in the final result. It was decided that only relevant parameters where either a large number of uncertainty or decisions with little basis have been made would be analysed. The three identified parameters include:

- **Time step** - these have been determined based on grid size, but the decisions throughout the selection may affect results in a significant way. The time step value will now be varied in the range of 5-60 min.
- **Fire start location** - the exact initial location is unknown, as the fire data from the satellite imagery begins at a larger time-step than the fire start. The fire start locations will be computed throughout different points along the range of first fire spread data available.
- **Colour mapping** - The assignation of colours to models was done manually. Although this was based on vegetation of the area, the discretisation and difference due to lighting may have changed it. For this, the adjacent fire models to the ones determined will be considered.

The results for time steps, start location, and colour mapping are shown in Figure 16.9a, Figure 16.9b, and Figure 16.9c, respectively. All analyses are done assuming ceteris paribus.

As can be seen, the results for the time steps and starting locations are fairly robust. However, the colour mapping has a fairly large variation, with the optimal mapping likely being somewhere in between the selected and an entire model upwards across all models.

Therefore, it is recommended that a better method for plant mapping is used in future versions. This could be done through options such as aerial imagery, field surveys, or LiDAR mapping.

16.9.Simulation Verification

The simulations defined above have been verified. This was done through the use of unit tests, system tests, and visual verifications. Due to the large number of tests implemented, this section will provide a general description of different types of tests.

Since the different simulations build upon each other, it was assumed that once a simulation was tested, its behaviour and results used in others would be nominal. However, the interactions between different simulations were still tested. This section will commence with models and simulations that are independent of other simulations, and will then transition to full system and interaction tests.

[6] See: https://www.hogeveluwe.nl/nl/ontdek-het-park/natuur-en-landschap/bomen, Accessed 01/05/2025.

Fire Propagation Models

All elements of the fire model must be tested. This includes the generation of an environment, extraction of features from the environment, the propagation speed by the NNs, and the spread area of the fire.

Environment Generation

The generation of the environment had four main types of tests: initialisation tests, value update tests, visualisation tests, and computational checks. Initialisation tests effectively entail ensuring that all processes upon the generation of a class work as intended. For the environment, it includes ensuring that all grids were implemented as intended and that the passed values were set - these are often the simplest type of tests. Then, value update tests essentially verified that changing a value in the environment automatically updated the values of all properties dependent on the changed value, e.g., ensuring that changing a ground material at a particular grid point automatically changes its colour and its propagation speed. Visualisation tests included the plotting of the environment as a whole, the risk map plotting, the slope plots, etc. of simplified and areas where the values should be clear, e.g., plotting a 4 by 4 grid with particular fuel types. These serve as wider tests, often spanning over multiple methods, but also serving to ensure that any later use of visualisations for other verifications or checks are not constrained by the visualisation itself. Lastly, computational checks are tests where a value is expected out of a particular method, e.g., that the dead fuel moisture for a particular temperature, relative humidity, slope, etc. results in the same value as that described by Rothermel [43] for the same conditions.

Extraction of Values

The extraction of values was tested through value and visual tests. For the extraction of weather, a historical day was selected at random and the results of the extraction were tested against manually obtained values for the same date. Quantisations of all high-resolution data into lower resolution grids were also tested numerically, as well as the mapping points to particular grid locations. Meanwhile, for topology and dendrology extraction, visual tests were used, where an area with characteristic altitude changes and a large vegetational biodiversity are present would be extracted and passed onto the environment, which would then be plotted (with its altitude and colour based on the extracted altitude and materials). The plots were then compared to the same area in high-accuracy maps, such as Google Earth, ensuring that these were passed on effectively.

Spread Speed Neural Networks

The spread speed of NNs was verified directly against the source of the data upon which it was trained, namely, BehavePlus6.0[7]. This was done using a classic ”train-validation-test” split, where the training set is used to create the model, the validation set determines when the model converges (to avoid over-/under-fitting), and the test set is used to determine the quality of the model. The average test error is 23.4%, which although quite high for a simulation of this scale, is acceptable considering that these are equally distributed in both the positive and negative directions. This means that for a full fire simulation, which will contain a large number of time steps, the sum of residuals is expected to tend towards zero.

The predictions for the GR9 model over the entire range of slopes and wind speeds are shown in Figure 16.10, while the exact values from the BehavePlus6.0 software are shown in Figure 16.11.

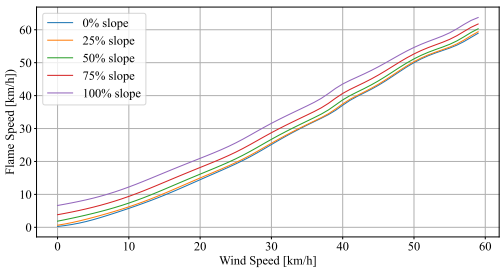

Figure 16.10: Predictions from the NN of the GR9 model implemented by FireFlight

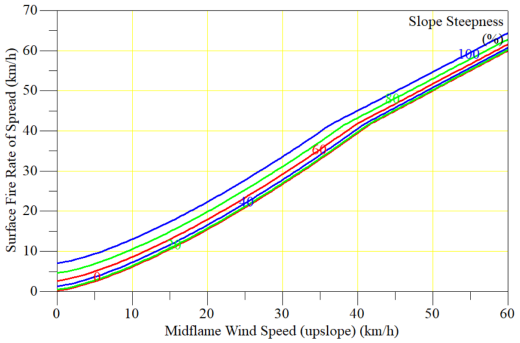

Figure 16.11: Exact solutions of the GR9 model (from BehavePlus6.0)

From these plots, it is clear that the NN generalises decently, although there are some fluctuations in the values. This is due to the small size of the dataset being interpolated by the NN, essentially being its guess of what the underlying function is between the trained points.

Fire propagation

The fire propagation was tested in three main ways, namely comparison tests, computational tests, and visual tests. The comparison tests included assessing expected traits of the model, e.g., that the fire propagation was larger in the direction

[7] See: https://www.frames.gov/catalog/57066. Accessed 19/05/2025.

of the wind, or that the number of fires and perimeters increases for the Huygens mode. The computational tests included ensuring that the initialisation points are generated in the correct positions, that given a certain velocity, the fire area for a simplified fire is correct, and that the perimeter is being calculated correctly. Lastly, visual tests including plotting the propagation in a virtual terrain with obstacles, and observing that the fire behaves as intended (moves around obstacles, accelerates in faster-burning vegetation, etc.).

Path

The path had two main types of test, including computational tests and performance tests. The first consisted testing for exact results, such as ensuring that the path did include a certain number of occurrences of high-risk paths, or that the results for simple grids (that could be tested manually verified) were correct. Meanwhile, the performance tests (which essentially test whether or not the method runs a particular case within a certain number of time) were implemented as the algorithm implemented does not scale very well, with a time complexity of $\mathcal{O}(n^2)$ (which is good considering that the problem solved in NP-Hard), thus, any gains in performance massively reduce computational time. These are important as the path depends on the wind, hence, it is important that the simulation is faster than the time it takes for the wind to change direction. These tests are the only tests that are failing, as the path determination algorithm has not been effectively optimised.

Swarm Coordination

The swarm coordination was verified through three main types of tests. Firstly, unit tests were used to ensure computations were outputting the correct values. For example, if a UAV had another UAV in front of it, but was told to accelerate, this would raise an error, and it meant that debugging, or a change to the algorithm, was required. The same process was repeated for all other computations performed by all swarming models. Secondly, as the main goal of this code is collision avoidance, system tests were used to check if any two UAVs were ever within the minimum separation distance, and the conclusion was that they were never so. To push this even further, two UAVs were initialised only $10\,\mathrm{m}$ apart, and it was observed that they immediately began separating until the minimum separation distance requirement was met. The third type of test used was visual tests, where several animations, each with a different combination of parameters (number of UAVs, initial distance between UAVs, initial fire size, among others), were used to check whether all UAVs behaved properly. This included checking whether they made any unreasonably large changes in speed or heading, whether they transitioned smoothly between the ”Cruise to fire” and ”Circulating fire” modes, whether they detected the fire at the correct distance, and whether they eventually became evenly spaced when circulating the fire. With unit tests, system tests, and visual tests completed and passed, the swarm coordination algorithm can now be seen as a reliable collision avoidance mechanism.

Suppression

To verify the suppression model, the method used was very similar to the coordination model. Unit tests were used to check for errors with computations, such as the needed turn or descent rate to suppress, or the distance from the fire. System tests were then used to check whether suppression was performed correctly. This meant checking that the UAVs started the dive and finished it at the correct altitude, that they deployed the water at the correct location, and more. And once again, visual tests were used with several parameter combinations to ensure that the dive was performed smoothly and at the correct time, and that the water was correctly deployed. Although significant debugging was required, in the end all tests passed and the suppression was thus correctly modelled.

Integration

The integration tests are tests for the interactions of different aspects, including the interactions of the aforementioned systems tested, the tests between data and simulations, and elements which required the interactions of other simulations (such as the UAV).

The main types of tests done were computational tests, edge-case tests, and evidently, integration tests. The computational tests included aspects such as ensuring that the UAV position changed by the amount expected during cruise, that the propagation computed for the grid matched the values expected from the propagation alone, or that the UAV did in fact transition between modes if fires were detected. The edge-cases included aspects such as how the UAV would behave if it were outside of the operational area, that the fire touches an edge of the area defined, or that the UAVs do not take-off if the wind speed is greater than their maximal speed. Lastly, the integration tests include testing for setting of the extracted features into the environment, that the UAVs can be defined in an arbitrary configuration within the environment, and that the UAVs respond to changes in the environment correctly.

Testing Summary

A wide range of tests — including unit tests, system tests, and visual inspections — were applied to individual simulation components as well as their integration. In fact, the coverage target set in Chapter 5 of 90% was met, with an impressive total coverage of 97.2% across classes, with the lowest being in the `fire.py` class, still exceeding the target with a total

line coverage of 92%.

Independent modules such as the environment generation, value extraction, fire spread speed NNs, fire propagation mechanics, and pathfinding algorithms were each rigorously tested for correctness and performance. Although most tests passed successfully, some limitations were noted, such as the relatively high error in the neural network prediction of fire spread speeds (23%) and the inefficiency of the pathfinding algorithm.

Integration tests confirmed that the interaction between systems, such as fire propagation and UAV behaviour, functioned correctly under typical and edge-case conditions. Overall, the system is robust, but improvements - particularly in NN training data, colour mapping accuracy, and pathfinding optimisation — are recommended for enhanced performance and reliability.

16.10.Simulation Validation

The final stage in ensuring that the models used provide acceptable data is validation. This refers to the comparison of model results to the real world. Evidently, since many of the simulations regard UAVs with the specific design or non-physical aspects (such as paths), they cannot be validated. However, the fire simulation is intended for replicating the real-world behaviour of wildfires, with its value being entirely tied on its ability to approximate a real wildfire.

Simplified Fire Model

Before validating a full fire, it is imperative to ensure that the simplified fire is representative of the real world. This is as the simplified fire is the basis of the full fire model, and is already the product of various models.

The simplified model will be validated using the same approach as the ELMFIRE model validation procedure[8] (which is also based on the Rothermel Mathematical model). This consists of simulating a simple case, with a flat environment and homogeneous GR2 fuel (as defined by Scott and Burgan [50]), and comparing it to the results of the test with an equal simulation configuration[1]. The inputs (homogeneous throughout area) are the same as those used in the ELMFIRE validation. Specifically:

- Fuel Model: GR2 (102)
- Live herbaceous fuel moisture: 30%
- Dead fuel moisture index: 3%
- Wind speed: $16.09\,\mathrm{km{\cdot}h^{-1}}$ ($10\,\mathrm{m{\cdot}h^{-1}}$)
- Slope steepness: 0%

The results of the model, compared to that of the exact solution from ELMFIRE[6] are shown in Figure 16.12 and Figure 16.13, respectively.

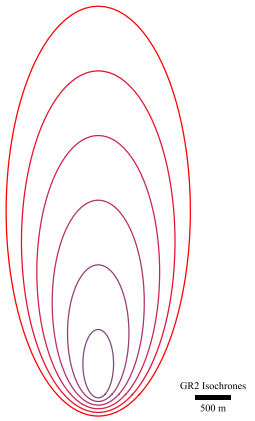

Figure 16.12: Isochrone lines of FireFlight corresponding to fire front position from 1 h hour to 6 h at an hourly interval.

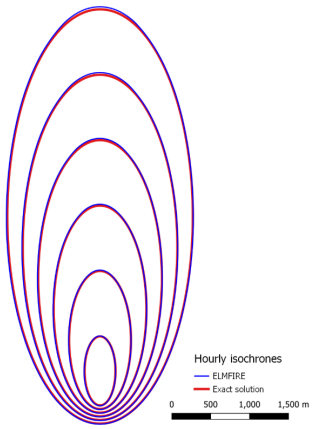

Figure 16.13: Isochrones of ELMFIRE Simulation and Test Results (”Exact Solution”).

Complete Fire Model

The validation above serves to verify that the basic simulation works effectively. However, such a simulation was for an artificial test in a controlled environment, which may not accurately reflect the real world. Hence, despite the simulation not being designed for large-scale simulation of fires, this section describes a validation with a real-world wildfire. This is valuable to determine the validity of results when monitoring fires that are already large and its ability to map environments effectively.

[8] See: https://elmfire.io/verification/verification_01.html. Accessed 26/05/2025.

The data for the real fire was obtained from the Portuguese Large Wildfire Spread database (PT-FireSprd) database [62], which has a collection of large Portuguese wildfires that occurred between 2015 and 2021 and their progressions. Out of these, the August 16th 2021 Castro Marim fire was selected for the following reasons:

1. Steady wind speed - The wind speed throughout the duration of the fire was invariable, which is desirable, as the simulation assumes constant wind-speed.
2. Minimal effect due to firefighting - the effect on firefighting on the fire was minimal, thus, the fire propagation is effectively a purely natural propagation.
3. Large variation in altitude and materials
4. Detailed progression present - can evaluate progression at any point in time.
5. Characteristic shape

Using the procedure described in Section 16.1, the environment around Castro Marim (before the fire) was replicated virtually, and the meteorological conditions were obtained using historical weather data[9] and post-fire analyses [62]. Lastly, a point fire was introduced into the environment, and the simulation was run for a time equivalent to that of the total fire duration.

The results of the propagation of the simulation and the real fire in a discretised environment are shown in Figure 16.15 and Figure 16.14, respectively, and the overlapped comparison between the two in Figure 16.16a.

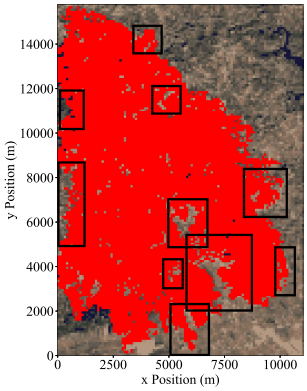

Figure 16.14: Real/Exact (discretised) area of the August 16th 2021 Castro Marim wildfire (data from Benali et al. [62]).

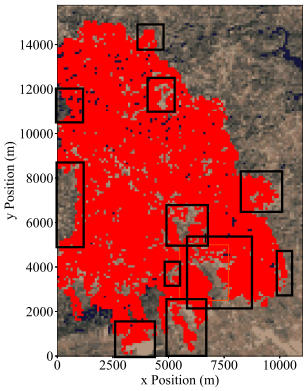

Figure 16.15: FireFlight prediction of fire using Castro Marim conditions on the August 16th 2021.

The results presented are those at the end of the 33 h of burning during which the fire took place, using a 100×100 m resolution. The results warrant close examination, as the predicted and real fires exhibit a striking visual similarity—not only in the overall "horseshoe" shape, but also in fine-grained, characteristic details. Figure 16.14 and Figure 16.15 have been annotated with specific features that appear consistently in both the real and simulated fires, underscoring the model's ability to reproduce detailed spatial patterns.

Furthermore, a statistical analysis was conducted on the final fire area to quantify the quality of the model. Although the model does not work on a cell-by-cell basis, it is still useful to analyse it in such a manner as it offers insight into the spatial accuracy, particularly in terms of shape and area correspondence.The key performance metrics of the model are as follows:

- F1 score = 78.2%
- Accuracy = 79.9%
- Jaccard index[10] = 65.4%

These are indicative that the model performs well, with minimal misclassification, as shown by the confusion matrix in Figure 16.16b.

[9] See: https://www.wunderground.com/history/daily/pt/castro-marim/LPFR/date/2021-8-16. Accessed 17/06/2025

[10] Jaccard index (or Jaccard similarity) is a measure of similarity between two sets, being equal to the cardinality of their union over that of their intersection

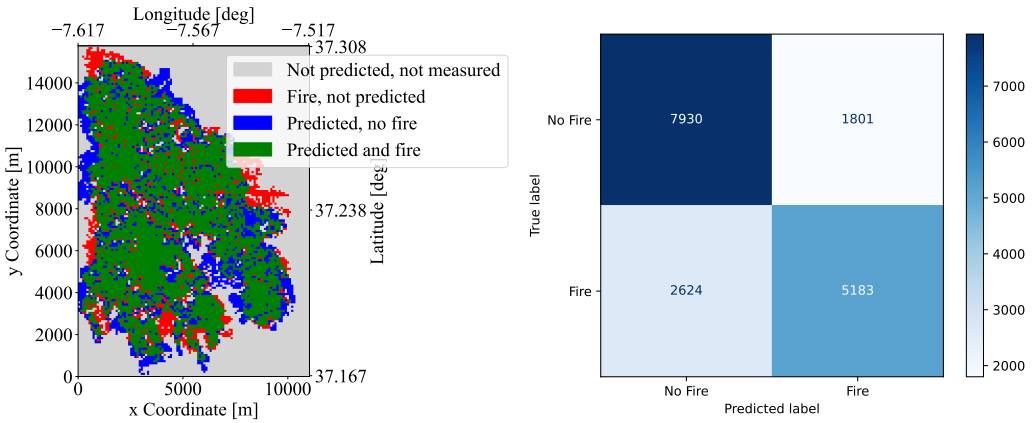

(a) Area comparison between prediction and exact solution

(b) Confusion matrix

Figure 16.16: Prediction evaluation for August 16th 2021 Castro Marim Wildfire

In fact, it is unexpectedly accurate considering that the fire simulation was not implemented for such long fires, as discussed in Table 16.1. In addition, it is clear from Figure 16.15 is only having a lower predictive success due to the noise within its temporal updates, causing it to skip certain grid cells (as that was not what it was designed for). Hence, these values are clearly underestimations of the actual effectiveness of the model.

16.11.Simulation Recommendations

Throughout the simulations section, multiple recommendations have been made. These include:

- Using a larger dataset to train the neural networks to decrease the error.
- Implement burnout and local weather variations
- Optimise genetic algorithm convergence
- Use more robust colour mapping.

With these, the simulation would likely yield more accurate and robust results.

17 Technical Resource Budgets

Technical performance measurement (TPM) describes the strategy for developing and maintaining realistic estimations for limited or expensive resources. Identifying these resources is crucial as it significantly supports the design team in focusing on the most relevant design decisions. Furthermore, it allows them to discard unfeasible design options, resulting in an efficient research and development process. The TPM strategy will be explained in Section 17.1, followed by the identification, explanation and justification of the key parameters in Section 17.2. This shows the parameters estimated at the beginning of the project, and the current parameters of the design.

17.1.TPM strategy

In the beginning of the project, parameters were chosen and quantified using statistical data, simple calculations, experience, or educated guesses to obtain valuable results from the TPM procedure. To account for uncertainties in the initial parameters, contingencies were applied. These reached both low and high percentages, allowing flexibility for future development stages, while providing first indications of parameter magnitudes. Contingencies started with large values for most parameters, but changed dynamically with advancements in the design process, as individual components and the holistic picture became clearer over time. To monitor the parameters during each stage of the project, the following values are estimated, measured or tested [63]:

1. The actual value of the parameter at the current design stage (without contingency).
2. The target value, which is equal to the specification value minus the contingency, valid for a nominal development process. This is the value that the group aims for.
3. The current value, which is equal to the actual value plus a contingency, reflecting on the current status of the design.
4. The specification value, which includes all approved waivers (includes contingency).

While tracking these parameters, comparison of the actual value with the target value and the current value with the specification value is needed. If the actual or current value exceeds the respective limits, one of the following actions is required [64]:

1. Decrease the uncertainty in the design (bread-boarding, tests, design review).
2. Change the specification value (therefore also altering the target value).
3. Modify the design.

The choice of an appropriate measure depends strongly on the situation and can be unique for each case.

The system engineer has and will continue to play the primary role in managing the budgets. He allocated the budgets to the respective subsystems and monitored them during the project. Moreover, changes in the budget proposed by any project member are first discussed with him to ensure that they do not threaten the mission's success.

17.2.TPM Parameters

In this section, the TPM parameters will be identified. Moreover, their relevance for the project will be briefly described, along with their influence on the design. The relevant parameters are shown in Table 17.1.

Table 17.1: Overview of TPM parameters.

TPM Parameter	Description
Mass [kg]	The mass budget ensures each subsystem stays within its allocated mass, directly influencing performance and cost-effectiveness.
Power [W]	Power consumption is budgeted to design a sufficiently capable battery. Power usage affects UAV endurance and total mass.
Cost [€]	Costs must be estimated early and monitored throughout design to ensure compliance with the allocated budget.

In the start of the design process, solely design options had been explored, resulting in little information on the final system. This is why the initial confidence was very low for each TPM parameter. To cover this uncertainty, the group added an initial contingency of $40\,\%$ to each of the parameters [65]. These have of course been revisited while making design decisions and have decreased significantly up to this point. Furthermore, only the target and specification values were obtained at the start of design. Now that specific designs have been chosen and analysed, the actual and the current value have been added to check the feasibility. Lastly, it is assumed that each parameter value represents a conservative estimate, as different configurations can largely differ in performance. Below, the TPM parameters will be discussed.

Mass

The overall mass is given as a requirement by the customer, at 80 kg, but a breakdown into the UAV subsystems is needed to ensure the requirement is met. Table 17.2 shows the preliminary estimate obtained using a combination of requirements, literature, and engineering judgement, and the current estimate, obtained through analysis and design parameters.

Table 17.2: Comparison of initial and current mass budget for the UAV.

Subsystem	Actual Mass [kg]		Target Mass [kg]		Margin [%]		Current Mass [kg]		Specification Mass [kg]	
	Init.	Curr.	Init.	Curr.	Init.	Curr.	Init.	Curr.	Init.	Curr.
Structure	n/a	17.0	12.0	18.9	40	10	n/a	18.9	20.0	21.0
Power Sources	n/a	18.1	9.6	19.8	40	10	n/a	20.1	16.0	22.0
Payload	n/a	15.9	15.0	18.0	40	10	n/a	17.7	25.0	20.0
Avionics	n/a	1.4	2.4	1.8	40	10	n/a	1.6	4.0	2.0
Propulsion	n/a	12.3	9.0	13.5	40	10	n/a	13.7	15.0	15.0
Total	n/a	**64.7**	**48.0**	**72.0**	n/a	n/a	n/a	**72.0**	**80.0**	**80.0**

The mass has been divided into the structure (fuselage, landing gear, wing, booms, and empennage), power sources (main battery, auxiliary battery, and fuel), payload (water and camera), avionics, and propulsion system (engine and VTOL propellers). The only specification mass that increased significantly was the power sources, but this occurred due to the size of the battery required for VTOL propulsion being higher than anticipated. Figure 17.1 shows that the actual mass is lower than the target mass, and the current mass is lower than the specification mass, so, none of the actions specified in Section 17.1 are required. To show a more detailed timeline of the changes in the mass budget throughout the design, Figure 17.1 shows the progression of several mass values over a number of iterations. It demonstrates that the overall masses decreased with each iteration, apart from the battery mass, which must be larger than was expected due to the high power needs of the VTOL propellers. The mass first drops significantly between the midterm and final report due to the payload requirement dropping from 40 to 18 kg. After that, the reduction of MTOW is about 10%, which is deemed insufficient for an iteration of the design. This is especially true since the weight decrease means that the UAV can execute the mission with a safety margin for possible increases in component masses when finalising the design and weighing the first prototype. It can also be used to execute a more difficult mission such as extended range, as demonstrated in Section 12.4, or a denser payload that fits in, or is equivalent to the suppression tank volume.

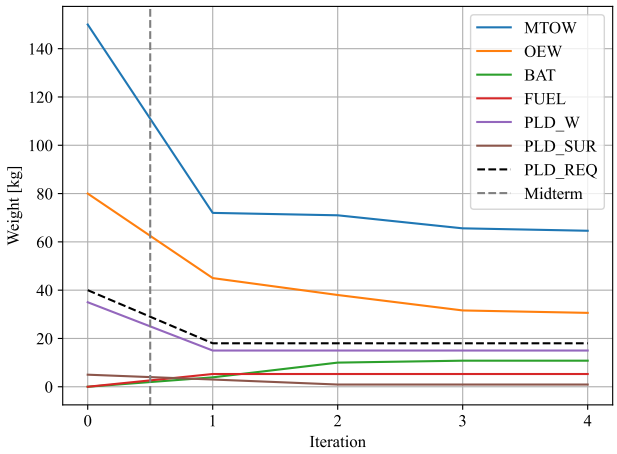

Figure 17.1: UAV mass change with iterations. Includes MTOW (maximum take-off weight), OEW (operational empty weight), BAT (battery mass), FUEL (fuel mass), PLD_W (water payload), and PLD_SUR (surveillance payload) and PLD_REQ (Payload Requirement).

Power

During operation, the battery must be capable of providing power to all electric subsystems. These subsystems include the payload sensors and cameras, as well as the avionics and electric propulsion systems. The initial power budget and its updated version is shown in Table 17.3.

Table 17.3: Comparison of initial and current mass budget for the UAV.

Subsystem	Actual Power [W]		Target Power [W]		Margin [%]		Current Power [W]		Specification Power [W]	
	Init.	Curr.	Init.	Curr.	Init.	Curr.	Init.	Curr.	Init.	Curr.
Payload	n/a	30	30	35	40	10	n/a	34	50	40
Avionics	n/a	340	30	380	40	10	n/a	380	50	420
Propulsion	n/a	22 600	15 000	25 000	40	10	n/a	25 100	25 000	28 000
Total	n/a	**23 000**	**15 060**	**25 500**	n/a	n/a	n/a	**25 600**	**25 100**	**28 500**

The specification power required by the avionics increased significantly over the initial value. However, the value shown

is for the peak power, meaning that all components are on at the same time, which will rarely occur. Nonetheless, this is a manageable power seeing that we already have the requirement for a large battery due to the VTOL propellers' power needs. The propellers' specification power increased slightly, but this is because of efficiency considerations and a safety factor that was applied for high-wind conditions. Once again, the actual power is lower than the target power, and the current power is lower than the specification power. This means that the actions specified in Section 17.1 are not required.

Costs

The target price given by the Dutch customer is €500 000 per year for 20 year mission lifetime including amortisation costs. Conservatively, the Dutch customer will be estimated as one of 30 customers assuming 30 operational centres will purchase a single system.

Target Operational Costs

The initial estimate of operating costs was €325 000. This was slightly over the 50 % split between acquisition and operational costs estimated in existing literature [66], with the resulting acquisition budget being approximately €3.5M distributed over 20 years.

Target Production Cost

From acquisition budget a portion will be attributed to production costs including hardware, assembly, integration and organizational overhead. Consumer heavy lift UAVs, with an estimated hardware and assembly cost of €25 000 per unit, were initially taken and broken down by percentage. During the operational assessment it was clear that chemically propelled UAVs were critical to meet range requirements. As such after the class I weight estimation an updated upper bound total cost total was computed through linear regression of price per kilogram payload for similar aircraft of €60 000, and lower bound at €40 000. An overview of the budgets used per sub-system is presented in Table 21.3. Percentages were based on engineering judgement and sanity checks with existing components and UAV breakdowns where available. The upper bound was used when calculating operations and costs. Each subsystem was then given a requirement to not exceed the upper bound, and given target for the lower bound costs.

Table 17.4: UAV Swarm Target Costs

Item	Percentage	Lower Bound Spec. Class I [2025 €]	Upper Bound Spec. Class I [2025 €]
Structure	0.25	10,000	15,000
EPS	0.2	8,000	12,000
Payload	0.25	10,000	15,000
Avionics	0.15	6,000	9,000
Propulsion	0.15	6,000	9,000
Total	1	40,000	60,000

18 Sustainability Implementation

After having performed all subsystem analyses, the results of the sustainable development strategy are reflected in this chapter by discussing the direct implementations of sustainability within each subsystem. In Section 18.1, all subsystems where sustainability was implemented were analysed and related to the sustainability indicators. Furthermore, Section 18.2 provides an estimate of the CO2 equivalent of the UAV system and divides it into separate phases.

18.1.Subsystem Sustainability Implementation

In this section, the sustainability of each part of the report will be discussed separately. Here, for each subsystem, the measures will be related to the sustainability indicators.

18.1.1.Costs

In order to confirm the design is financially sustainable, the cost of the system must be below the purchase price to create a return on investment. At the beginning of the project, cost budgets were assigned to each subsystem based on the cost price given as a requirement. Throughout each step of the design, costs were closely monitored and budgets updated if significant changes were anticipated. During design choices, cost was considered as a driving factor. In addition, maximising effectiveness was core to ensure that the customer is able to justify the spending and target systems are sold. In the project costs, the end-of-life budget is allocated to make sure items are correctly disposed of or recycled.

18.1.2.System Trade-Offs

In the system trade-offs, sustainability has been implemented by using it as a performance parameter for every trade-off matrix. Within the trade-offs, sustainability is treated with great importance, leading to high criteria weights. Therefore, it directly drives the configuration choices and makes the design more sustainable. In the trade-offs, sustainability is primarily taken into account considering the indicators energy efficiency, energy consumption, pollutant emission, share of renewable energy, share of recyclable materials, required space, and ecosystem disruption while also considering aspects of economic and social sustainability as the research and development costs, production and operation costs as well as reliability and availability.

18.1.3.Stability and Control

For the stability and control subsystem, sustainability has been considered in various ways. When iterating the design to obtain the final component positioning, it was aimed to design the aircraft as aerodynamic and compact as possible, reducing costs, mass and drag. In addition, the removable components were positioned on the OEW location to reduce the required tail size, resulting in a lightweight and efficient design. Moreover, the UAVs are designed to be inherently stable and the VTOL system was positioned equidistant around the OEW location, reducing the control actuator usage and increasing VTOL efficiency. Relating these considerations to the sustainability indicators, energy consumption, pollutant emission, required space, production costs and reliability are considered.

18.1.4.Structural Design

The initial target for recyclable materials was optimistically 80% of OEW. It was attempted to design with aluminium for recyclibility, this was however unfeasible for the wingbox. Using carbon fibre for the wingbox, fuselage en empennage, the estimate is 10.8kg of non-recyclable material out of the total structure budget of 22.24kg, approximately 50% recyclability. This must be closely monitored and communicated with stakeholders. Disassembly and access to internal components were core to design requirements to minimize operational costs and improve maintainability. The dissassembly facilitated recycling and also replacement of minimal parts in the event of component failure.

18.1.5.Propulsion Design

The propulsion system is key to maximising sustainability since it produces emissions and noise. Despite some emissions being unavoidable due to an ICE engine being used, the system still minimizes them by using a modern efficient engine with an electric starter meaning it can be shut off when not in use such as when VTOL operations are underway. The VTOL system itself is fully electrically powered, ensuring the most power hungry phases of the mission are performed by an electric power system. With this, pollutant emissions, energy consumption and the share of renewable energy are considered an minimised within the limitations of successfully performing the mission.

Noise is an essential part of sustainability and a restriction on tip speed is imposed to propellers. The Mach number must be kept under 0.75 from the usual 0.92, ensuring the noise is reduced to meet all regulations. Furthermore this increases efficiency again as less energy is lost to noise and other compressibility effects, influencing the noise production and ecosystem disruption indicators.

18.1.6.Aerodynamic Analysis
The aerodynamic analysis focused on maximizing the lift-to-drag ratio and minimising drag at cruise in order to extend the UAV's range and reduce fuel consumption. This objective guided the airfoil selection process, directly contributing to the performance indicators of 'energy efficiency' and 'operational cost', as a more aerodynamically efficient wing results in lower fuel demands. Additionally, the empennage design was performed with aerodynamics in mind: the choice of a U-tail configuration serves a dual purpose by integrating the landing mechanism into the tail structure. This eliminates the need for separate landing gear, thereby reducing drag and further improving aerodynamic efficiency.

18.1.7.Flight Performance
Within the flight performance analysis, several sustainability indicators are addressed through the investigation. 'Noise production' is addressed through its analysis and checking if it complies with EASA guidelines. It is minimised by reducing propeller tip speed. 'Energy efficiency' is emphasized through engine-propeller matching and ensuring the efficiency is at its maximum possible. 'Pollutant emissions' like CO_2 and NO_x have been quantified based on specific fuel consumption, allowing for an estimation of environmental impact over the lifecycle. 'Functionality' is assessed by elucidating the aircraft's abilities for its flight phases and turning. Lastly, the 'share of renewable energy' is supported by ensuring the electric component of the flight profile is maximised.

18.1.8.Embedded Systems
Although sustainability was not a primary driver in the design of the embedded systems, certain design choices that contributed to it indirectly. The integration of multiple domains onto a single compact baseboard reduces cable mass, structural volume, and required power routing. Interfacing via standard protocols (UART, CAN, USB, etc.) enables modular component replacement, contributing to maintainability. These aspects support the sustainability indicators of energy consumption, required space, and operational cost.

18.1.9.Operations and Logistics Concept
Solar panels were considered for power supply, but remain an option for the customer as it can limit the deployment locations due to the significant increase in ground footprint. The solar panels also have their own concerns with recyclability and in terms of rare earth materials used in their manufacturing process. The ground station is also built to be temporary to not disrupt ecosystems. However, the water and fuel needed for operations are extensive and unfortunately non-negotiable. These considerations relate to the following sustainability indicators: the pollutant emissions, energy consumption, share of renewable energy, required space, water consumption, ecosystem disruption.

18.1.10.Simulation
Several simulations incorporated sustainability. Firstly, the path optimisation was done to minimise the total distance that a UAV must fly to surveil the entire operational area. By optimising this, the amount of fuel that will be consumed by the UAV will be minimised, and thus reducing the carbon footprint of the system. A second model where sustainability is heavily taken into account is the fire detection. While it would be possible to keep the CNN running at all times, it was decided that it would only be turned on after a fire is detected by the infrared camera. This drastically reduces the power needs of the UAV, as a CNN is computationally heavy. Finally, the coordination model ensures that a large distance is kept between all UAVs, minimising the risk of crashes. This reduces the impact of the system on the environment, as having a crash over the forest would negatively impact the ecosystem.

18.1.11.Suppression System
To account for sustainability in the suppression system, a sacrifice on the suppression effectiveness was made. The most effective materials for fire suppression are foams, retardants, and gels. However, these are also toxic, so, it was decided that a less effective material, water, would be used for all suppression operations. This protects both plant and animal life in the areas that the system will be operating in.

18.2.Life Cycle Assessment
In this section, the climate impact of the UAV swarm during the entire operational lifetime will be discussed. For this, a life cycle assessment tool provided by TU Delft[1] will be used, which divides the operational phases into manufacturing, transport, use and end-of-life.

To perform this analysis, the strategy will be discussed for each step with the provided reasoning for the values used. With this tool, the main goal is to obtain an estimate for the CO2 impact of the FireFlight project. CO2 is the main parameter that was considered, as it is one of the strongest drivers of climate change. The respective CO2 values are obtained from a database included in the tool. The tool allows for the provision of an uncertainty of the values. As most values can only be estimated at this stage of the design, a margin of 30 % will be employed for all estimates.

[1] See: https://www.ecocostsvalue.com/data-tools-books/tool-in-excel/. Accessed: 21-06-2025.

For the manufacturing impact, the system was divided into its components. The items considered are carbon fibre, aluminium, battery, electronics, VTOL System and paint. Here, each component of the MTOW has been assigned to one of these categories with its respective mass, except the water payload. Furthermore, the number of items per functional unit has been set to 35 for each component, as 35 UAVs will be operating at the same time. For the energy usage while manufacturing the UAV, a total amount of 1800 MJ has been estimated.

For the impact of transportation, it has been conservatively estimated that each component will be shipped a distance of 20000 km before arriving at the assembly location. This includes the transport of the raw material, but also the transport of components that are bought from a different country and continent. In addition to that, the refuelling trucks are taken into account. It is expected that each truck will transport 25000 litres at a time, and during the lifetime, a total amount of 1236167 litres will be used, based on an operation time of four months a year, while operating with 70 % capacity during daytime and 30 % capacity during the night. Estimating the truck travel distance to be 100 km and with a required amount of 50 fuel refills during the entire lifespan, the CO2 impact can be obtained.

Next, analysing the operation time, fuel and electricity of the UAV needs to be taken into account. The total usage for the mission can easily be calculated from the operation strategy and amounts to 1,034,852 kg of fuel and 5,478 MJ of electrical energy for the swarm lifetime. Using the estimated CO2 impact in Chapter 12 for the fuel and the provided CO2 impact from the database, the total operational CO2 equivalent can be calculated.

Lastly, the end-of-life analysis is performed similarly to the manufacturing analysis. Thus, each component is considered separately. For aluminium, the good recyclability characteristics result in a negative contribution towards the equivalent CO2 emissions, while components as the battery are not well recyclable and strongly influence the total end-of-life emissions.

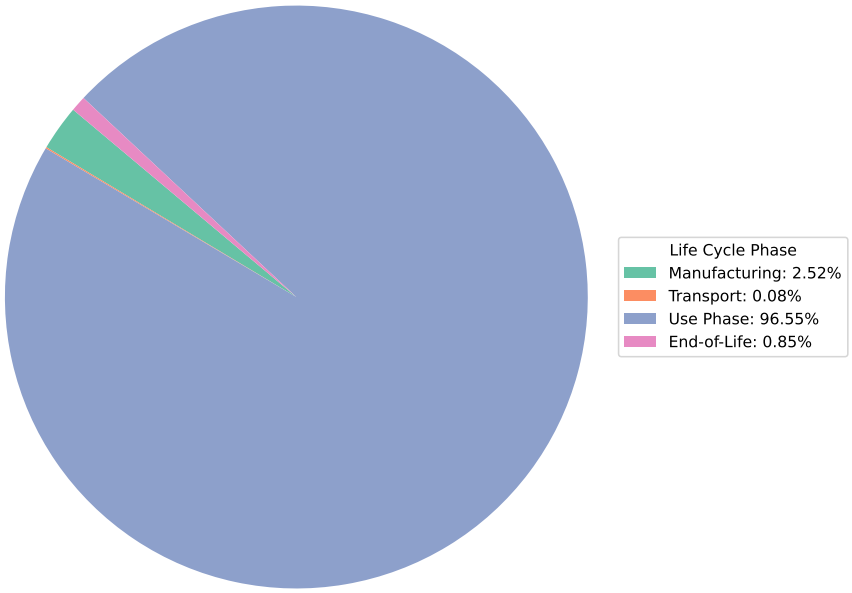

Figure 18.1: CO2 equivalent (%) during the UAV lifecycle, divided into the manufacturing, transportation, use and end-of-life phases

Figure 18.1 and Table 18.1 provide a direct overview of the CO2 impact of the UAV project. From this estimate, it can be seen that the propulsion fuel has by far the largest impact on the system, while other impacts seem almost negligible. Therefore, for future work, it is recommended to analyse the feasibility as well as the mission and the CO2 impact of replacing unleaded petrol with sustainable aircraft fuel.

Table 18.1: Life cycle assessment for CO2eq (kg) for the VTOL UAV production, transport, use, and end-of-life phases

Category	kg CO2eq/Quantity	Quantity	kg CO2eq
Manufacturing (Materials)			
Carbon Fibre	85.601	10.81 kg × 35	32,387
Aluminium	11.759	8.43 kg × 35	3,470
Battery	85.227	12.80 kg × 35	38,182
Electronics	42.264	2.31 kg × 35	3,417
VTOL System	3.184	9.25 kg × 35	1,031
Paint	4.363	0.76 kg × 35	116
Subtotal Materials			**78,602**
Manufacturing (Energy)			
Electricity (NL)	0.110	1,800 MJ × 35	6,952
Total Manufacturing			**85,554**
Transport			
Shipping (Container)	0.002	1.7344 t × 20,000 km	68
Refuelling Truck	0.019	25.8 t × 5,000 km	2,488
Total Transport			**2,556**
Use Phase			
Fuel (Petrol incl. combustion)	3.17	1,034,852 kg	3,280,480
Electricity (NL)	0.110	5,478 MJ	605
Total Use Phase			**3,281,084**
End-of-Life			
Carbon Fibre Disposal	23.410	10.81 kg × 35	8,857
Aluminum Recycling	-3.209	8.43 kg × 35	-947
Battery Recycling (worst case)	44.590	12.80 kg × 35	19,976
Electronics Recycling	1.000	2.31 kg × 35	81
VTOL System Recycling	2.800	9.25 kg × 35	907
Paint Recycling	4.320	0.76 kg × 35	115
Total End-of-Life			**28,989**
Total CO2eq			**3,398,183**

19 Technical Risk Management

Detailed subsystem design has introduced an additional set of technical risks. These risks are identified, analysed and mitigated with a risk map in Section 19.1 and with the method of Reliability, Availability, Maintainability, and Safety (RAMS) in Section 19.2.

19.1.Risk Map

The approach to identifying and assessing risks, as well as mitigation and contingency measures, remains unchanged from previous reports. Risk identifiers (IDs) are altered to reflect the specific subsystem to which they relate. The updated IDs are defined as follows: **R-AUT-XX** for UAV/swarm autonomy-related risks, where ”R” stands for risk and ”XX” refers to the sequential index of the risk; **R-COM-XX** for communication risks; **R-ES-XX** for embedded systems risks; **R-FPC-XX** for flight performance and control risks; **R-GS-XX** for ground station risks; **R-PM-XX** for project management risks; **R-PP-XX** for propulsion and power risks; **R-SEI-XX** for systems engineering and integration risks; **R-SM-XX** for structures and materials risks; **R-UI-XX** for user interface (UI) risks. The risk analysis is presented in Table 19.1.

Figure 19.1 and Figure 19.2 represent the pre- and post-mitigation technical risk maps, respectively. Each point represents a risk, plotted based on its estimated likelihood and severity. The orange-shaded region marks the risk mitigation zone, representing non-tolerated risks. For these combinations of likelihood and severity, the risk is deemed unacceptable and mitigation action is required [67]. Upon reassessing the likelihood and severity of each risk following the implementation of mitigation measures (Figure 19.2), almost all points are seen to shift outside the risk mitigation zone.

R-SEI-03, R-SEI-04, and R-PM-09 remain inside of the mitigation zone. The mitigation measures are insufficient in lowering its risk to an acceptable level; the handling of the aforementioned risks should therefore be contingency-focused, such that the team can act promptly and precisely following occurrence of this risk. Note that there are several risks that lie exactly on the boundary, thus requiring close monitoring.

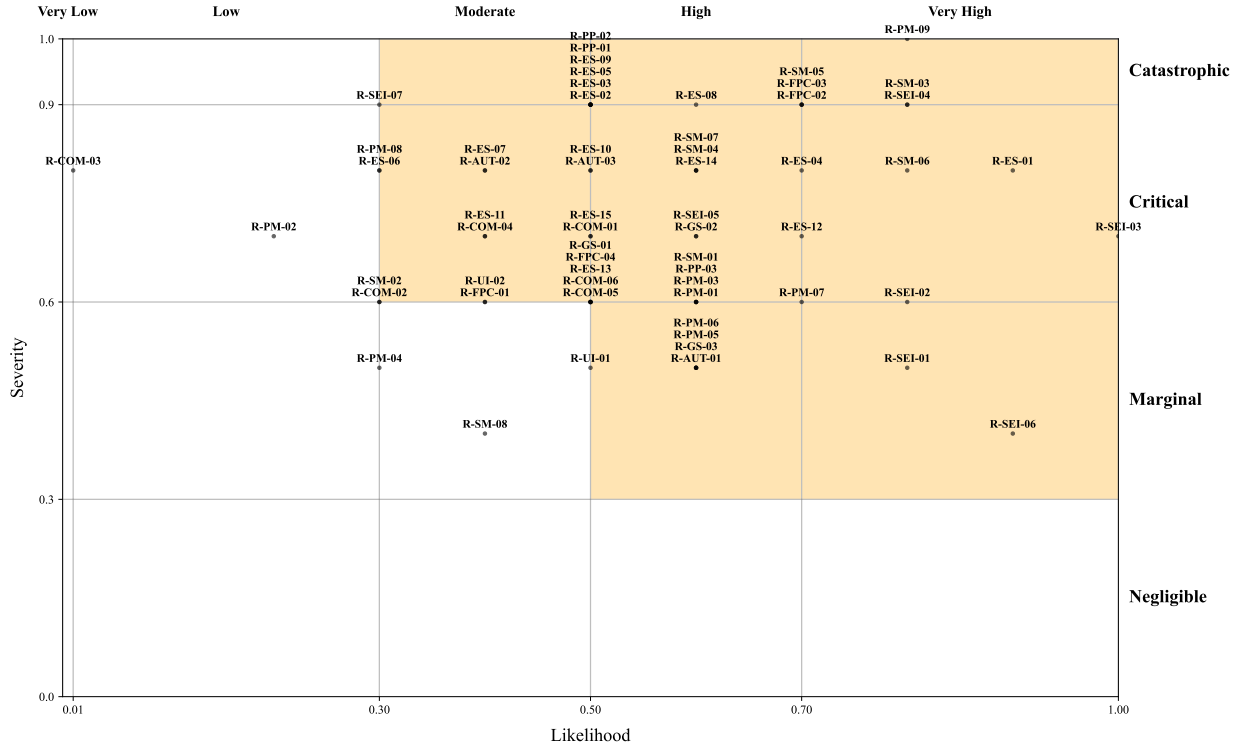

Figure 19.1: Pre-mitigation technical risk map.

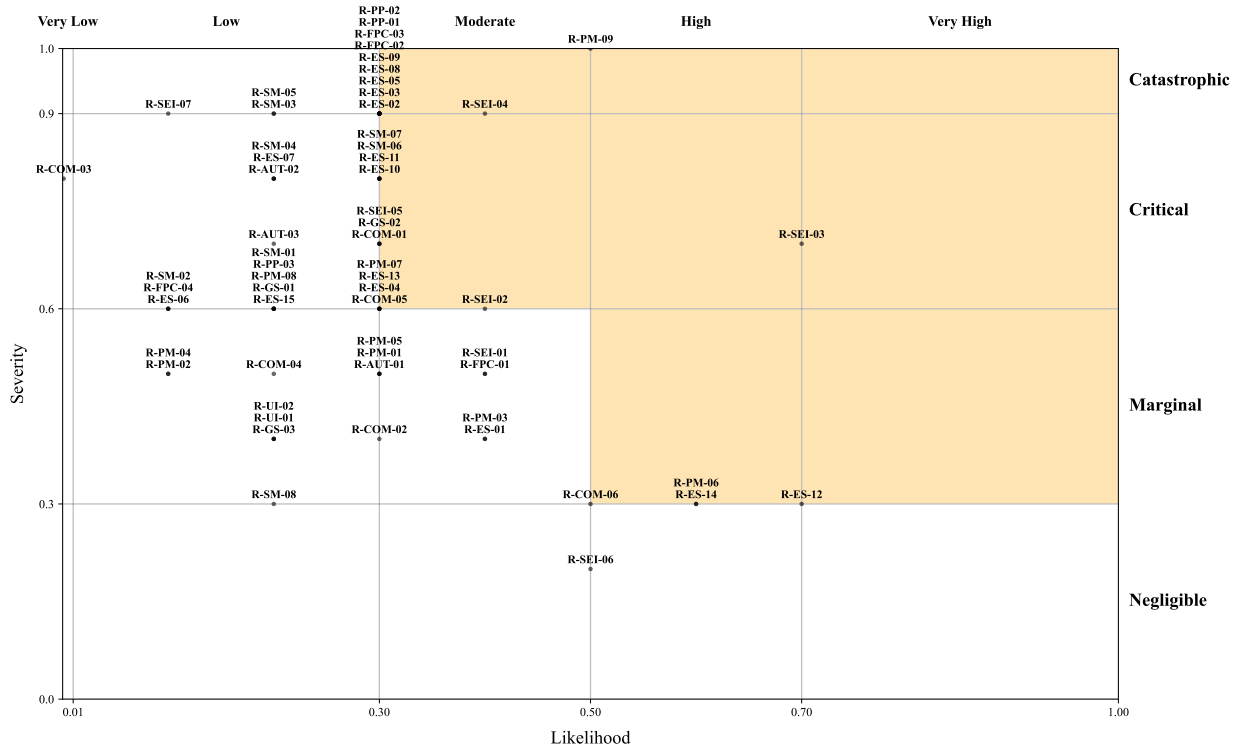

Figure 19.2: Post-mitigation technical risk map.

Table 19.1: Technical risk overview including mitigation and contingency considerations, as well as pre- and post-mitigation risk. L, S, and R refer to pre-mitigation Likelihood, Severity, and Risk, respectively. L_m, S_m, and R_m refer to post-mitigation values.

Identifier	Description	L	S	R	Impact	Mitigation Action	LM	SM	RM	Contingency Plan	Responsible
R-AUT-01	False positive in fire detection.	0.6	0.5	0.3	Wasted suppressant, misdirected resources, mission inefficiency.	Use sensor fusion and define required degree of sensor agreement.	0.3	0.5	0.15	Log and report event. Update detection model.	Fire Dpt.
R-AUT-02	Incorrect obstacle avoidance behaviour.	0.4	0.8	0.32	UAV crashes into other UAVs or environment.	Perform proper V&V perform tests in representative environment to assess avoidance behaviour.	0.2	0.8	0.16	Stop UAV operations, and resort to testing. Locate issue in code and debug.	Operations & Automation Dpt.
R-AUT-03	CNN is unable to generalise unseen fire scenarios	0.5	0.8	0.4	Failure to detect fires.	Train the model on diverse fire datasets; incorporate uncertainty estimation.	0.2	0.7	0.14	Revert to manual validation.	Control, Propulsion & Electrical Dpt.
R-COM-01	UAV-GS communication link loss during mission.	0.5	0.7	0.35	Loss of coordination and sync. between UAV swarm members.	Use redundant communication links.	0.3	0.7	0.21	Perform autonomous emergency landing.	Operations & Automation Dpt.
R-COM-02	Channel congestion from simultaneous data streams.	0.3	0.6	0.18	Increased latency, loss of telemetry or command responsiveness.	Prioritise critical messages; design for bandwidth margins.	0.3	0.4	0.12	Suppress non-critical messages; switch to backup communication link. Reduce update frequency/data rate.	Operations & Automation Dpt.
R-COM-03	Interception by external actors (e.g. spoofing, jamming, etc).	0.01	0.8	0.008	Loss of comms, navigation disruption, or UAV takeover attempts.	Use encrypted links, implement jam detection.	0.001	0.8	0.0008	Enable emergency landing.	Operations & Automation Dpt.
R-COM-04	Sync errors across the UAV swarm.	0.4	0.7	0.28	Loss of coordination, flight instability, conflicting behaviors.	Design decentralised backup UAV behaviours; synchronised clocks.	0.2	0.5	0.1	Perform emergency landing.	Operations & Automation Dpt.
R-COM-05	Data desynchronisation between UAV and GCS.	0.5	0.6	0.3	Fire detection and supression errors.	Time-stamped data packages, synchronised clocks across systems.	0.3	0.6	0.18	Manual sync.	Control, Propulsion & Electrical Dpt.
R-COM-06	4G network loss during high-data transmission.	0.5	0.6	0.3	Loss of situational awareness at GCS, delayed commands.	Implement fallback to RF modem.	0.5	0.3	0.15	Pause non-critical streams.	Control, Propulsion & Electrical Dpt.
R-ES-01	Sensor degradation over time or in adverse conditions.	0.9	0.8	0.72	Reduced accuracy or failure in nav, detection, or control.	Use redundant sensors; track sensor health telemetry; implement recalibration procedures.	0.4	0.4	0.16	Replace sensors.	Fire Dpt.
R-ES-02	Navigation system failure during flight.	0.5	0.9	0.45	UAV goes off course, risk of collision and crashes.	Flight check-lists; test navigation system under representative conditions (high temperatures, smoke, debris, etc.)	0.3	0.9	0.27	Activate manual mode and attempt emergency landing procedure.	Operations & Automation Dpt.
R-ES-03	Control system failure during flight.	0.5	0.9	0.45	UAV could lose stability, control, collide or crash.	Flight check-lists; redundancy.	0.3	0.9	0.27	Activate manual mode; attempt emergency landing.	Control, Propulsion & Electrical Dpt.
R-ES-04	Overheating of onboard avionics near fire hotspots.	0.7	0.8	0.56	Loss of power to internal systems, hardware damage.	Thermal shielding; cooling systems; heat-tolerant avionics.	0.3	0.6	0.18	Abort , return to base. Perform check-lists and assess damage.	Control, Propulsion & Electrical Dpt.
R-ES-05	Failure of onboard fault detection.	0.5	0.9	0.45	Unchecked subsystem degradation, cascading failures.	Test FDI logic in simulation and hardware-in-the-loop.	0.3	0.9	0.27	During maintenance, assess damage and repair.	Control, Propulsion & Electrical Dpt.
R-ES-06	Actuator saturation.	0.3	0.8	0.24	Reduced control authority, degraded flight performance or instability.	Anti-windup mechanisms; implement margins.	0.1	0.6	0.06	Emergency landing . Perform check-lists, assess damage.	Control, Propulsion & Electrical Dpt.
R-ES-07	Hardware interface mismatches between subsystems.	0.4	0.8	0.32	Communication failure, sensor misreads, system inoperability.	Define and verify interface standards early; conduct interface testing.	0.2	0.8	0.16	Check-lists during maintanence. Assess problem and repair.	Control, Propulsion & Electrical Dpt.
R-ES-08	Software-hardware integration conflicts.	0.6	0.9	0.54	System crash, unpredictable behaviour	Simulate hardware-in-the-loop; define and enforce the interface contracts.	0.3	0.9	0.27	Ground all UAVs and debug.	Control, Propulsion & Electrical Dpt.
R-ES-09	Payload release malfunction.	0.5	0.9	0.45	UAV cannot release payload to extinguish fire.	Test release mechanism under multiple conditions.	0.3	0.9	0.27	Fly UAV back to base. Check for failure mode and repair. If necessary, redesign and replace.	Fire Dpt.
R-ES-10	Payload sensor failure during mission.	0.5	0.8	0.4	Cannot perform fire detection.	Flight check-lists; regular maintanence; redundant sensors.	0.3	0.8	0.24	Land UAV at GS and replace faulty sensor.	Fire Dpt.

Continued on next page

Table 19.1: Technical risk overview including mitigation and contingency considerations, as well as pre- and post-mitigation risk (continued).

Identifier	Description	L	S	R	Impact	Mitigation Action	LM	SM	RM	Contingency Plan	Responsible
R-ES-11	Payload actuator failure.	0.4	0.7	0.28	Fire suppressant not deployed during critical window, fire propagates.	Test under diverse thermal and vibrational conditions.	0.3	0.8	0.24	Re-task another swarm UAV for suppression.	Control, Propulsion & Electrical Dpt.
R-ES-12	Onboard mission planning logic conflicts with external commands.	0.7	0.7	0.49	Erratic behaviour.	Implement arbitration logic with precedence hierarchy.	0.7	0.3	0.21	Freeze current decision branch, operator manual override.	Control, Propulsion & Electrical Dpt.
R-ES-13	Companion computer overload	0.5	0.6	0.3	Drop in frame rates, delayed decisions, missed targets/detections.	Optimise models for edge devices, monitor CPU usage, distribute computation.	0.3	0.6	0.18	Manual override, retrain models post-mission.	Control, Propulsion & Electrical Dpt.
R-ES-14	GNSS-denied environments impair navigation and/or coordination.	0.6	0.8	0.48	Navigation drift, swarm desync.	Fuse GNSS/INS to allow deadreckoning.	0.6	0.3	0.18	Return to last known position.	Control, Propulsion & Electrical Dpt.
R-ES-15	Flight controller overload from simultaneous commands.	0.5	0.7	0.35	Control delays or failure.	Monitor CPU usage, define command priority queue.	0.2	0.6	0.12	Manual override.	Control, Propulsion & Electrical Dpt.
R-FPC-01	Payload movements not sufficiently accounted for in Flight dynamics model.	0.4	0.6	0.24	Loss of stability.	Package payload such that movements have minimal impact.	0.4	0.5	0.2	Move packaging around for payload to have minimal shifts/movements.	Systems Eng.
R-FPC-02	Loss of UAV aerodynamic stability due to strong wind gusts or thermals near fire	0.7	0.9	0.63	Loss of control, collisions, crashes, mission failure.	Design for high wind tolerance. Redundancy in sensors.	0.3	0.9	0.27	Controlled mission abort and return to base.	Aerodynamic Dpt.
R-FPC-03	UAV fails during vertical transition phase.	0.7	0.9	0.63	Structural damage.	Control loop redundancy, extensive transition simulations.	0.3	0.9	0.27	Revert to vertical hover, initiate landing	Aerodynamic Dpt.
R-FPC-04	Payload release mid-manoeuvre causes CG shift.	0.5	0.6	0.3	Instability, reduced flight performance, collision.	Coordinate release timing with flight controller.	0.1	0.6	0.06	Abort manoeuvre.	Aerodynamic Dpt.
R-GS-01	Insufficient GS power backup during outage.	0.5	0.6	0.3	Inability to recharge UAVs or maintain comms; mission interruption.	Monitor GS power health and emit alerts; define backup systems based on worst-case-scenario.	0.2	0.6	0.12	Use back-up systems; pre-defined autonomous operations; land all UAVs and suspend operations.	Operations & Automation Dpt.
R-GS-02	GS fuel or suppressant tank under-capacity	0.6	0.7	0.42	Downtime; fires go unsupressed.	Implement sensor feedback, size tanks with margins.	0.3	0.7	0.21	Emergency refill, re-task UAVs.	Operations & Automation Dpt.
R-GS-03	UAV cannot be refuelled or resupplied within 5 min.	0.6	0.5	0.3	GS congestion; reduced fire response speed.	Optimise UAV queueing at GS, optimise UAV distribution across GS.	0.2	0.4	0.08	Delay non-critical UAV dispatches.	Operations & Automation Dpt.
R-PM-01	Delayed interface definitions.	0.6	0.6	0.36	Concurrent design mismatches.	Define interfaces early via N2 chart; version control.	0.3	0.5	0.15	Identify mismatches; adapt design.	Systems Eng.
R-PM-02	Underestimate component costs.	0.2	0.7	0.14	Components more expensive than in budget.	Check component cost with several suppliers. Apply cost safety factor.	0.1	0.5	0.05	Allocate more resources, assess impact product cost for customer.	Finance Manager
R-PM-03	Supplier cost increases.	0.6	0.6	0.36	Components are more expensive than accounted for in budget.	Investigate multiple suppliers to reduce dependency on single supplier. Take margins in budgetting for mat. costs.	0.4	0.4	0.16	Research if other suppliers available. Assess impact on final product cost.	Finance Manager
R-PM-04	Underestimate production cost scaling in mass production.	0.3	0.5	0.15	Initial investment not returned. Product more expensive, lose costumer.	Account for mass production in concept choice.	0.1	0.5	0.05	Assess impact cost for costumer. Reduce cost in other ways (e.g. other mat, production methods).	Finance Manager
R-PM-05	Development time extensions.	0.6	0.5	0.3	Development stage becomes more expensive.	Track daily progress and keep Gannt chart updated.	0.3	0.5	0.15	Estimate impact on develement cost budget.	Project Manager
R-PM-06	Delays in component delivery.	0.6	0.5	0.3	Delay in production and assembly, costumer receives product later.	Keep reserve stock available in-house.	0.6	0.3	0.18	Find alternative suppliers and resources. Assess impact on budget and timeline.	Project Manager
R-PM-07	Incomplete risk identification early on.	0.7	0.6	0.42	Insufficient risk mitigation and contingency planning.	Discuss potential risks with engineers from each discipline and level in hierarchy.	0.3	0.6	0.18	Add risks that were missed later, redo risk analysis.	Risk Manager
R-PM-08	Infrequent contact with costumer.	0.3	0.8	0.24	Disagreement about req. in later stages may cause system to not comply with user needs.	Keep key stakeholders engaged and agree on initial req. Perform market analysis to ensure product viability.	0.2	0.6	0.12	Rely on other users in market for profit.	Systems Eng.
R-PM-09	Failure to meet regulatory and certification standards.	0.8	1	0.8	Product becomes unsellable to most costumers leading to a massive loss of investment. Redesign necessary, causing delays.	Decide which regulation class the UAVs should follow. Make clear overview on relevant regulations.	0.5	1	0.5	Assess impact and replan project. Request additional resources to cover cost.	Systems Eng.

Continued on next page

Table 19.1: Technical risk overview including mitigation and contingency considerations, as well as pre- and post-mitigation risk (continued).

Identifier	Description	L	S	R	Impact	Mitigation Action	LM	SM	RM	Contingency Plan	Responsible
R-PP-01	Power system failure during mission.	0.5	0.9	0.45	UAV could lose control, or crash.	Flight check-lists; use parts with high-reliability; redundancy.	0.3	0.9	0.27	Shut down non-essential subsystems. Attempt emergency landing.	Control, Propulsion & Electrical Dpt.
R-PP-02	Propulsion system failure during mission.	0.5	0.9	0.45	UAV crashes, potential mission failure.	Flight check-lists; redundancy.	0.3	0.9	0.27	Assess potential damage at base.	Control, Propulsion & Electrical Dpt.
R-PP-03	Misestimation of battery state of charge (SoC) in varying thermal conditions.	0.6	0.6	0.36	UAV runs out of power mid-mission.	Account for temperature in SoC estimation, apply safety margins.	0.2	0.6	0.12	Emergency landing protocol.	Control, Propulsion & Electrical Dpt.
R-SEI-01	Incomplete requirements.	0.8	0.5	0.4	Leads to wrong design choices.	Start with requirements early on.	0.4	0.5	0.2	Add req. and revise when it is noticed one is missing.	Systems Eng.
R-SEI-02	Integration failures from incompatibility between subsystems.	0.8	0.6	0.48	Redesign and delays.	Keep a close overview of interfaces between subsystems and regularly asses compatibility.	0.4	0.6	0.24	Investigate main assembly in CATIA and find solution with least changes and minimum performance impact.	Systems Eng.
R-SEI-03	Changing technical requirements during design.	1	0.7	0.7	Not comply with new req; redesign; delays; increase development costs; decrease quality.	Establish clear req. freeze. Keep in touch with stakeholders from early stage to agree on req.	0.7	0.7	0.49	Assess the impact of the new req. Replan project if necessary.	Systems Eng.
R-SEI-04	Inadequate simulation and testing environment.	0.8	0.9	0.72	Unvalidated design.	From research and experts, define environmental conditions to simulate.	0.4	0.9	0.36	Validate subsystems seperately, rent external test facilities.	Systems Eng.
R-SEI-05	UAV mass exceeding design thresholds.	0.6	0.7	0.42	Reduced endurance, increased stall speed, takeoff failure.	Track mass through design iterations; set strict margins; include mass budget checks in design reviews.	0.3	0.7	0.21	Communicate and discuss impact with stakeholders. Redesign and perform additional iterations.	Systems Eng.
R-SEI-06	Use of unproven technologies.	0.9	0.4	0.36	High development cost; potentially less reliable	Take cost as a trade-off criterion; extensive simulation and testing.	0.5	0.2	0.1	Evaluate impact in budgetting. Take conservative approach for first gen. design. Do proper V&V for reliability.	Systems Eng, Resp. Dpt. Eng.
R-SEI-07	Unvalidated design simulations.	0.3	0.9	0.27	Simulations are incorrect leading to potential mission failure.	V&V. E.g. sensitivity analysis, cross-verification with alternative methods, testing.	0.1	0.9	0.09	With immediate effect, suspend all operations for safety reasons. Review simulations and adjust model.	Systems Eng, Resp. Dpt. Eng.
R-SM-01	Not sufficiently accounting for debris and ash damage potential.	0.6	0.6	0.36	Damage to airframe and sensors, requiring more maintanence.	Perform tests in representative environment to assess impact of conditions.	0.2	0.6	0.12	Add additional shielding outside of airframe and sensors.	Structures Dpt.
R-SM-02	Thermal insulation failure.	0.3	0.6	0.18	Potential damage to components.	Determine operating temp. range and apply safety factor.	0.1	0.6	0.06	Add additional heat protection mat. to critical components.	Structures Dpt.
R-SM-03	Airframe structural fatigue.	0.8	0.9	0.72	Failure of airframe structure.	Analyse fatigue with loading cycle.	0.2	0.9	0.18	Repair fatigue damage for crack growth retardation; replace components.	Structures Dpt.
R-SM-04	Inadequate vibrational damping.	0.6	0.8	0.48	Sensor errors, bad image quality, imprecise payload deployment.	Perform a normal modes and frequency response analysis.	0.2	0.8	0.16	Mass/stiffness modifications; damping; tuned absorber.	Structures Dpt.
R-SM-05	Airframe failure under thermal stresses in high temperature.	0.7	0.9	0.63	Structural failure.	Determine operating temperature range from literature; safety factor.	0.2	0.9	0.18	Assess failure mode, locally reinforce to reduce stresses.	Structures Dpt.
R-SM-06	Resonance at operational frequencies.	0.8	0.8	0.64	Structural failure, reduced control precision.	Perform a normal modes and frequency response analysis.	0.3	0.8	0.24	Mass/stiffness modifications. Add damping. Use tuned absorber.	Structures Dpt.
R-SM-07	Underestimated load cases for structural design.	0.6	0.8	0.48	Structural failure.	Research combined and critical load cases early; apply safety factor.	0.3	0.8	0.24	Asses where failure has occurred and which failure mode, then locally reinforce structure to reduce stresses.	Structures Dpt.
R-SM-08	Mat. not available due to shortages or geopolitical factors.	0.4	0.4	0.16	Mat. costs increase, product more expensive. Alternative mat. less quality and overall performance.	Research mat. availability during selection; identify critical points in supply chain; determine fall-back options.	0.2	0.3	0.06	Use fall-back mat. and assess impact. Potentially redesign.	Systems Eng, Finance Manager, Resp. Dpt. Eng.
R-UI-01	Unintuitive / cluttered GCS interface layout.	0.5	0.5	0.25	Operator confusion, delayed decision making during critical events.	Apply UI/UX design principles; conduct usability testing with operators.	0.2	0.4	0.08	Fallback to simplified display mode; manual operator guidelines.	Control, Propulsion & Electrical Dpt.
R-UI-02	Inconsistent status indications or feedback signals on GCS.	0.4	0.6	0.24	Operator misunderstanding system status, leading to inappropriate actions.	Standardise all status indicators; define colour codes and alerts.	0.2	0.4	0.08	Switch to default indication set; trigger support script.	Control, Propulsion & Electrical Dpt.

19.2.Reliability, Availability, Maintainability, and Safety (RAMS)

Integrating Reliability, Availability, Maintainability, and Safety (RAMS) principles early in the design process ensures that the system can perform its intended firefighting missions effectively, efficiently, and safely. A well-executed RAMS strategy not only enhances operational performance, but also reduces downtime, simplifies maintenance, and mitigates risks to both equipment and the environment.

19.2.1.Reliability

Reliability is defined as the probability that a system performs its intended function without failure for a specified period of time. To maximise reliability, a redundancy philosophy and functional isolation has been used during the design process.

For example, the vertical and horizontal propulsion systems are mechanically decoupled. This ensures that in the event of a horizontal propulsion failure, the UAV can still maintain controlled vertical thrust and perform a safe landing. Vice versa, if the vertical propulsion fails, a horizontal landing can be performed where the landing gear breaks off to protect the fuselage.

Additionally, the battery system has been designed with endurance in mind. Each battery is rated for up to 500 charge-discharge cycles. Assuming the UAV performs two full cycles per day during the 4-month operational season, this translates to:

$$2 \text{ cycles/day} \cdot 30 \text{ days/month} \cdot 4 \text{ months} = 240 \text{ cycles/year},$$

meaning each battery can remain in reliable use for at least two operational seasons before replacement is necessary.

The system's Mean Time Between Failures (MTBF) is further increased by:

- Using industrial-grade components with proven reliability;
- Avoiding complex interdependencies between subsystems;
- Implementing a health monitoring system for early fault detection.

The ground station further improves system-level reliability by reducing dependency on human intervention. It is equipped with a robotic arm that performs:

- Autonomous battery swapping or recharging;
- Water reservoir refilling for firefighting payloads;
- Health monitoring via onboard diagnostics (e.g., battery temperature, fluid levels).

19.2.2.Availability

Availability is defined as the time that a system will be able to be used. The UAV system will only be operational during the Dutch fire season, which spans approximately T_{month} =4 months each year. About 70% of wildfires start during the high-risk period of the day, which is between 10:00 and 19:00 [1]. So the system works at H_{day} =70% capacity for T_{day} =9 hours (high-risk period) and at H_{night} =30% capacity for T_{night} =15 hours (outside high-risk period). Meaning that it has H_{single_day} =10.8 hours of full capacity per 24 hour day, determined by Equation 19.2. During the day no full capacity is used, 30% is kept for when fires break out or used as reserves when UAVs break down.

Given that the system operates only 4 months per year, the annual operational percentage of the system can be calculated using Equation 19.1:

$$H_{\text{operational}} = \frac{H_{\text{single day}} \cdot 30 \cdot T_{\text{month}}}{24 \cdot 365} \qquad (19.1) \qquad H_{\text{single day}} = (H_{\text{day}} \cdot T_{\text{day}} + H_{\text{night}} \cdot T_{\text{night}}). \qquad (19.2)$$

This comes to an operational availability of 15% over the span of a year, the low annual duty cycle supports longer component lifetimes and simplifies maintenance logistics, while still covering the periods of highest wildfire risk.

During deployment, the autonomous ground station also boosts system availability by reducing turnaround time. UAVs can autonomously land, refuel, and be redeployed without requiring human operators. This minimises downtime and ensures continuous coverage.

19.2.3.Maintainability

Maintainability refers to the ease and speed with which a UAV can be returned to its operational state after a failure. It encompasses inspection, fault detection, and repair processes. Maintenance is typically divided into two categories:

Scheduled Maintenance: These are planned procedures based on usage time or calendar intervals. For the UAV, this includes:

- Pre-flight and post-flight inspections;
- Motor and propeller checks;

- Battery health diagnostics;
- Full system maintenance every 200 flight hours[1].

Unscheduled Maintenance: These refer to repairs resulting from unexpected failures or incidents. Examples include:

- Component replacement due to crash or hard landing;
- Electronics troubleshooting due to environmental exposure;
- Firmware rollbacks after software issues.

The modular design of the UAV enables rapid swap-out of key components such as arms, sensors, or batteries, improving turnaround time and reducing downtime.

To improve maintainability:

- Diagnostic logs are stored onboard and uploaded after each mission;
- Critical components are accessible without full disassembly;
- Spare parts are standardized across UAV units.

19.2.4.Safety

Safety addresses how the UAV system protects both the environment and human operators from harm, particularly in the case of system failures.

Design Safety Features:

- Redundant flight control systems to handle sensor or actuator failure;
- GPS geofencing to prevent the UAV from entering no-fly zones;
- Return-to-home (RTH) function in case of lost signal or low battery.

Operational Safety Measures:

- Pre-flight safety checks and airworthiness validation;
- Weather condition thresholds (e.g., wind, visibility) for safe deployment;
- Real-time monitoring by a trained remote pilot during missions;
- Operators and maintenance personnel disable the launch/landing area when in the vicinity for propeller safety.

The ground station ensures safe operations through:

- Obstacle detection and avoidance for the robotic arm;
- Docking position validation before initiating recharging or refuelling;
- Emergency stop mechanisms and fault isolation for hazardous operations (e.g. water or fuel refilling under pressure).

The system continuously monitors key operational parameters (e.g., battery temperature, GPS integrity, actuator feedback). If critical thresholds are exceeded, the UAV or ground station autonomously initiates a return to a safe state. Manual override is available at all times, allowing human operators to take direct control if required.

In addition, both the UAV and ground station comply with EASA regulations regarding autonomous systems and ground-based robotics. All autonomous actions are logged for post-mission audit and safety certification purposes.

[1] See: HP Drones Maintenance Guide. Accessed 13-06-2025.

20 Compliance Matrix

The compliance matrix for all requirements is shown in Table 20.1. It contains each requirement, verification method and explanation, status and explanation, and value where applicable.

Table 20.1: Requirement list with verification.

ID	Requirement	Verification Method	Verification Explanation	Status	Value	Status Explanation
FINANCE						
REQ-SoS-FIN	The total cost of the SoS shall be €10 million over 20 years.	Analysis	Cost modeling and lifecycle cost analysis of all system components over 20-year period	Yes	€8.5M	
REQ-SoS-FIN-1	The total purchasing cost of all systems shall be at most €3 million.	Analysis	Summation of all procurement costs from vendors and suppliers	Yes	€2.7M	
REQ-SoS-FIN-2	The yearly total operational cost of the mission shall be at most €500 000 (2025).	Analysis	Annual operational budget analysis including all operational expenses	Yes	€426 000	
REQ-SoS-FIN-2.1	The yearly maintenance cost per UAV shall be at most €250 000 (2025).	Analysis	Per-unit maintenance cost projection based on component lifecycle	Preliminary Yes		Estimated €75 000
REGULATIONS						
REQ-SoS-REG	The SoS shall adhere to regulatory constraints.	Inspection	Review of compliance documentation for all regulatory requirements	Preliminary Yes	Designed to certification	Requires certification process
REQ-SoS-REG-1	The design shall adhere to regulatory constraints.	Inspection	Regulatory compliance checklist verification by qualified authority	Preliminary Yes	Designed to certification	Requires certification process
REQ-SoS-REG-1.1	The design shall adhere to environmental regulatory constraints.	Inspection	Environmental compliance certification by relevant authorities	Preliminary Yes		Designed for environmental impact minimization
REQ-SoS-REG-1.1.1	The dispensable payload shall meet EEA environmental standards.	Testing	Laboratory testing of payload materials for environmental compliance	Yes		The payload is water which is fulfils the requirements
REQ-SoS-REG-1.1.2	The batteries used shall be recyclable under EU regulations.	Inspection	Verification of battery recycling EU 2023/1542	Preliminary Yes	> 83%	EU mandates signinficant battery recycling by 2031
REQ-SoS-REG-1.1.3	The UAVs shall not be made with materials deemed highly toxic by the EPA.	Inspection	Review of material safety data sheets for all components	Yes	N.A.	No materials used fall under the highly toxic category.
REQ-SoS-REG-1.1.4	The operations in natural reserves/parks shall adhere to local conservation standards.	Inspection	Review of operational permissions from conservation authorities	Yes		The requirements for noise are met
REQ-SoS-REG-1.2	The design shall adhere to safety regulatory constraints.	Inspection	Safety compliance certification by relevant authorities	TBD		Requires certification process
REQ-SoS-REG-1.2.1	All UAVs shall be registered under the Netherlands Vehicle Authority.	Inspection	Verification of registration documentation for each UAV	TBD		Requires certification process
REQ-SoS-REG-1.2.2	The UAV design(s) must be certified by EASA.	Inspection	Review of EASA certification documentation	TBD		Requires certification process
REQ-SoS-REG-2	The SoS operations shall adhere to regulatory constraints.	Inspection	Regular audits of operational procedures against regulatory requirements	TBD		Requires certification process
REQ-SoS-REG-2.1	The SoS operations shall adhere to airspace regulatory constraints.	Inspection	Review of airspace compliance documentation and procedures	TBD		Requires certification process
REQ-SoS-REG-2.1.1	The operations of the SoS shall adhere to EASA policies.	Inspection	Operational compliance audits against EASA regulations	TBD		Requires certification process
REQ-SoS-REG-2.1.2	The operations of the SoS shall adhere to Class E airspace regulation.	Demonstration	Field demonstration of airspace compliance in operational environment	Preliminary Yes		Designed for Class E regulation

Continued on next page

Table 20.1 (continued): Requirement list with verification.

ID	Requirement	Verification Method	Verification Explanation	Status	Value	Status Explanation
REQ-SoS-REG-2.1.3	The operations of the SoS shall be overseen by at least one responsible operator.	Inspection	Verification of operator credentials and staffing logs	Preliminary Yes		Planned for in the operational concept
REQ-SoS-REG-2.2	The SoS operations shall adhere to security regulatory constraints.	Inspection	Security compliance audit of operational procedures	TBD		Requires certification process
REQ-SoS-REG-2.2.10	The GS shall support the restriction of unauthorized personnel from accessing to stationed UAVs.	Demonstration	Physical security demonstration of access control systems	Preliminary Yes		Planned for in the operational concept
DATA MANAGEMENT						
REQ-SoS-DAT	The SoS shall support data management.	Demonstration	End-to-end demonstration of data flow through the system	Preliminary Yes	N.A.	Data flow and communication pathways are defined; end-to-end functionality not yet tested.
REQ-SoS-DAT-1.1	The SoS shall enable data transmission.	Testing	Communication link performance testing under various conditions	Preliminary Yes	N.A.	Communication stack and links are specified; no performance testing conducted.
REQ-SoS-DAT-1.1.2	The UAV system shall maintain command reception from the GCS at an operational range of at least 20 km.	Testing	Field testing of communication range at maximum specified distance	Preliminary Yes	20–50 km	Radio link ranges validated in specs, not field-tested.
REQ-SoS-DAT-1.2	The SoS shall enable data storage.	Demonstration	Demonstration of data storage capabilities with sample datasets	Yes	N.A.	Onboard and GCS-based data storage supported and scalable.
REQ-SoS-DAT-1.2.3	The UTS shall log all user actions with timestamps.	Testing	Log verification testing with scripted user actions	TBD	N.A.	UTS interface and back-end logging system are not implemented
REQ-SoS-DAT-2	The SoS shall enable user-driven data management.	Demonstration	User interface demonstration of manual data management capabilities	Preliminary Yes		Data flow architecture concept routes user inputs to GCS and mission data to user; no tests conducted.
REQ-SoS-DAT-2.1	The UTS shall enable user control of the SoS systems.	Demonstration	Demonstration of user command execution through interface	Preliminary Yes	N.A.	Remote user communications hardware theoretically supports this; further testing required.
REQ-SoS-DAT-2.2	The user shall be able to input their operational conditions to the UTS.	Demonstration	Demonstration of user input functionality for operational parameters	TBD	N.A.	Data/communications architecture supports commands from UTS to GCS; conceptually supported but not tested or extensively considered.
UAV SWARM DEPLOYMENT						
REQ-SoS-DEP	The SoS shall enable the deployment of the UAV swarm.	Demonstration	Full-scale deployment demonstration of UAV swarm	Preliminary Yes		Planned for in the operational concept
REQ-SoS-DEP-1.1	The SoS manufacturing shall be sustainable.	Analysis	Life cycle assessment of manufacturing processes	TBD	N.A.	Life cycle assessment of manufacturing shall be done after preliminary design phase.
REQ-SoS-DEP-1.1.1	The UAV shall be manufacturable with existing manufacturing technologies.	Inspection	Manufacturing process verification at production facility	Yes	N.A.	Commonly used materials and manufacturing methods are used.
REQ-SoS-DEP-1.1.2	The percentage of defective UAVs shall not exceed 0.1%.	Analysis	Statistical quality control analysis of production data	TBD	N.A.	After preliminary design phase, knowing materials and production method of UAV, the analysis will be performed.
REQ-SoS-DEP-1.1.3	The UAV shall be made of at least 50% recyclable materials, by mass.	Analysis	Material composition analysis and recyclability assessment	Preliminary Yes	N.A.	The recyclability of some materials has been assessed, but need to analyze all to have number.
REQ-SoS-DEP-1.1.4	The UAV shall have a modular design.	Inspection	Design review of modular components and interfaces	Yes		UAV has been designed as modular
REQ-SoS-DEP-1.2	The SoS scaling up shall be modular.	Demonstration	Demonstration of system scaling with additional modules	Yes		The system inherently allows modular scaling up
REQ-SoS-DEP-1.2.1	The GS shall support UAV transportation.	Demonstration	Demonstration of UAV loading and transport procedures	Yes		GS is designed to transport the UAVs
REQ-SoS-DEP-1.2.2	The GS shall be able to command the retrieval of all UAVs within its operational area.	Testing	Field testing of UAV retrieval commands across operational area	Preliminary Yes	N.A.	Selected GS hardware supports return-to-base commands; not yet tested.
REQ-SoS-DEP-1.2.3	The GS shall track all UAVs currently within its operational control area.	Testing	Tracking accuracy testing with multiple UAVs in operation	Preliminary Yes	N.A.	Comms architecture design theoretically supports this; not yet tested.

Continued on next page

Table 20.1 (continued): Requirement list with verification.

ID	Requirement	Verification Method	Verification Explanation	Status	Value	Status Explanation
REQ-SoS-DEP-1.2.4	The SoS shall be able to coordinate between different operating modules.	Testing	Inter-module communication and coordination testing	Yes		The communication are designed for coordination between different modules
REQ-SoS-DEP-1.2.10	The SoS should be shippable through ISO-668 standard shipping containers.	Inspection	Dimensional verification against standard shipping container specifications	Yes		The ground station is designed as a containerised solution using ISO-668 standard shipping containers
REQ-SoS-DEP-2	The SoS shall allow for UAV operations deployment.	Demonstration	Field demonstration of UAV deployment procedures	Yes		System is designed for UAVs to be deployed
REQ-SoS-DEP-2.1	The SoS shall allow for UAV autonomous deployment.	Demonstration	Autonomous deployment sequence demonstration	Yes		System has been designed to operate autonomously
REQ-SoS-DEP-2.2	The SoS shall allow for UAV take-off and landing	Demonstration	Take-off and landing demonstration under various conditions	Yes		System is designed to allow UAV take-off and landing
UAV SWARM OPERATION						
REQ-SoS-OPS	The SoS shall enable the operation of the UAV swarm.	Demonstration	Comprehensive operational demonstration of UAV swarm capabilities	Yes		All necessary logistics have been considered which allow the operation of the UAV swarm
REQ-SoS-OPS-1	The SoS shall support the execution of mission functions.	Demonstration	Mission execution demonstration with defined objectives	Yes		The UAV and the Ground Station are designed to complete the defined missions
REQ-SoS-OPS-1.1	The SoS shall support operational area surveillance.	Demonstration	Surveillance mission demonstration in operational area	Yes	N.A.	
REQ-SoS-OPS-1.1.2	The SoS shall support round-the-clock operational area monitoring during high alert periods.	Testing	24-hour continuous operation testing during simulated alert	Yes		The system is designed to operate continuously over 24 hours
REQ-SoS-OPS-1.1.3	The entire operational area shall be covered every $10\,\mathrm{min}$ during regular daytime operations.	Testing	Coverage timing verification using position tracking data	Yes	$8.1\,\mathrm{min}$	
REQ-SoS-OPS-1.1.4	The entire operational area shall be covered every $30\,\mathrm{min}$ during regular nighttime operations.	Testing	Night-time coverage timing verification with position data	Yes	$19\,\mathrm{min}$	
REQ-SoS-OPS-1.1.5	The SoS shall be capable of performing fire suppression operations for at least $6\,\mathrm{h{\cdot}d^{-1}}$.	Testing	Endurance testing of fire suppression capabilities	Preliminary Yes	6 h	Water Supplies allow 6 hours of continuous suppression
REQ-SoS-OPS-1.1.6	The SoS shall be capable of performing firefighter support operations continuously.	Testing	Extended continuous operation testing with firefighter support scenarios	Yes		The system is designed to support firefighting operations continuously, given realistic continuous logistical support
REQ-SoS-OPS-1.2	The SoS shall support fire suppression within the operational area.	Demonstration	Demonstration of fire suppression capabilities in controlled environment	Yes		The UAV has been designed to carry and drop 15 L of water, which can suppress fire
REQ-SoS-OPS-1.2.1	The UAV shall have a minimum dispensable payload capacity of $15\,\mathrm{kg}$	Testing	Payload capacity testing with calibrated weights	Yes		UAV has been designed to carry $15\,\mathrm{kg}$ of dispensable water
REQ-SoS-OPS-2	The SoS shall manage flight aspects of the UAV swarm.	Demonstration	Flight management demonstration with multiple UAVs	Yes	N.A	
REQ-SoS-OPS-2.1	The SoS shall maintain flight performance.	Testing	Performance testing under various flight conditions	Preliminary Yes	N/A	Initial values suggest performance is maintained.
REQ-SoS-OPS-2.1.3	The AFCS shall enable autonomous UAV attitude control.	Testing	Attitude control testing under external disturbances	TBD	N.A.	Requires testing
REQ-SoS-OPS-2.1.8	The UAV system shall sustain forward flight against wind speeds of up to $110\,\mathrm{km{\cdot}h^{-1}}$ while carrying its maximum operational payload.	Testing	Wind tunnel testing at maximum specified wind speed	Yes		The UAV has been designed to fly with a maximum speed of 118 km/h
REQ-SoS-OPS-2.1.9	The UAV system shall identify buildings within an horizontal radius of $100\,\mathrm{m}$.	Testing	Building detection testing with various structures at specified range	Preliminary Yes	N.A.	The EO/IR gimbal camera and CNN layer are capable of object detection and classification; no field tests conducted.
REQ-SoS-OPS-2.1.10	The UAV system shall not fly within a horizontal distance of $20\,\mathrm{m}$ from buildings.	Testing	Obstacle avoidance testing with building proximity scenarios	Preliminary Yes	TBD	UAV image recognition planned, but not implemented nor tested.
REQ-SoS-OPS-2.1.16	The UAV shall have a MTOW of at most $80\,\mathrm{kg}$.	Inspection	Weight verification with calibrated scales at maximum configuration	TBD	N.A.	Inspection shall be done after prototyping.

Continued on next page

Table 20.1 (continued): Requirement list with verification.

ID	Requirement	Verification Method	Verification Explanation	Status	Value	Status Explanation
REQ-SoS-OPS-2.2	The SoS shall maintain UAV swarm coordination.	Demonstration	Swarm coordination demonstration with multiple maneuvers	Yes	n/a	A coordination model has been developed to ensure this.
REQ-SoS-OPS-2.2.2	The UAV system shall maintain nominal navigation performance for any visibility conditions.	Testing	Navigation testing under various visibility conditions	Preliminary Yes	N.A.	Nav sensor integration supports navigation under variable conditions; not field tested.
REQ-SoS-OPS-2.2.5	The UAV shall detect other UAVs within a sensing radius of 50 m.	Testing	UAV detection range testing with multiple UAVs	Yes	100 m	In the coordination model, UAVs are not allowed to be within less than 100 m of other UAVs.
REQ-SoS-OPS-2.2.13	The SoS shall provide capacity for up to 50 simultaneously operating UAVs.	Testing	System capacity testing with maximum number of UAVs	No		The system has been designed for 35 UAVs which is sized by the budget
UAV SWARM SUSTENANCE						
REQ-SoS-SUS-1	The SoS shall support SoS maintenance.	Demonstration	Maintenance procedure demonstration on operational system	TBD	N.A.	Demonstration of maintenance needs to be done after prototyping.
REQ-SoS-SUS-1.1	The SoS shall support SoS repairs.	Demonstration	Repair procedure demonstration on damaged components	TBD	N.A.	Demonstration of repairs shall be done after prototyping.
REQ-SoS-SUS-1.1.1	The GS shall be equipped with the tooling required to perform UAV repairs.	Inspection	Inventory verification of repair tools against maintenance manual	No		Currently, the GS is not account for tooling required for repair
REQ-SoS-SUS-1.2	The SoS shall maintain operational reliability.	Analysis	Reliability modeling based on component failure rates	TBD	N.A.	Reliability of individual components not yet known.
REQ-SoS-SUS-1.2.4	The SoS shall maintain a reliability of 99% throughout its operational lifetime of 20 years.	Analysis	Statistical reliability projection based on accelerated testing	TBD	N.A.	Reliability of individual components not yet known.
REQ-SoS-SUS-1.2.8	The GS shall support nominal operations for at least TBD h in the event of grid failure.	Testing	Power failure simulation testing with backup systems	Yes		The system does not depend on the grid
REQ-SoS-SUS-1.2.9	The GS shall have an operational lifespan of 20 years.	Analysis	Component lifetime analysis and replacement schedule planning	TBD		No analysis performed so far
REQ-SoS-SUS-1.2.13	The SoS shall have an expected uptime (including maintenance and repairs) percentage of at least 90%.	Analysis	Availability analysis using component reliability data	TBD		No analysis performed so far
REQ-SoS-SUS-2	The SoS shall support SoS servicing.	Demonstration	Service procedure demonstration on operational system	TBD	N.A.	Demonstration shall be done after prototyping.
REQ-SoS-SUS-2.1	The SoS shall be able to sustain UAV swarm power needs.	Demonstration	Power management demonstration during extended operation	Yes		Power supply was sized to support UAV swarm
REQ-SoS-SUS-2.1.1	The GS shall support full recharging/refuelling of UAV systems within 3 min.	Testing	Recharging/refueling time measurement from empty to full	Preliminary Yes		Fluid flows sized for requirement. Robotic arm kinematic analysis not yet performed
REQ-SoS-SUS-2.1.2	The GS shall have a capability of storing sufficient fuel to sustain 7 d of firefighting operations.	Inspection	Fuel storage capacity verification against consumption rate	Yes		The ground station has fuel capacity for 29 days of operations without refuelling
REQ-SoS-SUS-2.2	The SoS shall be able to sustain UAV swarm fire suppressant needs.	Demonstration	Suppressant resupply demonstration during simulated operations	Yes		The GS was designed to meet the demand for water needed for up to 6 h of continuous firefighting operations
REQ-SoS-SUS-2.2.1	The GS shall have a capability of storing sufficient suppressant to sustain 6 h of firefighting operations.	Inspection	Suppressant storage capacity verification against usage rate	Yes		The GS was designed to meet the demand for water needed for up to 6 h of continuous firefighting operations
REQ-SoS-SUS-2.2.2	The GS shall support payload reloading in under 3 min per UAV.	Testing	Payload reloading time measurement with operational procedures	Yes		The refueling pump has been sized for refilling the tank in 3 min

21 Project Outlook

After the preliminary design is complete and the system has most parameters defined, it is important to evaluate the costs and next steps for the project. This chapter shows the breakdown of total system costs in Section 21.1. The project ROI is outlined in Section 21.2. Finally Section 21.3 describes in detail the items remaining to finalize the project.

21.1.Cost Breakdown

The system cost of €10 million for a 20 year lifespan is given as user requirement, equating to €500 000/yr. In the initial estimates for the cost breakdown were allocated on statistical estimates and literature. In the design costs are built up from component selection. During the design phase fundamental changes in cost breakdown for aircraft were considered while refining operations, during this period a cost model was created to vary for iterative design.

21.1.1.Operating Expenses

Assuming 15 % of yearly cost due to maintenance[1], maintenance will be placed at €75 000 for UAV replacement parts. For operations team a €50 000 cost per FTE totalling to €67 000 per year. This assumes 4 operators working in shifts to monitor the system 24/7 for 4 months per year out of 12 as calculated in Section 19.2, assuming the operator will be trained and able to perform maintenance. Additional coordination costs may be offset to firefighting departments as some roles may overlap with existing positions. As such the total operational cost excluding fuel may be approximated at €150 000 per year.

For fuel-powered UAVs lifetime fuel cost for operation is

$$C_{\text{energy fuel}} = N_{\text{UAVs}} \cdot V_{\text{tank}} \cdot \frac{T_{\text{lifetime}} \cdot 24 \cdot 365}{E_{\text{hours}}} \cdot M_{\text{op}} \cdot C_{\text{fuel}}, \tag{21.1}$$

where

- V_{tank} is the fuel tank size,
- E_{hours} is the endurance in hours,
- M_{op} is the operating time multiplier[2],
- C_{fuel} is the cost of fuel.

A direct model is created to size the UAV swarm based on cost and performance. Aircraft cruise speed, range, endurance, payload and cost is gathered at every stage of the design to inform the model. The selection of a chemically propelled UAV negates the need for multiple ground stations.

The cost of a ground station is estimated based on the upper bound cost of a custom semi truck [3] multiplied by 3 as a very rough approximation for custom modification. This was cross checked with costs for robotic arm to confirm they would be in budget. It is critical to refine the estimate as the ground station is further developed.

Number of UAVs Calculation

Calculate number of UAVs possible with the available budget using Equation 21.2.

$$N_{\text{UAVs}} = \frac{B_{\text{total}} - N_{\text{stations}} \cdot C_{\text{station}} - C_{\text{energy}}}{C_{\text{UAV}}}, \tag{21.2}$$

where

- N_{UAVs} is the number of UAVs that can be acquired,
- B_{total} is the lifetime total budget subtracting personnel and maintenance cost,
- N_{stations} is the number of ground stations required,
- C_{station} is the cost per ground station,
- C_{energy} is the lifetime energy cost found by Equation 21.1,
- C_{UAV} is the cost per UAV.

21.1.2.System Cost Breakdown

The result of the cost model determines that 35 UAVs may be manufactured for €2.79 million and operated with a yearly operating cost of €292 000 (FY2025). The costs are broken down as follows into 20 year lifetime and yearly costs:

[1] See: https://www.linkedin.com/pulse/understanding-airplane-maintenance-costs-tabish-khan/. Accessed 09/05/2025

[2] This accounts for all non-operating UAVs and times over the course of the year.

[3] See: https://www.mylittlesalesman.com/news/how-much-does-a-semi-truck-cost-prices-factors Accessed 17/06/2025

Table 21.1: UAV swarm lifetime cost breakdown.

Item	Target Lifetime Cost (M€FY2025)	Target Yearly Cost (K€FY2025)	Percentage
Fuel Costs	2.99	150	38
Maintenance Costs	1.50	75	16
Personnel Costs	1.34	67	14
Purchase Cost UAVs	1.88	94	24
Purchase Cost GS	0.80	40	8
Total	**8.51**	**426**	**100**

Cost Model Sensitivity
Fuel costs are highly limiting the chemically propelled VTOL aircraft. As such, sensitive parameters are primarily the operating time multiplier and the number of UAVs in the swarm, as it significantly increases the fuel cost. For example, using 42 drones has net neutral profit, while using 37 drones allows a break even in 30 systems sold. The value of 35 is chosen as a balance between performance and profitability. Inversely, with a fixed total budget, increasing the operating time from 4 months to 5 months decreases the number of drones possible from 35 to only 30 drones. This makes the case for battery powered operation, however it was extensively analysed and determined infeasible due to the low range of electric aircraft. If the ground station cost increases by 50% which may be expected then the number of UAVs possible decreases to 32 if maintaining current profitability.

21.1.3.Project Costs

In addition, the total R&D and engineering life cycle cost must be estimated. Due to the high uncertainty and high number of stakeholders a 40% contingency is applied. Project costs are estimated as follows:

Table 21.2: UAV swarm development cost breakdown.

Item	Target Cost (€ M FY2025)	With 40% Contingency (€ M FY2025)
Conceptual Design	1	1
Detail Design	2	3
Software Development	3	4
Production Setup	1	1
Test Subsystems	2	3
Integrated Testing	3	4
Final Product V&V	2	3
Certification	1	1
Operations Setup and Training	2	3
Engineering Support	1	2
End of Life	2	3
Total	**20**	**28**

Based on an approximate engineering salary of €100 000 per FTE with a factor of 2.5 to cover all overheads, every €1M R&D budget may provide 4 FTE engineering capacity for design work. The breakdown considers a 10 week conceptual design phase with 10 engineers for 2FTE. An additional €500 000 is allocated for preliminary proof of concept creation and testing. Detail design is estimated in a similar manner with 8 FTE, and software development being 12 FTE based on team member experience.

A high proportion of the budget is allocated to subsystem and integrated field testing. This is critical due to the high number of stakeholders in this process. In addition budget for the facilities identified in Section 5.4 must be allocated. Certifications for light aircraft are estimated in the range of $ 1M [4]. This value will be taken to cover the regulating body review of compliance documents.

End of Life costs are estimated to be €3 million. If spread over all aircraft and ground stations in proportion to manufacturing cost this would approximate €29 000 per ground station and €2000 per UAV.

21.1.4.UAV Cost Breakdown

The final UAV cost was estimated as follows built up from subsystem design, shown in Table 21.3. The lower and upper bounds used to estimate the budgets is displayed, followed by the built up cost, then with margin applied. The estimates include assembly, while the final breakdowns take assembly out as separate cost. The breakdown of each system can be

[4] See: https://resources.sw.siemens.com/en-US/case-study-tlg-aerospace/. Accessed 01/05/2025

found in it's corresponding section, with assembly described in Chapter 9. The costs from structure and assembly are estimated based on engineering judgement and as such are given higher safety margin of 30%. As the costs for camera payload, avionics and propulsion are derived directly from purchase price, they are given lower margin of 10%. Note that water dispensing payload is costed under structure.

Table 21.3: UAV cost breakdown at end of preliminary design.

Item	Lower Estimate [€]	Upper Estimate [€]	Final Target [€]	Margin	Final Specification (€FY2025)
Structure	10,000	15,000	8,515	1.3	11,100
EPS	8,000	12,000	2,000	1.1	2,200
Payload	10,000	15,000	10,000	1.1	11,000
Avionics	6,000	9,000	5,350	1.1	5,900
Propulsion	6,000	9,000	4,320	1.1	4,800
Assembly	–	–	14,400	1.3	18,700
Total	40,000	60,000	44,585	–	53,700

21.2.Return on Investment

In the market analysis the global annual market for fire aerial firefighting 2023 US$ 2.2 billion, or 2025 €1.9 billion. The system may replace a segment of this combined market. It is estimated to cover 1% of this market. This approximates to purchase of 30 systems with €500 000 per year for all costs.

In order to improve yearly ROI, from the specified budget of €10 million it is possible to charge €4.2M as purchase cost, leaving yearly operations costs at €290 000. With this the total gross profit of 30 systems is €45 million. With estimated program cost of €28 million, this results in a lifetime net profit of €17 million. The ROI is predicted 15% over R&D timeline. This is calculated by considering the net profit divided by total manufacturing and the €28 million development cost.

21.2.1.Financial Recommendations

Increasing the purchase price from €2.7 million to €12.7 million would increase ROI to 290% over lifetime. This would mean penetrating 1.4% of the aerial firefighting market. For the customer this would be a total price of €1 000 000 per year, doubling the current asking price. However, based on the market analysis where estimates of a single wildfire damages can be in the range of this value [6], this may still be interesting to customers if the system can prevent a single large wildfire per year.

The additional value of cost sharing in the development is highly beneficial as many tangential markets are interested in coordinated drone swarms for example law enforcement and military. Sharing development cost over a larger customer base should be investigated compared to additional costs to modify the design. It is also critical to improve the project cost estimate as it affects the return significantly.

Inflation amount determines operating expenses increase and as such must be accounted for. True operating costs would grow at a rate of approximately 2%[5] per year resulting in an operating cost in the 20th year of €433 000. All project costs are calculated in 2025 euros for clarity and requirements have been defined as such. In addition, financing interest payments are not considered in amortization costs, and must be investigated further, however this is considered to be responsibility of the customer.

21.3.Project Continuation

As the design synthesis exercise concludes, the project enters into a new phase, where the detail would be fully fleshed out, missing data would be supplemented by acquiring hardware, the prototype would be assembled and test campaigns conducted to determine the final design that finally enters production and is sold to the client. After, the product design team provides continuous support, working on maintenance, updates, upgrades and providing end of life support, connecting clients and recycling services if decommissioning cannot be performed by FireFlight.

21.3.1.Project Design and Development Logic

A framework for organising future project stages is developed to ensure the product has a basis for continuation beyond the conclusion of the design synthesis exercise. The logic is presented in Figure 21.1 below and is broadly divided into four major components: prototype development, verification and validation, production and manufacturing and finally the activities connected to the launch of the product as a business venture.

[5] See: https://tradingeconomics.com/euro-area/inflation-cpi Accessed 17/06/2025

Prototyping activities are further divided into the product thread and operations thread, which follow the design and implementation of the UAV and support equipment and operational items respectively. The design is first finalized, completing all detailed activities to enable prototype manufacture. The required materials and components are sourced and a draft prototype is manufactured utilising rapid development techniques such as 3D printing. The subsystems are tested and integrated with design implementations used to inform prototype improvement. Finally a full integration test is performed with a simulated mission.

Designs are continuously verified and validated with testing. The activities are informed from prototype development and used in combination with clients and stakeholders and their imposed requirements. After integrated testing of the prototype is performed, V&V is used to determine the final approach for manufacturing. The final design is informed by both tests and stakeholders. V&V activities are also carried out during manufacturing, and with the final product to ensure quality and reliability for clients. Any defects or detriments are used to optimise designs and manufacturing lines to comply with all stakeholders. Finally, continuous V&V takes place during the product's operational lifetime though client reports, maintenance findings and potential incident reports.

Full scale manufacturing design is already considered in prototype development with jig designs being tested alongside the prototype. Lessons learnt are then implemented and suppliers are sourced, so that a manufacturing line can be created and optimised. Concurrent manufacturing is employed to a limited extent due to the predicted lower order volume in the first batch. Manufacture of spare parts is continued and continuously improved to provide post-launch support.

Throughout the process and as already mentioned, client and stakeholder interaction is taking place, where current clients are consulted, new markets are explored, and meetings implementing feedback take place sales are negotiated. Certification and client approval is obtained during and after prototype testing to allow for final modifications. Documentation consisting of tests report form prototype testing, manuals and conditions for operation and certification documentation are delivered to the clients. Finally the product is delivered and support after launch as well as reviews and improvements are noted to be used in the manufacturing stage.

During the operational phase, the actual decisions are left up to the client. The company provides support to the clients by updating the system if security and safety vulnerabilities are found, performance is improved, and the system made more reliable. In addition, maintenance is performed if requests are made, and spare parts are produced for existing systems to allow for 20 years of life time. Finally end-of-life (EOL) activities are performed by recycling broken parts that were replaced during operations, refurbishing units that need maintenance and using components of totalled units to maintain other components, providing a circular economy environment. Note that the actual EOL and operating activities are left up to the client as this is a versatile system, but support is given by FireFligth throughout.

21.3.2.Project Gantt Chart

The activities planned for project continuation and successful launch outlined in Subsection 21.3.1 must be adapted to a timeline. A Gantt chart is created with quarterly resolution, fitted to fiscal quarters to couple key milestone reporting with financial reports. The timeline begins after the conclusion of the Design Synthesis Exercise, describes prototyping, which takes place in 2025, 2026 and early 2027 with testing and V&V running concurrently in late 2026 and 2027. Manufacturing preparation commences in late 2027 and takes place throughout 2028 with some time reserved in 2029 for resolving issues, client tests, and delays. The product is finally launched in Q2 2030, in time for the European fire season. Support of the product is guaranteed to be available for 20 years after launch, as software and hardware updates, as well as maintenance support.

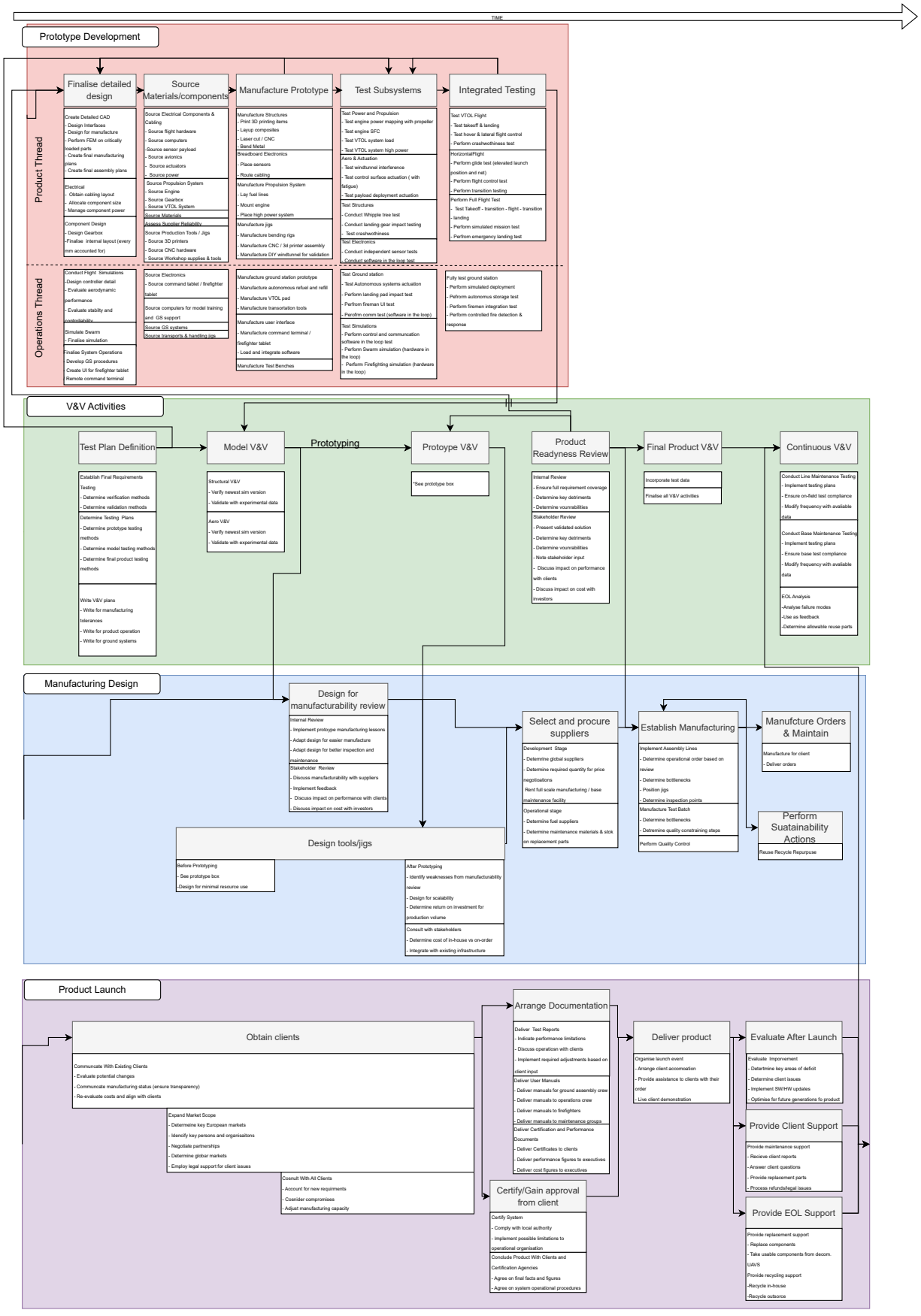

Figure 21.1: Project design and development logic.

ID	Task	2025 FQ3	2025 FQ4	2026 FQ1	2026 FQ2	2026 FQ3	2026 FQ4	2027 FQ1	2027 FQ2	2027 FQ3	2027 FQ4	2028 FQ1	2028 FQ2	2028 FQ3	2028 FQ4	2029 FQ1	2029 FQ2	2029 FQ3	2029 FQ4	2030 FQ1	2030 FQ2	2030 FQ3	2030 FQ4	Continuous - until EOL
1	Prototype development																							
1.1	Finalise detailed design																							
1.1.1	Create Detailed CAD																							
1.1.1.1	Design interfaces																							
1.1.1.2	Design for manufacture																							
1.1.1.3	Perform FEM on critically loaded parts																							
1.1.1.4	Create final manufacturing plans																							
1.1.1.5	Create final assembly plans																							
1.1.2	Electrical																							
1.1.2.1	Obtain cabling layout																							
1.1.2.2	Allocate component size																							
1.1.2.3	Manage component power																							
1.1.3	Component Design																							
1.1.3.1	Design gearbox																							
1.1.3.2	Finalise internal layout (every mm accounted for)																							
1.1.4	Conduct Flight Simulations																							
1.1.4.1	Design controller detail																							
1.1.4.2	Evaluate aerodynamic performance																							
1.1.4.3	Evaluate stability and controllability																							
1.1.5	Simulate Swarm																							
1.1.5.1	Finalise simulation																							
1.1.6	Finalise System Operations																							
1.1.6.1	Develop GS procedures																							
1.1.6.2	Create UI for firefighter tablet / Remote command terminal																							
1.2	Source Materials/components																							
1.2.1	Source Electrical Components & Cabling																							
1.2.1.1	Source flight hardware																							
1.2.1.2	Source computers																							
1.2.1.3	Source sensor payload																							
1.2.1.4	Source avionics																							
1.2.1.5	Source avionics																							
1.2.1.6	Source actuators																							
1.2.1.7	Source power																							
1.2.2	Source Propulsion System																							
1.2.2.1	Source Engine																							
1.2.2.2	Source Gearbox																							
1.2.2.3	Source VTOL System																							
1.2.3	Source Materials																							
1.2.4	Assess Supplier Reliability																							
1.2.5	Source Production Tools / Jigs																							
1.2.5.1	Source 3D printers																							
1.2.5.2	Source CNC hardware																							
1.2.5.3	Source workshop supplies & tools																							
1.2.6	Source Electronics																							
1.2.6.1	Source command tablet / firefighter tablet																							
1.2.7	Source computers for model training and GS support																							
1.2.8	Source GS systems																							
1.2.9	Source transports & handling jigs																							
1.3	Manufacture Prototype																							
1.3.1	Manufacture Structures																							
1.3.1.1	Print 3D printing items																							
1.3.1.2	Layup composites																							
1.3.1.3	Laser cut / CNC																							
1.3.1.4	Bend metal																							
1.3.2	Breadboard Electronics																							
1.3.2.1	Place sensors																							
1.3.2.2	Route cabling																							
1.3.3	Manufacture Propulsion System																							
1.3.3.1	Lay fuel lines																							
1.3.3.2	Mount engine																							
1.3.3.3	Place high power system																							
1.3.4	Manufacture jigs																							
1.3.4.1	Manufacture bending rigs																							
1.3.4.2	Manufacture CNC / 3d printer assembly																							
1.3.4.3	Manufacture DIY windtunnel for validation																							
1.3.5	Manufacture ground station prototype																							
1.3.5.1	Manufacture autonomous refuel and refill																							
1.3.5.2	Manufacture VTOL pad																							
1.3.5.3	Manufacture transortation tools																							
1.3.6	Manufacture user interface																							
1.3.6.1	Manufacture command terminal / firefighter tablet																							
1.3.6.2	Load and integrate software																							
1.3.7	Manufacture test benches																							
1.4	Test Subsystems																							
1.4.1	Test Power and Propulsion																							
1.4.1.1	Test engine power mapping with propeller																							
1.4.1.2	Test engine SFC																							
1.4.1.3	Test VTOL system load																							
1.4.1.4	Test VTOL system high power																							
1.4.2	Aero & Actuation																							
1.4.2.1	Test windtunnel interference																							
1.4.2.2	Test control surface actuation (with fatigue)																							
1.4.2.3	Test payload deployment actuation																							
1.4.3	Test Structures																							
1.4.3.1	Conduct Whipple tree test																							
1.4.3.2	Conduct landing gear impact testing																							
1.4.3.3	Test crashworthiness																							
1.4.4	Test Electronics																							
1.4.4.1	Conduct independent sensor tests																							
1.4.4.2	Conduct software in the loop test																							
1.4.5	Test Ground station																							
1.4.5.1	Test autonomous systems actuation																							
1.4.5.2	Perform landing pad impact test																							
1.4.5.3	Perfrom fireman Lift test																							
1.4.5.4	Perofrm comm test (software in the loop)																							
1.4.6	Test Simulations																							
1.4.6.1	Perform control and communcation software in the loop test																							
1.4.6.2	Perform swarm simulation (hardware in the loop)																							
1.4.6.3	Perform firefighting simulation (hardware in the loop)																							
1.5	Integrated Testing																							
1.5.1	Test VTOL Flight																							
1.5.1.1	Test takeoff & landing																							
1.5.1.2	Test hover & lateral flight control																							
1.5.1.3	Perform crashworthiness test																							
1.5.2	HorizontalFlight																							
1.5.2.1	Perform glide test (elevated launch position and net)																							
1.5.2.2	Perform flight control test																							
1.5.2.3	Perform transition testing																							
1.5.3	Perform Full Flight Test																							
1.5.3.1	Test takeoff - transition - flight - transition - landing																							
1.5.3.2	Perform simulated mission test																							
1.5.3.3	Perfrom emergency landing test																							
1.5.4	Fully test ground station																							
1.5.4.1	Perform simulated deployment																							
1.5.4.2	Peform autonomus storage test																							
1.5.4.3	Perform firemen integration test																							
1.5.4.4	Perform controlled fire detection & response																							
2	V&V Activities																							
2.1	Test Plan Definition																							
2.1.1	Establish Final Requirements Testing																							
2.1.1.1	Determine verification methods																							
2.1.1.2	Determine validation methods																							
2.1.2	Determine testing plans																							
2.1.2.1	Determine prototype testing methods																							
2.1.2.2	Determine model testing methods																							
2.1.2.3	Determine final product testing methods																							
2.1.3	Write V&V plans																							
2.1.3.1	Write for manufacturing tolerances																							
2.1.3.2	Write for product operation																							
2.1.3.3	Write for ground systems																							
2.2	Model V&V																							
2.2.1	Structural V&V																							
2.2.1.1	Verify newest sim version																							
2.2.1.2	Validate with experimental data																							
2.2.2	Aero V&V																							
2.2.2.1	Verify newest sim version																							
2.2.2.2	Validate with experimental data																							
2.3	Protoype V&V																							
2.4	Product Readyness Review																							
2.4.1	Internal Review																							
2.4.1.1	Ensure full requirement coverage																							
2.4.1.2	Determine key detriments																							
2.4.1.3	Determine vulnerabilities																							
2.4.2	Stakeholder Review																							
2.4.2.1	Present validated solution																							
2.4.2.2	Determine key detriments																							
2.4.2.3	Determine vulnerabilities																							
2.4.2.4	Note stakeholder input																							
2.4.2.5	Discuss impact on performance with clients																							
2.4.2.6	Discuss impact on cost with investors																							
2.5	Final Product V&V																							
2.5.1	Incorporate test data																							
2.5.2	Finalise all V&V activities																							
2.6	Continuous V&V																							
2.6.1	Line Maintenance Testing																							
2.6.1.1	Implement testing plans																							
2.6.1.2	Ensure on-field test compliance																							
2.6.1.3	Modify frequency with available data																							
2.6.2	Base Maintenance Testing																							
2.6.2.1	Implement testing plans																							
2.6.2.2	Ensure base test compliance																							
2.6.2.3	Modify frequency with available data																							
3	Manufacturing Design																							
3.1	Design for manufacturability review																							
3.1.1	Internal Review																							
3.1.1.1	Implement prototype manufacturing lessons																							
3.1.1.2	Adapt design for easier manufacture																							
3.1.1.3	Adapt design for better inspection and maintenance																							
3.1.2	Stakeholder Review																							
3.1.2.1	Discuss manufacturability with suppliers																							
3.1.2.2	Implement feedback																							
3.1.2.3	Discuss impact on performance with clients																							
3.1.2.4	Discuss impact on cost with investors																							
3.2	Design tools/jigs																							
3.2.1	Before Prototyping																							
3.2.1.1	*See prototype box																							
3.2.1.2	Design for minimal resource use																							
3.2.2	After Prototyping																							
3.2.2.1	Identify weaknesses from manufacturability review																							
3.2.2.2	Design for scalability																							
3.2.2.3	Determine return on investment for production volume																							
3.2.3	Consult with stakeholders																							
3.2.3.1	Determine cost of in-house vs on-order																							
3.2.3.2	Integrate with existing infrastructure																							
3.3	Select and procure suppliers																							
3.3.1	Development Stage																							
3.3.1.1	Determine global suppliers																							
3.3.1.2	Determine required quantity for price negotioations																							
3.3.1.3	Rent full scale manufacturing / base maintenance facility																							
3.3.2	Operational stage																							
3.3.2.1	Determine fuel suppliers																							
3.3.2.2	Determine maintenance materials & stok on replacement parts																							
3.4	Establish Manufacturing																							
3.4.1	Implement Assembly Lines																							
3.4.1.1	Determine operational order based on review																							
3.4.1.2	Determine bottlenecks																							
3.4.1.3	Position jigs																							
3.4.2	Determine inspection points																							
3.4.2.1	Manufacture Test Batch																							
3.4.2.2	Determine bottlenecks																							
3.4.2.3	Determine quality constraining steps																							
3.4.3	Perform Quality Control																							
3.5	Manufcture Orders & Maintain																							
3.5.1	Manufacture for client																							
3.5.1.1	Deliver orders																							
3.6	Perform Sustainability Actions																							
3.6.1	Reuse Recycle Repurpuse																							
4	Project Launch																							
4.1	Obtain clients																							
4.1.1	Communcate With Existing Clients																							
4.1.1.1	Evaluate potential changes																							
4.1.1.2	Communcate manufacturing status (ensure transparency)																							
4.1.1.3	Re-evaluate costs and align with clients																							
4.1.2	Expand Market Scope																							
4.1.2.1	Determeine key European markets																							
4.1.2.2	Identify key persons and organisaitons																							
4.1.2.3	Negotiate partnerships																							
4.1.2.4	Determine global markets																							
4.1.2.5	Employ legal support for client issues																							
4.1.3	Cosnult With All Clients																							
4.1.3.1	Account for new requirments																							
4.1.3.2	Cosnider compromises																							
4.1.3.3	Adjust manufacturing capacity																							
4.2	Arrange Documentation																							
4.2.1	Deliver Test Reports																							
4.2.1.1	Indicate performance limitations																							
4.2.1.2	Discuss operation with clients																							
4.2.1.3	Implement required adjustments based on client input																							
4.2.2	Deliver User Manuals																							
4.2.2.1	Deliver manuals for ground assembly crew																							
4.2.2.2	Deliver manuals to operations crew																							
4.2.2.3	Deliver manuals to firefighters																							
4.2.2.4	Deliver manuals to maintenance groups																							
4.2.3	Deliver Certification and Performance Documents																							
4.2.3.1	Deliver Certificates to clients																							
4.2.3.2	Deliver performance figures to executives																							
4.2.3.3	Deliver cost figures to executives																							
4.3	Certify/Gain approval from client																							
4.3.1	Certify System																							
4.3.1.1	Comply with local authority																							
4.3.1.2	Implement possible limitations to operational organisation																							
4.3.2	Conclude Product With Clients and Certification Agencies																							
4.3.2.1	Agree on final facts and figures																							
4.3.2.2	Agree on system operational procedures																							
4.4	Deliver product																							
4.4.1	Organise launch event																							
4.4.1.1	Arrange client accomodation																							
4.4.1.2	Provide assistance to clients with their order																							
4.4.1.3	Live client demonstration																							
4.5	Evaluate After Launch																							
4.5.1	Evaluate Improvement																							
4.5.1.1	Detertmine key areas of deficit																							
4.5.1.2	Determine client issues																							
4.5.1.3	Implement SW/HW updates																							
4.5.1.4	Optimise for future generations to product																							
4.6	Provide Client Support																							
4.6.1	Provide maintenance support																							
4.6.1.1	Recieve client reports																							
4.6.1.2	Answer client questions																							
4.6.1.3	Provide replacement parts																							
4.6.1.4	Process refunds/legal issues																							
4.7	Provide EOL Support																							
4.7.1	Provide replacement support																							
4.7.1.1	Replace components																							
4.7.1.2	Take usable components from decom. UAVS																							
4.7.2	Provide recycling support																							
4.7.2.1	Recycle in-house																							
4.7.2.2	Recycle outsorce																							

22 Conclusion

The goal of this report was to document the detailed design of a firefighting UAV swarm system, building upon the design decisions and considerations. This was done by performing detailed subsystem design, with functions and requirements being specified and applied for each subsystem. The main results of such a process are shown in Table 22.1.

Table 22.1: Design Results Conclusion

Item	Value	Unit	Item	Value	Unit	Item	Value	Unit
$MTOW$	65	kg	$P_{h_{\max}}$	2600	W	System Cost	2.7M	EUR
OEW	31	kg	N_{prop}	4+1	-	$P_{\text{VTOL}_{\max}}$	22.4	kW
W_{PLD}	18	kg	R	350	km	A_{covered}	400	km^2
S	1.87	m^2	L/D_{cruise}	11.7	-	h_{VTOL}	30	m
b	4.32	m	t_{refill}	180	s	N_{UAV}	35	-
L_t	1.7	m	t_{VTOL}	240	s	h_{cr}	450	m
S_h	0.32	m^2	t_{loiter}	300	s	Cost ops	292K	EUR/yr
S_v	0.18	m^2	Cost GS	800K	EUR	$V_{\text{H}_{\max}}$	33	m/s
V_{cr}	25.9	m/s	Cost UAV	54K	EUR	t_{detect}	220	s

The final system design addresses the market gap identified in wildfire surveillance and suppression operations. The 35-UAV swarm system with VTOL fixed-wing configuration achieves the critical balance between operational efficiency and mission effectiveness. With a maximum take-off weight of $64.6\,\text{kg}$ per UAV and an operational range of $350\,\text{km}$, the system can provide complete coverage of a $400\,\text{km}^2$ area while maintaining sufficient payload capacity for both surveillance equipment and water suppression loads.

The comprehensive risk management framework successfully identified and mitigated technical risks through systematic analysis of likelihood and severity. The verification and validation plan encompasses requirements validation, model verification, sensitivity analysis, and product validation, ensuring system reliability and safety. Sensitivity analysis confirmed design robustness, with key values such as MTOW, aerodynamic properties, and mission effectiveness remaining stable under parameter variations. The post-DSE development roadmap provides a clear path to market readiness through prototyping, manufacturing, validation, and certification phases, with total program costs estimated at €28 million.

The detailed design demonstrates technical feasibility, operational effectiveness, economic viability, and environmental responsibility. Through careful detail design from the engineering team, FireFlight is positioned to significantly impact wildfire management capabilities in autonomous aerial firefighting systems. A render of the final design is visible in Figure 22.1 and Figure 22.2 with the three-view drawing available in Appendix A.

Figure 22.1: Phoenix UAV render.

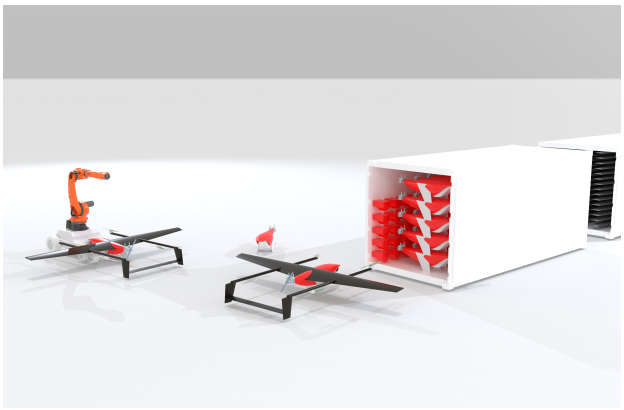

Figure 22.2: Ground station operations of FireFlight swarm.

References

[1] Cathelijne R. Stoof et al. “In temperate Europe, fire is already here: The case of The Netherlands”. In: *Ambio* 53.4 (Apr. 2024), pp. 604–623. ISSN: 0044-7447. DOI: 10.1007/s13280-023-01960-y.

[2] Margreet van Marle and H. J. Agricola. *Wildfire Risk Prediction: A Review*. Tech. rep. Deltares, Apr. 2021.

[3] Jakob Zscheischler et al. “Future climate risk from compound events”. In: *Nature Climate Change* 8.6 (June 2018), pp. 469–477. ISSN: 1758-678X. DOI: 10.1038/s41558-018-0156-3.

[4] Brian Verhoeven et al. *Wildfire Signal ’23*. Tech. rep. © Nederlands Instituut Publieke Veiligheid, Jan. 2023.

[5] *Wildfire Management Market Report 2024-2029*. Tech. rep. Institute for Defence and Government Advancement, 2024.

[6] Edwin Kok et al. *SCENARIO’S NATUURBRANDEN*. Tech. rep. Arnhem: Brandweer Nederland, Feb. 2023.

[7] Stoof Kok E. *2024 Forest Fires in Europe, Middle East and North Africa 2023*. Tech. rep. Publications Office of the European Union, 2024. DOI: 10.2760/8027062.

[8] Robert Mahoney et al. *Remotely Piloted Aircraft Systems in Bushfire Management: A NATIONAL ROADMAP*. Tech. rep. Bushfire Research Centre of Excellence, Dec. 2024.

[9] Mohammad Hosein Abbasi et al. “A framework to identify and prioritise the key sustainability indicators: Assessment of heating systems in the built environment”. In: *Sustainable Cities and Society* 95 (Aug. 2023), p. 104629. ISSN: 22106707. DOI: 10.1016/j.scs.2023.104629.

[10] Reza Sabzevari. *Cyber Physical Systems*. 2025.

[11] Jan Roskam and Chuan-Tau Edward Lan. *Airplane Aerodynamics and Performance*. Lawrence, Kansas: DARcorporation, 1997.

[12] Falk Götten et al. “Empirical Correlations for Geometry Build-Up of Fixed Wing Unmanned Air Vehicles”. In: 2019, pp. 1365–1381. DOI: 10.1007/978-981-13-3305-7{_}109.

[13] Richard Octonius and Neno Ruseno. “Endurance estimation in hovering flight based on battery power requested on quadcopter UAV”. In: *Angkasa: Jurnal Ilmiah Bidang Teknologi* 14.2 (Nov. 2022). ISSN: 2581-1355. DOI: 10.28989/angkasa.v14i2.1226.

[14] Jay Gundlach. *Designing Unmanned Aircraft Systems*. 2012.

[15] Daniel P. Raymer. *Aircraft Design, a Conceptual Approach*. Washington D.C.: AIAA, 1989.

[16] Johanning Andreas and Scholz Dieter. *Propeller Efficiency Calculation in Conceptual Aircraft Design*. Tech. rep. Hamburg University of Applied Sciences (HAW), 2013.

[17] Freeman Hugh B. *Comparison of full-scale propellers having r. A. F.-6 and clark y airfoil sections*. Tech. rep. NACA, 1931.

[18] Henk de Swardt. *Electric Motor Losses Quantified: A Comprehensive Study of Motor Losses*. Tech. rep. Timken Power System, 2023.

[19] P. J. Gelabert et al. “Maximum tree height in European Mountains decreases above a climate-related elevation threshold”. In: *Communications Earth & Environment* 5.1 (Feb. 2024), p. 84. ISSN: 2662-4435. DOI: 10.1038/s43247-024-01246-5.

[20] T.H.G. Megson. *Aircraft Structures for Engineering Students*. Fourth Edition. 2007. ISBN: 978-0-75066-7395.

[21] Yao Sun, Kuangye Zhang, and Guobin Gong. “Material properties of structural aluminium alloys after exposure to fire”. In: *Structures* 55 (Sept. 2023), pp. 2105–2111. ISSN: 23520124. DOI: 10.1016/j.istruc.2023.07.027.

[22] Christos Kassapoglou. *Design and Analysis of Composite Structures*. 2010.

[23] Marina Prieto, Mara S. Escarti-Guillem, and Sergio Hoyas. “Aerodynamic optimization of a VTOL drone using winglets”. In: *Results in Engineering* 17 (Mar. 2023), p. 100855. ISSN: 25901230. DOI: 10.1016/j.rineng.2022.100855.

[24] Thomas Hughes. *CFD Study of Flow over a Simplified Car (Ahmed Body) Using Different Turbulence Models*. Tech. rep. 2018. URL: https://www.researchgate.net/publication/325451944.

[25] Arthur W Carter. *Pressure Distributions on a Wing Having NACA 4415 Airfoil Sections with Trailing-Edge Flaps Set at 0 and 40*. Tech. rep. NASA, 1971.

[26] İbrahim Halil GÜZELBEY, Yüksel ERASLAN, and Mehmet Hanifi DOĞRU. “Effects of Taper Ratio on Aircraft Wing Aerodynamic Parameters: A Comperative Study”. In: *European Mechanical Science* 3.1 (Mar. 2019), pp. 18–23. DOI: 10.26701/ems.487516.

[27] R. Vos, M.F.M. Hoogreef, and B.T.C. Zandbergen. “Lecture 4: Analysis of aircraft configurations”. In: *AE1222-II: Aerospace Design and Systems Engineering Elements I* ().

[28] Gesang Nugroho, Galih Zuliardiansyah, and Azhar Aulia Rasyiddin. “Performance Analysis of Empennage Configurations on a Surveillance and Monitoring Mission of a VTOL-Plane UAV Using a Computational Fluid Dynamics Simulation”. In: *Aerospace* 9.4 (Apr. 2022), p. 208. ISSN: 2226-4310. DOI: 10.3390/aerospace9040208.

[29] Egbert Torenbeek. “Torenbeek - Subsonic Airplane Design”. In: (1976).

[30] R Vos, M.F.M. Hoogreef, and B.T.C. Zandbergen. *AE1222-II: Aerospace Design and Systems Engineering Elements I - A/C Preliminary Sizing (class I weight estimiation method)*.

[31] F. Oliviero. *AE3211-I Systems Engineering and Aerospace Design*. Delft, 2024.

[32] Charles R. Chalk et al. *Background Information and User Guide for Mil-F-8785B (ASG), ’Military Specification-Flying Qualities of Piloted Airplanes’*. Tech. rep. Buffalo, NY: Cornell Aeronautical Lab Inc., Aug. 1969.

[33] M. H. Sadraey. *Aircraft Design: A Systems Engineering Approach*. 1st ed. New Hampshire: Daniel Webster College, 2013.

[34] J.A. Mulder et al. *Flight Dynamics Lecture Notes*. Delft, Mar. 2013.

[35] Labane Chrif and Zemalache Meguenni Kadda. “Aircraft Control System Using LQG and LQR Controller with Optimal Estimation-Kalman Filter Design”. In: *Procedia Engineering* 80 (2014), pp. 245–257. ISSN: 18777058. DOI: 10.1016/j.proeng.2014.09.084.

[36] *Aeronautical Information Manual*. Oct. 2017.

[37] Carmine Varriale. *AE2230-I Flight & Orbital Mechanics: Lecture 05 - Cruise Range*. 2024.

[38] Robert Camilleri and Aman Batra. “Assessing the environmental impact of aircraft taxiing technologies”. PhD thesis. Shanghai, China: International Council of the Aeronautical Sciences, Sept. 2021.

[39] *Environmental Protection Technical Specifications applicable to VTOL-capable aircraft powered by non-tilting rotors*. Dec. 2023.

[40] Dhaval Joshi, Dipankar Deb, and S. M Muyeen. “Comprehensive Review on Electric Propulsion System of Unmanned Aerial Vehicles”. In: *Frontiers in Energy Research* 10 (May 2022). ISSN: 2296-598X. DOI: 10.3389/fenrg.2022.752012.

[41] Marta Portugal and André C. Marta. “Optimal Multi-Sensor Obstacle Detection System for Small Fixed-Wing UAVs”. In: *Modelling* 5.1 (Dec. 2023), pp. 16–36. ISSN: 2673-3951. DOI: 10.3390/modelling5010002.

[42] European Commission. “Commission Implementing Regulation on the Rules and Procedures for the Operation of Unmanned Aircraft”. In: *Official Journal of the European Union* 2019/947 (2024).

[43] Richard C. Rothermel. *A Mathematical Model for Predicting Fire Spead in Wildland Fuels*. Tech. rep. Ogden, Utah: USDA Forest Service, 1972.

[44] Marcos Llobera. “Modeling visibility through vegetation”. In: *International Journal of Geographical Information Science* 21.7 (Aug. 2007), pp. 799–810. ISSN: 1365-8816. DOI: 10.1080/13658810601169865.

[45] Thomas Szirtes. “Applied Dimensional Analysis and Modeling - Chapter 18”. In: *Applied Dimensional Analysis and Modeling*. Elsevier, 2007, pp. 527–657. DOI: 10.1016/B978-012370620-1.50024-1.

[46] Khaled Atamnia, Abdesselam Lebaroud, and Saikat Adikari. “Forward-Looking Model Dedicated to the Study of Electric Vehicle Range Considering Drive Cycles”. In: *The Scientific Bulletin of Electrical Engineering Faculty* (Apr. 2021). ISSN: 2286-2455. DOI: 10.2478/sbeef-2021-0011.

[47] Michael Reader-Harris. *Orifice Plates and Venturi Tubes*. Springer, 2015.

[48] Dominique Legendre et al. “Air tanker drop patterns”. In: *International Journal of Wildland Fire* 23.2 (2014), p. 272. ISSN: 1049-8001. DOI: 10.1071/WF13029.

[49] Philippe Bodino et al. *Guide d’emploi des moyens aeriens en feux de forets*. French. Tech. rep. Ministere de L’Interieur, Direction de la defense et de la securite civiles.

[50] Joe H. Scott and Robert E. Burgan. *Standard Fire Behavior Fuel Models: A Comprehensive Set for Use with Rothermel’s Surface Fire Spread Model*. Tech. rep. USDA, June 2005.

[51] K. Little et al. “Cross-landscape fuel moisture differences impact simulated fire behaviour”. In: *International Journal of Wildland Fire* 33.9 (Sept. 2024). ISSN: 1049-8001. DOI: 10.1071/WF24019.

[52] Cameron Foale. “The Directional Propagation Cache: Real-time Acoustic Simulation for Immersive Computer Games”. PhD thesis. Ballarat: University of Ballarat, July 2016.

[53] Renata M.S. Pinto et al. “Probabilistic fire spread forecast as a management tool in an operational setting”. In: *SpringerPlus* 5.1 (Dec. 2016), p. 1205. ISSN: 2193-1801. DOI: 10.1186/s40064-016-2842-9.

[54] Sakshi Patni and Bharti Sharma. “Genetic Algorithms for Decision Optimization”. In: May 2024, pp. 29–39. DOI: 10.4018/979-8-3693-2073-0.ch003.

[55] Alireza Shamsoshoara et al. “The FLAME dataset: Aerial Imagery Pile burn detection using drones (UAVs)”. In: *IEEE Dataport* (Nov. 2020).

[56] Bryce Hopkins et al. “FLAME 2: Fire detection and modeLing: Aerial Multi-spectral imagE dataset”. In: *IEEE Dataport* (Aug. 2022).

[57] Sarah Flanary et al. “FLAME 3 - Radiometric Thermal UAV Imagery for Wildfire Management”. In: *IEEE Dataport* (Dec. 2024).

[58] Alireza Shamsoshoara et al. “Aerial imagery pile burn detection using deep learning: The FLAME dataset”. In: *Computer Networks* 193 (2021). ISSN: 13891286. DOI: 10.1016/j.comnet.2021.108001.

[59] Olaf Ronneberger, Philipp Fischer, and Thomas Brox. “U-Net: Convolutional Networks for Biomedical Image Segmentation”. In: *Medical Image Computing and Computer-Assisted Intervention – MICCAI 2015*. May 2015.

[60] Hartwig Adam et al. “Rethinking Atrous Convolution for Semantic Image Segmentation”. In: *ArXiv* (Dec. 2017).

[61] C. W. Reynolds. “Flocks, Herds, and Schools: A Distributed Behavioral Model”. In: *SIGGRAPH*. 1987, pp. 25–34.

[62] Akli Benali et al. “The Portuguese Large Wildfire Spread database (PT-FireSprd)”. In: *Earth System Science Data* 15.8 (Aug. 2023), pp. 3791–3818. ISSN: 1866-3516. DOI: 10.5194/essd-15-3791-2023.

[63] Ir. R.J. Hamann and M.J.L van Tooren. *Systems Engineering & Technical Management - Part 1*. Tech. rep. 2006.

[64] Ir. R.J. Hamann and M.J.L van Tooren. *AE3-S01: Systems Engineering & Technical Management Techniques - Part 1*. Tech. rep. July 2006.

[65] Gabi Karpati et al. *Resource Management and Contingencies in Aerospace Concurrent Engineering*. Tech. rep. Pasadena: NASA Goddard Space Flight Center Greenbelt, Sept. 2013.

[66] Ricardo Valerdi. “Cost Metrics for Unmanned Aerial Vehicles”. In: *Infotech@Aerospace*. Reston, Virigina: American Institute of Aeronautics and Astronautics, Sept. 2005. ISBN: 978-1-62410-069-7. DOI: 10.2514/6.2005-7102.

[67] Prof. Dr. Eberhard Gill. *AE3211-I Systems Engineering & Aerospace Design: Lecture 3 - Risk Management & Concurrent Engineering*. 2025.

A Three-View Drawing